Spectroscopy of Planetary Systems with Space-based Telescopes

Billy Nelson Edwards

A dissertation submitted in partial fulfillment

of the requirements for the degree of

Doctor of Philosophy

of

University College London.

Department of Physics & Astronomy

University College London

December 20, 2019

I, Billy Nelson Edwards, confirm that the work presented in this thesis is my own. Where information has been derived from other sources, I confirm that this has been indicated in the work.

For my sisters, though I doubt they will ever bother to read it...

Publications:

1) Edwards et al. 2018, Exoplanet Spectroscopy and Photometry with the Twinkle Space Telescope, Experimental Astronomy, 47, pp. 29-63

2) Edwards et al. 2018, Remote-sensing Observations of Major Solar System Objects with the Twinkle Space Telescope, JATIS, 5(1), 014006

3) Edwards et al. 2019, Small Bodies Science with the Twinkle Space Telescope, JATIS, 5(3), 034004

4) Edwards et al. 2019, An Updated Study of Potential Targets for Ariel, ApJ, 157, 242

5) Edwards et al. 2020, Original Research By Young Twinkle Students: Ephemeris Refinement of Transiting Exoplanets, MNRAS (submitted)

6) Edwards 2020, Terminus: A Simulator for Exoplanet Observations with Space-based Telescopes, in prep

7) Edwards et al. 2020, ExoWebb: A JWST Radiometric Simulator, in prep

8) Edwards et al. 2020, ARES III: WASP-76 b, A Tale of Two Spectra, in prep

9) Bean et al. 2018, The Transiting Exoplanet Community Early Release Science Program for JWST, PASP, 130, 114402

10) Changeat, Edwards et al. 2019, Toward a More Complex Description of Chemical Profiles in Exoplanet Retrievals: A Two-layer Parametrisation, ApJ, in press

11) Skaf, Bieger, Edwards et al. 2020, ARES I: Characterising Hot Jupiters WASP-127 b, WASP-79 b and WASP-62 b with Hubble WFC3 Transmission Spectra, ApJ (submitted)

12) Pluriel, Whiteford, Edwards et al. 2020, ARES II: The Two Faces of KELT-7 b, ApJ (submitted)

13) Tinetti et al. 2018, A Chemical Survey of Exoplanets with Ariel, Experimental Astronomy, 46, pp. 135-209

Impact Statement

Understanding the capabilities of future instrumentation is fundamental in ensuring their design is viable, well before construction begins. The tools developed and discussed here have been used to explore the performance of the Twinkle Space Telescope for a variety of scientific endeavours. Twinkle is the first independent space observatory from Blue Skies Space Ltd (BSSL). BSSL aims to break the current bespoke, publicly-funded model for astronomy and astrophysics missions and employ a commercial approach to create new opportunities for cutting-edge science. Their vision is to enable cost-effective, quickly-delivered scientific instruments for users worldwide through a service-based model. Initially these models demonstrated that the Phase A design of Twinkle would give the spacecraft significant capacities for performing spectroscopic observations of both Solar System bodies and extrasolar planets. Now, these models are now being employed during Phase B reviews with Airbus and ABB, to compare the performances of different designs, ensuring the spacecraft's capabilities are enhanced or, at the very least, sustained. The outcomes of ongoing simulations are driving the evolution of this mission as well as the discussions with industry and scientists.

Ariel is ESA's fourth medium class mission. The ESA contribution is capped at €450 million (including launch) while the payload is being built by a consortium of 17 ESA countries alongside NASA and potentially JAXA, all of whom will work ten years to build the mission. The design for Ariel will soon be frozen and thus a crucial activity has been to validate that the instrumentation would be capable of achieving the mission's science objectives. My study into the performance of Ariel on currently-known and predicted exoplanets demonstrated this compliance and the work resulted in the creation of the Mission Reference Sample (MRS), a list of planets which Ariel could observe. The MRS is now being utilised in a number of studies, each of which aims to explore, verify and optimise the Ariel

mission, including scheduling exercises, retrieval population studies, and preparatory observations. Thus this work has been pivotal in ensuring the mission will be scientifically successful.

In the case of the James Webb Space Telescope, the design has long been fixed. However, while this powerful observatory has a plethora of observing modes, little appears to have been done to understand the optimal modes of operation. Finding efficient ways of using the spacecraft is essential given the cost of the mission, around $10 billion. Hence, ExoWebb has been developed to allow for such studies to be undertaken and its outputs are already being used by a number of researchers, helping to facilitate effective and efficient use of the most sensitive space-based telescope ever constructed.

Finally, I have been involved with engaging citizen astronomers through the ExoClock initiative, as well as education outreach through the ORBYTS program, with the aim of providing the opportunity for them to become involved in active scientific research and to be culturally connected to upcoming space missions. Such projects are crucial for inspiring the next generation of scientists and strengthening public support for astronomy.

Abstract

In the next decade, the field of exoplanetary science will be revolutionised by space-based instruments which are specifically designed for transit and eclipse spectroscopy. Current instruments provide low resolution data which has a low signal to noise ratio (SNR) over a narrow wavelength range. Upcoming missions JWST, Twinkle and Ariel will deliver broad spectral coverage, with a higher resolution and SNR, allowing for the atmospheres of hundreds of exoplanets to be probed. These missions will move the exoplanet field from an era of detection into one of characterisation, allowing for the identification of the molecular species present and their chemical profile, insights into the atmospheric temperature profile, and the detection and characterisation of clouds. However, to maximise the science gain of these missions, much preparatory work must be completed.

Simulating the expected performance is fundamental as it allows for the capability of the instrumentation to be understood. Studies can then be undertaken to access the potential impact of the mission and explore possible degeneracies or biases that may arise when fitting the simulated data. These pre-emptive studies are crucial in ensuring that, when the mission is flying, the data collected is analysed in a suitable manner. The nature of these observations necessitates caution as they will be of a far higher quality than current data, invalidating the assumptions and simplifications currently made during fitting, and will undoubtedly lead to serendipitous results. In the publication of these, we must be sure that the anomalous result is due to the exotic nature of the object studied, not errors within the data reduction or analysis. This thesis presents an overview of current data, discusses the creation of simulators for upcoming missions along with applications of these models,

and describes a project to engage high-school students and citizen astronomers in exoplanet science.

Acknowledgements

The work presented here is far from a solo effort and there are many to whom I am grateful. To my supervisors, Giovanna Tinetti and Giorgio Savini, for their guidance, patience, investment and faith in me. To Marcell Tessenyi, Enzo Pascale, Ingo Waldmann and Ian Stotesbury, for inspiring me and being excellent mentors. To Gordon Yip, Quentin Changeat, Angelos Tsiaras, Nikos Nikolaos, Ahmed Al-Refaie, Mario Morvan and many others at UCL and further afield, who have stimulated me intellectually as well as keeping me sane with their camaraderie. To my friends, for ensuring I had a life outside of work, for their mockery of my seemingly everlasting student status, and for keeping me well fed throughout these leaner years. Finally, to my family, for their love, encouragement and tolerance, throughout my life.

Contents

1 Introduction **21**

2 Planetary and Exoplanetary Spacecraft **28**

2.1 Fly-by and In-situ Missions 28

2.2 Remote-sensing Missions 30

2.2.1 AKARI 30

2.2.2 WISE/NEOWISE 30

2.2.3 Hubble 31

2.2.4 Spitzer 32

2.2.5 CoRoT 33

2.2.6 Kepler 33

2.2.7 TESS 34

2.3 Future Missions 34

2.3.1 Proposed Small Bodies Missions 35

2.3.2 CHEOPS 36

2.3.3 PLATO 37

2.3.4 WFIRST 37

2.3.5 EXCITE 38

2.3.6 Missions Beyond 2030 38

3 Spacecraft Studied Here **41**

3.1 JWST 42

3.1.1 NIRISS 42

3.1.2 NIRSpec . . . 42
3.1.3 NIRCam . . . 43
3.1.4 MIRI . . . 43
3.2 Twinkle . . . 43
3.3 Ariel . . . 45

4 Planetary Science with Twinkle **47**
4.1 Target Availability . . . 51
4.1.1 Outer Planets . . . 52
4.1.2 Moons . . . 52
4.1.3 Dwarf Planets and Other Major Celestial Bodies . . . 54
4.2 Instrumentation Performance and Data Quality . . . 57
4.2.1 Angular size . . . 57
4.2.2 Estimate of the signal received from a target . . . 58
4.2.3 Instrumental Performance and Noise . . . 62
4.2.4 Determining Observability . . . 62
4.3 Discussion . . . 64
4.3.1 Suitability of Targets . . . 64
4.3.2 Background Slits . . . 67
4.3.3 Potential Impact . . . 69
4.4 Conclusions . . . 70

5 Small Bodies Science with Twinkle **71**
5.1 Methodology . . . 73
5.1.1 Instrument Sensitivity . . . 73
5.1.2 Pointing and Tracking Restrictions . . . 74
5.1.3 Target Availability . . . 75
5.2 Results . . . 77
5.2.1 Number of Observable Asteroids . . . 77
5.2.2 Size of Potential Observable Asteroids . . . 80
5.2.3 Comets . . . 80

5.3 Discussion . . . 81
5.3.1 Characterising composition and mineralogy of primitive asteroids . . . 85
5.3.2 Composition of Comet Comae . . . 89
5.3.3 Composition and Mineralogy of S-complex and V-type asteroids . . . 90
5.3.4 Rotationally Resolved Spectral Data Sets . . . 92
5.4 Conclusions . . . 94

6 Current Exoplanet Observations from Space 95
6.1 Spitzer . . . 96
6.2 Hubble WFC3 . . . 98
6.3 Combining Instruments . . . 102
6.4 Conclusions . . . 109

7 Modelling The Performance of Future Space-based Telescopes 111
7.1 Creation of Catalogue of Exoplanets . . . 113
7.1.1 Known Exoplanets . . . 114
7.1.2 Future Planet Discoveries . . . 115
7.2 Building A Radiometric Model . . . 115
7.2.1 Signal Calculation . . . 117
7.2.2 Atmospheric Signal . . . 119
7.2.3 Modelling Light Curves . . . 122

8 Potential Targets for Ariel 125
8.1 Creating a List of Potential Targets . . . 126
8.1.1 ESA Radiometric Model . . . 126
8.1.2 Ariel Radiometric Model . . . 127
8.1.3 The 3 Tier Approach . . . 127
8.1.4 A List of Potential Targets for Ariel . . . 128
8.1.5 Creation of an Example Mission Reference Sample . . . 132
8.2 Characterisation of Small Planets . . . 135

8.3 Discussion . . . 139
8.3.1 Dependence of Predicted Yields on the Accuracy of Planetary Occurrence Statistics . . . 139
8.3.2 Scheduling of Observations . . . 140
8.3.3 Tiering System for Smaller Planets . . . 141
8.3.4 Next Steps and Final Selection of the Mission Reference Sample . . . 141
8.4 Conclusions . . . 142

9 Characterising Exoplanets with Twinkle 144
9.1 Targets within Twinkle's Field of Regard . . . 145
9.2 Assessing Target Suitability . . . 145
9.2.1 A Radiometric Model for Twinkle . . . 147
9.2.2 Spectral Retrievals . . . 156
9.3 Earth Obscuration . . . 165
9.4 Discussion . . . 169
9.4.1 Complimentary with Other Facilities . . . 171
9.4.2 Earth Obscuration . . . 172
9.4.3 Scheduling . . . 172
9.4.4 Future Planet Discoveries . . . 173
9.5 Conclusion . . . 173

10 Further Applications of Radiometric Models 175
10.1 Uses In The Literature . . . 176
10.2 Exploring Two Layer Chemistry . . . 178
10.2.1 Methodology . . . 179
10.2.2 Retrieving a 1-layer input with a 2-layer parametrisation . . . 181
10.2.3 Comparison of the 1-layer and 2-layer retrievals . . . 182
10.2.4 A more realistic example: WASP-33 b . . . 186
10.2.5 The need for non-isochemical profiles . . . 188
10.2.6 Should we always use the 2-layer model? . . . 191

10.3 Comparing Facilities . . . 194
10.3.1 Hot-Jupiters . . . 194
10.3.2 K2-18 b . . . 197
10.4 Conclusions . . . 206

11 Maintaining Exoplanet Ephemerides 210
11.1 Ground-based Follow-up . . . 211
11.1.1 Exoplanet Transit Database . . . 213
11.1.2 ExoWorlds Spies . . . 213
11.1.3 ExoClock . . . 214
11.2 Space-based Follow-up . . . 214
11.2.1 TESS . . . 215
11.2.2 Hubble and Spitzer . . . 216
11.2.3 CHEOPS . . . 217
11.2.4 Twinkle . . . 220
11.2.5 Cubesats . . . 221
11.3 An Example Ephemeris Refinement Project . . . 221
11.3.1 Target Selection . . . 222
11.3.2 Data Acquisition . . . 223
11.3.3 Data Reduction and Analysis . . . 225
11.3.4 Results . . . 227
11.3.5 Next Steps . . . 231
11.4 Conclusions . . . 232

12 Conclusion 233

Bibliography 236

List of Figures

1.1 In-situ images of various Solar System bodies 22
1.2 Hubble Spatial Scan Data 25
1.3 Example of a directly imaged planet: Fomalhaut B, as seen by the Hubble Space Telescope. Image credit: NASA/ESA. 27

2.1 Tubes in Space 40

4.1 Saturation limits for JWST instruments 49
4.2 Proposed observation strategies for observing Jupiter with NIRCam (top left), Titan with NIRSpec (top right) and Uranus (bottom left) and Neptune (bottom right) with different MIRI IFUs. All figures taken from [1]. 50
4.3 Twinkle Field of Regard 52
4.4 Observability of Outer Planets 53
4.5 Observability of Moons 54
4.6 Observability of Dwarf Planets 55
4.7 Observability of Major Asteroids 56
4.8 Noise Levels 63
4.9 Twinkle Sensitivity for Single Observation (SNR=10) 65
4.10 Twinkle Sensitivity for Multiple Observations (SNR=10) 66
4.11 Observing Moons with Background Slits 69

5.1 Twinkle Sensitivity for Single Observation (SNR = 100) 78
5.2 Twinkle Sensitivity for Multiple Observations (SNR = 100) 79
5.3 Number of Observable Asteroids 81

5.4 Size of Observable Asteroids 82
5.5 Number of Observable Comets 83
5.6 Infrared spectra obtained by AKARI for a number of small bodies highlighting the variety of spectral fatures in the 2.5-3 μm region. Figure reproduced from [2]. 87
5.7 Example Asteroid Spectra 92

6.1 G141 Spectra 100
6.2 G141 Post 101
6.3 The study of ten hot jupiters, achieved by combining data from Hubble and Spitzer, by Sing et al. [3] 102
6.4 G102 spectra 104
6.5 G102 and G141 best fit solutions 106
6.6 Posteriors for G102 and G141 107
6.7 WASP-121 b spectrum and T-P profile 108
6.8 Posteriors for WASP-121 b 109

7.1 Sky Locations of Currently-Known and Predicted Exoplanets 116
7.2 Terminus Structure 123

8.1 Simulated Ariel data for a planet similar to Wasp-39 b 129
8.2 Stellar Histograms for Ariel Tier 1 Catalogue 130
8.3 Planetary Histograms for Ariel Tier 1 Catalogue 130
8.4 Number of Potential Planets in Tiers 1 & 2 131
8.5 Sky Locations of Potential Targets for Study with Ariel 131
8.6 Planet Radius & Temperature Distribution of Example MRS 133
8.7 Potential Phase-curve Targets for Ariel 134
8.8 Simulated Tier 1 Data of LHS 1140 c for Different Atmospheric Weights 138
8.9 Histogram of current TESS Objects of Interest in the southern hemisphere and the Barclay predictions for the same sectors [4]. 140

9.1 Sky Locations of Currently-Known and Predicted Exoplanets 146
9.2 Number of Suitable Planets - Ch0 148
9.3 Number of Suitable Planets - Ch1 149
9.4 Number of Suitable Planets - Ch2 149
9.5 Achievable Resolving Power with Planet Radius - Ch0 150
9.6 Achievable Resolving Power with Planet Radius - Ch1 151
9.7 Achievable Resolving Power with Planet Radius - Ch2 152
9.8 Achievable Resolving Power with Star Magnitude - Ch0 153
9.9 Achievable Resolving Power with Star Magnitude - Ch1 154
9.10 Achievable Resolving Power with Star Magnitude - Ch2 155
9.11 Spectral retrieval of HD 209458 b 158
9.12 Posteriors for spectral retrieval of HD 209458 b 160
9.13 Spectral retrieval for GJ 3470 b 161
9.14 Posteriors for spectral retrieval for GJ 3470 b 162
9.15 Spectral retrieval for 55 Cnc e 163
9.16 Posteriors for spectral retrieval for 55 Cnc e 164
9.17 Screenshot from Freeflyer 166
9.18 Observable transits of HD 209458 b with Twinkle in 2023 167
9.19 Retrieval results for simulated observations of all available light curves of HD 209458 b during 2023 168

10.1 Example of a 2-layer chemical profile with H_2O 180
10.2 Posterior distributions of a 1-layer input atmosphere retrieved using the 2-layer model 183
10.3 Observed input spectrum obtained with a 2-layer CH_4 profile 184
10.4 Best retrieved solutions obtained with 1-layer and 2-layer retrievals . 185
10.5 Chemical and temperature profiles for the input atmospheric models 186
10.6 Posteriors of the constant and 2-layer retrievals 187
10.7 Outcome of the WASP-33 b retrieval simulations 189
10.8 Posterior distributions for the retrieval of WASP-33 b 190
10.9 Opacity contribution functions 192

10.10 Posterior distribution for the retrieval of a constant H_2O input profile 193
10.11 WASP-69 spectra with Twinkle, JWST and Ariel. 195
10.12 Retrieval posteriors for WASP-69 b 196
10.13 Retrieval posteriors for F-69b 198
10.14 JWST comparision for bright and faint targets 199
10.15 Current observational data of K2-18 b. 200
10.16 Simulated forward models with Ariel for the 3 scenarios of K2-18b . 202
10.17 Simulated forward models with JWST for the 3 scenarios of K2-18b 203
10.18 Summarising plots of the retrieval posteriors for the 3 atmospheric scenarios 204
10.19 Retrieval posteriors for the atmospheric scenario 1 206
10.20 Retrieval posteriors for the atmospheric scenario 2 207
10.21 Retrieval posteriors for the atmospheric scenario 3 208
10.22 Retrieval posteriors for the 10 Ariel transits 209

11.1 TESS observations of Kepler-18 b, WASP-4 b and KELT-15 b . . . 217
11.2 Predicted error on the transit depth with one CHEOPS observation . 219
11.3 Simulated observations of a Jupiter-sized planet orbiting a G-type star at different SNRs 219
11.4 Sky location of potential planets for study with Ariel 220
11.5 Observed minus calculated mid-transit times for all planet studied . 230
11.6 Projected Uncertainties in the Transit Times 231

List of Tables

3.1 Wavelength ranges and spectral resolutions of Twinkle's instrumentation. 45

3.2 Wavelength ranges and spectral resolutions of Ariel's instrumentation 46

4.1 Number of Observations Required Per Target 58

4.2 Average photon flux (photons/m^2/s) per spectral bin for targets considered here and the assumed parameters used in the calculation. Many of the albedos have been acquired for the JPL Solar System Dynamics Service and the original sources have been cited where possible. 60

4.3 Instrument properties over each channel 63

5.1 Main spectral features of some common minerals within the 0.4 - 4.5 μm spectral region, take from the RELAB database[5] 83

7.1 List of the opacities used within Tau-REx for the atmospheric models presented here. 121

8.1 Resolution of Ariel's 3 Tiers 128

8.2 Classification Bounds 133

8.3 Mission time required to achieve different observation goals 134

8.4 Mission Time Required to Achieve Tier 1 Resolutions for Smaller Planets 137

9.1 Planetary characteristics utilised for simulating atmospheric retrievals 157

9.2 Parameters of the simulated atmospheric retrievals with Tau-REx . . 157

9.3 The original and retrieved abundances for each planet from the simulated retrievals with Tau-REx 159

10.1 Input parameters used for WASP-69 b simulations and the priors for the retrievals. 195
10.2 Parameters used for our 3 atmosphere scenarios 199
10.3 JWST instrument setups used in ExoWebb for this work. 201
10.4 Cases investigated with Ariel and JWST 201

11.1 Number of planets that could be follow-up from the ground 212
11.2 Number of planets within the Ariel target list for which a given SNR can be reached in 1 transit with CHEOPS 220
11.3 Data on exoplanets for which observations were acquired 222
11.4 General information about the observations conducted and analysed in this work 226

Chapter 1

Introduction

”We shall not cease from exploration,
and the end of all our exploring,
will be to arrive where we started,
and know that place for the first time”

T.S. Eliot, Four Quartets

The fields of planetary and exoplanetary science are highly complementary as both contribute towards a deeper understanding of planet formation and evolution. However, they can differ vastly in the methods in which they are studied. Planetary science is generally defined as the study of our own Solar System, which is achieved through two observational types: remote-sensing and in-situ. Spacecraft studies of Solar System bodies have increasingly contributed to our knowledge of these objects over recent years. In-situ spacecraft are usually capable of studying their target in detail, from taking measurements of local effects, such as the magnetosphere, to imaging the surface, or atmospheric, features of the body. The high spatial resolution images that can be gained give extraordinary insight but are also useful in a wider context, inspiring scientists and non-scientists alike by providing snapshots of far away worlds. Figure 1.1 highlights several notable examples.

While in-situ measurements undoubtedly provide the best means of understanding a target, dedicated lander, orbiting or fly-by missions are rare and thus remote sensing missions offer a great chance to observe an object of interest. Some targets can be viewed from ground-based telescopes at certain wavelengths (e.g.

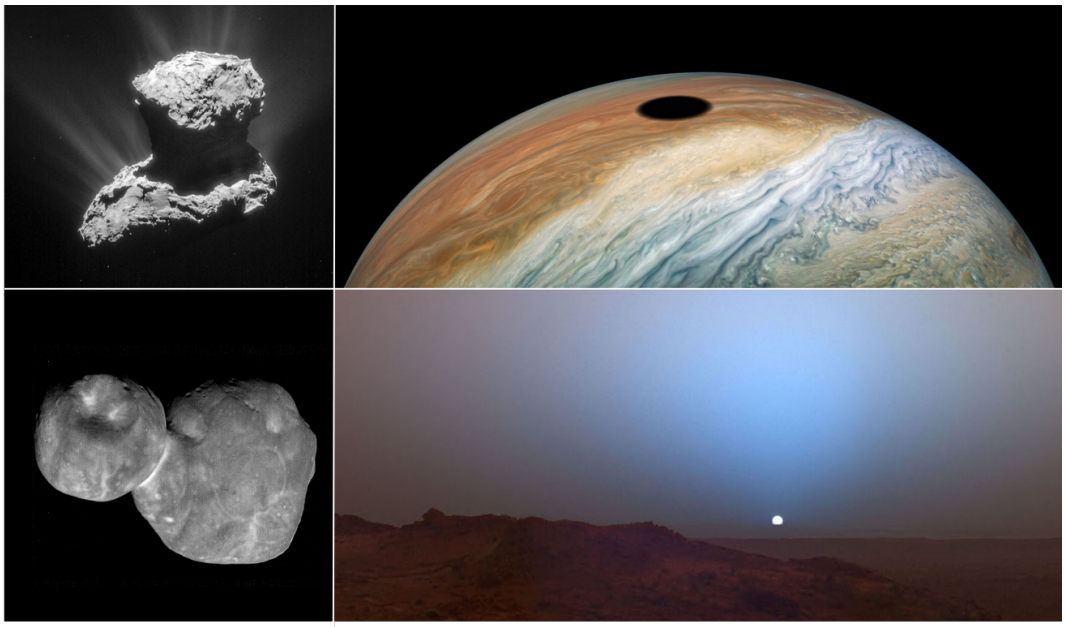

Figure 1.1: In-situ images of various Solar System bodies. Top left: Water sublimation from the comet 67P/ChuryumovGerasimenko, observed by Rosetta. Top Right: The shadow of Io crossing the face of Jupiter, as seen by the Juno spacecraft. Bottom Left: New Horizons image of Ultima Thule, the most distant object ever visited. Bottom Right: Martian sunset captured by the Curiosity rover. Image credits: ESA/NASA.

visible) but significant issues are encountered in other bands due to atmospheric absorption, particularly if observing at infrared (IR) or ultraviolet (UV) wavelengths. Additionally, ground observations can be affected by weather and atmospheric distortion. Space telescopes avoid these issues and thus are fundamental to increasing our knowledge of planetary science. However, space-based observatories are more expensive, are more limited in size and the instrumentation carried, have finite lifetimes and generally can't be repaired or upgraded. Therefore it is crucial to invest in both ground and space-based facilities to ensure a wide ranging program of scientific inquiry can be undertaken.

Potential targets for observation within our local stellar environment are diverse and each offers insight into the Solar System as a whole. Asteroids and comets are remnants of the earliest celestial bodies, providing a means of investigating the formation of the planets we know today. Studying the building blocks of the Solar System, as well as the larger bodies to have formed, enhances our understanding of

planet formation and evolution. Images taken on Earth, or by spacecraft in near-Earth orbits, are limited by the distance to the target, which reduces the spatial resolution, degrading the information content. While a great deal can be achieved with imaging, spectroscopic observations allow the mineralogy of the surface to be uncovered. Instead of the science data product being a spatially separated measure of flux, the flux's wavelength dependence is ascertained, with the target often becoming a point-like source[1].

Spectroscopic observations, particularly at visible and infrared wavelengths, allow the composition of the surfaces and atmospheres of these objects to be determined and hints of these formation and evolutionary processes to be gleaned. Although many small bodies have been discovered, and basic characteristics such as size and orbital parameters are known for many of them, only a small percentage have been characterised through spectroscopy. A lack of spectroscopic data means that our understanding of these objects, and thus the formation and evolution of our Solar System, has been limited. A broader understanding of the chemical diversity of asteroids and comets would facilitate a number of inquires including the identification of the source regions for Earth's water and organics and uncovering how and when the differentiation of planetismals, protoplanets and eventual planets occurred.

Currently, exoplanets can only be studied through remote-sensing but many methods exist for finding and characterising these planets and their atmospheres. One of the most successful methods is through observing the dip in flux seen when the planet transits the disc of the host star; i.e. it passes between the observer and the host star. The change in flux is proportional to the square of the ratio of planet to star radius. Therefore, if the stellar radius is well-known, the transit method provides the planetary radius along with the period (by observing multiple transit events). However, this method does not usually provide the mass, except through observing transit time variations, which are difficult to detect and require a system to have at least two planets. Luckily, another highly successful detection technique,

[1]Note that hyper-spectral imaging provides both wavelength and spatial information.

radial velocity, does provide constraints on the mass. When used together, these techniques provide an excellent characterisation of the basic planetary parameters (radius, mass, equilibrium temperature, semi-major axis etc.).

However, while many planets have been detected and it is thought that planets are common in our galaxy (e.g. [6, 7, 8, 9, 10]), our current knowledge of their atmospheric, thermal and compositional characteristics is still very limited. Currently, the most widely used atmospheric characterisation technique is transit and eclipse spectroscopy. As discussed, during a transit, the planet blocks out a portion of the stellar light and if an atmosphere is present, the depth of this transit will vary with wavelength due to the different opacities of molecules within the gaseous envelope. During the majority of an orbit the planetary and stellar signals are intertwined. However, during eclipse, the planet passes behind the star and thus the star is the sole contributor. By comparing this to the out of eclipse signal, the emission of the planet can be acquired as a fraction of the stellar signal.

Space telescopes such as Hubble and Spitzer, as well as some ground-based observatories, have used this technqiue to identify the key molecules present in the atmospheres of a handful of planets while also detecting the presence of clouds and probing the thermal structure (e.g. [11, 12, 13, 3, 14, 15, 16]). However, the breadth and quality of currently available data is limited by the absence of a dedicated space-based exoplanet spectroscopy mission and therefore progress in this area has been slower than desired. An example of the data products obtained by Hubble's Wide Field Camera 3 (WFC3) is given in Figure 1.2, showing the processed detector image as well as the spectrum recovered. While this data can lead to ground-breaking results, it is not as eye-catching as the images in Figure 1.1 and the planet cannot be individually resolved.

Additionally, spectroscopic observations by Hubble, Spitzer and many ground-based instruments are taken at relative low resolution ($R<100$) meaning individual spectroscopic lines cannot be resolved. However, high resolution spectrographs ($R\sim100{,}000$), such as HARPS [19] or CRIRES [20], can be used to resolve these and molecular species can be identified by using their unique fingerprint to match

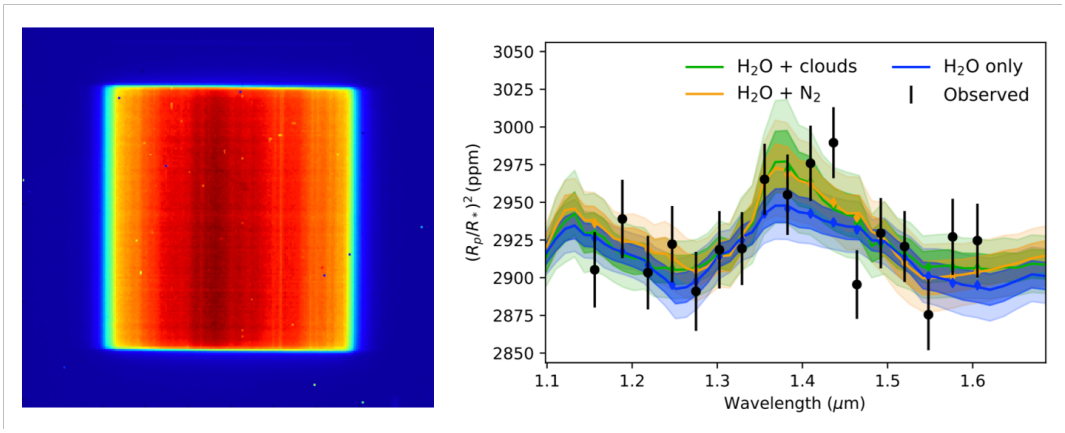

Figure 1.2: Typical data obtained with the Hubble Space Telescope WFC3 when observing exoplanets in scanning mode. Left: Example spatial scan spectral image [17]. Right: Example spectra (black points) obtained with WFC3 [18]

the observed spectra. This is in contrast to the potential ambiguities in the interpretation of planet spectra observed at low-resolution when many lines, and molecules, contribute to each data point within the spectrum. However, the cross-correlation method is not 100% precise as it only considers one molecule at a time and this can be limited by lines from multiple molecules overlapping. For example, water has absorption lines across a wide range of wavelengths and these can dominate weaker lines. Additionally, observing through the atmosphere of the Earth means the measured transmission spectrum lacks an absolute empirical normalisation. This means that absolute atomic abundances cannot be extracted from the data. Therefore, due to the contrast in capabilities, high and low resolution spectroscopy have the potential to be used together in a highly complementary fashion. Notable detections include the presence of atomic iron and titanium in KELT-9 b [21] and of high-altitude winds on HD 209458 b [22].

Direct imaging, as the name implies, is the only exoplanet detection and characterisation techniques that directly resolves the planetary contribution. The method tries to image the planet's thermal emission in-situ by blocking out the light of its host-star to reveal the significantly fainter planetary companion. Figure 1.3 shows the Fomalhaut system as imaged by Hubble. The methodology, instrumentation and data reduction and analysis are all cutting-edge, demonstrating the difficulty of observing these distant objects and there is a stark contrast when compared to images

of bodies within our Solar System. Here the planet only occupies a few pixels and can be easily lost in the noise. Many of the directly imaged planets are very young as they still radiate from the heat of their recent formation [23, 24, 25]. Hence, studying this population gives us a window into early planet formation. To understand the formation and evolution history of our own solar system, it is paramount to study the widest possible range of planetary systems and ages. Therefore, more detections via direct imaging would greatly impact the field. Direct imaging also permits atmospheric characterisation as the spectra of the planet can be directly obtained. These spectra are composed of reflected light from the host star as well as emission of the planet itself. Constraints on this technique include the inability to measure the planetary mass or radius and that the received flux is also dependent upon the distance to the planetary system. These parameters must therefore be included with the fitting process but there are correlations between them which can make deducing a single solution difficult. Combined direct imaging observations with other methodologies (e.g. radial velocity for the mass or transit photometry/spectroscopy for the radius) would increase the information content of these studies, enhancing our understanding of these worlds. Perhaps the most complementary method to direct imaging is astrometry where the motion of the star is monitored and used to infer the presence of planets. Gaia is anticipated to discover thousands of planets [26] and the results of these studies could be used to guide future direct imaging surveys which currently have a very low detection rate.

We have just begun the detection and characterisation of other planetary systems and the discoveries made so far have perhaps posed more questions than they have answered. From the planets detected thus far it is evident that our Solar System is far from the standard paradigm. In fact, no planetary system has been detected which could be considered a Solar System twin and the discovered planetary architectures have been diverse. Current key questions, which each of these methods of atmospheric characterisation have the potential to contribute towards answering, include how chemically diverse are the atmospheres of extrasolar planets and if there is an underlying correlation between a planet's basic characteristics (e.g. size, tem-

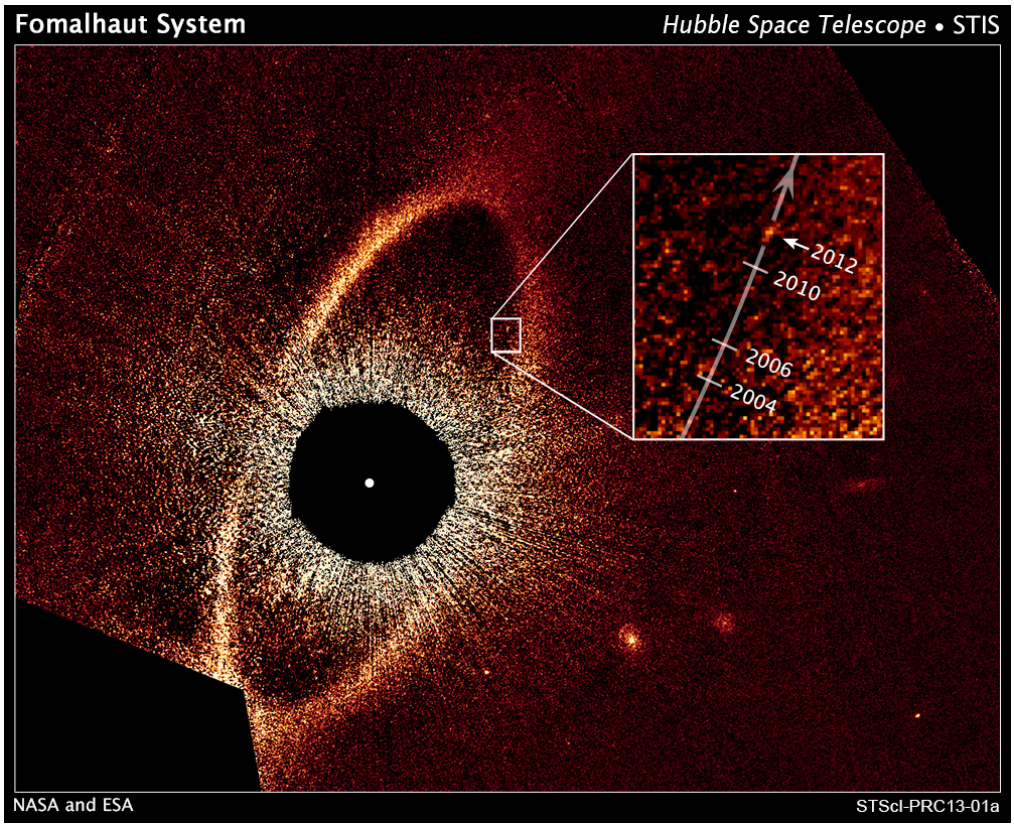

Figure 1.3: Example of a directly imaged planet: Fomalhaut B, as seen by the Hubble Space Telescope. Image credit: NASA/ESA.

perature, metallicity of the host star) and chemical species present in its atmosphere.

Upcoming space-based telescopes will generally focus on low resolution transit/eclipse spectroscopy. This thesis presents work that has been done in preparation for these missions, which are likely to revolutionise the fields of planetary and exoplanetary science, and the models being used to simulate their performance will be described. The capabilities of these future facilities will then be demonstrated, highlighting the improvements in data quality and quantity, and the potential impact discussed. In fact, the quality of the exoplanet spectra from these missions is likely to be such that current data analysis techniques will be inadequate. Hence an approach to increase the complexity of our analysis, without implying certain physical regimes, is discussed. A key aim of much of the work presented here is to ensure the maximum scientific gain from upcoming facilities. Thus the final chapter focuses on efforts to increase the efficiency of these next generation telescopes including an outreach project working with students from high schools in London.

Chapter 2

Planetary and Exoplanetary Spacecraft

> ”With every passing hour, our solar system comes forty-three thousand miles closer to globular cluster M13 in the constellation Hercules, and still there are some misfits who continue to insist that there is no such thing as progress”
>
> Kurt Vonnegut, The Sirens of Titan

Over the last 60 years, a wide variety of satellites have been launched for scientific research and spacecraft studies have characterised bodies ranging from 10 m asteroids in our Solar System to planets orbiting other stars. Here I will present a brief overview of the key planetary and exoplanetary spacecraft launched to date, and some notable achievements in each field, before discussing future missions, excluding those studied ind epth in this work which are described in Chapter 3.

2.1 Fly-by and In-situ Missions

In December 1962 the Mariner 2 spacecraft performed a fly-by of Venus, becoming the first successful mission to closely study another planet, passing just 34,773 km from the surface. Despite issues with attitude control and solar panel output during

the cruise phase, Mariner 2 provided several key scientific discoveries, including confirming a slow retrograde rotation rate for Venus, measuring a predominantly carbon dioxide atmosphere and finding no detectable magnetic field. The spacecraft also showed that the solar wind streams continuously through interplanetary space and allowed for the value of the astronomical unit to be refined [27]. Since Mariner 2, spacecraft have visited every planet within our Solar System as well as many other small bodies. Of particular note are the Pioneer 10 and 11, Verena 7, the Voyager Probes, the Viking Landers, Galileo, Cassini (and Cassini-Huygens) and New Horizons to name a few. These missions have often revolutionised our understanding of these fascinating places, delivering stunning images of surface features and a multitude of new discoveries.

Additionally spacecraft have massively contributed to our knowledge of the primordial bodies of our Solar System. Fly-by and rendezvous missions have provided in-situ observations of a handful of small bodies in extraordinary detail while sample return missions can offer unparalleled opportunities for studying the composition of the target bodies.

In 2014 Rosetta became the first spacecraft to rendezvous with, and orbit, a comet. Over the next two years Rosetta performed a detailed study of comet 67P/ChuryumovGerasimenko (67P) and deployed a lander, Philae, to perform in-situ science on the comet's surface [28]. Although hints of water-ice were detected within active regions of the comet, the surface was generally found to be dehydrated with some evidence for carbon-bearing compounds [29]. While the Rosetta mission, along with other studies, excludes comets as being the source of the bulk terrestrial water due to their generally high D/H ratio, they may have been responsible for delivering significant amount of organics [30].

The Origins, Spectral Interpretation, Resource Identification, Security, Regolith Explorer (OSIRIS-REx) arrived at Bennu, a carbonaceous asteroid whose regolith may record the earliest history of our solar system, in December 2018. The NASA mission aims to retrieve 60 grams of material from the asteroid and return it to Earth by late 2023. The sample should enable a greater understanding of the

formation and evolution of the Solar System and potentially provide hints about the source of organic compounds that led to the development of life on Earth [31].

2.2 Remote-sensing Missions

In 1946 – more than a decade before the launch of Sputnik – Lyman Spitzer proposed the development of a large, space-based observatory that would not be hindered by Earth's atmospheric distortion and span a broad range of wavelengths [32]. Since this ground-breaking concept was conceived, numerous space-based telescopes have been launched for a diverse array of scientific research. Highlighted here are those that have been at the forefront of discovery in planetary and exoplanetary science in the last decade.

2.2.1 AKARI

AKARI was an infrared astronomy satellite which was developed by the Japanese Aerospace eXploration Agency (JAXA) and launched in 2006 [33]. Over its 6 year life, AKARI surveyed 96% of the sky and contributed to a wide range of infrared astronomy, including galaxy evolution, stellar formation and evolution, interstellar media, and Solar System objects. AKARI's infrared camera (IRC) operated from 1.8 - 26.5 μm [34] and was used for several asteroid surveys. These included a catalogue of albedos and sizes for over 5000 asteroids with measurements in two mid-infrared bands (9 and 18 μm) during the cryogenic phase of the mission [2]. Additionally a spectroscopic survey of tens of asteroids was conducted over 2.5 - 5 μm using the grism of the near-infrared channel of the IRC [35].

2.2.2 WISE/NEOWISE

The Wide Infrared Survey Explorer (WISE) is a medium-class space telescope, launched in 2009, which acquired infrared images of the entire sky over four bands centred on the wavelengths 3.4, 4.6, 12, and 22 μm [36]. During the main mission, NEOWISE (Near-Earth Object WISE), the asteroid hunting section of the project, detected and reported diameters and albedos for $>$158,000 asteroids, including $\sim$700 Near-Earth objects (NEOs, [37]). After the end of the cold mission and several years of hibernation, the spacecraft was reactivated in September 2013,

exculsively for asteroid science [38]. NEOWISE has since detected several hundred more NEOs and thousands of Main Belt Asteroids using the 3.4 and 4.6 μm bands, providing albedos and diameters for these newly discovered objects [39, 40, 41].

2.2.3 Hubble

Launched in 1990, the Hubble Space Telescope (HST) fulfilled the lofty vision of Lyman Spitzer with instrumentation covering the UV, visible and near infrared. With a 2.4 m diameter mirror, HST has provided extraordinary data over a vast range of scientific disciplines. Hubble's Space Telescope Imaging Spectrograph (STIS) has three detectors, each with a different field of view and spectral range, and the most widely used for planetary, and exoplanetary, science has a 52x52 arcsecond field of view, covering the visible and near-infrared spectrum from 0.2 - 1.03 μm. STIS has observed water vapour above the polar regions of Europa, one of Jupiter's icy moons, providing the first circumstantial evidence of water plumes erupting off the moon's surface [42]. STIS spectra of the exoplanet HD 209458 b facilitated the first detection of the planet's atmosphere, allowing for the identification of several atmospheric constituents, including hydrogen, oxygen and sodium [43], and has since been extensively used for atmospheric characterisation [e.g. 44, 45, 46].

The Hubble Wide Field Camera 3 (WFC3) consists of two channels, UVIS and IR, which cover 0.2 - 1.0 μm and 0.8 - 1.7 μm respectively with a variety of filters available for each. In the field of small bodies, WFC3, in particular the UVIS channel, has been utilised for the characterisation of comet nuclei and coma [e.g. 47, 48] and these studies have included the discovery of a binary main-belt comet [49] and the observation of an increase in activity due to a comet-asteroid impact [50].

WFC3 has also delivered spectroscopic data of exoplanets, with tens of planets being studied through transmission spectroscopy [e.g. 15, 16, 51] and several more have been characterised via eclipse measurements [e.g. 52, 53, 54]. One of the most remarkable findings in the exoplanet field was recently announced when, through the use of Hubble data, the atmosphere of K2-18 b, a 2.24 $R_{\oplus}$ planet orbiting in the habitable zone of its star, was discovered to contain water vapour [18].

Although WFC3 has been an outstanding facility for detecting water in exoplanet atmospheres, it was not designed for observations of this type and its narrow wavelength coverage leads to degeneracies in the retrieved atmospheric solutions. Analysis of data from Hubble is discussed in Chapter 6 along with the limitations of these spectra.

2.2.4 Spitzer

The Spitzer Space Telescope (SST) is, along with Hubble, part of NASAs Great Observatories Program. Launched in 2003, Spitzer carries an Infrared Array Camera (IRAC), an Infrared Spectrograph (IRS) and a Multiband Imaging Photometer (MIPS). The IRS was split over four sub-modules with operational wavelengths of 5.3 - 40 μm ([55]) and has not been operational since Spitzer's helium coolant was depleted in 2009. Since the cool phase of Spitzer's mission ended, only the IRAC has remained operational though with reduced capabilities. Spitzer has been used extensively for studying small bodies (e.g. [56, 57, 58, 59]) including the Explore-NEOs program [60] which was a 500 hour survey to determine the albedos and diameters for nearly 600 NEOs during the warm mission phase. The CO and CO_2 emission of comets has also been observed with Spitzer [61].

Additionally, Spitzer has been a key facility for exoplanet observations via transit and eclipse spectroscopy (e.g. [62, 63]) and phase curves (e.g. [64, 65]). Although the data is not collected simultaneously, Spitzer data has often been combined with observations from STIS and WFC3 to give an extended wavelength coverage [e.g. 3, 66]. Spitzer observations have also been utilised to find and characterise earth-sized planets within the TRAPPIST-1 system [e.g. 67, 68, 69]. Finally, the refinement of exoplanet ephemerides, the knowledge of their orbits and thus the time of the next transit, has also been performed with Spitzer for targets which are amenable to atmospheric characterisation with upcoming facilities [e.g. 70, 71, 72]. Spitzer was launched into an Earth trailing orbit and the line-of-sight between Earth and the spacecraft is now close to the Sun which has reduced the communications bandwidth. Due to this, and the lack of the cryogenic capability, Spitzer has not been granted a funding extension and thus will cease operations in January 2020.

2.2.5 CoRoT

The Convection, Rotation and planetary Transits (CoRoT) satellite was launched in 2006 with the objectives of studying asteroseismology and finding short-period, transiting exoplanets [73]. Over the course of the seven year mission, 32 exoplanets were confirmed along with several hundred candidates. Notable achievements include the first optical measurement of a secondary eclipse (CoRoT-1 b, [74]) and the first confirmed rocky exoplanet (CoRoT-7 b, [75]). CoRoT was the first spacecraft dedicated to the detection of transiting extrasolar planets, paving the way for facilities such as Kepler and TESS.

2.2.6 Kepler

The scientific objective of the Kepler Mission was to explore the structure and diversity of planetary systems. To do this, the mission surveyed over half a million stars during its nine year life. The science aims of Kepler included determining the percentage of terrestrial and larger planets that are in, or near, the habitable zone of a wide variety of stars [76]. The Kepler mission provided an excellent means of understanding the occurence of planets within our galaxy. Although the transit technique is naturally biased towards large planets in short periods, knowledge of this selection bias can be used to understand the planetary population that is required to match the detections. Perhaps the most serendipitous finding of the mission is the abundance planets with radii between that of Earth and Neptune (1.0-3.9 $R_{\oplus}$) as our Solar System has no example of these intermediate planets, yet they are by far the most common in the Kepler sample (e.g. [77, 7, 9, 78]. In late 2011, the Kepler team announced the discovery of the first Earth-sized planets orbiting a Sun-like star in the Kepler-20 system [79].

After the failure of two reaction wheels, the primary mission of Kepler ended in May 2013 as the spacecraft was unable to achieve accurate pointing. However, an ingenious solution, using the photon pressure of the sun, allowed the spacecraft to point at fields close to the ecliptic plane for periods of around 83 days and achieve a photmetric precision of 400 ppm [80]. The extended mission, known as K2, lasted until October 2018 when the spacecraft's fuel was finally depleted. K2 compounded

the success of the initial Kepler survey and led to numerous discoveries including nearly 400 confirmed exoplanets, using optical phase curves to confirm planet candidates and, as with the primary mission, had significant engagment with citizen scientists who confirmed many planets and planet candidates [e.g. 81].

To date, over 2700 planets have been confirmed using data from the Kepler mission, accounting for roughly 87% of the transiting exoplanets detections thus far. The abundance of Kepler data has allowed for studies into exoplanet demographics which have resulted in findings such as the "Fulton Gap", a factor of 2 deficit in the occurrence rate distribution at 1.5 -2.0 $R_\oplus$ [82], which had previously been predicted due to photoevaporation (e.g. [83]).

2.2.7 TESS

The Transiting Exoplanet Survey Satellite (TESS, [84]) launched in April 2018 and is anticipated to detect over 4500 planets around bright stars and more than 10,000 giant planets around fainter stars during its two year primary mission [4]. Of these, several hundred are expected to be Earth-sized and super-Earth-sized planets and an extensive ground-based program aims to measure masses for many of these. Using four wide-field cameras, TESS will survey at least 200,000 main-sequence stars over almost the entire sky with observational periods of between 1 month and 1 year. TESS aims to detect a rich catalogue of planets which are amenable for atmospheric characterisation by finding planets around stars which are 30-100 times brighter than those surveyed with Kepler/K2. Already, over 1000 TESS candidates have been found and tens of planets have been confirmed [e.g. 85, 86]. The mission was recently funded for a two year extension which will see the spacecraft survey the ecliptic as well as re-observing portions of the sky covered in the primary mission.

2.3 Future Missions

In the context of remote-sensing, the only currently available space-based facilities are Hubble and Spitzer. Thus, at the time of writing, no space telescope capable of infrared spectroscopy beyond 1.7μm is operational. This has limited progress in the fields of asteroids, comets and exoplanets. However, many missions have been

proposed or are currently in development.

2.3.1 Proposed Small Bodies Missions

Several mission concepts have been studied and submitted to calls by ESA and NASA. Medium class proposals to ESA include CASTAway which aims to explore the main asteroid belt with a telescopic survey of over 10,000 objects, targeted close encounters of 10 - 20 asteroids and serendipitous searches to constrain the distribution of smaller objects (<10m, [87]). CASTAway's proposed payload consists of a 50 cm diameter telescope with a spectrometer covering 0.6 - 5 μm (R = 30-100), a thermal imager (6 - 16 μm) for use during flybys, a visible context imager and modified star tracker cameras to detect small asteroids. Spectral features related to hydroxyl (OH), water (ice and gas), and hydrated silicates, are either partially or fully obscured in Earth-based observations due to Earth's water-rich atmosphere and the 2.5 - 3 μm region is especially prohibitive. CASTAway is designed to be able to detect such features.

Main Belt Comets are objects in stable asteroid-like orbits which lie within the snow line but exhibit comet-like activity [88, 89] and 18 such active bodies are currently-known. Castalia is a proposed ESA mission to rendezvous with the Main Belt Comet 133P/Elst-Pizaroo to perform the first characterisation of this intriguing population, making the first in-situ measurements of the water in the asteroid belt and measuring isotope ratios as well as plasma and dust properties [90].

Although CASTAway and Castalia were not implemented by ESA, a new small bodies mission, Comet Interceptor [91], has been accepted for ESA's F Class call. The mission aims to encounter a dynamically new comet (i.e. one that is entering the inner Solar System for the first time) as well as making solar wind measurements. The rendezvous target is likely be a long period comet discovered by the Large Synoptic Survey Telescope (LSST) and characterisation of this pristine object will be achieved with a compact, agile set of spacecraft. Although they are far rarer than long-period comets, Comet Interceptor may also have the capability of encountering an interstellar object passing through our Solar System. Comet Interceptor will launch with Ariel in 2028.

NEOCam is a proposed NASA Discovery class mission and is currently funded for an extend Phase A study. Launching to the Sun-Earth L1 Lagrange point, NEOCam will detect and characterise NEOs with a particular focus on those that could potentially impact Earth (i.e potential hazardous asteroids, PHAs) and will build on the work from NEOWISE. NEOCam's primary science objectives are: (i) assess the present-day risk of near-Earth object (NEO) impacts, (ii) study the origin and ultimate fate of asteroids, (iii) find suitable NEO targets for future exploration by robots and humans. To facilitate this, NEOCam consists of a 50 cm telescope operating at two photometric channels which are dominated by NEO thermal emission, 4.2 - 5.0 μm and 6 - 10 μm, in order to better constrain the objects' temperatures and diameters. NEOCam's field of view is significantly larger than that of NEOWISE, allowing the mission to discover tens of thousands of new NEOs with sizes as small as 30 - 50 m in diameter [92].

Upcoming all-sky surveys also offer potential for the characterisation of small bodies. These include Euclid, a mission to map the geometry of dark matter in the Universe, which is expected to provide spectra for $\sim$100,000 asteroids from 0.5 - 2 μm [93]. Selected earlier this year, Spectro-Photometer for the History of the Universe, Epoch of Reionization and ices Explorer (SPHEREx), is a NASA medium-class explorer mission due for launch in 2023. SPHEREx will observe the whole sky over the spectral range 0.75-5 μm at low resolution (R$\sim$35-140) and is expected to provide spectra of tens of thousands of asteroids [94].

2.3.2 CHEOPS

The CHaracterising ExOPlanet Satellite (CHEOPS) is dedicated to searching for exoplanetary transits by performing ultrahigh precision photometry on bright stars already known to host planets [95]. CHEOPS is ESA's first S-Class mission and is expected to launch in December 2019. With a 32 cm aperture, CHEOPS aims to accurately measure the radii of exoplanets for which ground-based spectroscopic surveys have already provided mass estimates [96]. The majority of the targets studied by CHEOPS will be those found by TESS but ground-based facilities such as the Next Generation Transit Survey (NGTS, [97]) will also provide suitable plan-

ets. By probing the mass-radius relation for small planets, strict constraints can be placed upon the density which can be used to approximate their composition and suggest whether they are rocky or gaseous. Additionally, CHEOPS will study the energy transport from the day side to the night side of exoplanets and provide targets for future ground and space-based facilities which have spectroscopy capabilities to allow for atmospheric characterisation.

2.3.3 PLATO

The PLAnterary Transits and Oscillation of stars (PLATO) mission was selected in 2012 as ESA's third medium class mission. Scheduled for launch in 2026, PLATO will use 24 cameras with an instantaneous sky coverage of 2232 square degrees to discover exoplanets around bright nearby stars [98]. The final mission strategy has not yet been selected but is likely to included a long stare of at least two years at the same area of sky. This should allow for the detection of a number of small, rocky planets within the habitable zone around sun-like stars. PLATO data products will also allow for the seismic analysis of stars to determine their mass with an accuracy of 1% [99]. This in turn will place tight constraints on the age of the system, improving our understanding of planetary and stellar evolution.

2.3.4 WFIRST

In 2010, the Wide Field InfraRed Survey Telescope (WFIRST) was selected as the top priority for the next decade of astronomy in the decadal survey undertaken by the United States National Research Council. After further study, WFIRST was approved in 2016 for development and launch. While the primary focus of WFIRST is on probing the expansion history of the Universe and precisely measuring the effects of dark energy, it is also envisioned that the instrumentation will be suitable for finding and characterising exoplanets [100, 101]. WFIRST intends to achieve this through two methods: microlensing and direct imaging. The planets discovered via this methods will probe different parameter spaces to those detected via the transit or radial velocity techniques, providing complementary statistics on planet occurrence rates [102, 103].

WFIRST has been slated for launch in the mid-2020s but, largely due to cost and schedule overruns of the James Webb Space Telescope, has recently received reduced funding and has twice been proposed for cancellation, including in the FY20 budget. Thus, the future of WFIRST is, unfortunately, uncertain.

2.3.5 EXCITE

Although not technically a space-based facility, the EXoplanet Climate Infrared TElescope (EXCITE) also cannot be labelled as a ground-based observatory. EXCITE is a proposed high altitude balloon dedicated to obtaining phase curves of exoplanets via an infrared spectrograph covering 1-4 μm at R$\sim$50 [104]. At balloon altitudes (40 km), Earth's atmosphere is stable and nearly transparent. Hence a balloon can observe from a space-like environment at a small fraction of the cost. EXCITE would launch from, or close to, Antarctica, meaning many targets would not set and thus short period planets could be observed for the entirety of their orbit. For bright targets, EXCITE could deliver sensitivities similar to Hubble WFC3 though crucially, over a wider spectral range.

2.3.6 Missions Beyond 2030

NASA is currently considering four large mission concepts for operation in the late 2030s. Of these, three offer the potential for contributions to exoplanet science.

The Large UltraViolet Optical and InfraRed surveyor (LUVOIR) will be a general purpose observatory with time allocated via peer review in line with HST, Spitzer and JWST. As the name suggests, LUVOIR with be capable of performing observations from the ultraviolet to the infrared (0.1 - 2.5 μm) with imaging and spectroscopic instruments. While it is envisioned that its instruments could be used to study anything from plumes of water on Enceladus to cosmic origins studies of the early universe, a key scientific aim for LUVOIR is a census of Earth-like exoplanets. The mission intends to find and study at least 28 habitable planet candidates, and to discover at least 1 Earth-like planet orbiting an FGK star (at 95% confidence), assuming an occurrence rate of habitable conditions of 10%[1].

[1] https://asd.gsfc.nasa.gov/luvoir/resources/docs/LUVOIR_FinalReport_2019-08-26.pdf

Based on heritage from Spitzer, the Origins Space Telescope's scientific objectives, with regards to exoplanets, are understanding how the conditions for habitability develop during planetary formation and whether planets orbiting M-dwarfs support life[2]. These goals will be pursued via a 5.9 m diameter mirror, cooled to 4.9 K, and instrumentation providing spectroscopy from 2.8 - 588 μm. Over its lifetime, it is thought Origins should be able to study the atmospheres of at least 28 temperate, terrestrial worlds orbiting M and K-dwarfs, distinguishing between tenuous, clear and cloudy gaseous envelopes.

The Habitable Exoplanet observatory (HabEx) aims to directly image exoplanetary systems via the use of a starshade which will obscure the light from the host star, increasing the contrast ratio and revealing the planet. With this technology, HabEx intents to image and characterise habitable exoplanets, searching their atmospheres for signs of water and other biosignature gases, including oxygen and ozone[3]. HabEx's instrumention covers from the UV to near-infrared (0.115 - 1.8 μm) and, as with all the missions considered for the 2020 decadal survey, has extensive capabilities for many other areas of astrophysics including galactic and Solar System science.

The final competitor for the next great observatory is Lynx, a X-Ray telescope with a 2 m^2 effective area, allowing it to unveil stellar and galactic evolution as well as probe the dawn of black holes[4]. While there is no guarantee that the decadal committee will select one these missions, it is likely that the highest priority flagship mission will have a design similar to one of them.

[2] https://asd.gsfc.nasa.gov/firs/docs/OriginsVolume1MissionConceptStudyReport.pdf
[3] https://www.jpl.nasa.gov/habex/pdf/HabEx-Final-Report-Public-Release.pdf
[4] https://wwwastro.msfc.nasa.gov/lynx/docs/LynxConceptStudy.pdf

Figure 2.1: Tubes in Space: A collage of space-based telescopes. Left to right, top to bottom: AKARI, WISE, Hubble, Spitzer, CoRoT, Kepler, TESS, CHEOPS, Euclid, JWST, SPHEREx, Twinkle, NEOCam, WFIRST, PLATO, Ariel, LUVOIR, HabEx, Origins and Lynx. (Not to scale).

Chapter 3

Spacecraft Studied Here

> ”You talk as if a god had made the Machine,” cried the other. ”I believe that you pray to it when you are unhappy. Men made it, do not forget that. Great men, but men. The Machine is much, but not everything.”
>
> E.M. Forster, The Machine Stops

Space-based observatories are generally equipped with highly specialised instrumentation that allows for cutting-edge science to be achieved. Facilities are often publicised as revolutionary, with the capabilities described as if they mirror perfection in the minds of those who have built them and will use them. While such endeavours are the culmination of years of intense study and undoubtedly offer new and exciting opportunities to acquire data, each has its limits. Diversity is required; instruments probing different spectral regions, and with differing sensitivity and resolution, must be built so that a vast array of scientific projects can be undertaken. With many observatories operating simultaneously, it is key to understand the niche of each to allow for all facilities to be used effectively and efficiently. In this thesis, the performance of three upcoming space missions is studied and an overview of these, listed in order of their anticipated launch date, is given here.

3.1 JWST

The James Webb Space Telescope (JWST) is currently expected to be launched in March 2021. Often heralded as the successor to Hubble, JWST has been in development since the early 1990's and has been subject to a series of delays and cost overruns. JWST will be a general observatory and will cater to various science cases including a wide range of exoplanet targets [105, 106, 107] and Solar System science (e.g. [108, 109, 110]). Although a good fraction of JWST observation time is expected to be allocated for exoplanet science (e.g. [111, 112]), for a space observatory of this scale, over-subscription is likely to be an issue and not all interesting science cases will necessarily require the sensitivity and accuracy of JWST. The mission will operate from the second Lagrangian point, L2, which provides a stable thermal and orbital environment. The facility will have instruments covering visible, near-infrared and mid-infrared wavelengths. The specifications of these, and the useful modes for planetary and exoplanetary science are outlined below.

3.1.1 NIRISS

The Near-InfraRed Imager and Slitless Spectrograph (NIRISS) is the Canadian contribution to JWST and, as with every instrument on the spacecraft, it has a number of different operating modes, each with a variety of science cases [113]. The single object slitless spectroscopy (SOSS) mode of NIRISS enables medium-resolution (R$\sim$700) spectroscopy at 0.6-2.8 μm, in three cross-dispersed orders for a single bright target. The SOSS mode is optimised to carry out time-series observations and thus is well-suited to observing transiting exoplanets, providing extremely high precision observations with excellent spectro-photometric stability [107]. This is achieved by defocusing the spectral orders in the cross-dispersion direction, allowing brighter objects to be observed without saturating the detector.

3.1.2 NIRSpec

The Near-Infrared Spectrograph (NIRSpec) aboard JWST is capable of low (R$\sim$100), medium (R$\sim$1000) and high (R$\sim$2700) resolution spectroscopy over the spectral band 0.6 - 5.3 μm [114]. NIRSpec has a variety of operating modes

including slit spectroscopy, with a 1.6" x 1.6" aperture (S1600A1) designed for exoplanet transit spectroscopy. Due to its wavelength coverage, spectral resolution and sensitivity, NIRSpec is expected to be a powerful tool for atmospheric characterisation [115].

3.1.3 NIRCam

The JWST Near-Infrared Camera (NIRCam) has two 2.2' x 2.2' fields of view that are capable of spectroscopic observations via two grisms which provide resolutions of R$\sim$1600 [116]. When providing time-series grism observations, NIRCam operates from 2.4-5.0 μm with a variety of filters available. Although NIRSpec is likely to be more widely used for transiting exoplanets, NIRCam also offers the potential for atmospheric characterisation [117].

3.1.4 MIRI

The Mid-Infrared Instrument (MIRI) provides coverage of 4.9 - 28.8 μm and will provide atmospheric characterisation of exoplanets through direct imaging [118]. For exoplanet transit (and eclipse) spectroscopy, the MIRI low resolution spectrometer (LRS) also offers a slitless spectroscopy mode [119]. MIRI offers access to wavelengths that are not covered by any current, or any upcoming, instruments for exoplanet science and thus facilities unique science cases such as the detection and characterisation of silicate clouds [120].

3.2 Twinkle

The Twinkle Space Mission is a new, fast-track satellite designed for launch in 2023. It has been conceived for providing faster access to spectroscopic data from exoplanet atmospheres and Solar System bodies, but it is also capable of providing spectra of bright brown dwarfs and stars. Twinkle is equipped with a visible (0.4 - 1 μm) and infrared (1.3 - 4.5 μm) spectrometer (split into two channels at 2.42 μm). The satellite has been designed to operate in a low Earth, Sun-synchronous orbit [121, 122].

Twinkle is a general observatory which is being managed by Blue Skies Space Ltd. (BSSL). Scientists will be able to purchase telescope time and Twinkle will

provide on-demand observations of a wide variety of targets within wavelength ranges that are currently not accessible using other space telescopes or accessible only to oversubscribed observatories in the short-term future.

Twinkle is currently entering a Phase B design review and thus the technical specifications, taken from the Phase A study, may change. Twinkle's scientific payload consists of a telescope with a 0.45 m aperture, a Fine Guidance Sensor (FGS) and both a Visible and Near-Infrared (NIR) spectrometer which can be operated simultaneously. The Exoplanet Light Visible Spectrometer (ELVIS) is a visible spectrometer channel which is based upon the Ultraviolet and Visible Spectrometer (UVIS) flown on the ExoMars Trace Gas Orbiter. For the Mars application, the UVIS instrument used a dual telescope configuration: nadir (downward viewing of the surface for total atmospheric column measurements) and solar occultation observations (looking at the Sun through the atmosphere from orbit to measure vertical profiles). The telescopes were connected to a single spectrometer via a fibre optic selector link. This telescope and selector system is not required in the Twinkle application as the spectrometer is positioned in the visible beam of the main Twinkle telescope.

The main modification to the spectrometer design is the use of an alternative grating and associated coatings to optimise the spectral range to the visible to near IR range between 0.4 - 1 μm with a resolving power of R$\sim$250 [121]. Other planned changes include a minor electronics component change on the detector board and relocation of the main electronics board stack to improve thermal isolation and allow the detector to run at a lower temperature. Changes to the firmware code within the electronics will optimise the operations (e.g. CCD readout modes) and integration times for the Twinkle application [121]. This instrument is referred to as Channel 0 (Ch0). For the Phase A study, an e2v CCD-230-42 detector was assumed for the visible channel but this is currently under further discussion.

The design of Twinkle's near infrared (NIR) spectrometer is detailed in Wells (2016) [123]. The NIR spectrometer will split the light into two channels (1.3 - 2.42 μm and 2.42 - 4.5 μm) to provide broadband coverage while also ensuring

appreciable spectral resolution. For shorter wavelengths (λ <2.42 μm), the NIR spectrometer will have a resolving power of 250 while for longer wavelengths (λ >2.42 μm) this will be reduced to 60 [123]. These are referred to as Channels 1 and 2 (Ch1, Ch2) respectively and the spectrometer delivers a diffraction-limited image over both channels. In the instrument design, a set of coupling lenslets is adopted to create an image of the aperture on the detectors. These lenses produce several spectra on the detector, with the spectrum from the star slit in the centre with three spectra from the background slits on either side [123]. The two channels use different halves of the same detector (assumed to be produced by Selex in the Phase A study). Due to this layout, the two IR channels (Ch1 & Ch2) must be read out simultaneously whilst the visible instrument (Ch0) can be read out independently. This current design features a spectral gap at 1 - 1.3 μm and the instrumentation is summarised in Table 3.1.

Instrument Name	Wavelength Range [μm]	Resolution
Ch0	0.4 - 1.0	250
Ch1	1.3 - 2.42	250
Ch2	2.42 - 4.5	60

Table 3.1: Wavelength ranges and spectral resolutions of Twinkle's instrumentation.

The satellite will be placed in a low Earth (600-700 km), Sun-synchronous (dawn-dusk) polar orbit with a period of 90-100 minutes. The orientation of the satellite's orbit is constant with respect to the Sun but dictates that Twinkle's instrumentation may have to be re-targeted during an orbit to avoid Earth's limb. The boresight of the telescope will be pointed within a cone with a radius of 40° which is centred on the anti-sun vector (i.e. the ecliptic). The field of regard could potentially be expanded to ±60° from the ecliptic for non-demanding targets.

3.3 Ariel

Further into the future, the Ariel space mission will conduct a population survey of the atmospheres of ∼1000 transiting exoplanets over a wide wavelength range (0.5 - 7.8 μm) followed by a detailed study of a number of selected planets [124]. Ariel, ESA's M4 mission, aims to deliver a comprehensive catalogue of planetary spec-

tra, which will yield molecular abundances, chemical gradients and atmospheric structures [125, 126]. Ariel is expected to be launched in 2028.

Ariel's telescope is an off-axis 0.6 m^2 Cassegrain with an elliptical primary mirror, that is cooled to less than 70 K. The flux collected by the primary aperture feeds two separated instrument modules. A dichroic mirror splits the flux into two beams at 1.95 μm. The first beam is directed to an instrument module containing three photometers (VISPhot, 0.5 - 0.6 μm; FGS-1, 0.6 - 0.80 μm; FGS-2, 0.80 -1.1 μm) and a slitless spectrometer (NIRSpec, 1.1 - 1.95 μm) with spectral resolving power, R $\sim$ 20. The two photometers, FGS-1 and FGS-2, operate as Fine Guidance Sensors (FGS), providing both scientific photometric data and pointing information for the attitude and orbital control system (AOCS). The second instrument module, fed by the beam with wavelengths longer than 1.95μm, hosts the Ariel Infrared Spectrometer (AIRS), which consists of two channels covering the 1.95 - 3.9 μm and 3.9 - 7.8 μm band with a spectral resolving powers of R$\sim$ 100 and R$\sim$ 30 respectively. A summary of Ariel's instrumentation is given in Table 3.2. For more detail on the Ariel design see [125, 127].

Instrument Name	Wavelength Range [μm]	Resolution
VISPhot	0.5 - 0.6	
FGS 1	0.6 - 0.81	Photometric Bands
FGS 2	0.81 - 1.1	
NIRSpec	1.1 - 1.95	20
AIRS Ch0	1.95 - 3.9	100
AIRS Ch1	3.9 - 7.8	30

Table 3.2: Wavelength ranges and spectral resolutions of Ariel's instrumentation

Chapter 4

Planetary Science with Twinkle

> ”If you see a whole thing - it seems that it’s always beautiful. Planets, lives... But up close, a world’s all dirt and rocks.”
>
> Ursula K. Le Guin

Spectroscopic observations of Solar System bodies, particularly at visible and infrared wavelengths, allow the composition of the surfaces and atmospheres of these objects to be determined and hints of their formation and evolutionary processes to be gleaned. The highest level of detail is usually obtained via interplanetary missions but remote-sensing from Earth, or Earth orbit, also provides the opportunity to study a vast array of objects. Space-based observing avoids the issues of telluric contamination and is vital for studying hydration features in the Solar System and beyond. Herschel, Hubble and Spitzer have succeed in characterising many Solar System bodies [e.g. 47, 57, 128] and JWST is expected to contribute significantly to our understanding of our own planetary system due to the improvements in sensitivity and spatial resolution, as well as spectral resolution and coverage, that will be offered. Our own Solar System serves as a benchmark against

Contributions: This chapter is based upon a study which I led and has been published in a peer-reviewed journal (Edwards et al. 2019, Remote-sensing Characterisation of Major Solar System Bodies with the Twinkle Space Telescope, JATIS, doi: 10.1117/1.JATIS.5.1.014006.). Giorgio Savini, Giovanna Tinetti and Marcell Tessenyi also contributed significantly to this work.

which all other planetary systems are compared, and the insights gained into the physical processes governing the formation and evolution of our own system are by extension also relevant to the field of exoplanet science.

While the MIRI instrument would be quickly saturated, studies of Mars with NIRSpec could include the monitoring of gases, aerosols and dust in the Martian atmosphere over the entire disk [1]. However, due to the brightness of Mars, only observations beyond 2.5 μm would be possible, as shown in Figure 4.1, though the potentially measurable atmospheric signatures still include CO and H_2O.

Studies of the dynamical processes and molecular compositions of the gas giants of our system offer insight into the behaviour of large extra-solar planets and JWST could complement and enhance observations made in previous decades by Galileo, Cassini, Juno and New Horizons. Our understanding of the atmospheres of giant planets is determined by our knowledge of the relationships between heat transport, atmospheric dynamics, and chemical processes. JWST may be able to study the relationship between atmospheric chemistry and dynamics by exploring disequilibrium species such as phosphine (PH_3) and arsine (AsH_3), including the spatial variations of these moelcules [1]. Saturation will again be an issue but, by selecting the appropriate filter and fast readout speed, observations of Jupiter and Saturn should be achievable with NIRCam, NIRSpec and MIRI. The spectra of these planets in the wavelengths covered by these instruments is dominated by methane absorption which appears as dark features. Hence, any reflective aerosols seen are located high in the atmospheres, above the majority of the methane. This probing of the upper troposphere, or lower stratosphere, provides information on the variation of atmospheric properties, such as wind speed, as a function of altitude [1]. For NIRCam observations, bright targets may have to strandle all four of the subarrays as shown in Figure 4.2.

Uranus and Neptune are, due to their distance from Earth, challenging to characterise and until the era of space-based telescopes and ground-based adaptive optics, individual features could not be spatial resolved. Substantial improvements over existing capabilities are expected with JWST, particularly due to the spatial

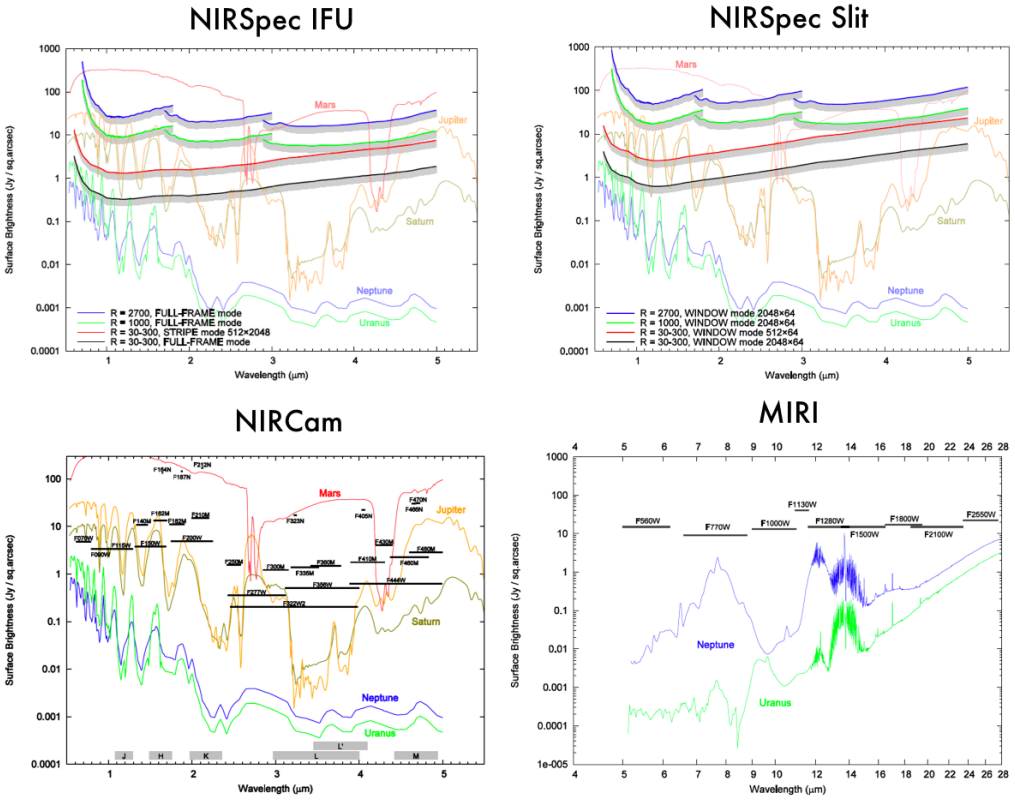

Figure 4.1: Saturation limits for NIRSpec (in integral field unit (IFU) and slit modes), NIRCam and MIRI plotted over the spectra of the outer Solar System planets. Figure adapted from [1].

resolution. Observations of these planets with the facility could lead to assessments of cloud layers and hydrocarbon distribution, with repeated observations offering the possibility of detecting temporal variations. Studies with MIRI of Uranus and Neptune would probe the thermal structure of the planets, with emission features due to CH_4 and other hydrocarbons likely to be detectable, and providing valuable data sets on photochemical processes in these ice giants. The angular size of the outer gas giants with respect to the fields of view of several MIRI IFUs is shown in Figure 4.2.

Additionally JWST will offer excellent opportunities for studying the moons of the Solar System. Of particular interest are icy moons, such as Europa and Enceladus, where water plumes erupting off the moon's surface may be detectable and Titan, the only moon with an atmosphere.

This chapter considers the possibility of using a small satellite in a low Earth

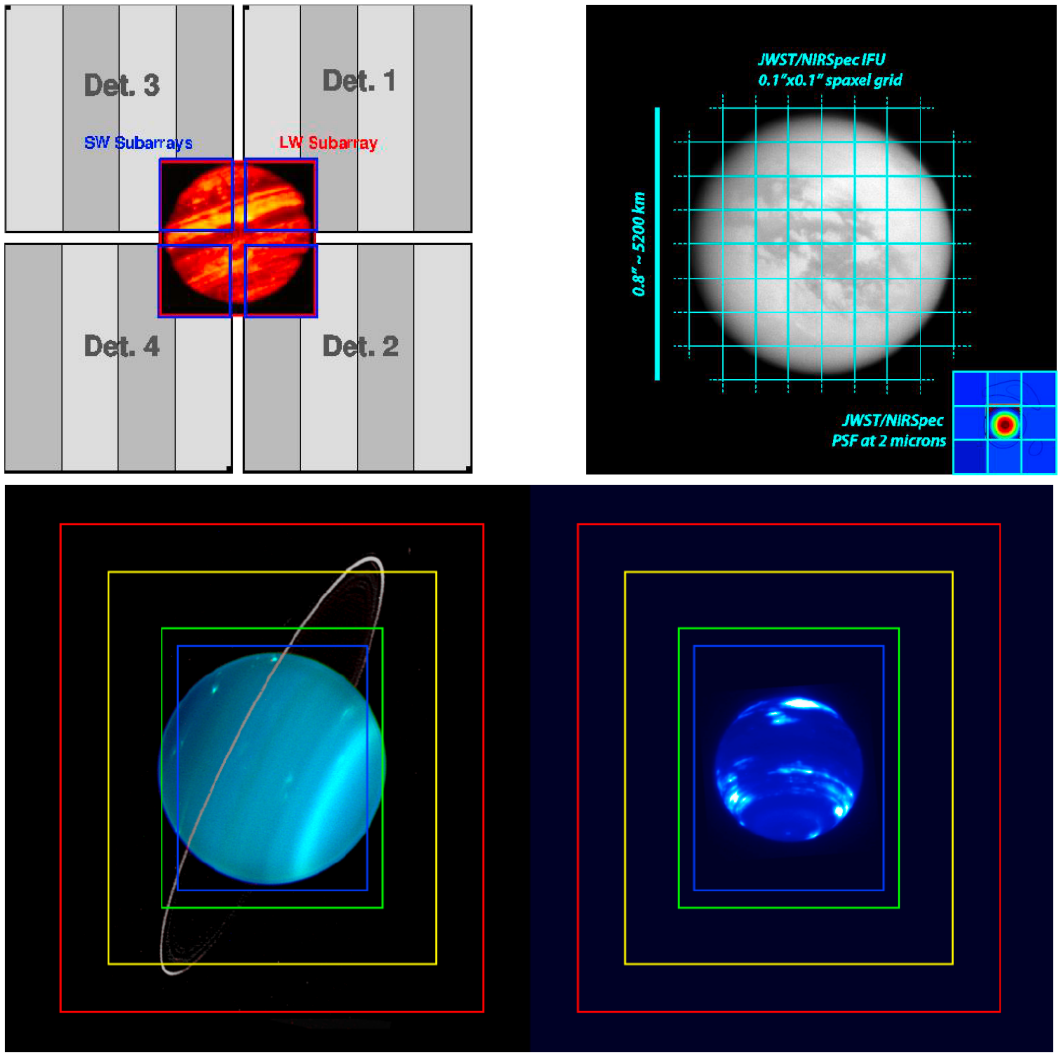

Figure 4.2: Proposed observation strategies for observing Jupiter with NIRCam (top left), Titan with NIRSpec (top right) and Uranus (bottom left) and Neptune (bottom right) with different MIRI IFUs. All figures taken from [1].

orbit, Twinkle, to perform spectroscopic remote sensing observations of major Solar System objects. Such a facility could provide observations of targets which are too bright to be observed JWST, complementing the latter facilities capabilities. Firstly, the timescales over which major objects, such as planets, dwarf planets and major asteroids, will be observable is assessed. This analysis is then extended to planetary moons which potentially incur an additional observational constraint.

Having established a potential schedule for observing targets, the ability of Twinkle to obtain scientific data is evaluated. The sensitivity and saturation limits of each of Twinkle's spectrometers is calculated for a given signal to noise ratio

(SNR) and compared to the photon flux from a selection of Solar System bodies. The effect of combining multiple observations is also explored.

4.1 Target Availability

Twinkle has a design life of seven years but, with no expendables, has the potential to operate for far longer. A precise launch date for the mission is still under discussion: for the purpose of this work a 'first light' date of 1st January 2022 was chosen and the following analysis was completed with a mission end date of 1st January 2032. Due to the periodicity of observation windows for Solar System objects, the launch date has little effect on the availability of most targets.

Twinkle's field of regard is centred on the anti-sun vector and the time period in which targets can be viewed is limited. When considering the observations of celestial bodies, it is therefore key to determine how Twinkle's field of regard varies over time and when, and for how long, targets will be within this field.

Figure 4.3 shows the variation in the declination of the centre of Twinkle's field of regard with right ascension. Note that, due to its sun-synchronous orbit, the right ascension of the centre of Twinkle's field of regard varies by 360° over the period of a year and that the declination variation is sinusoidal over the same period. The white circles indicate the extent of the telescope's field of regard at a given point. The centre of the field of regard is located on the ecliptic at all times.

A model has been created to calculate Twinkle's field of regard for any date. Therefore, if the celestial co-ordinates of an object for a given date are known, it can be deduced whether this lies within Twinkle's observable range. The future ephemerides of the planets and other celestial bodies can be predicted with high accuracy by the Jet Propulsion Laboratory's Horizons system[1]. By comparing these predicted values to those of Twinkle over the lifetime of the mission, it can be determined when each object will be within Twinkle's field of regard and for how long.

[1] https://ssd.jpl.nasa.gov/horizons.cgi

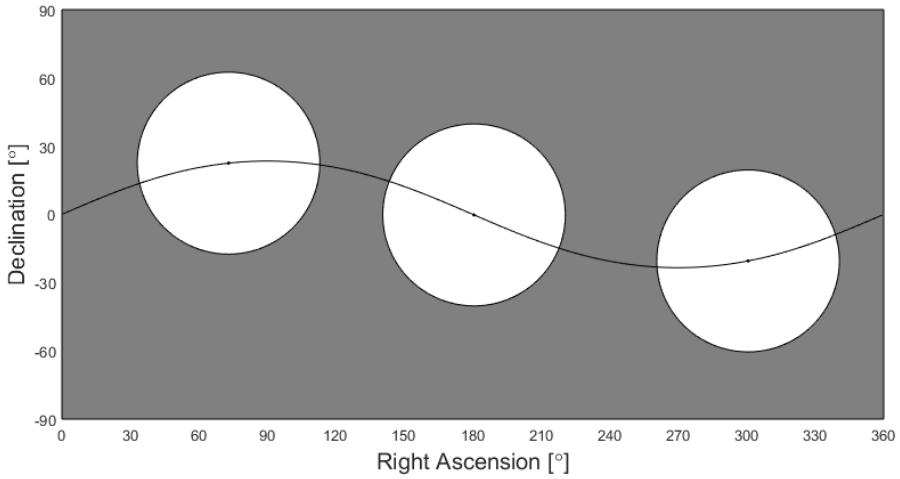

Figure 4.3: Variation in right ascension and declination of the centre of Twinkle's field of regard and indication of its extent at a given time.

4.1.1 Outer Planets

Figure 4.4 displays the observational periods for the outer planets over the period considered and shows that, generally, the further the planet is from Earth, the longer the time period for which it can be observed. The outer planets are also found to have regular observation windows. As Twinkle's field of regard is centred on the anti-sun vector, it will not be possible to observe the inner planets of the Solar System.

4.1.2 Moons

Observations of one set of potential targets within the Solar System, planetary moons, incur an additional constraint. The moon of interest could be obscured behind the planet or be transiting across the face of the planet. In the case of the moon being behind the planet obviously no spectral data can be obtained. When the moon is transiting across the planet, observations are likely to be subject to contamination by emission from the planet. Therefore, for two segments of its orbit, a moon cannot be observed by Twinkle. The percentage of time for which a moon is viewable can be determined by calculating the time spent in front of, or behind, the host planet.

Figure 4.5 displays the orbit of Phobos and Triton over a period during which

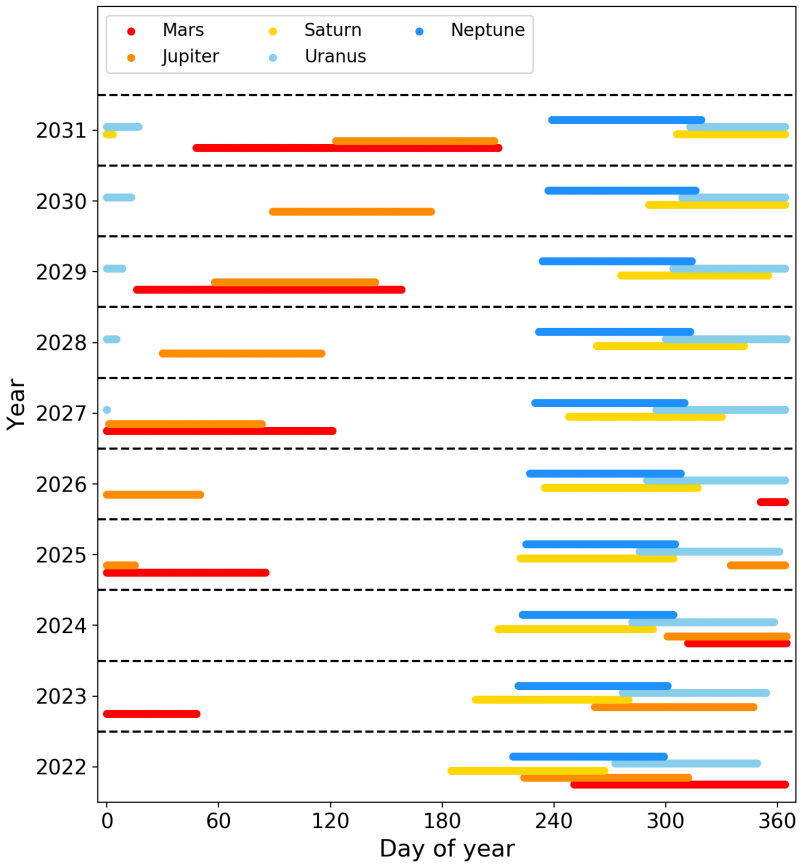

Figure 4.4: Periods for which the outer planets lie within Twinkle's field of regard from 1st January 2022 to 1st January 2032. Due to Mars' close proximity to Earth and Twinkle's field of regard, Mars is only observable every other year.

Mars and Neptune lie within Twinkle's field of regard. It should be noted that difficulties may be encountered if observations are performed when the moon is close to the limb of its host planet due to stray light. As the angular size of planetary moons is generally small compared to the size of Twinkle's slits, a gap between a moon and the planet's limb is desirable to reduce this stray light. The appropriate size of this gap is likely to vary depending upon the target. Increasing the gap reduces the likelihood of the planet contributing to the spectra. However, requiring a large gap reduces the time for which a moon can be viewed.

If one wishes for separation between the edge of the slit and the planet, a gap

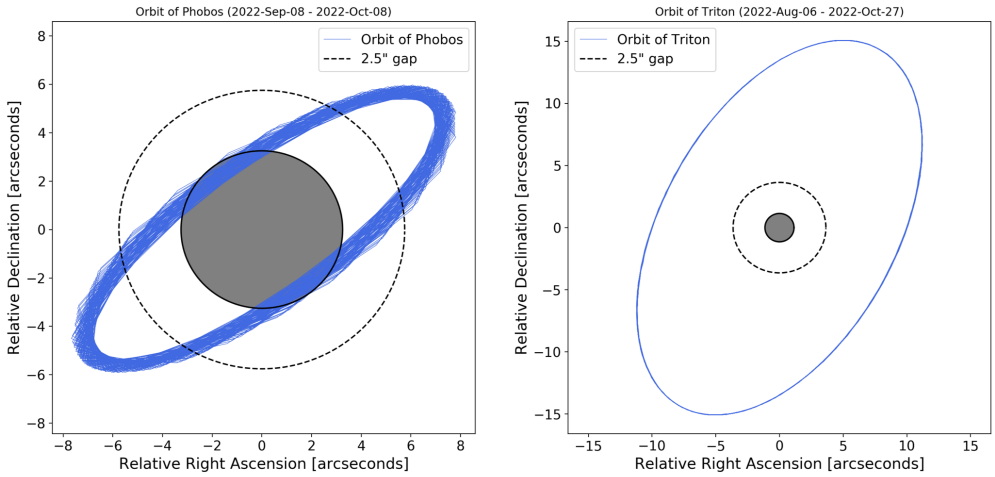

Figure 4.5: Left: Orbit of Phobos during some of the period for which Mars is within Twinkle's field of regard. Right: Orbit of Triton when Neptune is potentially viewable. The host planets are represented by the shaded central circles (to scale). Note the orbital period of Phobos and Triton are 7.38 hours and 5.88 days, respectively.

of 2.5 arcseconds could be considered minimum as (assuming the slit is centred on the moon) this provides a gap of at least 1 arcsecond between the edge of the slit and the planetary limb.

It is found that, in the majority of cases, the moons are viewable for large proportions of their orbits but that observable periods change over longer time frames due to the changing inclination of the moon's orbit with respect to an observer on Earth.

4.1.3 Dwarf Planets and Other Major Celestial Bodies

In the same way as for planets, the analysis was conducted for other celestial bodies. The possibility of viewing dwarf planets as well as major asteroids and Trojans was explored and the observation periods for these objects are shown in Figures 4.6 and 4.7. We again find that the more distant a target, the smaller the variation in observable period over the lifetime of the mission.

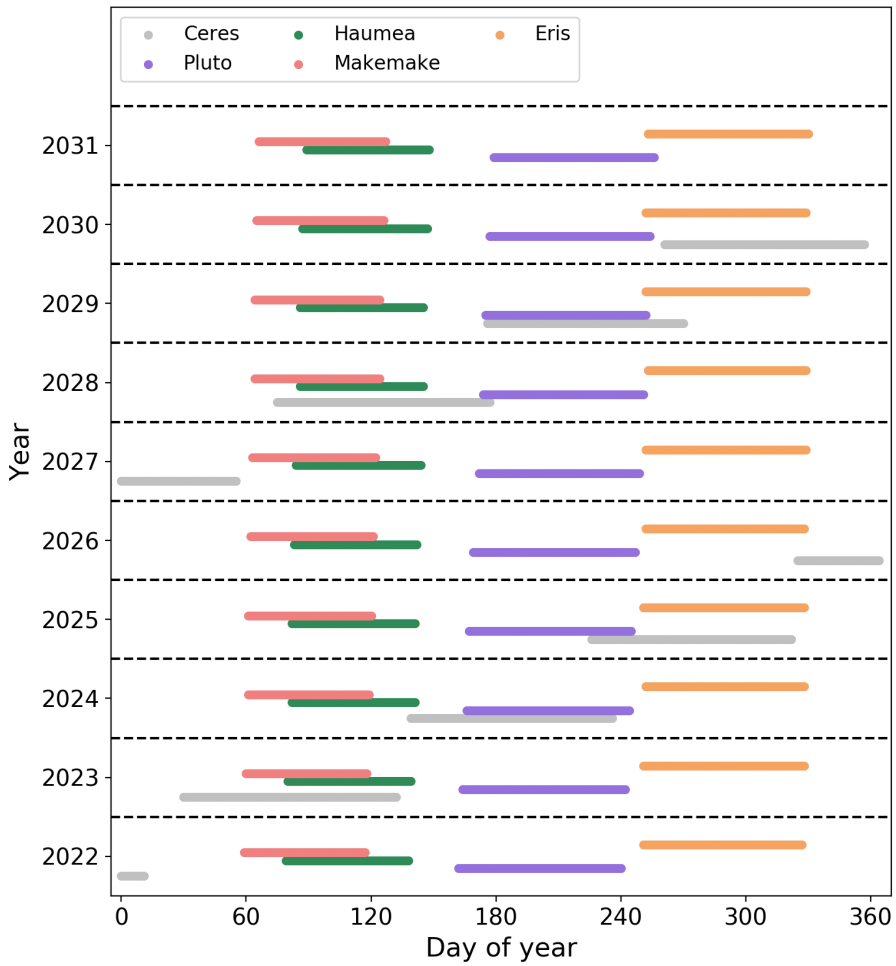

Figure 4.6: Period for which the dwarf planets lie within Twinkle's field of regard from 1st January 2022 to 1st January 2032.

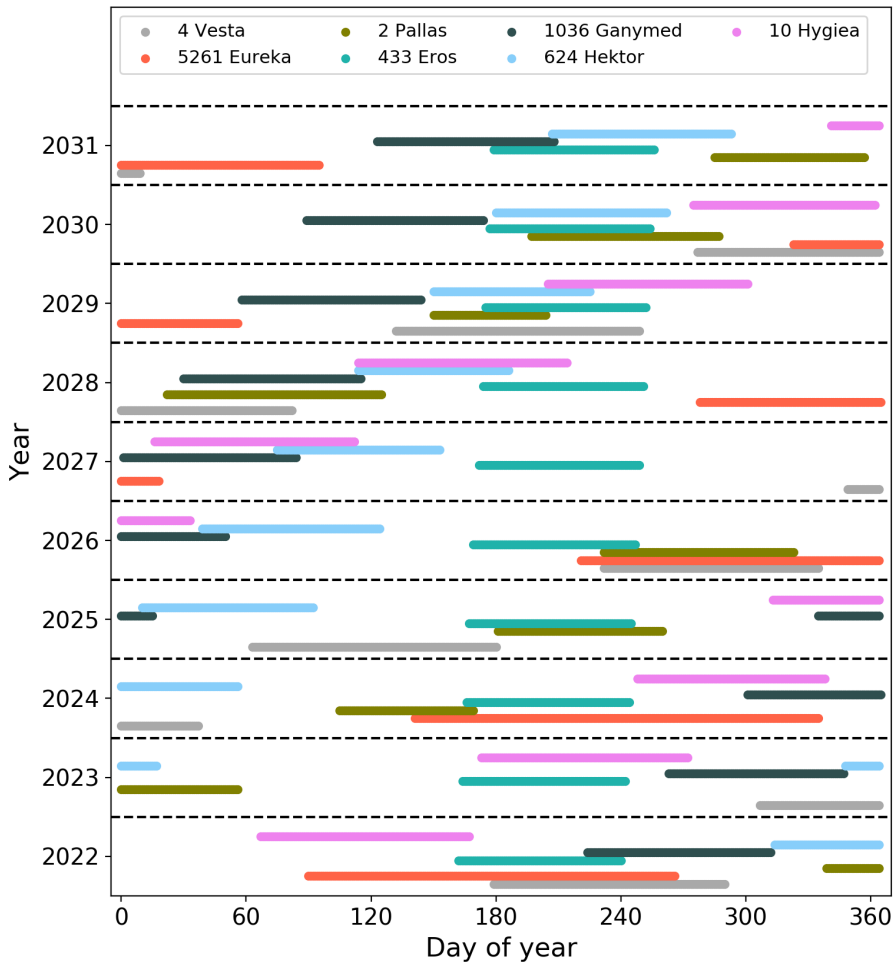

Figure 4.7: Period for which the major asteroids considered here lie within Twinkle's field of regard from 1st January 2022 to 1st January 2032.

4.2 Instrumentation Performance and Data Quality

Once it has been concluded an object is viewable, the performance of Twinkle's instrumentation and the potential quality of scientific data must be ascertained. The specifications of the instrumentation have not been definitively established and any changes will impact the conclusions drawn here. However, the following analysis is readily adaptable to new instrumentation parameters.

4.2.1 Angular size

As discussed in Section 3.2, the slits for each spectral band have different angular sizes. From JPL's Horizons system, the angular diameter of a target at a given time can be found. As demonstrated, the observation windows for viewing a target can be determined and thus the average angular diameter of a target when viewable can be calculated. This angular size can be compared to the angular size of Twinkle's star and background slits for each spectral band to ascertain whether the target can be viewed in its entirety in one observation.

If a target is too large to view in one observation, an estimate of the number of observations required to fully map the target is critical to both the total time needed to observe the entire target and the average signal to noise ratio associated with each observation. In the case where only one observation is needed, all photons from the target's visible disc are collected in one spectrum. If multiple spectra are taken then the number of photons received from a given observation area is dependent on the total number of photons from the target and the number of observations needed to map the target (i.e. if 4 observations are needed, a constant surface brightness is assumed and thus that a quarter of the total number of photons contributes to each spectrum).

An estimate to quantify the required number of observations is given by dividing the target's angular area by that of the viewing slit of Twinkle. If the planet were to be totally mapped this lower bound is unachievable as the shape of the viewing slit does not tessellate to form a circle. However, for the purpose of defining the fraction of photons from the viewed segment of target, this approximation is valid. Here we assume the star slit is used for observations and the number required to

Table 4.1: Approximate number of observations required for each instrument to cover the entire visible face of a target using the star slit.

Target	Angular Diameter [arcseconds]	Approximate Number of Observations		
		Ch0	Ch1	Ch2
Mars	16.02	806	127	37
Jupiter	46.17	6697	1055	306
Europa	1.03	4	1	1
Saturn	16.74	881	139	41
Titan	0.74	2	1	1
Uranus	3.78	45	8	1
Neptune	2.35	18	3	1
Triton	0.13	1	1	1
Pluto	0.10	1	1	1

map the entire visible face of various targets is shown in Table 4.1.

The photon flux received may vary due to planetary features (for instance the bands on Jupiter) and may also be affected by limb darkening. Hence the exposure time needed for a desired signal to noise ratio could fluctuate depending upon the type of observation carried out. However, this difference should be relatively small due to the brightness of such a target.

The targets in question are also rotating, the rate of which will dictate the length of time necessary to allow Twinkle to gain spectral data for the whole surface of the object. In general, these rotation times are low compared to the observation window, allowing plenty of time for observations of any side of the object.

4.2.2 Estimate of the signal received from a target

Assuming that the systematic noise characteristics of the instrument are constant for any target, the exposure time needed for a desired signal to noise ratio is dictated by the number of photons received per second. When observing a Solar System target, the flux received originates from two sources, the reflection of solar radiation and the radiation emitted from the target itself. Thus, the flux received at Earth from a target body is given by:

$$F_{Target} = F_{Reflected} + F_{Emitted} \tag{4.1}$$

The flux from the target due to reflected solar radiation is given by:

$$F_{Reflected} = \frac{Solar\,Flux\,at\,Target\,(Wm^{-2}nm^{-1}) \times A \times \pi R_T^2}{2\pi D_{E-T}^2} \tag{4.2}$$

where R_T is the radius of the body, D_{E-T} is the separation between the target and Earth and the A is the bond albedo, the fraction of incident radiation which is reflected in the direction of the observer. It is assumed that the visible face of the body reflects solar radiation uniformly over a half sphere of radius D_{E-T}.

The previously described analysis determines when a target could be viewed by Twinkle and was used to calculate the average Sun-target separation as well as the Earth-target distance. We use the ASTM E-490 solar spectral irradiance [129] to calculate the reflected light from the target body.

The geometric albedo of the target, as well as its radius, can be acquired from a variety of sources and thus the photon flux of solar radiation reflected by the target at the observer can be obtained. The values used here are contained in Table 4.2. The amount of radiation reflected by a target in the direction of the observer depends upon the phase angle, the angle formed between the Sun, target and observer. The geometric albedo, p_v, was used to calculate the bond albedo, A, of a target from:

$$A = p_v \times q(\chi) \tag{4.3}$$

where $q(\chi)$ is the phase integral which, for planetary bodies, can be estimated as that for a diffuse sphere and is given by:

$$q(\chi) = \frac{2}{3}\Big((1 - \frac{\chi}{\pi})\cos(\chi) + \frac{1}{\pi}\sin(\chi)\Big) \tag{4.4}$$

where χ is the phase angle [130]. Given that Twinkle's field of regard is centred on the ecliptic, and the orbits of major bodies have small inclinations, observations will generally occur at low phase angles and thus a phase angle of 10° has been assumed (i.e. $q \approx 0.657$). Geometry effects such as coherent backscatter have been omitted.

Modelling the target as a black body, the flux received at Earth due to emission

from the target can be determined. Here the effective temperature has not been derived but instead literature values have been used which are also given in Table 4.2. For a solid body, the surface temperature is used and for the gaseous planets the temperature at 1 bar is taken. It is assumed that the body radiates uniformly over a sphere with radius equal to the average Twinkle-target distance.

For all targets in the shorter infrared band (Ch1) and the visual band (Ch0), as well as the vast majority of targets in the longer infrared band (Ch2), it is found that the contribution of emitted radiation is negligible. The exception is the Martian satellites which have an emission contribution of approximately 18% in the second infrared band.

Table 4.2: Average photon flux (photons/m^2/s) per spectral bin for targets considered here and the assumed parameters used in the calculation. Many of the albedos have been acquired for the JPL Solar System Dynamics Service and the original sources have been cited where possible.

Target Name	Radius	Geometric Albedo	Temperature [K]
Mars	3.39E+06	0.15[131]	210
Phobos	1.11E+04	0.071[132]	233
Deimos	6.20E+03	0.068[133]	233
Jupiter	6.99E+07	0.52	165
Ganymede	2.63E+06	0.435[134]	103
Callisto	2.41E+06	0.18[134]	118
Io	1.82E+06	0.625[135]	118
Europa	1.56E+06	0.7[136]	113
Himalia	8.50E+04	0.675	124
Amalthea	8.35E+04	0.091[137]	160
Thebe	4.93E+04	0.047[137]	124
Elara	4.30E+04	0.035	124
Saturn	5.82E+07	0.47	134
Titan	2.57E+06	0.2[138]	94
Rhea	7.64E+05	0.949[139]	76
Iapetus	7.36E+05	0.6[138]	110

Dione	5.62E+05	0.85[139]	87
Tethys	5.31E+05	1.229[139]	86
Enceladus	2.52E+05	1.375[139]	75
Mimas	1.98E+05	0.962[139]	64
Hyperion	1.35E+05	0.3[138]	93
Uranus	2.54E+07	0.51[140]	76
Titania	7.89E+05	0.27[140]	70
Oberon	7.61E+05	0.23[140]	75
Umbriel	5.85E+05	0.21[140]	75
Ariel	5.79E+05	0.39[140]	60
Miranda	2.36E+05	0.32[140]	60
Neptune	2.46E+07	0.41	72
Triton	1.35E+06	0.719[141]	58
Proteus	2.10E+05	0.096[142]	51
Nereid	1.70E+05	0.155[143]	51
Larissa	9.70E+04	0.091[142]	51
Galatea	8.80E+04	0.079[142]	51
Despina	7.50E+04	0.09[142]	51
Thalassa	4.10E+04	0.091[142]	51
Naiad	3.30E+04	0.072[142]	51
1 Ceres	4.70E+05	0.09[144]	168
Pluto	1.19E+06	0.3	50
136108 Haumea	5.75E+05	0.84[145]	50
136372 Makemake	7.15E+05	0.81[146]	42
136199 Eris	1.16E+05	0.96[147]	43
5261 Eureka	1.30E+03	0.39[148]	250
433 Eros	8.42E+03	0.25[149]	230
4 Vesta	2.63E+05	0.38[150]	150
2 Pallas	2.56E+05	0.16[151]	164
10 Hygiea	2.16E+05	0.07[152]	164

1036 Ganymed	1.58E+04	0.218[37]	160
624 Hektor	1.13E+05	0.034[2]	122

4.2.3 Instrumental Performance and Noise

Not all incident photons will be detected due to instrument inefficiencies. The optical and quantum efficiencies are shown in Table 4.3 along with the instrument plate scale.

A model was created to estimate the noise contributions from various sources. The detector is assumed to be cooled to 70 K whilst the telescope has been modelled at 180 K. Excluding the target signal, Figure 4.8 shows the background from each source with the dark current dominating most wavelengths for long exposures although the telescope is dominant at longer wavelengths. For short exposures the read noise dominates and the contribution from the instrument box is only significant in Ch2 ($\ll 10^{-4}$ for the other channels). Due to this background signal the detector will saturate at longer wavelengths within $\sim$600 seconds, even for faint targets. Additionally a read noise of 18 e^-/pix rms was assumed.

4.2.4 Determining Observability

By setting a requirement of SNR = 10, we calculate the ability of Twinkle to observe an object at the highest resolving power for each channel using the star slit. The photon flux (photons/m^2/s) received from a target was calculated across each spectral bin. Within each channel, the photon flux varies due to the variance in solar output with wavelength. Thus, for ease of representation, the average flux per spectral bin was calculated for each channel.

The signal to noise ratio of an observation can be determined from:

$$\text{SNR} = \frac{N * QE * \eta}{\sqrt{N_\gamma + (N * QE * \eta)}} \sqrt{t_{EXP}} \tag{4.5}$$

where t_{EXP} is the exposure time, N_γ is the total number of non-signal-generated electrons (per spectral bin per second), QE is the quantum efficiency, η is the optical

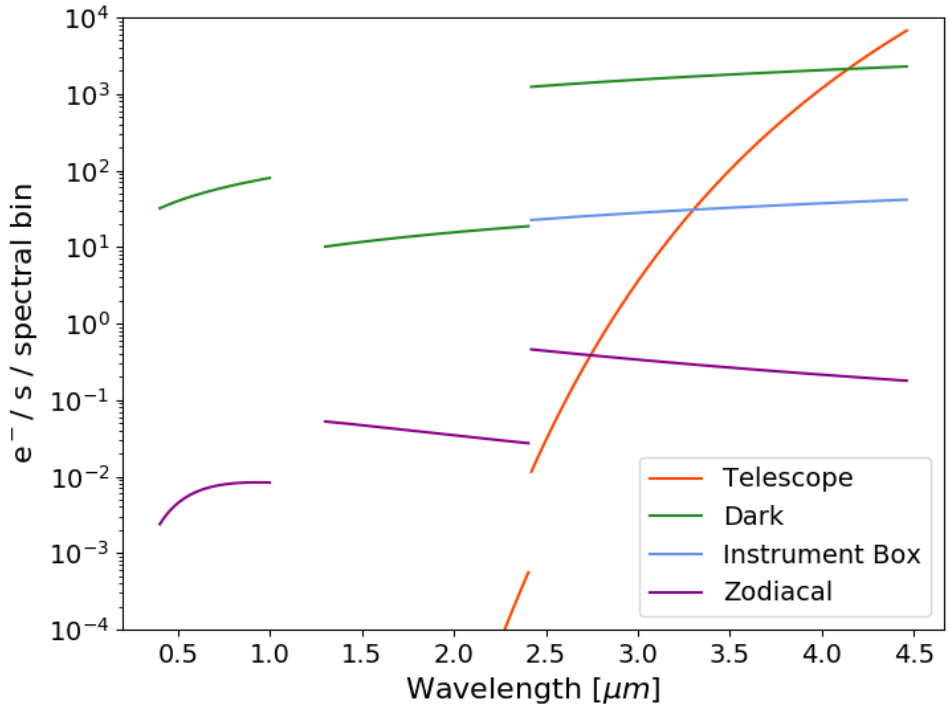

Figure 4.8: Number of photons per second per spectral bin from different background sources when operating at R∼250 (λ <2.42 μm) and R∼60 (λ >2.42 μm).

Table 4.3: Instrument properties over each channel.

Instrument Property	Ch0 (0.4 - 1μm)	Ch 1 (1.3 - 2.42μm)	Ch 2 (2.42 - 4.5μm)
Optical Efficiency	0.80	0.45	0.61
Quantum Efficiency	0.7	0.7	0.7
Plate Scale (arcsec /μm)	0.007	0.027	0.7
Telescope Emissivity	0.02	0.02	0.02

efficiency and N is the number of photons (per spectral bin per second) from the target. This was rearranged to obtain the minimum photon flux needed to meet the SNR requirement within a given integration time.

By comparing the photon flux from a target with the minimum required to achieve SNR = 10, the Solar System objects which could be observed by Twinkle were determined. For some bright sources, saturation can be an issue and thus the maximum photon flux from a target that could be observed for a given integration time was also calculated. We assume a max continuous integration time of 300

seconds.

These sensitivity and saturation limits are plotted in Figure 4.9 and, if an object lies between these limits for a given exposure time, Twinkle can achieve spectra at the instrumentation's native resolution with an SNR >10. We find that very bright objects such as Mars could only be observed with short exposure times due to saturation of the detectors. Targets such as Neptune could be observed in around 1 second whilst spectra of dimmer objects (e.g. Deimos) could be obtained in 60 seconds.

By combining multiple observations, some fainter object could be observed by Twinkle. We find that with less than 10 observations with exposure times of 300 seconds, Pluto could be observed at Twinkle's native resolution as shown in Figure 4.10. The sensitivity limit of Twinkle could be further increased by binning down the spectra, reducing the resolution but increasing the number of photons per spectral bin.

Thus, we find that many celestial bodies could be observed at a high spectral resolution (R$\sim$250, λ <2.42 μm; R$\sim$60, λ >2.42 μm) with short exposure times ($\ll$ 300 seconds). On the other hand, some bodies are too small, faint or distant and are found to require many observations. The potential exists to bin the spectra to lower resolutions to increase the SNR and thus allow faint objects to be observed.

4.3 Discussion

This first iteration of assessing Twinkle's performance for Solar System science has shown that many objects are potentially observable with Twinkle. Twinkle is currently entering a Phase B design review and thus the technical specifications may change. An updated analysis will be published when the design is finalised.

4.3.1 Suitability of Targets

From the analysis presented here, it can be concluded that, for each object, an ideal viewing period will exist and this is when the target is closest to the Sun (and Earth), at a low phase angle, close to the centre of Twinkle's field of regard. This will ensure the highest photon flux. The photon fluxes calculated here are averages of

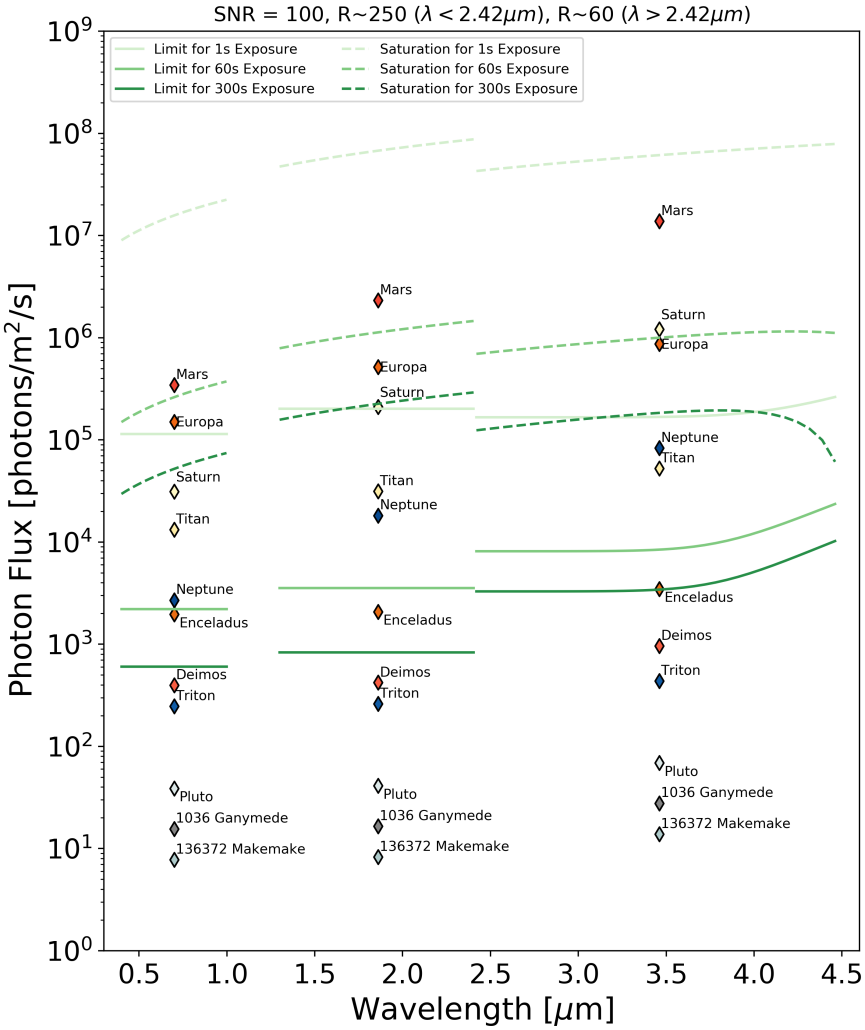

Figure 4.9: The average photon flux received per spectral bin at Earth for various Solar System bodies at their average distance during observable periods with Twinkle. Additionally the sensitivity and saturation limits of Twinkle are plotted for single observations with various exposure times using the star slit assuming a SNR $>$10 is required.

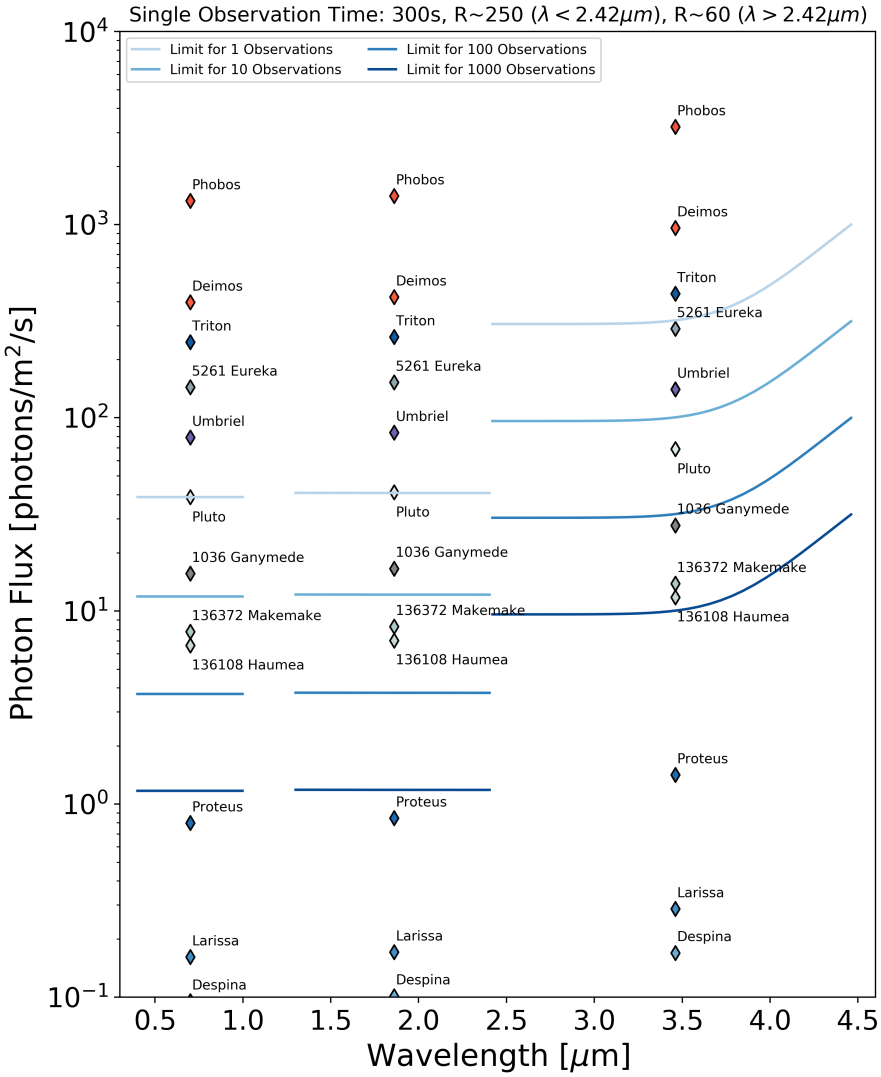

Figure 4.10: The average photon flux received per spectral bin at Earth for various Solar System bodies at their average distance during observable periods with Twinkle. Additionally the sensitivity limits of Twinkle are plotted for a given number of 300 second observations with the star slit.

the expected performance. Thus, an observation at a specified time may achieve better or worse performance than predicted here, depending upon the instantaneous geometry of the observation. The capability of Twinkle to view a target also varies over the spectral bins. Targets have been assessed by the number of observations required to achieve high resolution spectroscopic data with a signal to noise ratio of 10. If this level of resolution or quality is not needed, the capability of Twinkle to observe this object may change. For example, in the infrared, many spectral features can be broad and thus a resolving power of 250 (or 60) may not be necessary.

It is therefore concluded that, although some targets will not be suitable for observations with Twinkle, there is the potential to observe, with a relatively small space telescope, a significant number of objects. The resolution and quality of data achievable will vary with each spectral bin and with the length and number of observations undertaken. Reducing the required signal to noise ratio will considerably increase the ease for which Twinkle could obtain data from a target.

For planets and large moons, the integration times are, in many cases, shown to be short enough that spectroscopic observations of these bodies can be undertaken in a single exposure. For faint, small or distant targets the integration times are longer and in several cases are too large to obtain high quality data in one observation. Combining multiple observations of a target will increase the data quality obtainable as will binning the spectra to a lower resolution.

We find that Solar System objects generally have long observing windows (up to 80 days) each year and these potential observing periods are also periodic over the timescale of the mission. As, in general, the observation window for an object is greater than the rotation period of the target, Twinkle could obtain global views of spatial variations. By re-observing an object over an extended period of time (i.e. years), observations with Twinkle could also be used to search for temporal variations.

4.3.2 Background Slits

Here, the capabilities of the star slit to observe Solar System objects has been assessed and, in the normal operation mode, the background slits are used to provide

measurements of zodiacal light in the direction of observation which is then subtracted from the observation of the target. When observing a planet, the zodiacal component will be small compared to the planetary contribution.

Therefore, the background slits could instead be used to provide spectra of a strip of the target. This increases the area covered in one observation and decreases the exposure time required although spatial resolution is also reduced. The star slit (or other background slit) could potentially be used to subtract any background. Utilising the background slit in this way would rapidly decrease the time taken to fully observe the visible face of a large target.

There may however be issues with using Twinkle in this way. The telescope is designed such that the FGS is used for fine pointing. In normal operations this will fix the star on pixels of the FGS CCD and keep its location fixed. As the spacecraft moves due to its orbit and other perturbations the FGS mirror tilts to keep the target positioned on this pixel. This ensures that the slit is pointed at the target for the entirety of the observation. For small targets, such as moons or asteroids, for which only one observation is required to map, the methodology is the same.

However, if multiple spectra need to be taken to map the object then this would require Twinkle to not only keep the telescope pointed at a given location but also be able to fine point within this object. This is vastly different from the primary mode of operation and thus a different mode would need to be devised. The slew time between these observations will also need to be accounted for in the mapping time and the precision to which these adjustments can be accomplished must be determined. Though potentially problematic, this mapping technique is certainly not inconceivable.

The background slits could also mitigate for the contribution of the planet when observing moons. The background slit could be used to observe the moon with its orientation being perpendicular to the planet-satellite direction, as shown in Figure 4.11, with the central background spectra focused on the moon. For moons, and other small objects, care will have to be taken to ensure that other background objects, such as bright stars, do not lie within the field of view, contributing to the

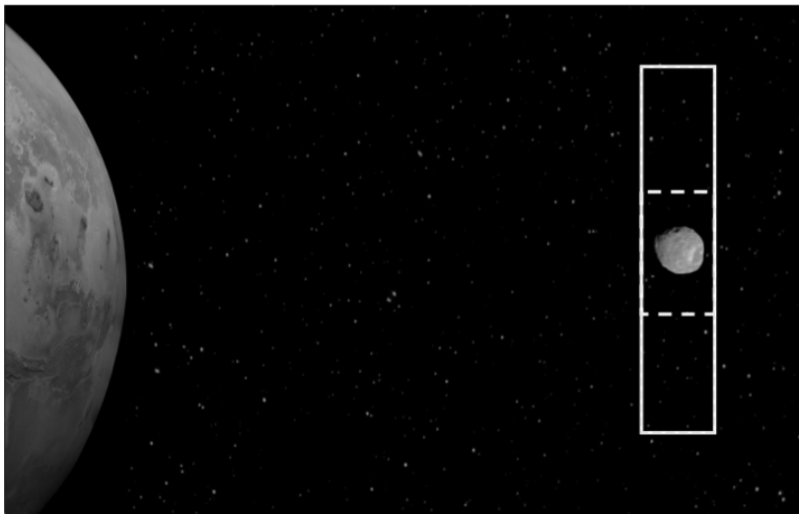

Figure 4.11: Potential use of background slit to view moons and mitigate for stray light from the host planet (not to scale). Original images credit: NASA.

received spectra. Additionally, as all three slits image onto the same detector, the other slits must be positioned away from very bright objects, such as the host planet of a moon, to avoid saturation. A final consideration is that the background slits observe different regions of the sky so multiple observations would be needed to obtain full spectral coverage.

4.3.3 Potential Impact

Twinkle therefore offers a capability that is not currently available: space-based spectroscopic observations of Solar System objects in the infrared beyond 1.7 μm. Unlike ground-based telescopes, Twinkle will not be inhibited by Earth's atmosphere and thus will be capable of detecting water features in the infrared that would be extremely difficult from the ground. In addition to hydration features, many silicates and organics have absorption features within Twinkle's 0.4 - 4.5 μm range. These are key for understanding the dispersion of water, metals and organics throughout the Solar System and provide insights into planetary formation and evolution. Several CO_2 ice bands also lie within Twinkle's wavelength coverage (e.g. those around 2 μm and the absorption feature at 4 - 4.4 μm which is blocked by telluric CO_2) which have been detected in various bodies including the moons of Jupiter [153, 91], Saturn [154] and Uranus [155]. Additional molecules found

in these satellites that may be detectable with Twinkle include condensed O_2 [156] as well as SO_2 [157]. Combining spectroscopic observations of major bodies with small bodies (asteroids and comets) enables a detailed view of the primitive and current state of the Solar System. Thus, further work will seek to understand the capability of Twinkle to observe small bodies within the Solar System.

4.4 Conclusions

The capability of the Twinkle space telescope to observe Solar System objects in visible and infrared wavelengths has been assessed in this chapter.

From comparing the celestial coordinates of potential targets with Twinkle's field of regard it has been found that, although the orbital characteristics of Twinkle impose constraints, the potential observation windows are still large. The duration and frequency of these observable periods varies, as does the trajectory of the object across Twinkle's field of regard. Planetary moons incur an additional constraint but obscuration by their host planet is found to be minor in the vast majority of cases although some observations may be hindered by stray light.

Solar System targets, for which Twinkle's capabilities allow for the acquisition of high quality, high-resolution spectroscopic data within a single observation is found to incorporate planets and some larger moons. The potential also exists for observations of smaller moons and large asteroids at high resolution while photometric observations should be possible for a vast number of objects. The capability of Twinkle to observe these objects varies with wavelength and, as the majority of photons received from bodies are reflected solar radiation, the longer infrared band has the lowest capabilities for viewing fainter objects, which is also due to higher instrumentation noise.

An obvious way of increasing the sensitivity limit is to combine multiple observations and this has been shown to expand the targets which Twinkle could observe. For each target an optimal approach is likely to exist and, by varying the resolving power, length and number of observations and the required signal to noise, the ability of Twinkle can be assessed on a case by case basis.

Chapter 5

Small Bodies Science with Twinkle

> ”When we try to pick out anything by itself, we find it hitched to everything else in the universe.”
>
> John Muir

As outlined in Section 2.3.1, the small bodies field currently lacks a space-based remote-sensing mission capable of selectively characterising thousands of asteroids and comets, through visible and near-infrared spectroscopy. While Ariel is not expected to be capable of Solar System science due to the lack of a non-sidereal tracking capability, JWST and Twinkle both present the possibility of investigating a multifarious selection of small bodies.

The capability of JWST for small bodies science has long been anticipated. Analysis of the sensitivity of NIRCam and NIRSpec suggests that, with an exposure time of 1000 s, almost any currently known main belt asteroid could be observed with an SNR $>$ 10 at R$\sim$100 [158]. For larger objects, these observations will provide both spectral and spatial information, facilitating the distinction of surface features and changes in surface mineralogy. While Hubble has been used extensively for spatial observations of asteroids [e.g. 159], it cannot simultaneously

Contributions: This chapter is based upon a study which I led and has been published in a peer-reviewed journal (Edwards et al. 2019, Small Bodies Science with the Twinkle Space Telescope, JATIS, doi: 10.1117/1.JATIS.5.3.034004). Sean Lindsay, Neil Bowles, Giorgio Savini, Giovanna Tinetti, Marcell Tessenyi and Claudio Arena also contributed significantly to this work.

provide this spectral information. Additionally, Hubble observations are interrupted due to Earth obscuration. This will not be an issue for JWST meaning an asteroid could be observed continuously over its rotation period instead of stitching together observations over several rotations.

Near Earth Objects (NEOs) are a particularly interesting population of bodies. With short dynamical lifetimes of few million years due to gravitational interactions, NEOs are constantly being depleted by Earth impacts while simultaneously being refreshed via capture. This population contains potentially hazardous asteroids (PHAs) which have a high probability of Earth impact but some of them also present the ideal targets for future resource utilisation. Hence, detecting and studying NEOs is deemed of critical importance for both planetary defence and future human exploration and exploitation. Around 75% of NEOs should be observable by JWST in a given year with MIRI anticipated to have the sensitivity to conduct photometric surveys of meter-sized NEOs, providing albedo and diameter measurements and opening a new parameter space for characterisation [110].

Another science case to which JWST is expected to contribute is the study of comets, in particular the expansion of our knowledge of gas coma orbital evolution and the detection of water ice in cometary nuclei and coma [160]. Main Belt Comets (MBCs) could also be studied and Hubble observations have, in some cases, quantified the volume of water outgassing but have yet to characterise the dust volume or particle size in the comae [49]. JWST could allow for such properties to be probed and objects with significant outgasing rates should be detectable out to 4.5 AU [160].

However, JWST is expected to be hugely oversubscribed and thus it is unlikely small bodies programs will receive enough time to study the hundreds, or even thousands, of objects required to form a true population study. Hence, although JWST will undoubtedly provide fantastic insights into a handful of small bodies, without a larger population study, progress in understanding these primordial objects will be slower than hoped.

The focus of this chapter is on the potential of Twinkle to observe and charac-

terise the small bodies of the Solar System. Twinkle's spectrometers cover a similar wavelength range to JWST NIRSpec, as well as the proposed CASTAway mission [87], and thus will be capable of detecting many of the same features. This spectral coverage is ideal for the compositional characterisation of mafic silicates, hydration features, and organics on asteroid surfaces and within comet comae. Here, Twinkle's ability to acquire high fidelity spectral data of many asteroids and comets within the Solar System is demonstrated, a description of which spectral features lie within Twinkle's spectral range that make it an ideal small bodies research facility is provided, and the research areas to which Twinkle could contribute most significantly are discussed.

5.1 Methodology

JPL's Horizons system[1] was accessed for $\sim$740,000 small bodies defined as NEOs, Inner, Main and Outer Belt asteroids or Trojan asteroids. Here, Near-Earth Objects (NEOs) include those that are classified by the Horizons database as Aten, Apollo and Amor. Atira asteroids are excluded as their orbits are contained entirely within the Earth's orbit and thus are not observable due to the field of regard of Twinkle always being centred upon the anti-Sun vector. Mars-crossing asteroids are classified here as Inner Belt asteroids. Additionally, the physical characteristics of $\sim$1000 comets were downloaded from the Minor Planet Centre[2]. The capability of Twinkle to observe these small bodies has been analysed using the methods described in Sections 5.1.1 - 5.1.3.

5.1.1 Instrument Sensitivity

For many small bodies within the Solar System, such as comets and asteroids, parameters such as albedo, radius and temperature are not precisely known. Therefore, the analysis described in Chapter 4, which was used for modelling Twinkle's capabilities to observe major Solar System bodies, cannot be applied. To assess Twinkle's performance when viewing such objects, the flux received has been esti-

[1] https://ssd.jpl.nasa.gov
[2] https://minorplanetcenter.net

mated from the visible magnitude of the body and the methodology for calculating the visible magnitude of small bodies is described in Section 5.1.3.

It is assumed that all photons received in Twinkle's visible and infrared wavelengths bands are from reflected solar radiation and that a target is small enough to be viewed in its entirety in one observation. The former is valid for Ch0 and Ch1 but provides an underestimation of the flux in the spectral band 2.42 - 4.5 μm while the latter assumption is true for all but the biggest, brightest objects (e.g. Ceres) which have angular diameters which are greater than the size of Twinkle's slits but have already been shown to be observable with Twinkle in the previous chapter. For each magnitude, the photon flux is calculated per spectral bin which can then be compared to the sensitivity and saturation limits of Twinkle for a given exposure time. The thermal emission of an asteroid can of course be significant, particularly for NEOs. By ignoring it we are underestimating the number of photons received and thus underestimating the exposure time required. When planning an actual observation with Twinkle, the thermal emission should of course be accounted for to avoid detector saturation. Here however, we attempt to classify an approximate number of potential targets rather than focusing on any individual objects. To reduce the number of assumptions in the calculation of the flux (e.g. surface temperature, diameter, albedo) we chose the simplified case of assuming just reflected solar radiation.

The minimum photon flux required to achieve SNR = 100 was calculated for various exposure times to find the sensitivity limit of Twinkle. Additionally the saturation limit was found by finding the maximum photon flux that could be observed in each spectral bin. The noise characteristics per spectral bin were identical to that of Chapter 4 (see Figure 4.8).

5.1.2 Pointing and Tracking Restrictions

Twinkle's FGS operates at visible wavelengths and the detailed tracking performance of the FGS will ultimately depend on the platform pointing accuracy. However, it is expected that the wide Field of View (FOV) of the FGS camera will allow bright sidereal targets to be tracked. The ability of Twinkle to track an object varies with brightness and there exists a faintest object which Twinkle can track using the

FGS. Current simulations suggest direct tracking will be possible for targets with visible magnitude of 15 or brighter. Further investigation is needed to fully ascertain the capability of the FGS and this will be performed as part of the Phase B study. For fainter targets, tracking could be simulated by scanning linear track segments. These linear track segments are linear in equatorial coordinate space; they are commanded as a vector rate in J2000 coordinates, passing through a specified RA and Dec at a specified time. The coordinates of the target can be obtained from services such as Jet Propulsion Laboratory's Horizons System. This method of tracking is by no means simple but has been employed on Spitzer (and will be for JWST). Including such a capability would be non-trivial but, given the current status of the mission, there is time to include and refine this capacity. Here we assume only on-target tracking is used.

The maximum tracking rate of Twinkle is also subject to further investigation. During the ExploreNEO program, Spitzer targets achieved a max rate of 543 mas/s [60] and JWST will be capable of 30 mas/s [110]. Twinkle's FGS is expected to be capable of tracking Mars (e.g. a rate of 30 mas/s) though its max rate may have a dependence on the brightness of the target.

5.1.3 Target Availability

As in Chapter 4, Twinkle was assumed to have a 'first light' date of 1st January 2022 and a 10 year mission life. To assess the number of small bodies which enter Twinkle's field of regard, JPL's Horizons system was accessed and ephemeris data obtained for all small bodies over the timescale 2022 to 2032 at 1 day intervals. This was compared to Twinkle's field of regard and, when a target could be observed with Twinkle, the visible magnitude, m, of the body calculated from:

$$m = H + 2.5log_{10}\Big(\frac{d_{S-T}^2 \times d_{O-T}^2}{q(\chi) \times (1AU)^4}\Big) \tag{5.1}$$

where d_{S-T} is the distance between the Sun and the target, d_{O-T} is the distance between the observer and the target, $q(\chi)$ is the phase integral and H is the apparent magnitude an object would have if it were at 1 AU from both the observer and the

Sun. The apparent magnitude of these bodies was calculated using d_{S-T} and H from the Horizons database. For planetary bodies (with an atmosphere), the phase integral can be estimated as that for a diffuse sphere [130]. However, airless bodies (i.e. asteroids although some have tenuous exospheres such as Ceres [161]) usually reflect light more strongly in the direction of the incident light. This causes their brightness to increase rapidly as the phase angle, the angle between the Sun, the observer and the target, approaches 0°. This opposition effect is dependent upon the physical properties of the body [162]. Therefore, q(χ) has been calculated from:

$$q(\chi) = (1-G)\phi_1(\chi) + G\phi_2(\alpha) \tag{5.2}$$

where G is the slope parameter (acquired from Horizons or assumed to be 0.15) and ϕ is given by:

$$\phi_n(\chi) = exp\Big(-A_n\Big(tan\frac{\chi}{2}\Big)^{B_n}\Big)$$

where A_1 = 3.332, A_2 = 1.862, B_1 = 0.631, B_2 = 1.218 [163, 164]. This is valid for phase angles below 120°. These assumptions therefore include phase angle effects but do not account for phase angle dependent spectral effects. However, these are still not well understood and, in all but the most extreme cases of large phase angle, are only minor effects.

This calculation was performed for three periods (1 year, 3 years and 10 years), each starting in 2022, to provide estimates of the number of asteroids observable with Twinkle over the mission life but also shorter time-spans. By monitoring an asteroid over time, the maximum brightness when observable with Twinkle could be obtained. The visible magnitude was utilised to calculate the number of photons received from the target in each spectral band. The rate of motion at a given time was also calculated to account for the capabilities of the FGS.

If not currently known (i.e. listed in the Horizons database[3]), the diameter (in

[3]https://ssd.jpl.nasa.gov/horizons.cgi

metres) of the observable asteroids have been determined from:

$$d = 10^{3.1236-0.5log_{10}(p_v)-0.2H} \tag{5.3}$$

where p_v is the geometric albedo [165]. For each target, three possible albedo classes are considered that represent a variety of asteroid taxonomies. The albedo classes are defined using average albedos for different taxonomic types as determined in [166], and are as follows: 1) taxonomic types with low average albedos near 0.05 including the C-complex and P- and D-types (possible X-complex); 2) taxonomic types with moderate average albedos near 0.20 including the S-complex and K-, L-,(possible X-complex) and M-types (X-complex); and 3) taxonomic types with high average albedos near 0.40 including V-type (similar to S-complex) and E-type (X-complex).

5.2 Results

5.2.1 Number of Observable Asteroids

By assuming a requirement of SNR = 100 and the discussed instrument characteristics, the capability of Twinkle to observe small bodies is determined by calculating the sensitivity and saturation limits of Twinkle's instrumentation for each spectrometer. These are plotted in Figure 5.1 and, if an object lies between these limits for a given exposure time, Twinkle can achieve spectra at the instrumentation's highest resolution with an SNR >100. At shorter wavelengths (λ<2.42 μm), targets of visible magnitudes brighter than $m_v \sim$13.5 could be observed at Twinkle's highest spectral resolution in 300 s while for longer wavelengths the magnitude limit for this exposure time is $m_v \sim$12. As discussed in Section 5.1, thermal emission has been ignored and thus the calculated flux at longer wavelengths is an underestimate for many small bodies.

By combining multiple observations, the faintest object which could be observed by Twinkle can be improved. We find that by stacking fewer than 100 observations, each with exposure times of 300 s, Twinkle could probe to visible magni-

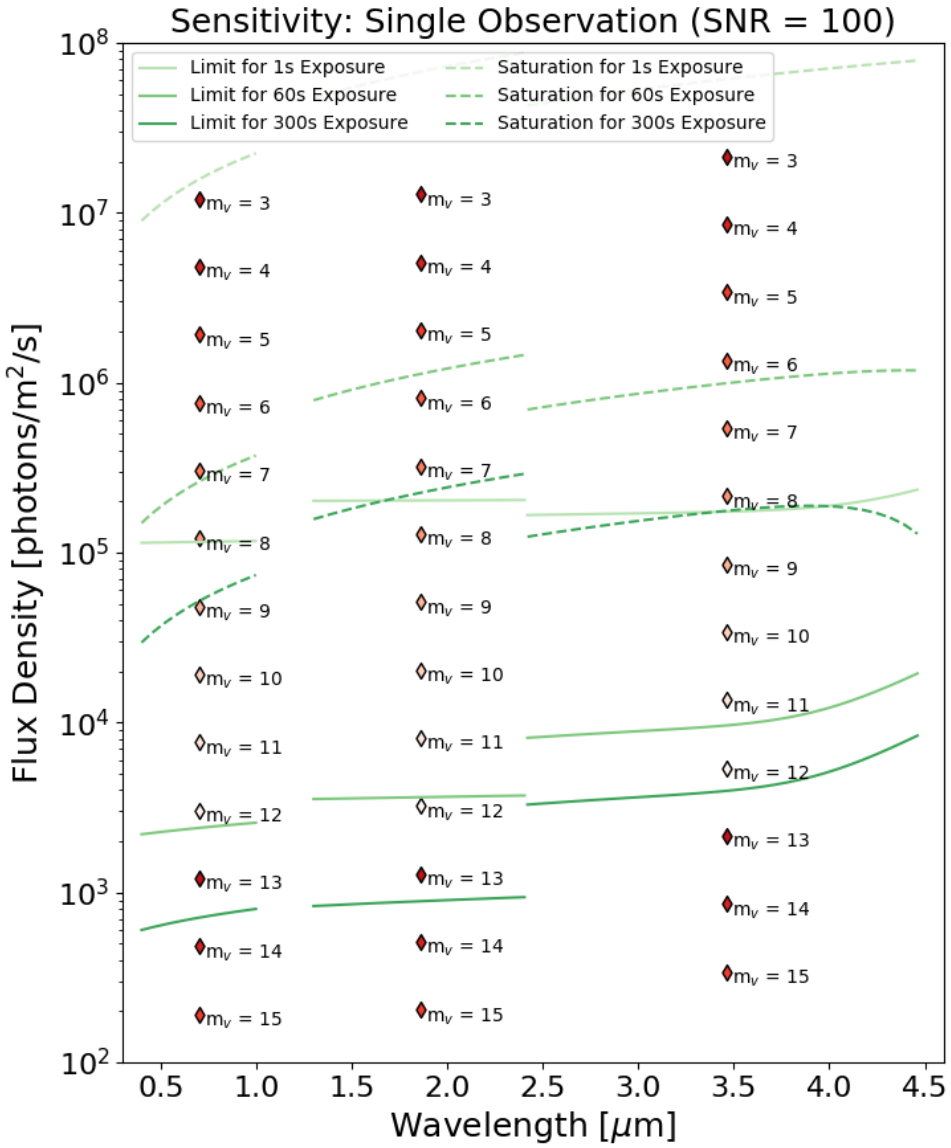

Figure 5.1: For a single observation of a given exposure time, the sensitivity and saturation limits of Twinkle assuming observational parameters of SNR = 100, R∼250 (λ <2.42 μm) and R∼60 (λ >2.42 μm). Additionally the average photon fluxes received per spectral band at Earth for small bodies of a given visible magnitude are plotted.

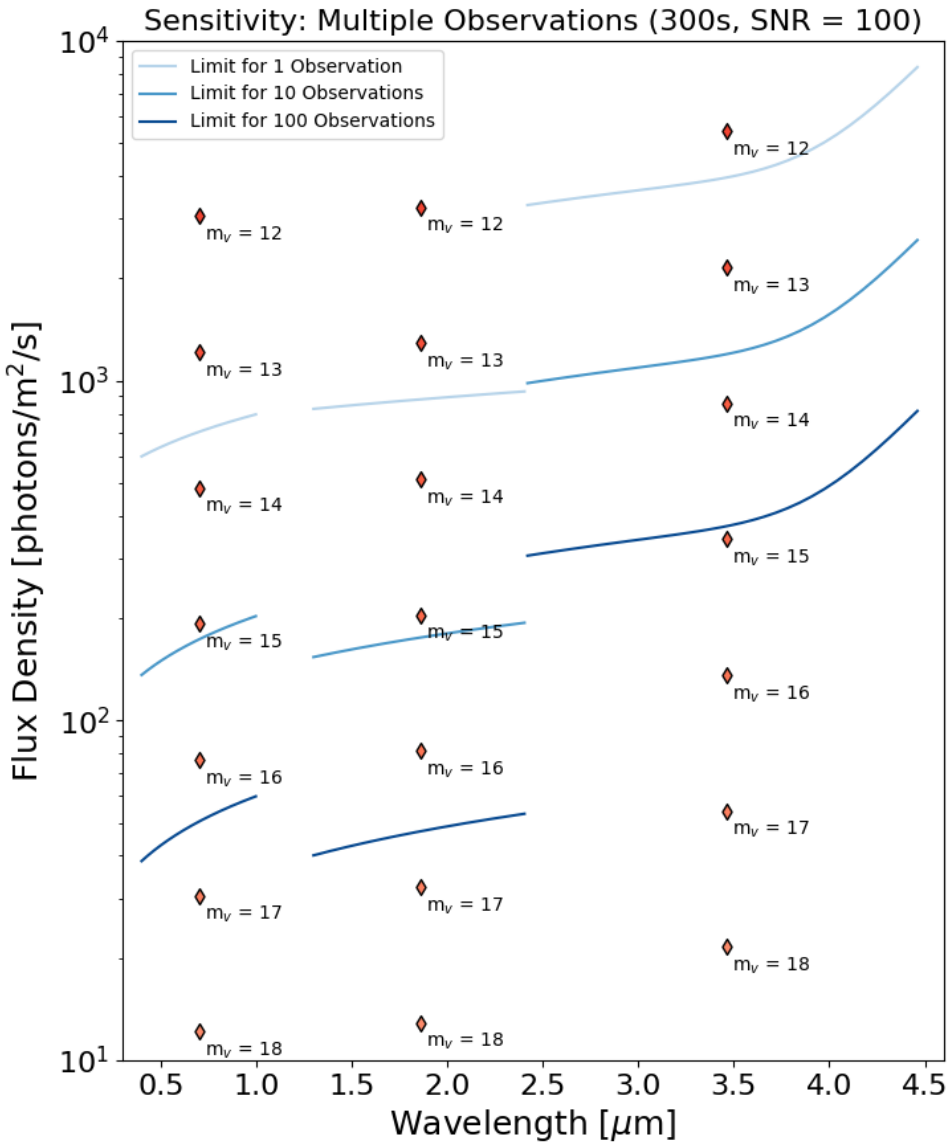

Figure 5.2: For multiple 300 second observations, the sensitivity and saturation limits of Twinkle assuming observational parameters of SNR = 100, R∼250 (λ <2.42 μm) and R∼60 (λ >2.42 μm). Additionally the average photon flux received per spectral band at Earth for a small body of a given visible magnitude are plotted.

tudes of m_v ~15-16.5 (Figure 5.2). The sensitivity limit of Twinkle could be further increased by binning down the spectra, reducing the resolution but increasing the number of photons per spectral bin.

The number of asteroids which Twinkle could characterise depends upon the brightness of targets when entering the field of regard, which dictates the possibility of tracking it with the FGS (without the need for linear tracking segments) and the data quality achievable. The cumulative number of asteroids of a given visible magnitude that enter Twinkle's field of regard with non-sidereal rates of <30 mas/s is shown in Figure 5.3. We find that several thousand Main Belt asteroids with a visible magnitude <15 enter Twinkle's field of regard over the time periods considered. Tens or a few hundred NEOs and Outer Belt asteroids are bright enough for on target tracking. Additionally, a handful of Trojans are bright enough to be tracked with the current FGS design as are tens of asteroids in the Inner Belt.

5.2.2 Size of Potential Observable Asteroids

For each asteroid which enters Twinkle's field of regard over the period 2022 - 2032, the maximum visible magnitude has been calculated as described. Additionally, the diameter, if not already known, has been determined assuming 3 different albedos (0.05, 0.2 and 0.4). Figure 5.4 shows the sizes of asteroid that Twinkle could characterise. The plotted value for the diameter is that calculated assuming an albedo of 0.2 while the error bars show the change in the diameter if the albedo is between 0.05 and 0.4. We find that the majority of potentially observable asteroids are large (>1 km) but there are also some possible targets with sizes of 100's of metres or less. If tracking via bright stars is employed and data resolution or quality can be sacrificed (i.e. spectral binning of spectra or SNR <100) then objects fainter than M_v = 15 could be observed with Twinkle which would allow for many asteroids with smaller diameters to be characterised.

5.2.3 Comets

The visible magnitude of ~1000 comets has been monitored over the period 2022 - 2032 and Figure 5.3 shows the change in this brightness for the most luminous

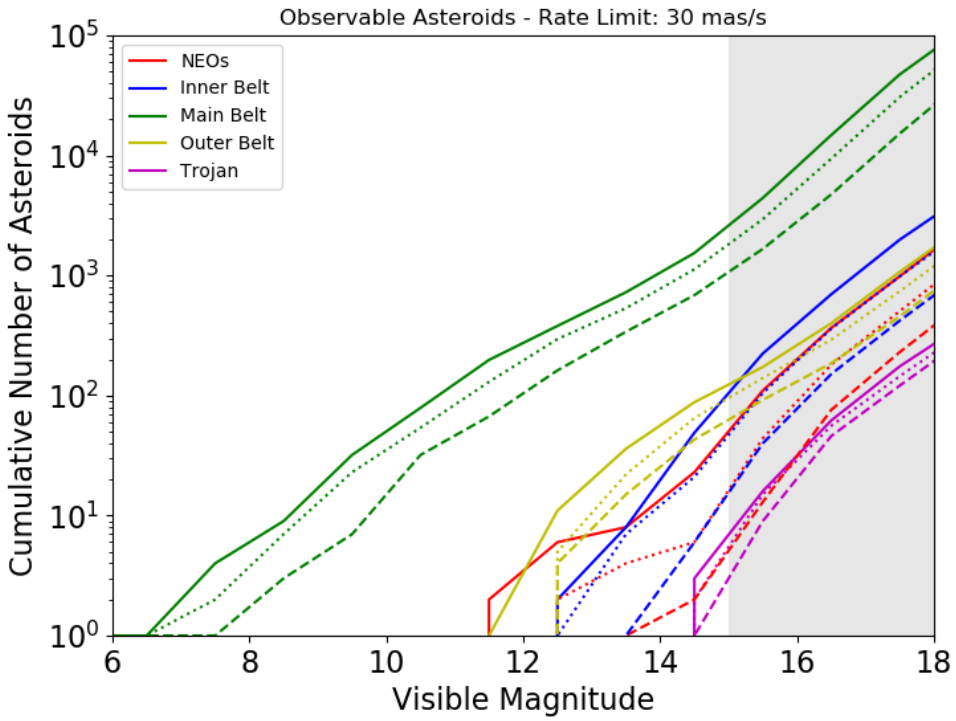

Figure 5.3: Cumulative number of asteroids of a given visible magnitude and type that enter Twinkle's field of regard over several time periods (dashed: 2022 - 2023, dotted: 2022 - 2025, solid: 2022 - 2032) with non-sidereal rates of $<$30 mas/s. The grey area indicates the cut-off due to the tracking capability of the current FGS design.

objects. Over a decade, $\sim$200 comets are found to be brighter than the current tracking limit of Twinkle's FGS and thus spectra with SNR $>$100 could be obtained for these over multiple observations at Twinkle's highest resolution. Again, increasing the sensitivity of the FGS, or utilising other tracking methods, would allow for more targets to be characterised and mean comets could be observed while they are further from the Sun (e.g. before they become active).

5.3 Discussion

With its wavelength coverage, position outside of Earth's atmosphere, instrument performance (Section 5.2), and stability capabilities, Twinkle is ideally suited to acquire high fidelity visible and near-infrared (VNIR) data for the small bodies of the Solar System. While Twinkle is well-suited to investigate asteroids of all types, the

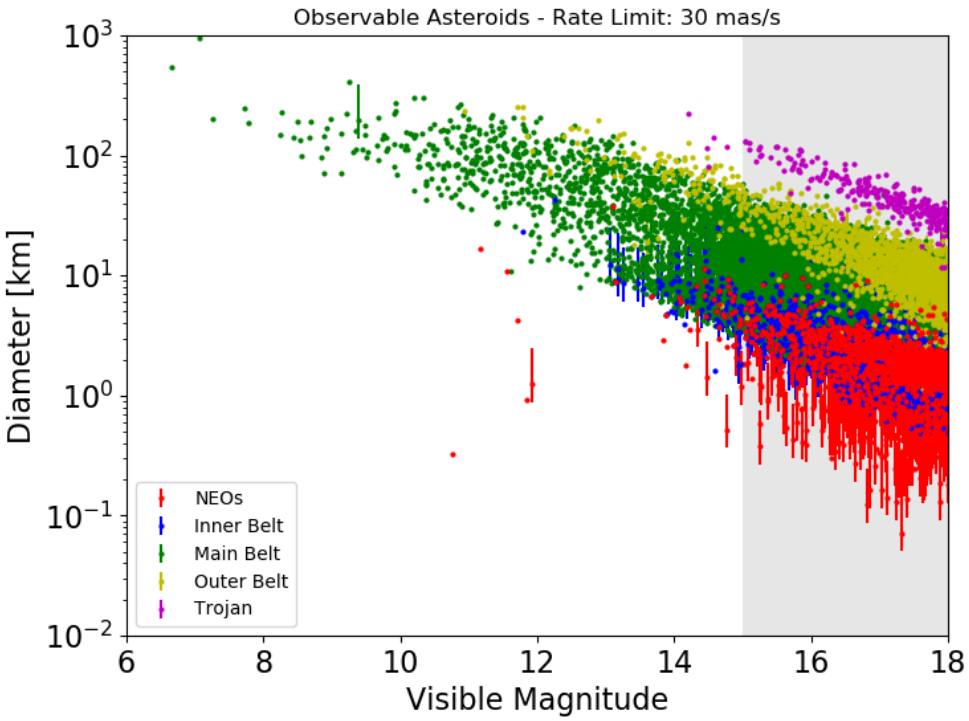

Figure 5.4: The diameters of asteroids which enter Twinkle's field of regard and the max visible magnitude they are observable at with non-sidereal rates of <30 mas/s. The grey area indicates the cut-off due to the tracking capability of the current FGS design.

most promising contribution the space-based observatory offers is to investigate the primitive asteroids. Twinkle's ability to fully resolve spectral features related to hydroxyl (OH), water (ice and gas), and hydrated silicates, which are either partially or fully obscured in Earth-based observations due to Earth's water-rich atmosphere, offers the opportunity to collect the best primitive asteroid VNIR data set to date. Currently, telluric (atmospheric) water features in the spectral data prevent a full characterisation of the primitive asteroids and comet comae. Such a characterisation is required to determine the composition and mineralogy of these objects and Table 5.1 contains various minerals with absorption features within Twinkle's spectral range. Without a large database of VNIR spectra free of atmospheric water contamination, our understanding of the composition of the most primitive bodies of the Solar System has been stunted.

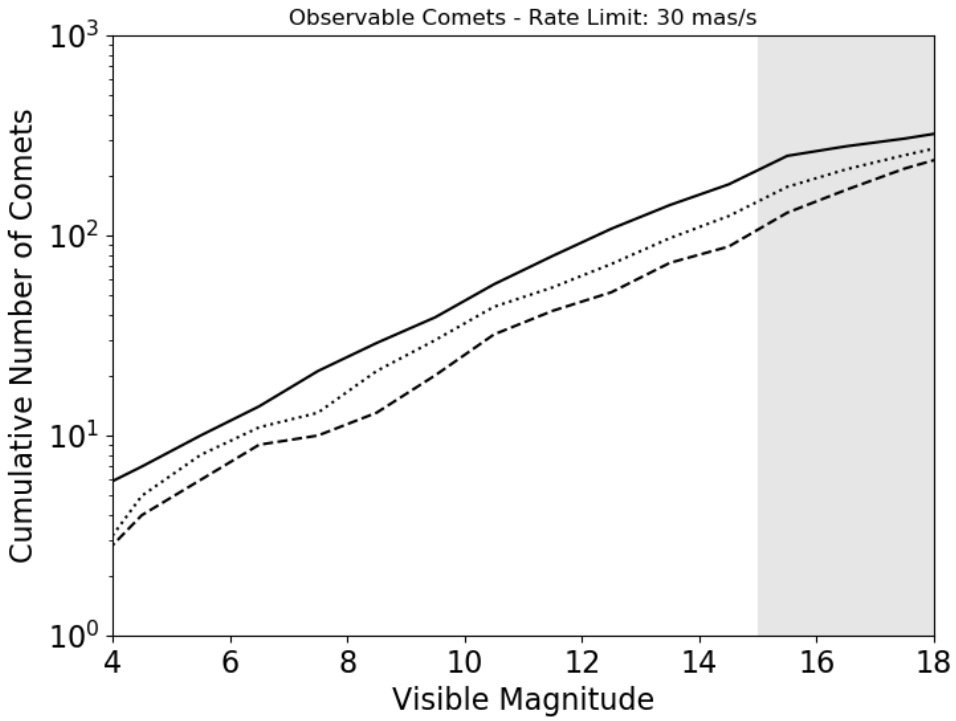

Figure 5.5: Cumulative number of comets of a given visible magnitude that enter Twinkle's field of regard over several time periods (dashed: 2022 - 2023, dotted: 2022 - 2025, solid: 2022 - 2032) with non-sidereal rates of <30 mas/s. The grey area indicates the cut-off due to the tracking capability of the current FGS design.

Table 5.1: Main spectral features of some common minerals within the 0.4 - 4.5 μm spectral region, take from the RELAB database[5]

Minerals	Main Spectral Features [μm]	Comments
Carbonates		
Calcite/Dolomite	1.85 - 1.87	
	1.97 - 2.0	
	2.12 - 2.16	
	2.30 - 2.35	
	2.50 - 2.55	
	3.40	
	4.00	
Oxides		

Chromite		0.49	
		0.59	
		1.3	At the edge of Channel 1
		2.0	
Spinel		0.46	
		0.93	
		2.80	
Organics			
e.g. n-alkanes,	numerous	1.7	
amino acids	including:	2.3	
		2.4	
Phosphates			
Apatite	OH - apatite	1.4	
		1.9	
		2.8	
		3.0	
	F - Cl apatite	2.80	
		3.47	
		4.00	
		4.20	
Silicates			
Olivine		0.86 - 0.92	
		1.05 - 1.07	Not currently covered
		1.23 - 1.29	Not currently covered
Pyroxene	Mg - Fe	0.91 - 0.94	
		1.14 - 1.23	Not currently covered
		1.80 - 2.07	
	Ca - Mg - Fe	1.2	Not currently covered
		2.0	

Feldspar	Na - Ca	1.1 - 1.29	Not currently covered
Phyllosilicate	e.g. saponite	1.35	
		1.8	
		2.3	
		2.8	
	e.g. serpentine	1.4	
		1.9	
		2.2	
		2.9	
		0.7	
		0.9	
		1.1	Not currently covered

5.3.1 Characterising composition and mineralogy of primitive asteroids

A characterisation of the composition and mineralogy of the primitive asteroids (C-complex, some X-complex, D-type, and potentially L-/K-type) remains unconstrained [166]. This is in part due to the fact that the surfaces of these asteroids contain abundant opaques (e.g. amorphous carbon), which leads to the spectra of these asteroids types being, for the most part, featureless. However, the primary problem with characterising the composition and mineralogy of primitive asteroids using VNIR spectroscopy is that almost all VNIR spectroscopic studies to date have been limited to ground-based observations. The few absorption features observed in primitive asteroids are associated with water and/or hydration (either chemically or physically absorbed), which are contaminated by atmospheric water in ground-based observing campaigns.

5.3.1.1 0.7 and 3 μm features

Two notable absorption features associated with primitive asteroids are the 0.7 μm and 3.0 μm features. These features are commonly observed in CM chondrites

as well as C-complex and M-type asteroids [167, 168, 169, 170, 171]. The 0.7 μm feature is not obscured by atmospheric water, but what compositional information it constrains is still an open question. This feature is often associated with phyllosilicates and attributed to Fe^{2+} - Fe^{3+} intervalence charge transfer [167, 168]. Regardless of its association with phyllosilicates, the 0.7 μm feature is not currently used as a diagnostic of phyllosilicate mineralogy or composition.

The 3 μm feature is, in many cases, a complex blend of several different features. The 3 μm band is associated with hydration and is due to a combination of possibilities: hydroxyl (OH), water ice, and water/hydroxyl associated with phyllosilicates [172, 173, 174, 175, 176, 177, 178, 170, 179]. The shape of this feature is dependent on the composition. For example, OH has band positions between 2.7 - 2.8 μm that vary based on the associated composition (i.e., OH in hydrated minerals) [172]. An OH-only 3 μm feature will have a sharp absorption drop off near 2.7 μm that transitions to a near-linear return to the continuum level for wavelengths long-ward of the feature minimum. Some studies have shown that the location of the OH band minimum in carbonaceous chondrites is an indicator of phyllosilicates and of the degree of aqueous alteration experienced [173, 175, 177, 180]. A 3 μm feature due entirely to water ice, on the other hand, will have a broader, more bowl-shaped minimum region [176, 179]. The water ice 3 μm feature is a composite of three absorption bands due to molecular vibrations located at near 3.0, 3.1, and 3.2 μm that shift slightly in wavelength location depending on whether the ice is crystalline or amorphous and as a function of temperature [176]. Additional to the contributions from water and hydroxyl, hydrated minerals, such as the phyllosilicates, also have spectral absorptions near 3 μm with band positions that vary based on mineral species and composition.

The large diversity of 3 μm band shapes and centres is used to divide the NIR spectra of asteroids with a 3 μm feature into four spectral groups (the sharp, or 'Pallas'-like, rounded or 'Themis'-like, 'Ceres'-like, and 'Europa'-like) [180], and divide the spectra of CM and CI chondrites into three spectral groups, with band positions tenuously associated with degree of alteration and composition of the phyl-

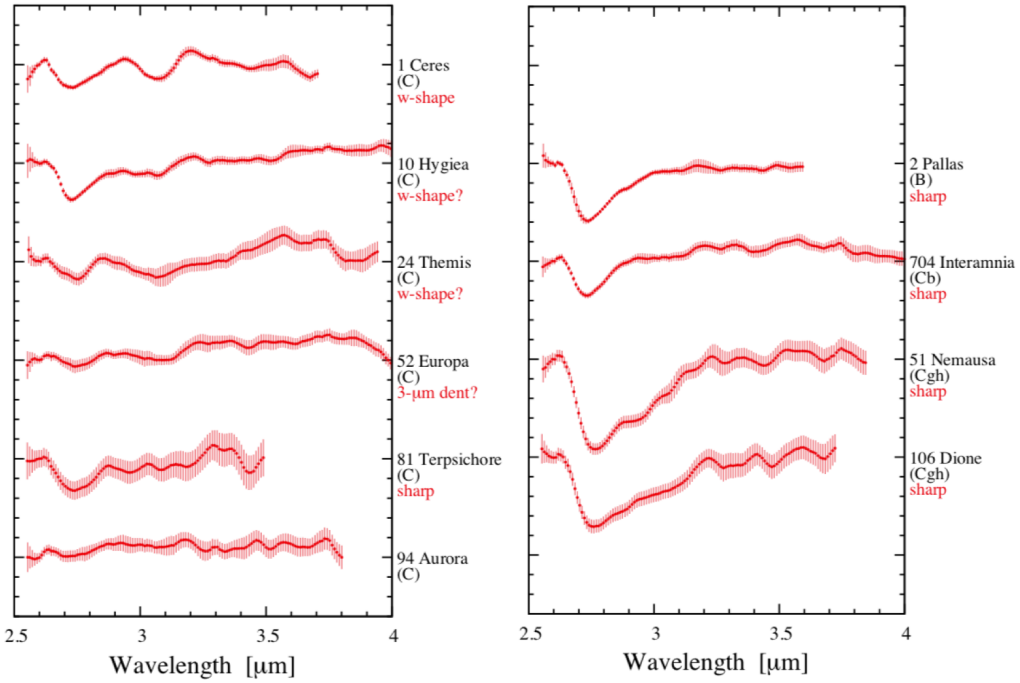

Figure 5.6: Infrared spectra obtained by AKARI for a number of small bodies highlighting the variety of spectral fatures in the 2.5-3 μm region. Figure reproduced from [2].

losilicate serpentine [179]. The relationship between these two groups is still not understood, and there have been no meteorite spectral matches to the 'Ceres'-like, 'Pallas'-like, or 'Europa'-like asteroid spectral groups [179, 180]. Examples of different 3 μm features as seen by AKARI are shown in Figure 5.6. The potential to resolve the problem will greatly benefit from spectral data sets of primitive asteroids obtained by a space-based telescope, such as Twinkle, coupled with further laboratory measurements of hydrated minerals and carbonaceous chondrites.

5.3.1.2 The 3.2 - 3.6 μm organics feature

The spectrum of C-complex asteroid 24 Themis exhibits a feature spanning 3.2-3.6 μm that has been associated with organic material on the surface [178, 170]. This feature is blended with the strong 3 μm absorption. By fitting a spectral model to the 3 μm feature which includes water ice coated pyroxene grains intimately mixed with amorphous carbon, [170] were able to extract the residual 3.2 - 3.6 μm feature. [170] use shape and position of the residual feature to suggest the presence

of organic material with CH_2 and CH_3 functional groups. However, an additional feature centred near 3.3 μm, indicative of aromatic hydrocarbons, may be required to provide a decent spectral match.

Currently, 24 Themis and 65 Cybele [181] are the only asteroids with spectroscopically confirmed detections of organics. Asteroid 24 Themis is the largest fragment in a large dynamical family of over 1600 asteroids located near 3.2 AU from the Sun [182] with indications that a significant percentage of them have the 0.7 μm feature implying aqueous alteration [183]. Several other studies also suggest that the Themis family has a variety of compositions, based on a large, observed NIR (1 - 2.5 μm: [184, 185]) and mid-infrared (5 - 14 μm: [181]) spectral diversity . This makes the Themis family a likely candidate to search for organics via an absorption near 3.3 - 3.6 μm. The largest (diameters 50 - 100 km) Themis family members are observable with high SNR for relatively short exposure times, making this group of asteroids targets of interest for Twinkle that could extend the number of detections of organics and our knowledge of organics in the asteroid belt. Additionally, the Themis family contains three of the newly discovered Main-Belt Comets (e.g. [186, 187, 89]), where a full 0.4 - 4.5 μm spectrum uncontaminated by atmospheric water would significantly benefit small bodies science.

5.3.1.3 Additional hydration features

The 1.4 and 1.9 μm features are of use in terrestrial studies, but have yet to be detected in asteroids, which is likely due to the presence of opaques and blocking by atmospheric water [172]. The 1.4 μm feature is the first overtone of the OH-band at 2.7 - 2.8 μm discussed previously. The 1.9 μm feature is a combination of water ice bending and OH stretching modes. While these features have yet to be observed in the NIR spectra of asteroids, they are expected to be present in asteroid spectra that exhibit a strong 3.0 μm feature. Twinkle's position as a space-based telescope offers the opportunity to provide the first detections of these features.

The 2.2 and 2.4 μm features are OH combination bands that generally appear in pairs [188], and so they are considered together here. These features are commonly used in Earth and Mars spectral studies to identify phyllosilicates, and they

have band centre positions that are diagnostic of Al and/or Mg composition [189]. They have been tenuously identified in some CM chondrites and as weak features in a few CI chondrites, but thus far there have only been tentative detections in asteroid spectra [171, 190, 191]. Given Twinkle's ability to obtain high SNR IR spectra for asteroids that show features related to OH, and its position above Earth's atmosphere, Twinkle has a high potential to identify these compositionally diagnostic features for C- and X-complex asteroids.

5.3.2 Composition of Comet Comae

Comets are considered to be reservoirs of some of the most primitive material in the Solar System. They formed out beyond the H_2O frost-line where ices can condense and become incorporated into growing planetesimals. As such, they contain a plethora of volatile ices, organics, and silicate material that has remained relatively unaltered since the comet forming epoch. This 'pristine' quality makes comets an ideal object to study to understand the origin and evolution of our Solar System. As discussed below, Twinkle will be able to observe the comae of these comets to detect water-ice, water-vapour, CO_2, and organics, all of which will add to our understanding of comets and the origins of water and organics in our Solar System.

As a comet nucleus approaches the Sun, the ices near the surface begin to sublimate, liberating material from the surface to form a temporary thin atmosphere of gases and dust (i.e., a comet coma). NIR observations of comet comae frequently reveal the gaseous phase of cometary volatiles: primarily H_2O vapour, but also as CO_2 and CO gas (e.g. [192, 193, 194]). However, over the past decade, there has been a growing number of detections of water-ice (at 2.0 and 3.0 μm) in the comae of comets made either with in-situ spacecraft measurements or ground-based measurements [195, 196, 192, 193, 194, 197, 198, 199]. Characterising the composition, size, and structure of these ice grains is a newly-emerging field in cometary science. This could be accessible with Twinkle and it offers the ability to increase our understanding of the initial stages of planet formation, the structure of the early solid grains in the Solar System formation, and the outer disk environmental conditions of the pre-protoplanetary disk of gas and dust.

In addition to the water-ice features, Twinkle has the opportunity to also detect water vapour (2.7 μm), organics (3.3 - 3.6 μm), and CO_2 (4.3 μm) as emission features in the comae of comets [200, 201, 202]. Measurements of the 4.3 μm CO_2 feature can be used to derive CO_2 abundances in comets. In turn, the abundance of CO_2 in comets constrains cometary formation and is the driver of activity on comets, especially at large heliocentric distances that are external to the frost-line. As atmospheric CO_2 heavily obscures the 4.3 μm feature, ground-based studies are unable to observe this feature, and the total number of comets with observed CO_2 features and derived abundances is small. Hence, Twinkle, as a space-based observatory with NIR spectral coverage capable of observing this feature, can potentially provide a highly valuable resource to the cometary science community. The Large Synoptic Survey Telescope (LSST) is expected to discover $\sim$10,000 comets, some of which will be entering the inner Solar System for the first time. Characterising these pristine objects, as well as short period comets which have undergone surfaces changes, would allow for a deeper study of comet evolution.

5.3.3 Composition and Mineralogy of S-complex and V-type asteroids

VNIR spectroscopy spanning 0.4 - 2.5 μm of the stony type asteroids (S-complex and V-type), with mafic mineral compositions primarily of pyroxene and/or olivine, are not strongly impeded by atmospheric water, and therefore there have been numerous spectroscopic studies of these types of bodies. The majority of these studies are performed using the SpeX instrument on the IRTF. Twinkle offers an additional resource to the small bodies community to acquire VNIR spectra of stony asteroid surfaces and provide complimentary data. However, Twinkle's current design may limit the characterisation of these stony asteroids as discussed in Section 5.3.3.1.

5.3.3.1 The 1.0 - 1.3 μm spectral gap

Twinkle's current design has a spectral gap between the visible and infrared spectrometers at 1.0 - 1.3 μm. Twinkle is currently in a Phase B design review and thus the instrument characteristics are being reassessed. If a channel that covers the 1.0 -

1.3 μm region were included, the following types of studies would become possible with Twinkle:

- **Characterisation of S-type asteroids to establish links to meteorite analogues.** A major goal of VNIR spectroscopic studies of asteroids is to establish meteorite analogue connections. This requires both high quality remote sensing data of asteroids, from a platform such as Twinkle, and several laboratory measurements of meteorites including reflectance spectra and a mineralogical analysis of the meteorites via methods such as electron microprobe or x-ray diffraction. Previous investigations have been successful in establishing such connections.

- **Identification of ordinary chondrite parent bodies.** Another key objective of spectral studies of asteroids is to identify a meteorite analogue, and in cases where a strong link exists between meteorite type and asteroid type, to leverage that information to identify asteroid families that could represent the parent bodies of those meteorites. Identification of such parent bodies extends our knowledge of the thermal structure of our protoplanetary disk, and of how each of the different OC meteorite groups formed. Hence, using Twinkle to obtain spectra of S-type asteroids in an effort to identify ordinary chondrite parent bodies would add significantly to our understanding of planetary formation, thermal history and evolution of protoplanets, and the dynamical evolution of the Solar System during the protoplanetary disk epochs.

- **Characterisation of Stony Asteroids** is limited by the spectral gap. Asteroids with mafic sciliates, olvine and pyroxene on their surfaces have two prominent absorption features near 1 and 2 μm (Figure 5.7) that are diagnostic of silicate mineralogy and composition [203] [204, 205, 206, 207, 208]. These two features, often referred to as Band I and Band II for the 1 and 2 μm bands, respectively, are commonly used to determine mineralogy (olivine-to-pyroxene ratio) and composition (molar percent Fe in olivine and pyroxene) of S-complex and V-type asteroids via band parameter analysis studies (e.g.

[209, 207, 210, 208, 211, 59, 212, 213, 214]).

- **Rotational variability.** The purpose and promise of rotationally-resolved spectra of asteroids in order to investigate surface heterogeneity is discussed for all asteroid types in Section 5.3.4.

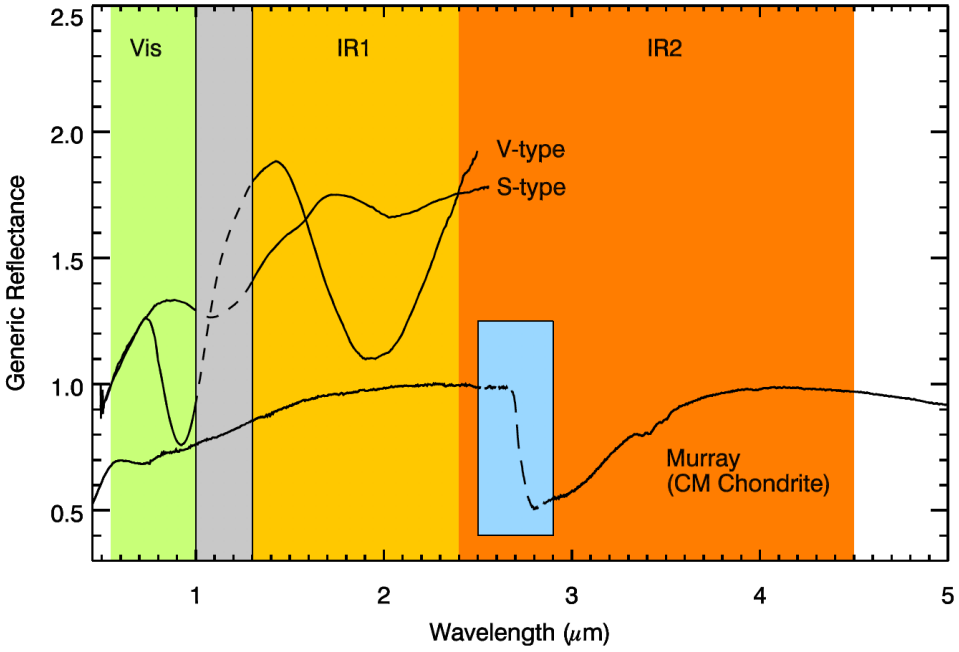

Figure 5.7: Example spectra of potential targets plotted over the visible (Vis) and two near-infrared (IR1, IR2) channels of Twinkle. The CM Chondrite, Murray, is representative of primitive, hydrous asteroids. The 0.7 μm and 3.0 μm features associated with hydrated primitive asteroids (see Section 5.3.1) are apparent in the spectrum of Murray. The small blue inset window represents the 3 μm portion of the spectrum obscured by Earth's atmosphere. The Earth's atmosphere can also obscure the spectrum near 1.4 and 1.9 μm (not shown). The generic S- and V-type asteroid spectra (from [210]) exhibit the 1 and 2 μm bands used to determine mafic mineralogy and compositions (see Section 5.3.3). The vertical grey bar highlights the spectral gap from 1.0 - 1.3 μm in the current Twinkle design. The spectrum for Murray was acquired from the RELAB database [5].

5.3.4 Rotationally Resolved Spectral Data Sets

Based on the exposure time estimates from Figure 5.1 and asteroid brightness from Figure 5.3, Twinkle will be able to obtain rotationally resolved spectra for a large number of Main Belt asteroids and some NEOs. Spectral variability is expected for asteroids due to a number of effects, including space weathering, composition

and grain size heterogeneity, thermal effects, and viewing aspect (i.e. phase angle of observation). Constraining any of these as the cause of spectral variability offers a tremendous opportunity to further our knowledge on the processes governing the formation and evolution of asteroids. For example, consider an S-type asteroid, which, as evidenced by experiments, is susceptible to changes in VNIR spectral slope and Band I parameters (depth, centre, and area) due to space weathering by irradiation and micrometeorite impacts [215, 216]. If subsurface material is brought to the surface via an impact event or rotational fission event (i.e., mass-shedding), this 'fresher' material, that has not been processed by space weathering, will have different spectral characteristics than the rest of the regolith on the surface, which would lead to spectral variations as a function of rotation. If detected, this would provide a valuable dataset to understand the rotational evolution and potential disruption of asteroids as well as how space weathering proceeds in different parts of the Solar System.

To date, rotational variability in VNIR spectra of asteroids has been observed from in-situ spacecraft measurements for 951 Gaspra, Ida and Dactyl by Galileo [217, 218], 433 Eros by NEAR [149], 4 Vesta from the Dawn spacecraft [219] and ground-based observations [220], as well as for a handful of NEOs. There have also been suggestions of spectral variability due to surface heterogeneity for other asteroids, but it is likely that these variations are caused by observational effects, such as viewing aspect or poor observing conditions, or different methodologies in data reduction methods [208, 210]. However, as mentioned previously there are many reasons to expect spectral variability on the surfaces of asteroids. Therefore, it is likely that the dearth of confirmed spectral variations due to surface heterogeneity is a result of the reliance on ground-based facilities for VNIR spectroscopy of a large population of asteroids. Considering the relatively short exposure times needed to acquire high signal to noise spectra with Twinkle, and its position as a space-based observatory, Twinkle could be an ideal telescope to conduct rotationally resolved spectral studies.

5.4 Conclusions

In this chapter, Twinkle's capabilities for small bodies science have been explored. I have shown the observatory will have the capability to acquire high SNR spectra for a large variety of asteroid types including a vast number within the Main Belt. Spectra at Twinkle's highest resolution and with SNR>100 could be obtained for asteroids brighter than $M_v = 12$ in <300 seconds. Combining multiple observations, or reducing the observational requirements, will allow many fainter objects to be characterised.

With respect to potential impact, Twinkle's strongest contribution to small bodies science could be the opportunity to investigate the composition of the primitive asteroids that exhibit features associated with hydration (water ice, hydroxyl, and phyllosilicates), which to date, is an area that has been severely limited due to atmospheric water contamination in ground-based observations. Twinkle also offers the opportunity to study of stony (S-complex and V-type) asteroids. Finally, with respect to asteroid science, Twinkle offers the potential to be the best resource to study rotational variation in spectra of asteroids, which is difficult to do with ground-based telescopes due to Earth's atmosphere generating spectral variations similar to what is expected for asteroids.

Additionally to asteroid science, Twinkle will have the capability of investigating the comae of bright comets, providing valuable data sets on CO_2 production and the presence of water-ice and organics in the comae. Therefore, Twinkle potentially provides a resource that would push our understanding of asteroids and comets, and hence the formation and evolution of the Solar System, well beyond its current state.

Chapter 6

Current Exoplanet Observations from Space

> ”With increasing distance, our knowledge fades, and fades rapidly. Eventually, we reach the dim boundary, the utmost limits of our telescopes. There, we measure shadows, and we search among ghostly errors of measurement for landmarks that are scarcely more substantial. ”
>
> Edwin Hubble

Transit light curves have proved a valuable technique for constraining the bulk and orbital parameters of exoplanets. Additionally, by observing at different wavelengths, the atmosphere of the planet can be probed, revealing the thermal structure and chemical composition. During transmission spectroscopy, light passes through the planetary limb and is absorbed or scattered by the atoms, molecules and condensates present. This interaction imprints a wavelength-dependent variation on

Contributions: The majority of the data reduction and analysis presented in this chapter has been conducted by myself but this work has not yet formed a formal publication. Angelos Tsiaras and Quentin Changeat have also contributed to this work.

the transit depth. While detections of the chemical composition have been carried out from the ground, in the last decade existing space-based instruments have been utilised to great effect. However, these instruments were not designed for studying exoplanets and thus have a number of limitations in sensitivity, wavelength coverage and systematic noise.

This chapter focuses on the use of this data. Spitzer observations from the literature are shown before the analysis of data from Hubble is described and results presented, highlighting its great capability for detecting water. Finally, the benefits, and issues, of combining data from multiple instruments are discussed.

6.1 Spitzer

Spitzer's Infrared Spectrograph (IRS) was one of the first instruments used to attempt to observe the atmospheres of exoplanets and the emission spectra of HD 209458 b found several features but these could not be matched to molecules [221]. IRS was then also used to observe the eclipse of another hot-jupiter, HD 189733 b, but the data was noiser than expected and the analysis was unable to say anything about the chemical composition of the atmosphere [222]. Subsequently another Spitzer instrument, the Infrared Array Camera (IRAC), took measurements of the transit of HD 189733 b and three photometric bands at 3.6, 5.8 and 8 μm were used in infer the presence of water [62, 223]. Further eclipse observations with IRS and IRAC then allowed for water to be distinguished in the emission spectra [224].

Since the end of the cold mission in 2009, only the 3.6 and 4.5 μm bands have been functional. Nevertheless, Spitzer IRAC has been used to study numerous exoplanets through transit and eclipse photometry although the two bands are not utilised simultaneously. A major issue in the analysis of Spitzer data has been the instrument systematics. The study of the atmospheres of transiting exoplanets requires a photometric precision, and repeatability, of around 100 ppm. This is beyond the original calibration plans of Spitzer, creating a necessity to disentangle the instrumental systematics from the astrophysical signals in raw datasets. Initial models of these systematics meant that different teams achieved discrepant results

with [225] refuting the claimed water detection in HD 189733 b. Further observations were taken with the Spitzer IRAC 3.6 μm band wherein the authors derived noticeably different planetary parameters to their original study, even though the same extraction method was used [226]. All these analyses attempted to correct instrument systematics by fitting parametric models, each of which is somewhat subjective. [227] proposed applying a non-parametric method to IRAC and used algorithms based upon Independent Component Analysis (ICA) to attempt to correctly extract the atmospheric signal. This method has the advantage of not making assumptions about the structure of the unknown systematics but often led to larger uncertainties on the extracted signal. Attempts to correct Spitzer data are still ongoing and recently a new method was proposed which reconstructs the stellar baseline during the transit. By training a probabilistic Long Short-Term Memory (LSTM) network to predict the next data point of the light curve during the out-of-transit, a transit-free light curve could be constructed. This is then used to normalise the actual light curve, without making assumptions about the instrument [228].

Observations using 6 broadband channels on the Spitzer Space Telescope claimed the first detection of a thermal inversion in the atmosphere of HD 209458 b [229, 230]. These results were attributed to the presence of a high-altitude absorber, the leading candidates being TiO and VO in the temperature regime of HD 209458 b. Evidence for the inversion was based upon the relatively high fluxes of the 4.5 and 5.8 μm channels compared with the 3.6 and 8.0 μm channels. However, when fitting occultation observations, not only are the molecular constituents free parameters but a T-P profile that varies with altitude must also be fitted. Such a large number of free parameters, and so few data points, can easily lead to over-fitting. Later observations of HD 209458 b showed no signs of a thermal inversion, suggesting that high-precision spectrophotometric observations are required to robustly infer thermal structures [231].

In other fields, eclipses have proven to be a powerful tool for "spatially resolving" distant objects and have long been utilised for studying binary stars and accretion disks [232, 233]. As the target of interest passes behind another object,

sections of the target are gradually masked, and later unmasked, providng a scan of surface. Theoretical studies for eclipse scanning presented the potential for characterising exoplanet atmospheres [234, 235] and have since been realised with Spitzer observations. [236] used the 8 μm channel of IRAC and found that the eclipse of HD 189733 b could not be explained by the occulation of a uniformly-bright disk. They therefore deduced that the atmosphere must have a large-scale hot spot and were able to produce a global distribution of the planet's brightness.

Spitzer has also been used to obtain a number of photometric phase curves. HD 189733 b was the testbed for one of the first phase curves and analysis of IRAC 8 μm data found that energy from the irradiated dayside is efficiently redistributed throughout the atmosphere [237]. Later observations at 3.6 and 4.5 μm were also taken which found that the minimum and maximum brightness temperatures were earlier then expected for an atmosphere in radiative equibrium, leading to claims of non-equilbirum chemistry on HD 189733 b [237]. A phase curve of the hot Super-Earth 55 Cnc e discovered that the peak emission was offset from the substellar point, a finding which was consistent with either an optically thick atmosphere or a planet devoid of an atmosphere but with low viscosity magma flows on the surface [64]. Additionally, recent Spitzer phase curves revealed the absence of a thick atmosphere on LHS-3844 b [65]. The planet, which has a radius of 1.3 $R_{\odot}$, had no observed phase variation and a day-side brightness temperature of 1040 K. The analysis ruled out atmospheres with surface pressures above 10 bar while thinner atmospheres would be unstable due to erosion by stellar wind.

Therefore, the analysis of Spitzer data has been a major challenge for the field and, given that JWST is using similar detectors, one can expect future missions to have their own peculiarities. Nevertheless, Spitzer has provided a vast amount of data for exoplanet science, helping researchers gain insights into distant worlds.

6.2 Hubble WFC3

WFC3 was installed on Hubble in May 2009 during the fifth, and final, Hubble servicing mission and, during the same operation, the STIS instrument was also

revived 5 years after an electronic failure rendered it inoperable. WFC3 has since been used extensively for transit and eclipse spectroscopy. Initially, transit spectra were collected in the standard Hubble staring mode (e.g. [51, 238, 239]). While these observations were successful in characterising the atmospheres of a number of planets, the brightness of the host stars meant a fast saturation time. At the time, most known planets were around bright stars and thus there was a limited choice of targets. The fast readout time also meant the SNR of the observations was relatively low. The addition of the spatial scan mode changed this, allowing Hubble to spread the stellar light in the cross-dispersion direction and thus increase the exposure time. However, the standard Hubble WFC3 pipeline is unable to reduce these images and thus new pipelines had to be developed.

One such pipeline is Iraclis [240]. Unlike staring spectra, spatially scanned spectra are affected by dispersion variations across the scanning direction, while also suffering from inclined spectra. Furthermore, scanning-mode observations include positional shifts that are an order of magnitude stronger than staring-mode observations. Iraclis has been designed to minimise these effects by including alternative calibration and extraction techniques. For instance, the coordinate system utislised in Iraclis is along the wavelength/scanning axes instead of the x/y axes of the detector. Iraclis starts with the raw images and performs a number of reduction steps. These include calculating the zero-red flux, accounting for detector non-linearity, the subtraction of dark current and sky background and correcting for gain variations, bad pixels and cosmic rays. The Iraclis software is open-source and available through GitHub[1].

Here we use Iraclis to analyse the Hubble scanning data collected for HAT-P-11 b which was first studied with WFC3 G141 in 2012. Although two observations were taken, one was unusable. The resultant spectrum is shown in Figure 6.1 along with the best fit solution from the atmospheric retrieval using Tau-REx [241]. The retrieval confirmed the presence of water (H_2O) and, as the posterior plot in Figure 6.2 shows, also suggests the presence of ammonia (NH_3) and carbon dioxide (CO_2).

[1] https://github.com/ucl-exoplanets/Iraclis

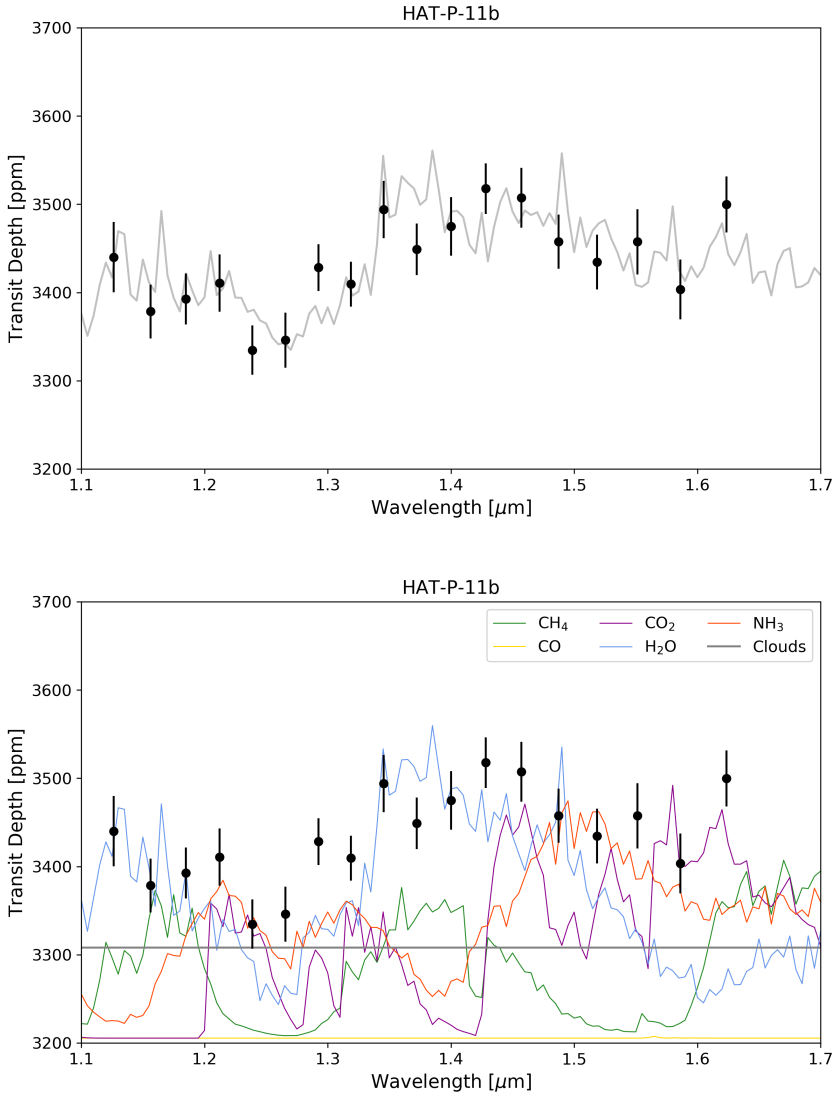

Figure 6.1: Best fit spectrum and molecule contributions for the WFC3 G141 observation of HAT-P-11 b.

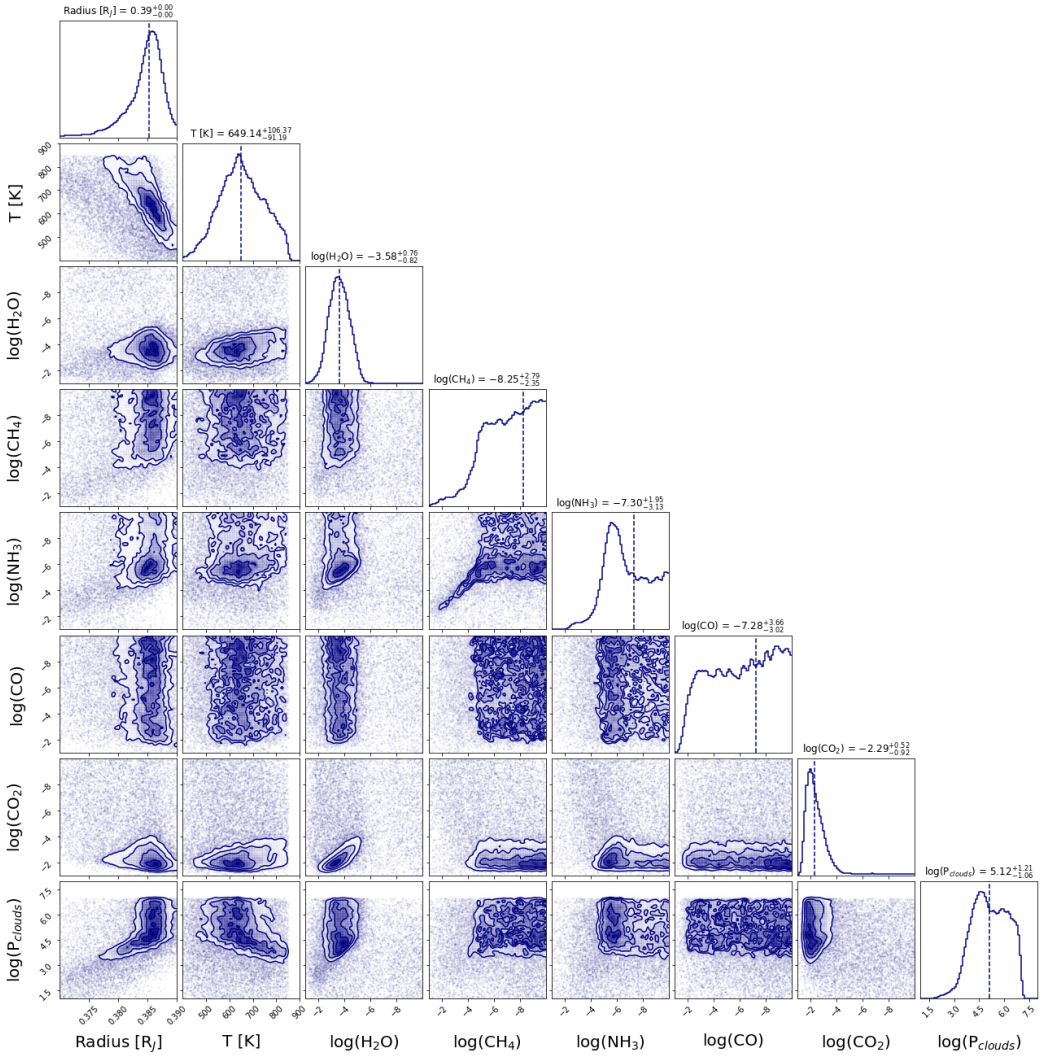

Figure 6.2: Posteriors distributions for the WFC3 G141 observation of HAT-P-11 b.

While the detection of water is likely to be robust thanks to the strong feature which occurs in the centre of the Hubble G141 wavelength range, the indicated presence of carbon dioxide is less reliable. The feature which leads to Tau-REx recovering carbon dioxide is based largely on the two data points around 1.6 μm which are at the edge of the instruments sensitivity. These data points are thus less reliable and the narrow wavelength range does not allow the whole of any feature due to carbon dioxide to be covered. A robust confirmation of the presence of molecules other than water would, for this planet, require a wider spectral coverage. The recovered abundance of carbon dioxide is also suspect (1 part per hundred).

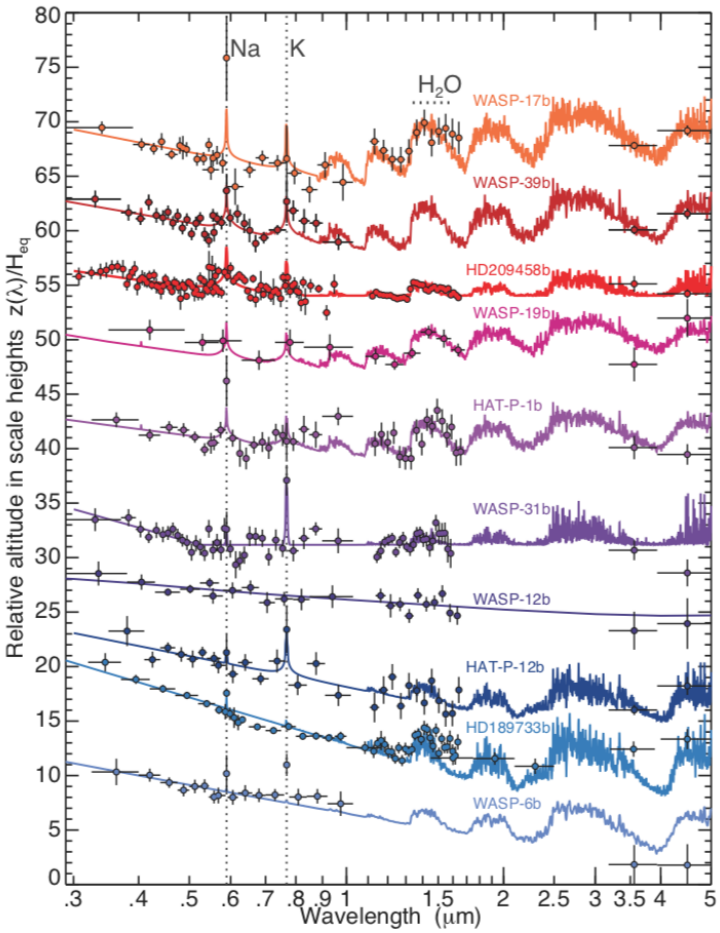

Figure 6.3: The study of ten hot jupiters, achieved by combining data from Hubble and Spitzer, by Sing et al. [3]

6.3 Combining Instruments

Due to the narrow wavelength coverage of current facilities, combining observations from different instruments has become the norm. Figure 6.3 shows a classic example of this: the study of ten hot-jupiters with Hubble STIS and WFC3 as well as Spitzer IRAC 1 and 2 [3]. While achieving a greater wavelength coverage is appealing, there are several underlying issues with such approaches. The first is that these observations are not simultaneous. Given that both the star and planet are likely to exhibit temporal variations this presents an obvious issue. Due to the quality of the data, the planet variation is likely to be of minor importance but stellar activity, particularly the presence and frequency of occulted and unocculted star spots poses a more serious concern (see e.g. [242]).

Additionally, instrument systematics could cause offsets in the recovered transit depth. If one is only analysing data from a single instrument, this offset will only have the effect of increasing the fitted planet radius. However, if multiple instruments are combined, each exhibiting different offsets (which are unknown to the observer), the data sets are then incompatible. Fitting the light curves as part of the retrieval can reveal this but cannot currently offer corrections for it and no study conducted thus far has checked the compatibility [243]. If the wavelengths of the combined instruments overlap, this can help to stitch together the observations. Unfortunately this does not necessarily provide the perfect solution to broadening the wavelength coverage.

HAT-P-11 b was also observed by Spitzer and Fraine et al. [17] combined these observations, along with 208 Kepler light curves, with the Hubble WFC3 observation. The study, which fitted the data via grid models instead of a Bayesian retrieval, concluded that HAT-P-11 b had a clear, water-rich atmosphere. Later analysis by [15], using only the Hubble data, confirmed the presence of water. Additionally, having been studied by Hubble WFC3 with the G141 grism, HAT-P-11 b was also observed with less frequently utilised G102 grism. These have some overlap and thus provide an opportune way of gathering spectroscopic data across 0.8-1.8 μm. Hence this new data has been analysed, again using Iraclis and Tau-REx.

While only 1 transit with G141 was taken, five were obtained with G102 to increase the SNR. Each of these was analysed with the same methodology as previously described resulting in the spectra shown in Figure 6.4. Immediately recognisable is the offset of one observation and inspection of the white light curve depths shows a large variation for this transit. The white light curves should, in theory, have the same depth and, as transit spectroscopy is a differential measurement, normalisation is required before combining observations. Therefore, the spectra had their white light curve depths subtracted from them. To normalise the spectra, an averaged value for the white light curves was then added. Next a weighted average was taken of these spectra to produce the final dataset which is also displayed in Figure 6.4.

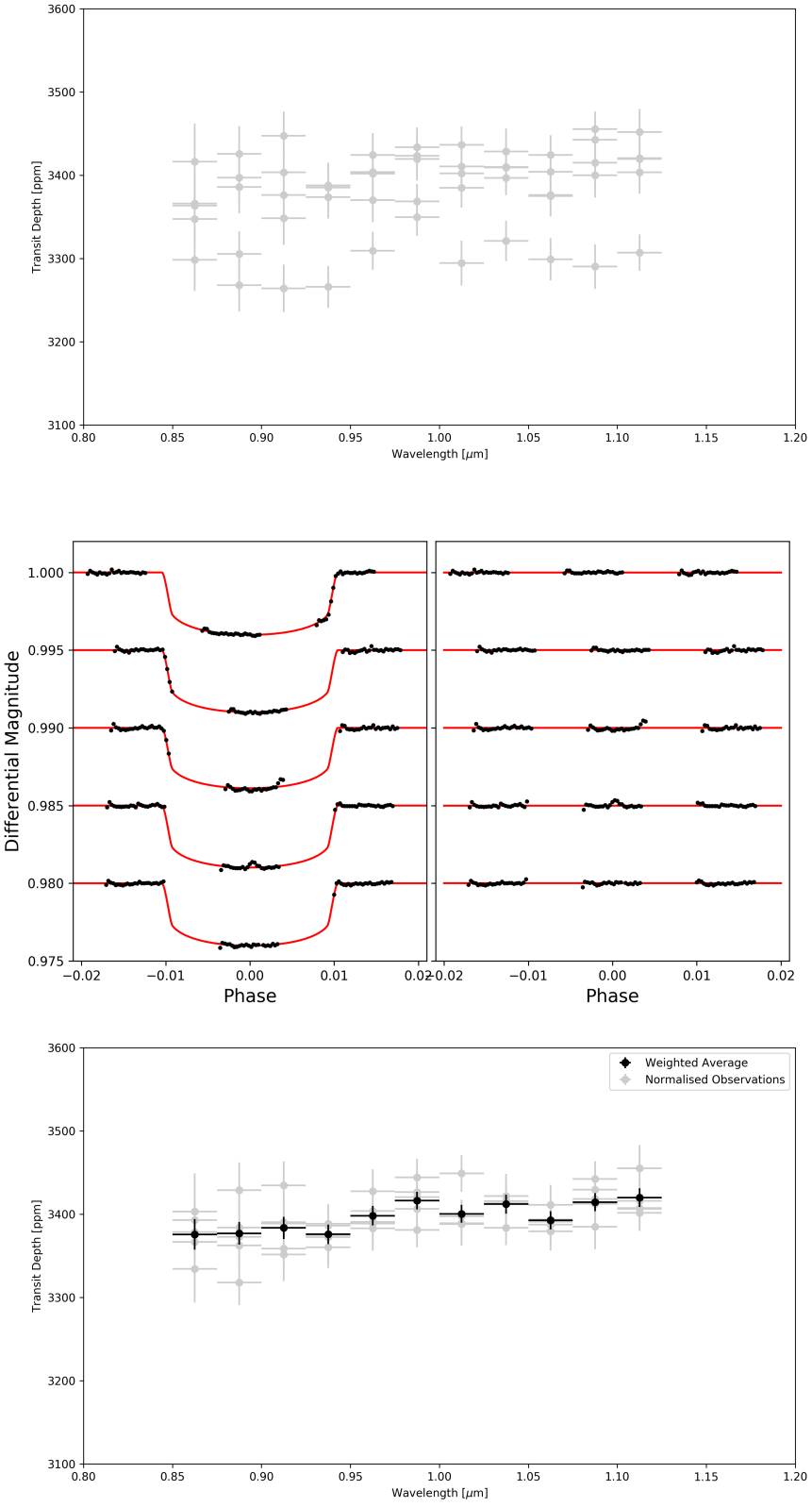

Figure 6.4: Top: Initial spectra from five Hubble WFC3 G102 transits. Middle: Fitted white light curves for each observation. Bottom: Normalised spectra and a weighted average spectrum of the five observations. The normalised spectra were achieved by subtracting the associated white light curve depth from each observation and adding an averaged white light curve depth.

This normalised and averaged spectrum was combined with that taken from G141 and this, along with the best fit solution from the previously discussed retrieval, is shown in Figure 6.5. When retrievals on the combined spectra are attempted, Tau-REx struggles to fit the data without an exceedingly large temperature (see Figure 6.6). The difficultly experienced fitting the data may well be due to stellar activity. HAT-P-11 is known to be active and to exhibit spots at two latitude locations [244, 245, 246]. Due to the high obliquity of its orbit, HAT-P-11 b transits these regions and thus has been seen to occult stellar spots [247, 248, 249, 250]. While some spot crossings can be seen in the light curve, and thus attempts can be made to account for them, unocculted star spots leave no obvious tracer but do cause an offset in the transit depth. The effect is wavelength dependent and could cause a slope offset of the order of 20ppm [251].

Therefore the methodology of normalisation applied here, which is the standard in the field, may not be adequate for this system. Further attempts to fit the data will try to fit an offset between the two Hubble spectra, caused by stellar activity, or to model out the stellar activity from the light curves themselves. This was recently achieved via machine learning methods for simulated Ariel data. Additionaly, the method developed by [243] of including light curves directly in the retrievals many be useful for determining whether the datasets are compatible. A recent paper analysed data from both Hubble WFC3 grisms as well as Spitzer IRAC and Hubble STIS observations of HAT-P-11 b. [252] found features which indicated water and/or methane in the Hubble spectra. However, the retrievals they performed on the Hubble data, fitting for radius, temperature, atmospheric metallicity and the C/O ratio, could not match the Spitzer transit depths. The time between the first and last observations for this study was nearly 6 years and the authors used ground-based monitoring of HAT-P-11 with a Cousins R filter to infer the spot coverage. Finally, the cloud model used here is a simple opaque layer and more complex models, such a Mie clouds [253], which have a wavelength variability, may well help to fit the data.

Another planet which has been studied with both Hubble grisms is WASP-121

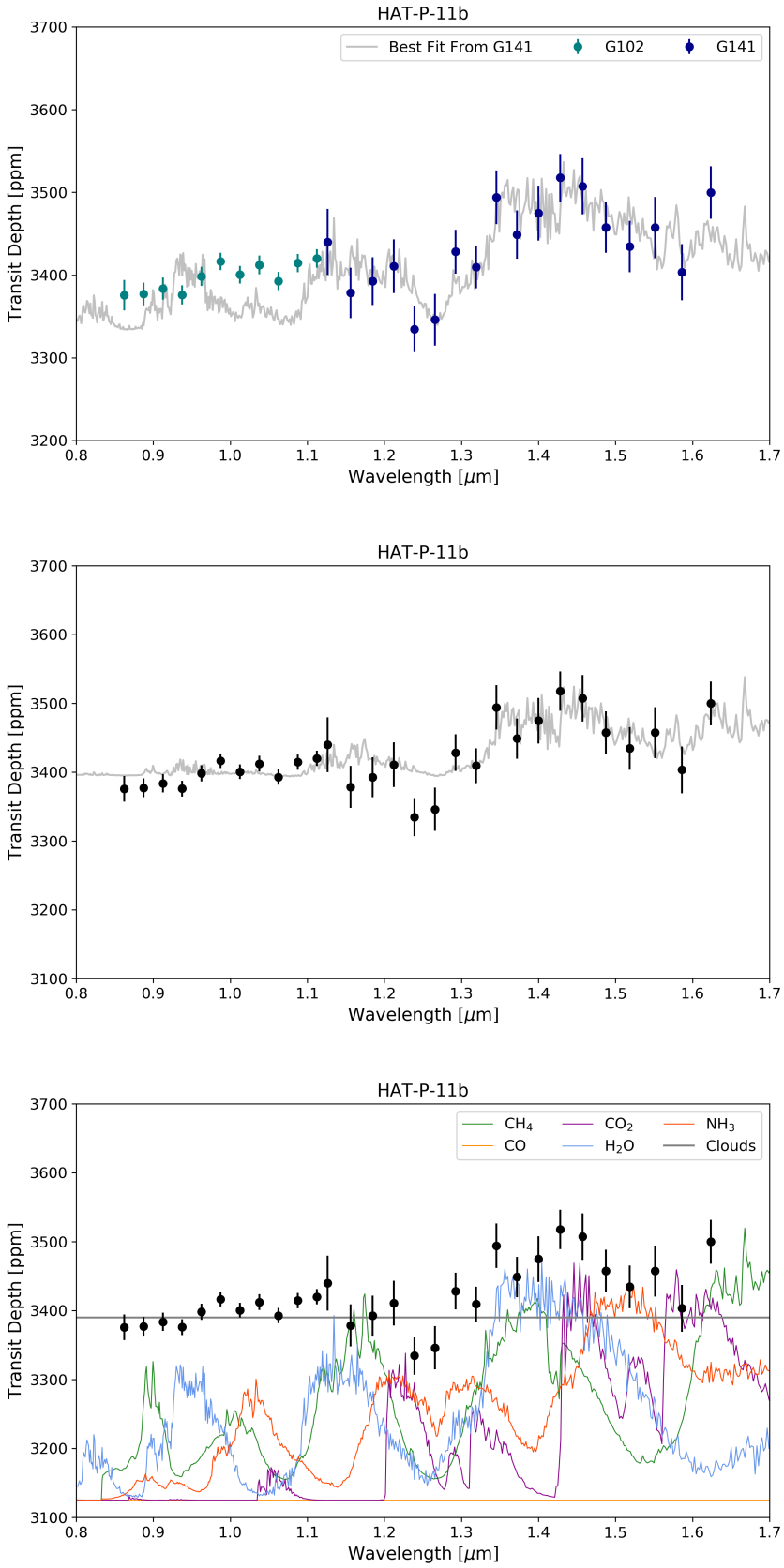

Figure 6.5: Top: Best fit spectrum from G141 of HAT-P-11 b, plotted behind the new data from G102, highlighting a poor fit to the new data. Middle: Best fit from the Tau-REx retrieval using data both grisms. Again the fitting is poor. Bottom: Molecular contributions for the brest-fit solution to both datasets.

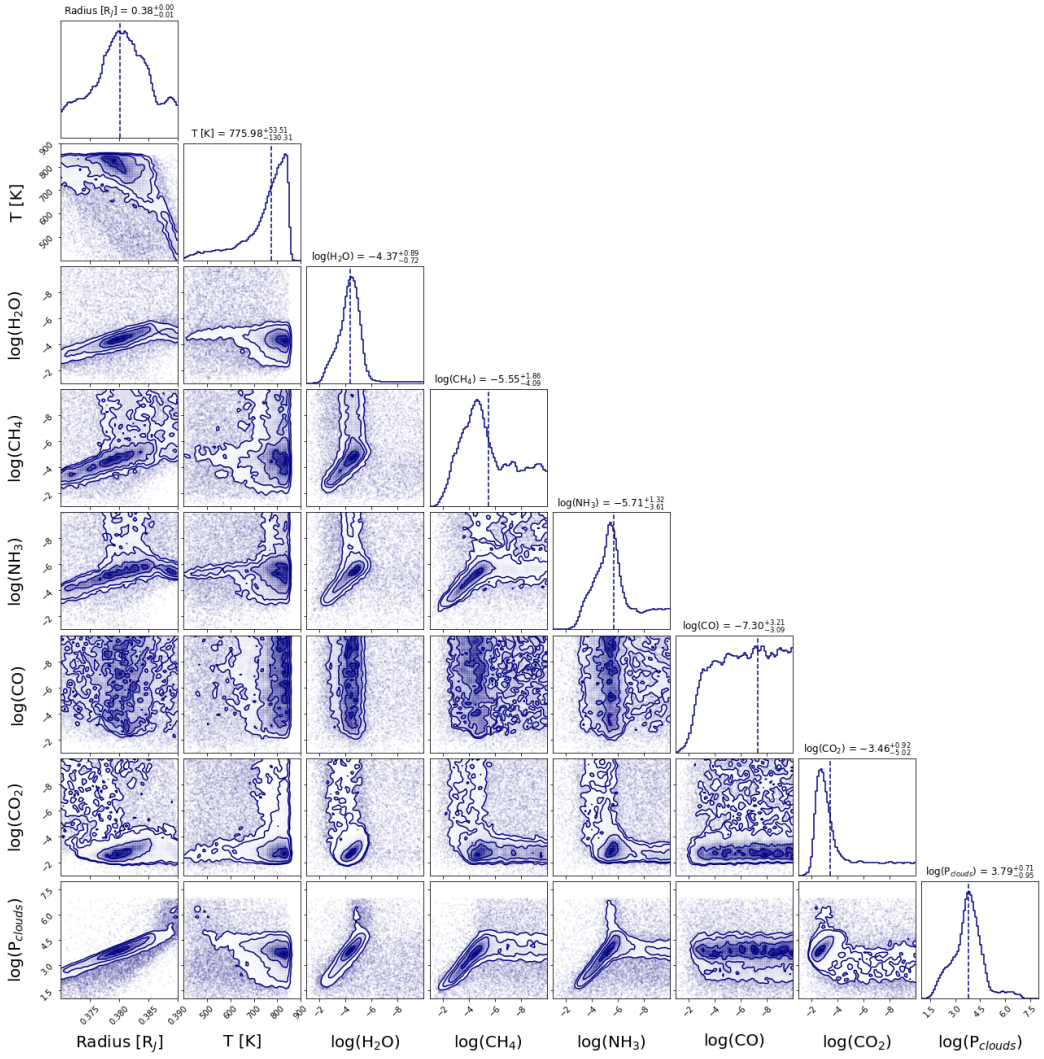

Figure 6.6: Posteriors for retrieval of HAT-P-11 b using both Hubble grisms. The final solution tends to temperatures which are far higher than the expected equilibrium temperature ($\sim$850K).

b, a hot-jupiter. However, unlike HAT-P-11 this planet was studied in emission. A single observation was taken with G141 and two with G102. Again Iraclis was used to reduce the data with a weighted average of the two G102 observations being taken to create the spectrum shown in Figure 6.7. The best fit model from TauREx suggests an atmosphere containing Vanadium Oxide (VO) as well as water (see Figure 6.8) which agrees with literature analysis of both the transmission and emission spectra [15, 254, 255]. Here, the star is far less active and, as emission spectra are generally less affected by stellar contamination [16], the two datasets provide an excellent probe into the nature of the planet.

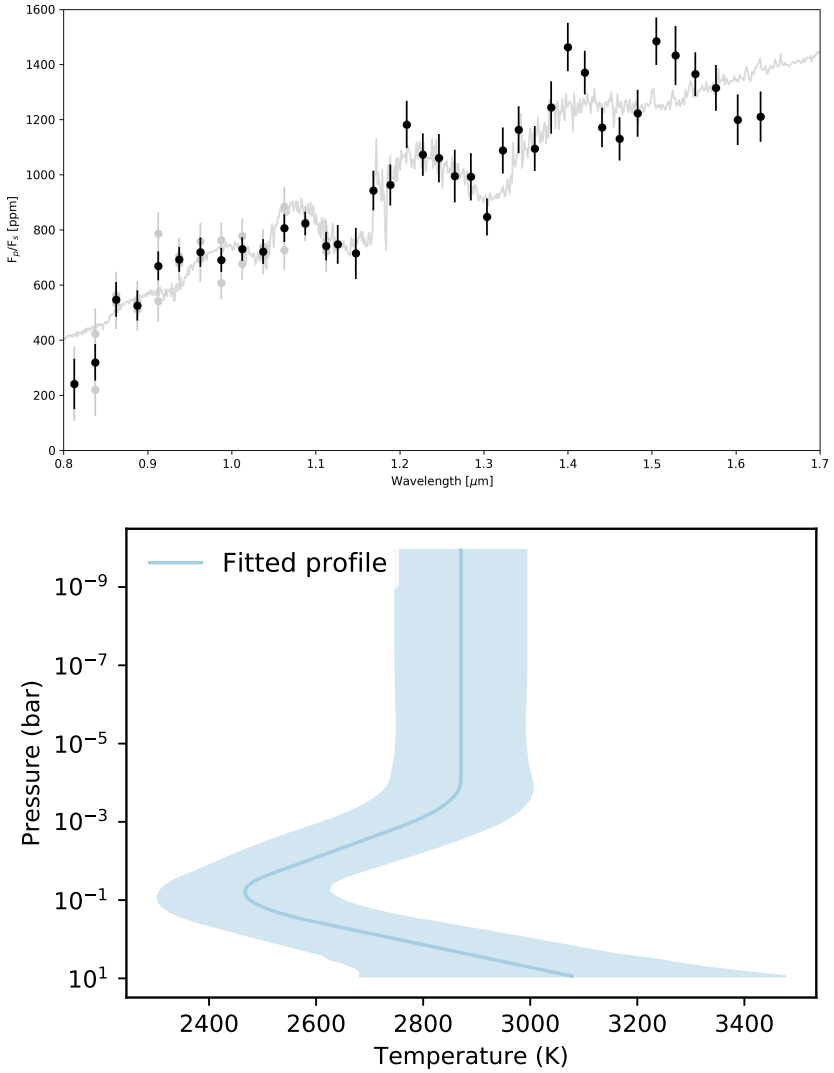

Figure 6.7: Top: Hubble spectrum for WASP-121 b and best fit solution from Tau-REx. Bottom: Retrieved temperature-pressure profile which suggests a thermal inversion in the atmosphere.

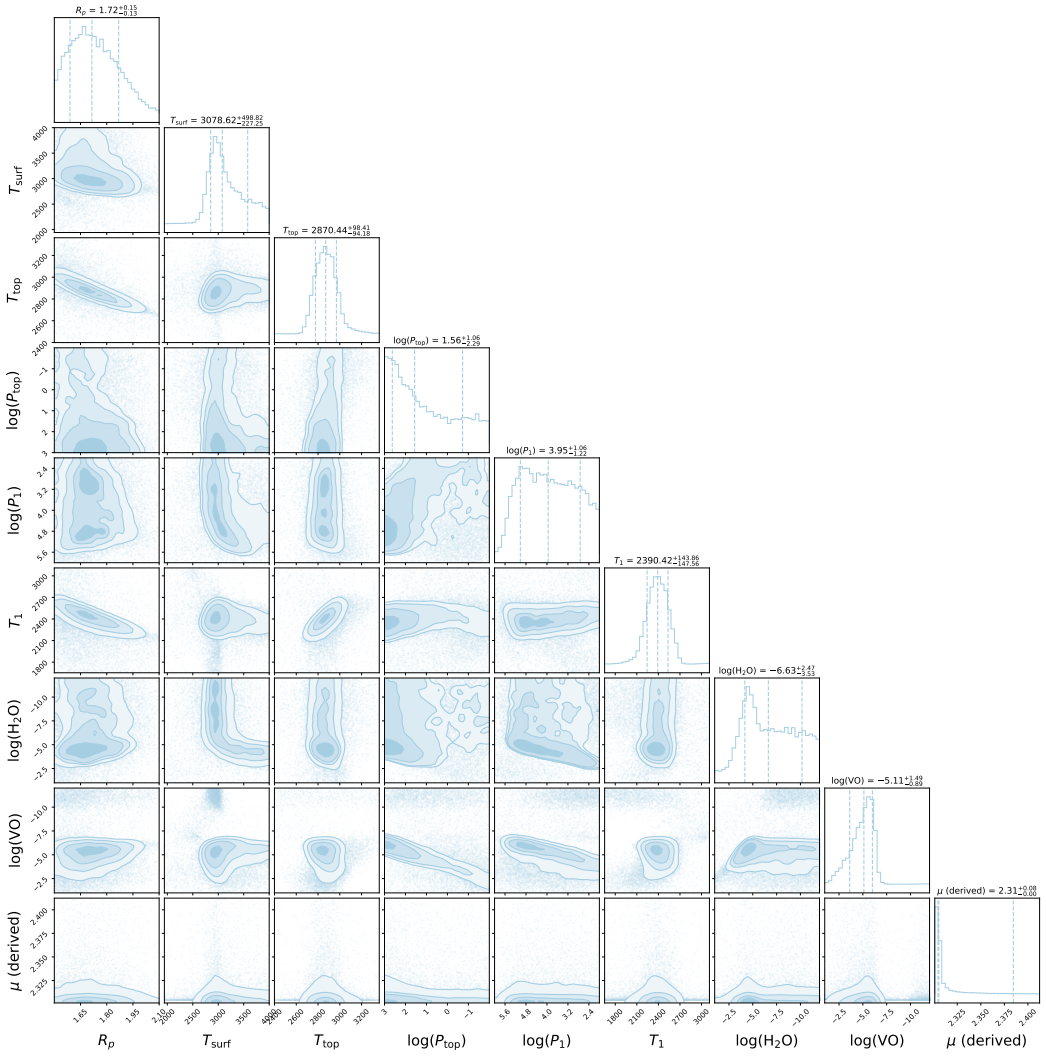

Figure 6.8: Posteriors from Tau-REx for the emission spectrum of WASP-121 b with Hubble grisms G102 and G141.

6.4 Conclusions

Space-based telescopes have provided the first true insights into the nature of extrasolar planets. With these facilities, numerous molecules have been detected. The wavelength coverage of WFC3 has been particularly successful at discovering water which has been found to be abundant in planets of all sizes. However, these instruments were not designed for exoplanet science and thus the data has several limitations, namely the narrow wavelength coverage which has led observers to combine data from multiple instruments. While this increases the spectral range there are potentially issues of incompatibility and studies are ongoing to understand

how the data analysis is affected by differing stellar activities or instruments systematics. Although any given observation can be subject to an offset via unocculted spots, future instruments which gather data over a wide wavelength range in a single observation will not be affected by differing offset between instruments. Hence, acquiring the data in one visit will help ensure that features seen within the spectra come directly from the planetary atmosphere.

Chapter 7

Modelling The Performance of Future Space-based Telescopes

> ”The chief contribution of such a radically new and more powerful instrument would be, not to supplement our present ideas of the unverise we live in, but rather to uncover new phenomena not yet imagined ”
>
> Lyman Spitzer

JWST, Twinkle and Ariel will perform spatially unresolved observations of exoplanets at various positions in their orbits around their host stars (it should be noted that JWST will also be capable of directly imaging planets, e.g. [118]). The stellar and planetary signals are gathered simultaneously with the planet signal comprising only a tiny fraction of the total. Differential measurements, that is observations with, and without, the planetary contribution, allow for this signal to be disentan-

Contributions: The creation of Terminus has been led by myself with the guidance of Giovanna Tinetti, Marcell Tessenyi, Giorgio Savini and Ian Stotesbury. A paper is in preparation. ExoWebb has been developed by myself with the help of Pierre-Olivier Lagage, Rene Gastaud and Ahmed Al-Refaie and a publication is planned. The development of ArielRad has been led by Lorenzo Mugnai and I have contributed to this and the accompanying paper (Mugnai, Edwards, et al., ArielRad: The Ariel Radiometric Model).

gled. Such measurements permit the observer to determine the transmission, reflection and emission spectrum of the exoplanet atmosphere.

During the development of an instrument, understanding the expected performance is critical to ensuring an optimal design or, at least, one which is capable of meeting the mission requirements within the technical and budgetary specifications. In the early phases of the design, simulations which are equivalent to back-of-the-envelope calculations, with many assumptions and simplifications, can prove the basic feasibility of the idea. As the design progresses and is refined, so too are the instrument models with various types used and required.

Static models, often referred to as radiometric or sensitivity models, are suitable for studying the instrument performance over a wide parameter space (i.e. for many different targets) as they are generally quick and require only rudimentary information about the instrumentation. These usually account for efficiency of the optics and simple noise contributions such as dark current, readout and instrument/telescope emission. Such a radiometric model was developed by Puig et al [256] for the Exoplanet Characterisation Observatory (EChO, [257]) to simulate the signal received in two cases: before/during/after primary transit, where the planet crosses the face of the star, and before/during/after secondary transit, also known as eclipse or occultation, where the planet passes behind the star.

More complex effects, such as jitter, stellar variability and spots, and correlated noise sources, require models which have a time-domain aspect. These also usually produce simulated detector images which can act as realistic data products for the mission, accounting for detector informaties such as correlated noise between pixels or inter- and intra-pixel variations. For example, ExoSim is a numerical end-to-end simulator of transit spectroscopy which is currently being utilised for the Ariel mission [258]. The tool has been created to explore a variety of signal and noise issues that occur in, and might bias, transit spectroscopy observations, including instrument systematics and the other effects previously mentioned. By producing realistic raw data products, the outputs can also be fed into data reduction pipelines to explore, and remove, potential biases within them as well as develop new reduction or

data correction methods. End-to-end simulators such as ExoSim are therefore powerful tools for understanding the capabilities of an instrument design. Additional time-domain simulators of note are MIRISim, for the JWST MIRI instrument, and Wayne which models Hubble spatial scans of exoplanets [259].

While the complexity of these types of tools can be hugely advantageous in understanding intricate effects, it can also be their biggest weakness. Such sophisticated models require a great deal of time to develop and run as well as an excellent understanding of all parts of the instrument design. They can therefore only be applied to highly refined designs and run for a small number of cases. The solution to the issue of complexity versus efficiency is to use both types of models. For Ariel, ExoSim is used to validate the outcomes of ArielRad (the Ariel Radiometric model [260]) for selected, representative targets. ArielRad is then used as the workhorse for modelling the capability of thousands of targets due to its superior speed.

Here, the creation and use of radiometric simulators is explored. The model from Puig et al. has been adapted and enhanced for modelling the performance of Ariel, Twinkle and JWST. These newer radiometric models (ArielRad [260], ExoWebb [261], and Terminus [262]) share many of the same features and capabilities. In this chapter the methodology behind these models is explained. All these models require planetary and stellar parameters as inputs and so creation of a catalogue of planets is discussed. Then the underlying assumptions and calculations of all these radiometric models are defined as is the need for a time-domain capability for Twinkle simulations.

7.1 Creation of Catalogue of Exoplanets

With over 4000 exoplanets currently detected, there are certainly many potential targets for atmospheric characterisation. However, in the time till the launch of JWST, Twinkle and Ariel, many more planets are expected to be discovered. To understand exactly how many potential targets each of these missions will have, a catalogue of known and predicted exoplanets was created.

7.1.1 Known Exoplanets

Exoplanetary data was downloaded from NASA's Exoplanet Archive in order to account for all confirmed planets before being filtered such that only transiting planets were considered. However, the major exoplanet catalogues are sometimes incomplete and thus an effort has been made to combine them (for a review of the current state of exoplanet catalogues see [263]).

Hence, the data was verified, and in some cases gaps filled, utilising the Open Exoplanet Catalogue [264], exoplanet.eu [265] and TEPCat [266]. Planets not included in the NASA Exoplanet Archive were not added to the analysis to ensure that only confirmed planets were utilised.

Unknown parameters, which are required for the radiometric models, were inferred based on the following assumptions:

- If the inclination, i, is known, the impact parameter is calculated from:

$$b = \frac{a\cos(i)}{R_*} \tag{7.1}$$

  where R_* is the host star radius and a is the semi-major axis.

- Else, it was assumed that $b = 0.5$ (i.e. the midpoint of the equator and limb of the star)

- Planetary effective temperature (T_p) is estimated from:

$$T_p = T_* \left(\sqrt{\frac{1-A}{\varepsilon}} \frac{R_*}{2a} \right)^{1/2} \tag{7.2}$$

  where T_* is the host star temperature and a greenhouse effect of $\varepsilon = 0.8$ and a planetary albedo of $A = 0.3$ ($T_P < 700$ K) or $A = 0.1$ ($T_p > 700$ K) are assumed [267, 268]

- Planetary mass (M_p) was estimated utilising Forecaster [269].

- Atmospheric molecular mass was assumed to be 2.3.

7.1.2 Future Planet Discoveries

TESS and other surveys are predicted to discover thousands of planets around bright stars. In the first two years of operation, TESS is anticipated to detect over 4500 planets around bright stars and more than 10,000 giant planets around fainter stars [4]. Here, these predicted TESS discoveries around brighter stars are incorporated into the analysis to highlight the capabilities of upcoming instruments to study anticipated future discoveries. The MAST archive[1] has been utilised to obtain stellar parameters for these planets by cross-referencing the Gaia catalogue. The first planets from TESS have begun to be discovered [e.g. 85] but these were separated from the other currently-known planets to avoid overlap with the predicted yield. The known and predicted exoplanets were compiled into a single dataset ($\sim$7000 planets) which has been used to provide an indicative look at the number and type of planets that could be observed. Figure 7.1 displays the location of currently-known planets and predicted TESS detections.

Potential discoveries by other surveys (PLATO, CHEOPS, SPECULOOS etc.) have not been included as, while predictions for these surveys have resulted in an estimate of the number of expected detections, no specific target coordinates and characteristics have been released. When such information becomes available, predicted/real detections from these surveys will be incorporated into this analysis. In any case, these surveys are expected to find thousands of planets which could be suitable for study, enhancing the population of planets from which the final target lists of the missions are selected. Hence, although these predicted yields have not been included, planets found by these surveys will be added to the sample as they are detected. Note that some simulations include only the currently-known planets to highlight the interesting discoveries made by TESS thus far.

7.2 Building A Radiometric Model

All the radiometric models presented here use the same basic assumptions and techniques which are described in the following sections.

[1] https://archive.stsci.edu

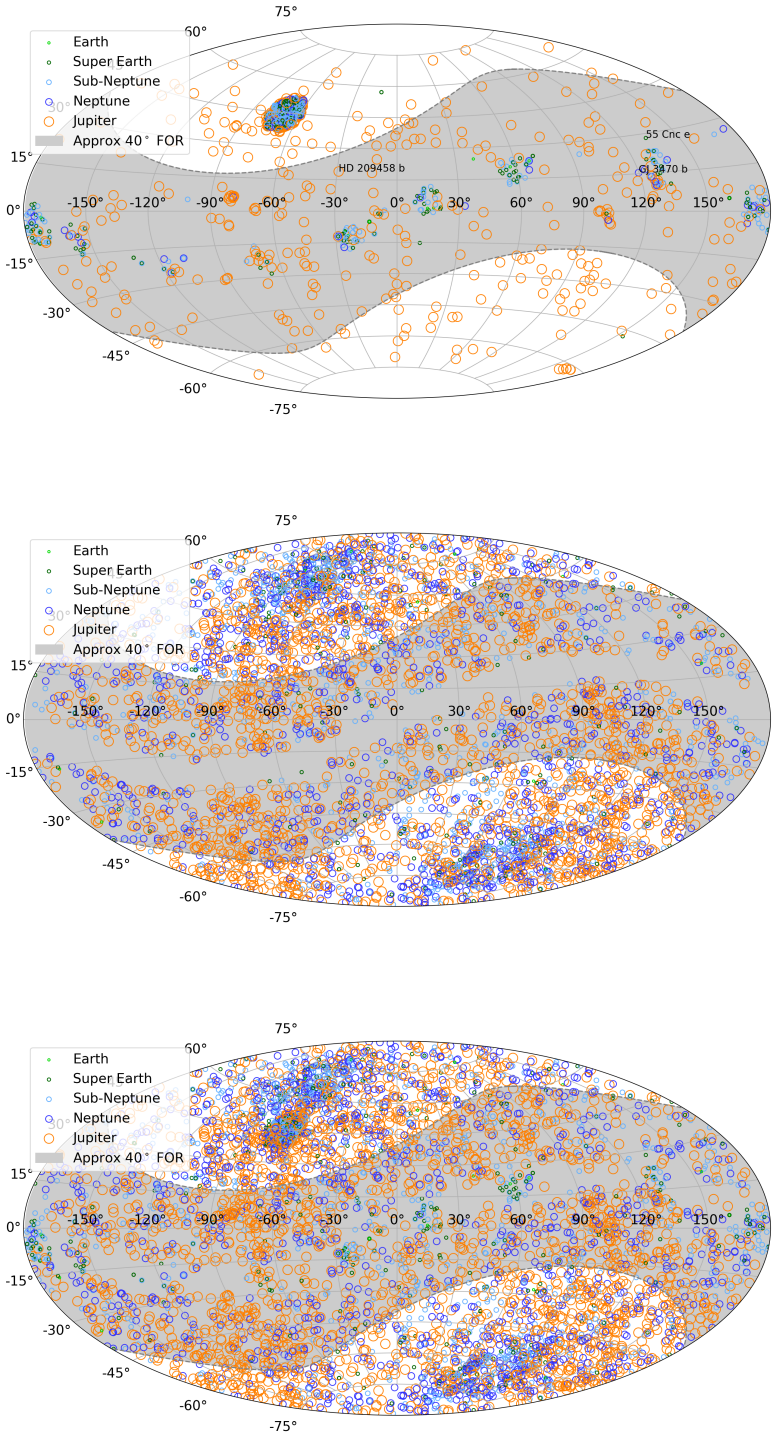

Figure 7.1: Top: Currently-known transiting exoplanets (excluding those discovered by TESS), their planetary classification and the sweep of Twinkle's field of regard. The initial Kepler field is the densely populated region at RA -70°, Dec 45° and the locations of some well-known exoplanets are noted. JWST and Ariel will have constant visibility of the ecliptic poles with a partial visibility of the whole sky at lower latitudes. Middle: Predicted TESS planet detections. Bottom: Currently-known planets and predicted TESS detections

7.2.1 Signal Calculation

Information about the target planet and its stellar host is loaded from the catalogue of transiting planets described in Section 7.1. Stellar emission is modelled by spectral energy distributions (SEDs) from the Phoenix atmospheric models [270]. The spectral irradiance from a host star at the aperture of the telescope is given by:

$$E_S(\lambda) = S_S(\lambda)(\frac{R_*}{d})^2 \tag{7.3}$$

where $S_S(\lambda)$ is the star spectral irradiance from the Phoenix catalogue ($\mathrm{Wm}^{-2}\mu\mathrm{m}^{-1}$) and d is the distance to the star. The effective collecting area of the telescope is then accounted for before the flux is integrated into the spectral bins of the instrumentation to give a photon flux per bin. The signal is then propagated through the instrument to the detector focal planes, taking into account the transmission of each optical component and the dispersion of the prism spectrometers as well as the quantum efficiency of the detectors. This provides a final signal, in electrons per second, from the star in each spectral bin. A variety of sources of noise are accounted for in each of the models. In addition to photon noise, dark current, readout noise, Zodiacal background emission, instrument and telescope emission, and jitter noise can be added. Some of these are wavelength dependent (e.g. Zodiacal background) while others are not (e.g. read noise).

As the duration of a transit/eclipse is generally orders of magnitude longer than the saturation time of the detector, many destructive readouts will be taken during an observation. The total noise variance per exposure, σ^2_{exp}, is given by:

$$\sigma^2_{exp} = \frac{12(n_g-1)}{n_g(n_g+1)} n_{pix}\sigma^2_{read} + \frac{6(n_g^2+1)}{5n_g(n_g+1)}(n_g-1)t_g i_{total} \tag{7.4}$$

from [271] where n_g is the number of groups (non-destructive reads) per exposure, σ_{read} is the read noise in e^-/pix rms, n_{pix} is the number of pixels in the spectral bin and t_g is the time for a single read. In the standard Terminus and ArielRad setup, correlated double sampling (CDS) is used (n_g =2) while ExoWebb automatically maximises the number of groups (up-the-ramp reads) that can be obtained before

detector saturation. This is the standard practice for JWST observations and can be used to help correct for cosmic ray impacts. Adding more up-the-ramp reads reduces the read noise but increases the photon noise contribution. As JWST will be photon noise limited for exoplanet observations, this technique slightly increases the noise per integration. i_{total} is the total flux in e^-/s and is defined as:

$$i_{total} = i_{sig} + n_{pix}(i_{dark} + i_{bdg}) \tag{7.5}$$

where i_{sig} is the total signal from the star in the spectral bin (e^-/s) while i_{dark} and i_{bdg} are the dark current and background signals respectively (in e^-/s/pix). The maximum integration time is set by the duration of a transit/eclipse event, T. Each model assumes the time spent during ingress (T_{12}) and egress (T_{34}) is negligible to the primary transit time (T_{23}) and thus T = T_{23} = T_{14}. The transit time can be calculated from:

$$T_{14} = \sqrt{1-b^2}\frac{R_* P}{\pi a} \tag{7.6}$$

for a given system where P is the orbital period. The error on the star signal over one transit duration is then given by:

$$\sigma_{Star} = \frac{1}{\sqrt{n_{int}}}\frac{\sigma_{exp}}{i_{sig}} \tag{7.7}$$

where n_{int} is the number of integrations over one transit duration which is calculated from:

$$n_{int} = \frac{T_{14}}{n_g * t_g i_{total}} \tag{7.8}$$

The measurement of the transit depth is a differential and thus the error on the transit depth is given by:

$$\sigma_{TD} = \sigma_{Star}\sqrt{1+\frac{1}{n_{T_{14}}}} \tag{7.9}$$

where $n_{T_{14}}$ is the number of transit durations observed out of transit (i.e. the baseline). For all simulations presented here, $n_{T_{14}}$ is set to 1.5 (i.e. 0.75 x T_{14} is spent before/after the main observation). This error is calculated for every spectral bin.

ArielRad assumes the sum of the detector reset times is negligible compared to the transit/eclipse time (i.e. $T_{Integration} \approx T_{14}$) while ExoWebb and Terminus account for a reset time.

7.2.2 Atmospheric Signal

7.2.2.1 Transit

During transit, the critical signal is the fraction of stellar light that passes through the atmosphere of the exoplanet. This is determined by the ratio of the projected area of the atmosphere to that of the stellar disk and thus is given by:

$$\frac{2R_p\Delta z(\lambda)}{R_*^2} \tag{7.10}$$

where Δz is the height of the atmosphere. The size of the atmosphere is taken to be equivalent to the height above 'sea-level' at which the pressure/density can be considered to be negligible. The pressure of an atmosphere at a height, z, as a fraction of that at 'sea-level' is given by:

$$p(z) = p_0 e^{\frac{-z}{H}} \tag{7.11}$$

where H is the scale height, the distance over which the pressure falls by 1/e. The model by Puig et al. assumes $\Delta z = 5H$ (at which point one is above 99.5% of the atmosphere). The scale height of the atmosphere is calculated from:

$$H = \frac{kT_pN_A}{\mu g} \tag{7.12}$$

where k is the Boltzmann constant, N_A is Avogadro's number, μ is the mean molecular weight of the atmosphere and g is the surface gravity determined from:

$$g = \frac{GM_p}{R_p^2} \tag{7.13}$$

where M_p and R_p are the mass and radius of the planet and G is the gravitional constant.

7.2.2.2 Eclipse

During eclipse, the signal is calculated form two sources; reflected and emitted light from the planet. Emission from the exoplanet day-side is modelled as a black body and the wavelength-dependent surface flux density is given by:

$$S_p(\lambda, T_p) = \pi \frac{2hc^2}{\lambda^5} \frac{1}{e^{\frac{hc}{\lambda k T_p}} - 1} \tag{7.14}$$

where T_p is the planet temperature. The product of the black body emission and the solid angle subtended by the exoplanet at the telescope gives the spectral radiance at the aperture:

$$E_p^{Emission}(\lambda, T_p) = S_p(\lambda, T_p) \left(\frac{R_p}{d}\right)^2 \tag{7.15}$$

in $Wm^{-2}\mu m^{-1}$. Additionally, a portion of the stellar light incident on the exoplanet is reflected. The strength of this reflected signal is strongly dependant on wavelength and can be significant at visible wavelengths. The flux of reflected light at the telescope aperture is calculated from:

$$E_p^{Reflection}(\lambda) = \alpha_{geom} S_s(\lambda) \left(\frac{R_*}{d}\right)^2 \left(\frac{R_p}{a}\right)^2 \tag{7.16}$$

where a is the star-planet distance (i.e. the planet's semi-major axis) and α_{geom} is the geometric albedo, which is assumed to be that of a Lambertian sphere ($\frac{2}{3}\alpha_{bond}$), wavelength-independent and at a phase of $\phi = 1$ (i.e. full disk illumination).

7.2.2.3 Signal to Noise Ratio

From these equations, and the error on the transit/eclipse depth, the signal to noise (SNR) on the atmospheric signal can be obtained. By setting a requirement on the SNR, the number of observations, and type of observation, needed for a given planet can be ascertained. For the purposes of most of the work presented here, an average SNR of 7 was assumed as a necessity to facilitate the characterisation of the atmosphere's molecular composition.

Opacity	Reference
H_2-H_2	[276, 277]
H_2-He	[278]
H_2O	[279, 280]
CH_4	[281, 282]
C_2H_2	[283]
HCN	[284]
NH_3	[285]
CO	[286]
CO_2	[287]
TiO	[288]
VO	[289]
PH_3	[290]
SiO	[291]
SO_2	[292]
H_2S	[293]

Table 7.1: List of the opacities used within Tau-REx for the atmospheric models presented here.

7.2.2.4 Atmospheric Modelling and Retrieval

Determining the composition of exoplanetary atmospheres, and thus gaining an understanding of the atmospheric properties, provides insight about the processes occurring on these planets.

To simulate emission and transmission forward models and atmospheric retrievals, the open-source exoplanet atmospheric retrieval framework Tau-REx [272, 241] has been used. This assumes a plane parallel atmosphere with 100 layers and includes the contributions of collision-induced absorption (cia) of H_2-H_2 and H_2-He, Rayleigh scattering and grey-clouds. Cross-section opacities calculated from the ExoMol database [273] where available, and from HITEMP [274] and HITRAN [275] otherwise, are also utilised. A list of opacities used can be found in Table 7.1.

Convolving the outputs of Tau-REx with those of a radiometric model provides a powerful data product: a simulated observation of an exoplanet atmosphere. This ”observed” spectrum can then be inserted into Tau-REx in retrieval mode, where the software attempts to fit the data and thus recover the input atmospheric parameters. The ability of Tau-REx to fit the data, and retrieve accurately the molecular

abundances and thermal structure of the atmosphere, can be used as a more meaningful measure of the data quality than the SNR. However, such analysis can be time consuming and the results are of course dependent upon the assumed atmospheric chemistry as well as the priors used for the retrieval. Therefore it is prudent to use the SNR calculation to prove an instrument's capability for a large number of targets while providing simulated data, and retrievals, for a small number of typical planets.

7.2.3 Modelling Light Curves

Observatories in low Earth orbits (e.g. Hubble, CHEOPS, Twinkle and an ever increasing number of cubesats) cannot always be continuously pointed at a target due to Earth obscuration. For transit, or eclipse, spectroscopy this causes gaps in the light curve, which reduces the information content and can diminish the science return of the observation. Terminus was developed to model the occurrence of these gaps to predict the potential impact on future observations. Terminus is currently base-lined on the Twinkle Space Telescope but the model can be adapted for any space-based telescope and is especially applicable to those in a low-Earth orbit.

The variance on a single observation is calculated from Equation (7.4) and is used to generate noisy light curves for each of the spectral bins. These noisy light curves are then fitted with a Markov Chain Monte Carlo (MCMC) algorithm to produce a spectrum complete with error bars. Prior to this, the gaps due to Earth obscuration can be added.

For fainter targets, a spectrum with a reduced resolution can be requested and Terminus will combine the light curves and provide a spectrum with a resolution as close to the desired as possible. While the default cadence is set by the saturation time of the detector it can lowered or exposures can be combined. Additionally, multiple transits (or eclipses) can be individually modelled, fitted and then combined.

Finally, once a spectrum has been generated, Tau-REx is then used to fit the data and retrieve the atmospheric parameters. This process is graphically summarised in Figure 7.2.

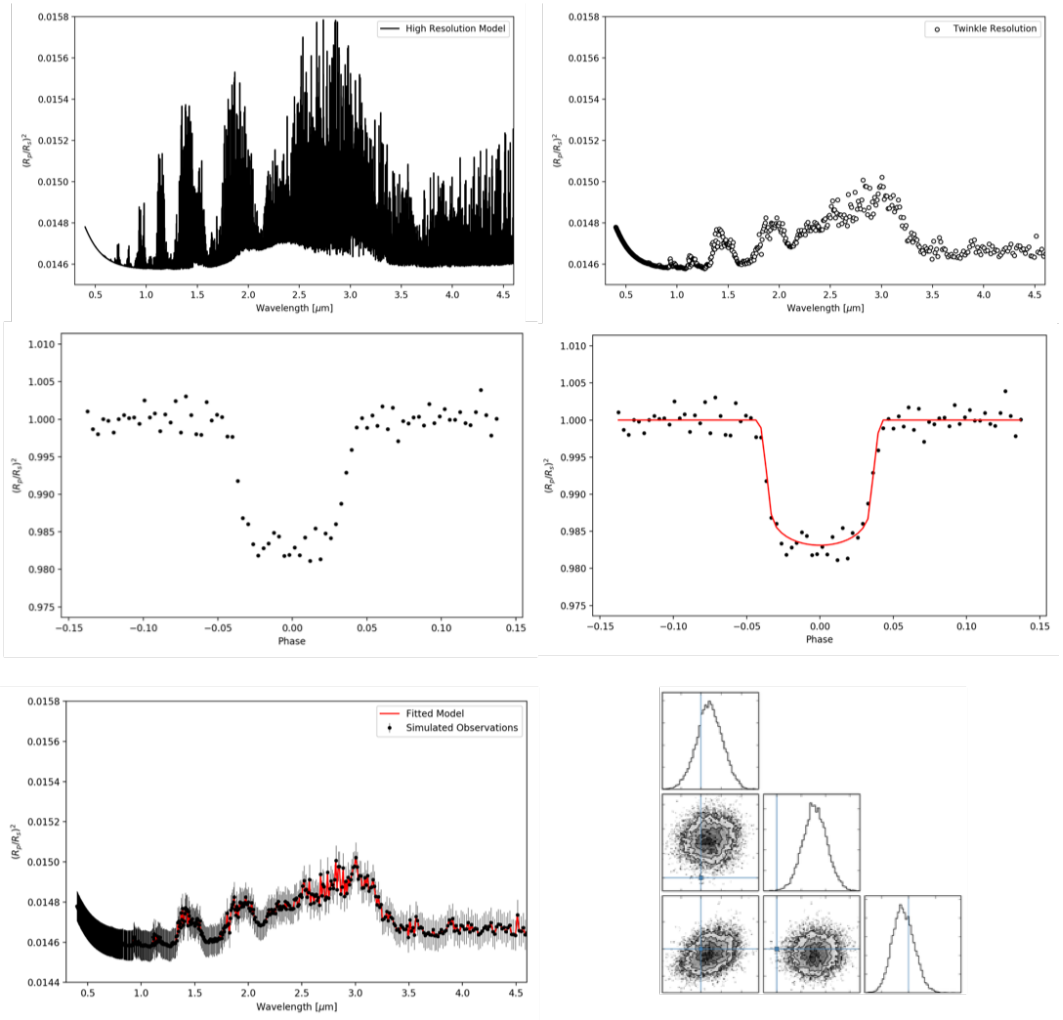

Figure 7.2: Overview of the structure of Terminus. Top left: Input spectrum generated by Tau-REx. Top Right: Binning of spectrum to instrument resolution. Middle Left: Creation of light curves. Middle Right: Fitting of light curves. Bottom Left: Retrieved spectrum. Bottom Right: Retrieved atmospheric composition.

While the basic signal calculation in Terminus is essentially identical to that of ArielRad and ExoWebb, the strength of this simulator is the creation of time-domain data. The standard output spectrum from ArielRad or ExoWebb adds no scatter on the transit depth (it is assumed to be perfectly recovered) while the transit depth for Terminus is that retrieved during the light curve fitting. These offsets caused by the MCMC fitting can be mimicked in data from a radiometric model by adding Gaussian scatter to the spectrum. However, adding Gaussian scatter to the individual exposures and fitting the subsequent light curves brings the simulations closer to reality, though with the disadvantage of a longer simulation time due to the

fitting process. If the added complexity of time-domain data is not required, Terminus can be run as a standard radiometric model to provide fast, but still accurate, estimations of the capabilities of a spacecraft's instrumentation, assuming full light curves are observed.

Chapter 8

Potential Targets for Ariel

> ”No sensible decision can be made any longer without taking into account not only the world as it is, but the world as it will be.”
>
> Isaac Asimov

During its 4-year mission, Ariel aims to observe $\sim$1000 exoplanets ranging from Jupiters and Neptunes down to Super-Earth size in the visible and the infrared with its meter-class telescope. The analysis of Ariel spectra and photometric data will deliver a homogeneous catalogue of planetary spectra which will allow for the extraction of the chemical fingerprints of gases and condensates in the planets' atmospheres, including the elemental composition for the most favourable targets. It will also enable the study of thermal and scattering properties of the atmosphere as the planet orbits around the star.

While Ariel will not be operational for nearly a decade, the design is scheduled to be fixed in 2020. It is therefore vital to attempt to predict the future state of the field to ensure that Ariel's design will allow it to meet the mission's science goals. During Phase A, a study of Ariel's capabilities to observe known and predicted

Contributions: I have led recent studies into potential targets for the Ariel mission and this has been published (Edwards et al., 2019, An Updated Study of Potential Targets for Ariel, ApJ, doi: 10.3847/1538-3881/ab1cb9). Giovanna Tinetti, Enzo Pascale and Lorenzo Mugnai also contributed to this work.

planets was conducted and a Mission Reference Sample (i.e a list of exoplanets to be observed during the primary mission life) of $\sim$1000 potential targets was created [126].

This chapter details the ongoing review of the capability of Ariel's instrumentation to observe currently-known planets and potential future detections. The catalogue described in Section 7.1 is analysed using ArielRad, the new Ariel simulator which is more suitable to capture the details and updates of Ariel's design as considered in Phase B (see Section 8.1.2). This exercise is being regularly repeated to incorporate new discoveries and verify that the mission's science goals can be achieved as the instrumentation evolves in Phase B.

Finally we focus part of our simulations and discussion on smaller planets, to refine some of the science objectives considered in Phase A for the mission and address new science questions emerging from the recent discoveries, e.g. the "Fulton gap" [82].

8.1 Creating a List of Potential Targets

8.1.1 ESA Radiometric Model

During Phase A, the ESA radiometric model [256] was utilised to assess the duration and type of observations needed to meet the mission requirements. Although the NIRSpec instrument will also be used for spectroscopy, the mission requirements are baselined on the AIRS channels, as these bands are typically the most demanding. The ESA Radiometric Model calculates the signal and noise contributions for exoplanet spectroscopic observations [256, 294]. This model simulates observational and instrumentation effects, utilising target characteristics to assess whether emission or transmission spectroscopy is preferable and to estimate the required number of observations to achieve a desired resolving power and signal to noise ratio (SNR). The ESA radiometric model requires the host star temperature to be in the range 3070-7200 K. The Mission Reference Sample during Phase A was obtained using this model [126].

8.1.2 Ariel Radiometric Model

The ESA radiometric model assumes that the systematic noise does not vary from target to target. The Ariel Radiometric model (ArielRad, [260]) has been developed to provide a comprehensive model of the instrument performance. While the ESA radiometric model assumes a constant instrument noise, ArielRad provides systematic noise on a case by case basis. The Ariel team has validated ArielRad against the ESA radiometric model and ExoSim [294] by running the simulators with the same instrument noise characteristics. ArielRad includes greater margins on the instrument noise and a noise floor of 20 ppm.

The ArielRad simulator is used to provide realistic noise models for all planets within the catalogue described in Section 7.1. These noise models are used to create a new list of potential targets, based on the expected performance from ArielRad. The FGS signal requirements for accurate pointing are now accounted for as these are not included in the ESA radiometric model but are key for target selection. In the ESA radiometric model, simulations were restricted to planets orbiting stars with temperatures in the range 3070-7200 K due to the stellar spectral energy distributions (SEDs) used. For ArielRad, this range is expanded to include early type stars and M-dwarfs such as Trappist-1 by using a broader range of SEDs from the Phoenix atmospheric models increasing the diversity of input catalogue.

8.1.3 The 3 Tier Approach

Planning of observations with Ariel is based around a tiered approach and Table 8.1 describes the requirements on each tier. As envisaged in Phase A, a survey tier aims to observe 1000 planets with low resolution spectroscopy to produce a statistically viable dataset of a diverse range of exoplanetary atmospheres. Tier 1 observations will help refine orbital and planetary parameters and constrain (or remove) degeneracies in the interpretation of mass-radius diagrams. Additionally, it will offer the opportunity to generate colour/colour and colour/magnitude diagrams and investigate what fraction of planets have a transparent atmosphere, are partially clouded or are completely overcast.

From this initial survey of planets, around half will be selected for spectro-

Table 8.1: Resolution of final dataset across each instrument in each tier

Instrument Name	Tier 1	Tier 2	Tier 3
NIRSpec	R$\sim$1	R$\sim$10	R$\sim$20
AIRS Ch0	R$\sim$3	R$\sim$50	R$\sim$100
AIRS Ch1	R$\sim$1	R$\sim$10	R$\sim$30

scopic follow-up: Tier 2 spectroscopic measurements are crucial for uncovering atmospheric structure and composition. Additionally, Tier 2 observations are critical to search for potential correlations between atmospheric chemistry and basic parameters such as planetary size, density, temperature, stellar type and metallicity. Tier 3 will consist of repeated observations of a select group of benchmark planets ($\sim$50-100) around bright stars which can be observed at high resolution within a small number of transits or eclipses to provide a very detailed knowledge of the planetary chemistry and dynamics (see [125] for an in-depth description of the tiering system and the mission science questions and requirements). Figure 8.1 shows simulated observations in each tier for a planet with parameters similar to Wasp-39 b. The addition of a Tier 4 – including phase-curves and an ad-hoc observational strategy for targets of interest which do not fit into the tier system – has been recently discussed in the Ariel team.

8.1.4 A List of Potential Targets for Ariel

From the noise models created by ArielRad, the catalogue of known and predicted planets was cut down to those for which an SNR $\geq$ 7 could be achieved on the atmosphere within a reasonable number of transits or eclipses. For Tier 1, there are over 2000 potential planets for which the science requirements can be reached with 5 observations or less, far more than the 1000 that will make up the MRS. Being over-saturated in the number of possible targets is useful as it allows for redundancy in the scheduling of observations and it means there is a large catalogue of planets to draw from to allow for a diverse sample to be observed. The distribution of various stellar and planetary parameters for these potential Tier 1 targets is shown in Figures 8.2 and 8.3. These show that (i) to achieve a sample of $\sim$1000 planets, Ariel does not need to observe faint stars (except for special targets of interest) (ii) there is a

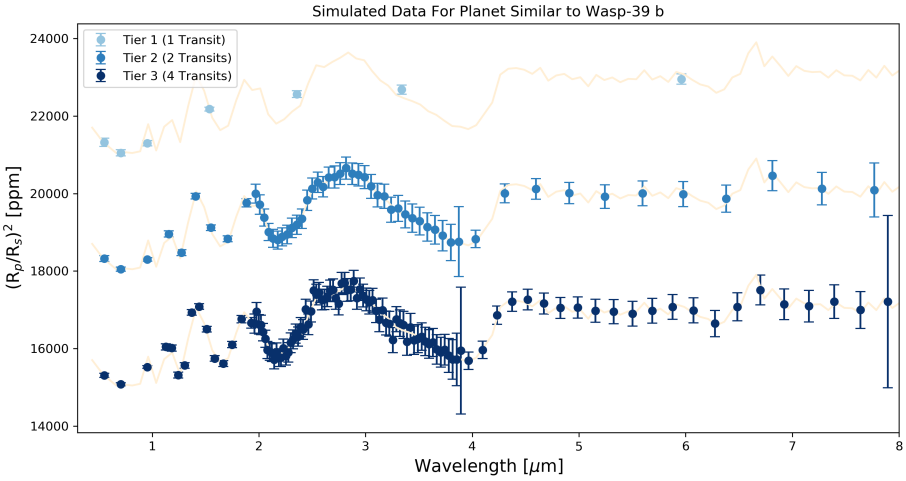

Figure 8.1: Simulated data for a planet similar to Wasp-39 b in each Tier. The atmosphere has been modelled in chemical equilibrium with solar metallicity and C/O = 0.5. The error bars are calculated using ArielRad and the spectra are offset for clarity. The larger errors at the red end of AIRS Channels 0 and 1 are due to a reduced sensitivity caused by optical filter cut-off, and detector sensitivity, respectively. This will however be mitigated by the cross-channel spectral overlap of the baseline design which is expected to reduce the error bars at the transition between channels 0 and 1.

large diversity in planet temperature and radius (iii) the stellar type of planet hosting stars is varied although FG stars are more dominant (iv) the majority of potential targets are located within a few hundred parsecs (v) most potential targets are close to their stars and have orbits of under 20 days (vi) although the metallicities of many of the host stars are unknown, there is a wide range of values included in the sample.

Additionally, $\sim$1000 planets are found to be potentially observable in Tier 2 and Figure 8.4 details the distribution of the number of observations required for these planets as well as those in Tier 1. We find that the number of observable Jupiters ($R_p > 7\ R_\oplus$) is approaching saturation at 5 observations while the number of suitable smaller planets are rising with increased observations. Ariel will have constant visibility of the ecliptic poles with a partial visibility of the whole sky at lower latitudes. The sky locations of possible planets for study in each tier with Ariel are shown in Figure 8.5 to be well distributed across the sky but with a noticeable gap close to the ecliptic due to a lack of TESS coverage in its primary mission.

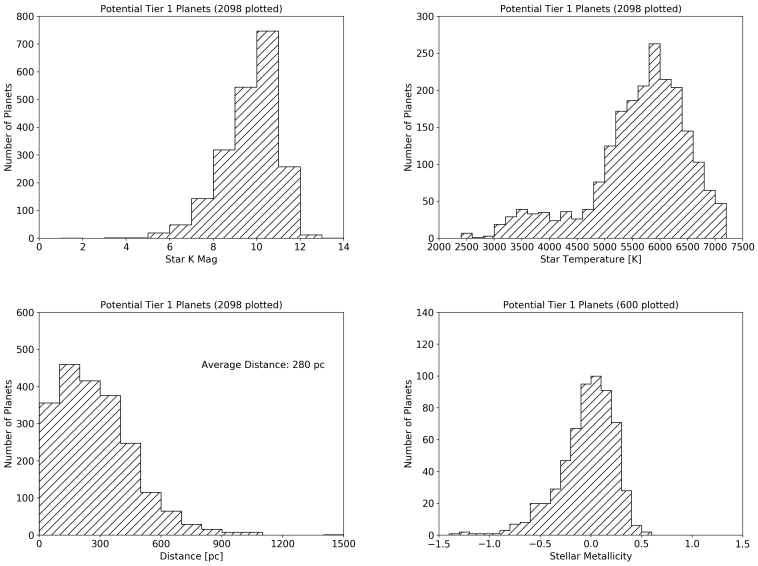

Figure 8.2: Histograms of the properties of the stellar hosts within the potential Ariel Tier 1 Catalogue. Metallicities were not available for all host stars.

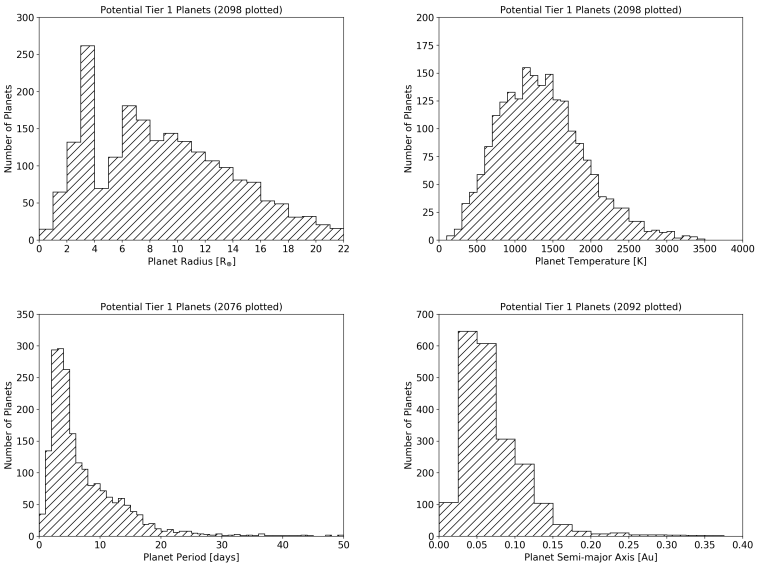

Figure 8.3: Histograms of the planetary properties within the potential Ariel Tier 1 Catalogue. In some cases, not all planets are plotted for aesthetic reasons.

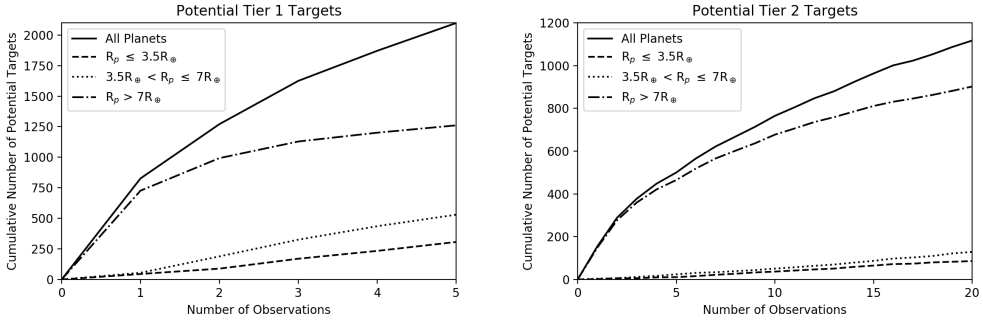

Figure 8.4: Cumulative number of planets that can be observed in Tiers 1 (left) and 2 (right) with a given number of transits or eclipses.

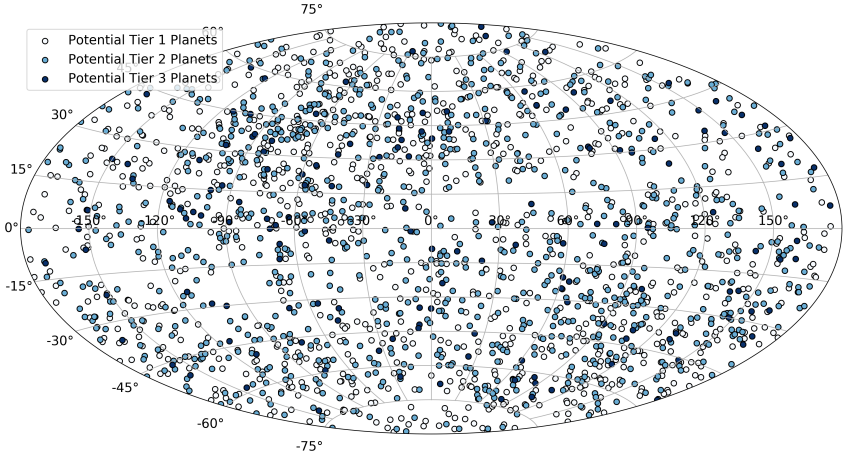

Figure 8.5: Sky locations of potential targets for study with Ariel. Having targets scattered across the entire sky is beneficial for the scheduling of observations.

8.1.5 Creation of an Example Mission Reference Sample

Ariel has a nominal life of 4 years (extendable to 6) including a 6-month commissioning and calibration phase. Additionally, scheduling constraints, such as telescope housekeeping, slewing between targets and data down-link, reduce the available science time. Ariel will therefore have $\sim$3 years of usable science time during its nominal life. Having established that there will be a large number of planetary atmospheres that are suitable for characterisation with Ariel we explore the number that could be observed over the mission lifetime.

The approach adopted during Phase A consisted of choosing a very diverse, and as complete as possible, combination of star/planet parameters while minimising the number of repeated observations by selecting the planets around the brightest stars. Here, we chose three main parameters to classify the potential targets by: stellar effective temperature, planetary radius and planetary equilibrium temperature. Each parameter is split into a number of classes and Table 8.2 summarises these distinctions. We bin the planets by these 3 parameters, and where possible, ensure that at least 2 planets within each bin are contained within the Mission Reference Sample. Future selections will also classify planets by their density and the metallicity of the host star. These five basic characteristics are thought to have a large impact on the chemistry and thus choosing planets with a broad range in these parameters should yield a multifarious exoplanet population for study.

Adopting this strategy we obtain a distribution of planets by radius and temperature as displayed in Figure 8.6. Planets selected for Tier 3 are also included in Tier 2 and, in turn, Tier 1 planets incorporate all those studied in Tier 2. Although not considered in-depth here, 10% of mission time is reserved for Tier 4 and we highlight potential targets for phase-curves in Figure 8.7. For larger planets, these are those which can easily be observed at Tier 2 resolutions in both transit and eclipse while for smaller planets, it is those that can be studied at Tier 1 resolutions in both methods. Phase-curve targets are also required to be on relatively short orbits and thus are generally found to be hot (or very-hot).

Different observing strategies have been discussed within the Ariel team in-

Table 8.2: Bounds used to classify potential planets to ensure a varied population of planets within the Mission Reference Sample.

Parameter	Class	Bounds
Stellar Effective Temperature	M	T_s <3955 K
	K	3955 K <T_s <5330 K
	G	5330 K<T_s <6070 K
	F	6070 K <T_s <7200 K
Planetary Radius	Earth/Super-Earth	R_p <1.8 $R_\oplus$
	Sub-Neptune	1.8 $R_\oplus$ <R_p <3.5 $R_\oplus$
	Neptune	3.5 $R_\oplus$ <R_p <6 $R_\oplus$
	Jupiter	6 $R_\oplus$ <R_p <16 $R_\oplus$
	Massive Jupiter	R_p >16 $R_\oplus$
Planetary Equilibrium Temperature	Temperate/Warm	T_p <500 K
	Very Warm	500 K <T_p <1000 K
	Hot	1000 K <T_p <1500 K
	Very Hot	1500 K <T_p <2500 K
	Ultra Hot	T_p >2500 K

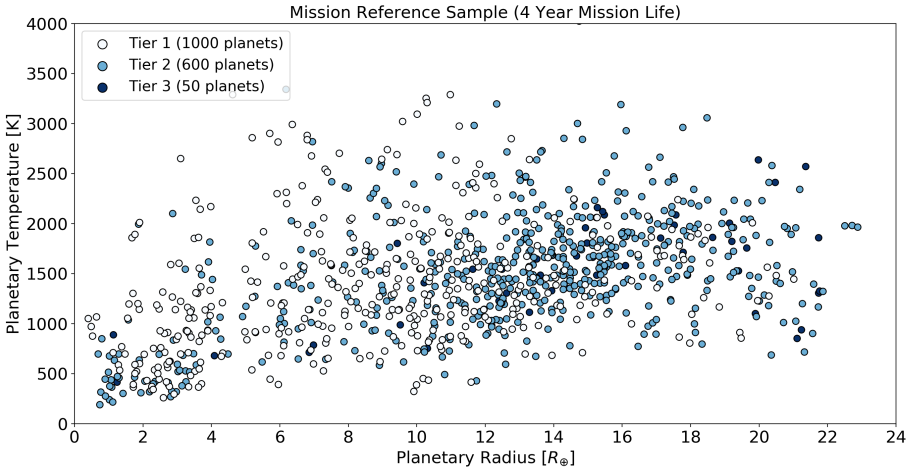

Figure 8.6: Planetary radius and temperature distribution of a potential Ariel mission reference sample from ArielRad

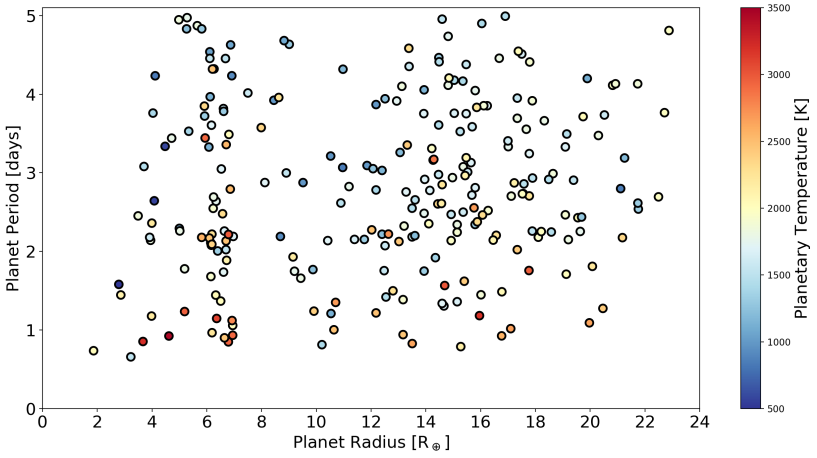

Figure 8.7: Potential phase-curve targets for Ariel. The colour of points highlights the planetary equilibrium temperature. Spectroscopic phase-curves should be possible for Jupiter-sized planets while smaller planets are suitable for multi-band photometric observations.

Number of Planets	Observation Requirement	Required Science Time [hours]
1000	Achieve Tier 1 resolutions	∼10,600
400	Increase resolution from Tier 1 to Tier 2	∼3,100
500		∼6,000
600		∼10,500
200	Achieve Tier 1 resolutions in second method	∼1,400
300		∼2,500
400		∼4,200
50	Tier 3 (5 repeated observations per planet)	∼1,700
-	Tier 4 (additional science time)	∼2,300

Table 8.3: Mission time required to achieve different observation goals. The total science time over the 4 year primary life is ∼24,800 hours. Note that for some bright targets (e.g. HD 209458 b), Tier 2 or 3 resolutions would be reached in a single observation.

cluding acquiring data in both transit and eclipse for some Tier 2 planets. Such observations would increase our ability to characterise the atmospheres of these targets but would reduce the total number of planets studied. Table 8.3 highlights the science time (i.e. time on target) required to achieve different observations. These discussions are ongoing and further studies will be undertaken but it can be seen that acquiring data in the secondary method (i.e. the method which gives a lower SNR) for some of the best planets will not require significant mission time. However, the total number of Tier 2 planets may have to be sacrificed to achieve this.

Hence, ArielRad simulations combined with the TESS yield suggested by [4] predict that Ariel will be able to observe 1000 planets within the primary mission (e.g. Figure 8.6). The number of planets within this updated version of Mission Reference Sample is similar to that of the Phase A study although we find an increase in the number of Tier 2 planets compared to the results of [126] on top of the 10% mission lifetime dedicated to Tier 4 planets. Therefore, from the input catalogue of currently-known and predicted planets, ArielRad simulations suggest Ariel should be more than capable of achieving the science requirement of characterising the atmospheres of hundreds of diverse extra-solar planets.

8.2 Characterisation of Small Planets

Section 8.1.2 shows that from the catalogue of known planets and predicted TESS detections ArielRad produces a Mission Reference Sample consistent with that created in Phase A with the ESA radiometric model and predicted targets by [126]. Choosing the Mission Reference Sample in this way naturally leads to a proportionally larger number of gaseous planets being selected for observation. However, warm and hot Super-Earths (and Earth-sized planets) are well within Ariel's capabilities, especially given that many more are expected to be discovered around bright stars thanks to TESS.

Smaller planets, particularly those which could be rocky, are an intriguing population of bodies, especially since the discovery of the "Fulton gap" at $\sim$1.8 $R_\oplus$ by the California-Kepler Survey (CKS) [82]. This distribution seemingly indicates two populations of small planets: those which have retained a volatile dominated atmosphere and those which are expected to have lost this more primordial envelope (e.g. [83]) or never had one. Characterising the atmospheres of planets with radii smaller than 3.5 $R_\oplus$, and in particular those within the transition region from rocky to gaseous, is fundamental in uncovering the nature of this population and would be very informative for planetary formation and evolution theories. More specifically, understanding whether the atmosphere is still primordial (i.e. H/He rich, possibly thick) or more evolved (i.e. richer in heavier elements, thin or completely absent)

may constrain formation (formed in situ or remnants of more massive bodies which have migrated to closer orbits) and evolution scenarios (e.g. hydrogen escaped, a secondary atmosphere which might hint at the interior composition).

Here we explore a different option for the Ariel MRS, with more emphasis on the interpretation of the nature of smaller planets, by specifically devoting mission lifetime to studying this dichotomy of small worlds.

In the Mission Reference Sample studied in Section 8.1.2, $\sim$110 planets with a radius less than 3.5 Earth radii were selected for study over around 600 observations ($\sim$2100 hours of science time) in all three tiers. These planets are located on both sides of the "Fulton gap". A key goal of Tier 1 is to discover the fraction of small planets with hydrogen/helium envelopes. For this reason, the number of required observations to detect an atmosphere is estimated assuming a low mean molecular weight so that if a planetary atmosphere has a primordial composition, this atmosphere should be detected with high confidence. Additionally, the atmospheric trace gases should be accurately constrained if the planet is observed in Tier 2 or 3. If no detection is made, the planet either has (i) an atmosphere with a higher molecular weight or (ii) opaque clouds across all wavelengths or (iii) no atmosphere at all.

In all likelihood, some fraction of these planets will have far heavier atmospheres (higher mean molecular weight) and thus will be harder to characterise, requiring more observations to obtain the observational requirements in each tier. In particular, additionally to the H/He atmospheric content, the fraction of H_2O present in an atmosphere is also very important to constrain formation/evolution scenarios and the delivery of volatiles to the inner part of the planetary system. "Water worlds", i.e. planets with a significant amount of H_2O on their surface or in the subsurface (e.g. [295]), or magma ocean planets with a steam atmosphere (e.g. [296]), are expected to have atmospheres with a large fraction of H_2O.

However, the characteristics of a planet's atmosphere (if present) cannot be known before observations are undertaken, unless these targets are observed previously with other facilities from space or the ground. To quantify the fraction of lifetime needed to characterise the atmospheric composition of small planets with

Table 8.4: Mission time required to achieve Tier 1 resolutions (at SNR >7) for the 113 small planets in the example MRS assuming different mean molecular weights. The total science time over the 4 year primary life is ∼24,800 hours. t_0 is the time spent observing small planets in Tier 1 of the standard MRS.

Atmospheric Mean Molecular Weight	Number of Planets	Required Science Time [hours]
2.3	All	∼1,000 (t_0)
5	50	t_0 + ∼360
	All	t_0 + ∼3000
8	50	t_0 + ∼1,100
	All	t_0 + ∼9,200
10	50	t_0 + ∼1,900
15	50	t_0 + ∼4,400
18	25	t_0 + ∼1,700
	50	t_0 + ∼6,400
28	25	t_0 + ∼4,300
	50	t_0 + ∼15,600

an atmosphere heavier than H/He, we select the small planets ($R_p < 3.5\ R_\oplus$) from the example MRS for further study. The science time required to achieve Tier 1 resolutions (with SNR > 7) for different atmospheric compositions is determined and compared to the Tier 1 time assumed in Section 8.1 (Table 8.4).

As expected, the required number of observations (and thus science time) rises with the increasing atmospheric weight. While the atmospheres of smaller planets will be easily probed if H/He dominated, heavier atmospheres would require significant mission time to observe. Distinguishing between primary and secondary atmospheres should be possible for all small planets studied here within a reasonable science time. However, the assumed noise floor of 20 ppm limits the characterisation at very high mean molecular weights where the signals become increasingly small. Smaller, cooler planets may also have a nitrogen based atmosphere and we find that, for the Earth-sized planets below 500 K in this chosen sample, 25-130 transits would be required to achieve Tier 1 resolutions if the atmospheres had a molecular weight of 28. Figure 8.8 shows simulated data for one such planet, LHS 1140 c [297], for various atmospheric weights. The dampening in the spectra due to a heavier atmosphere can clearly be seen. Generally, the best targets could be easily characterised regardless of their atmospheric composition while for others achieving the required signal uncertainty will be difficult if the atmosphere is dense. We

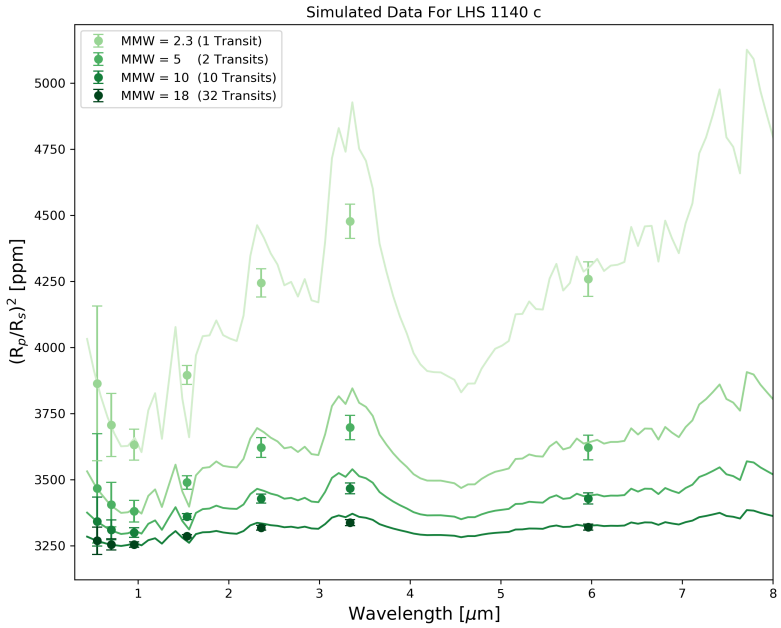

Figure 8.8: Simulated Tier 1 data of LHS 1140 c for different atmospheric weights. The atmosphere is modelled with 10^{-5} of H_2O and CH_4 and the mean molecular weight is varied by modifying the nitrogen ratio. The number of transits quoted is the requirement for an SNR >7 to be achieved on the atmosphere at Tier 1 resolutions.

note that the impact of clouds is expected to be well captured in the simulations for higher mean molecular weight, where signals are up to fourteen times smaller than the ones for atmospheres which are cloud-free and H/He-rich. Additional observations of the planet at different phases may provide further constraints on the cloud types and distribution (e.g. [298]). Observations of smaller planets could be undertaken in a tiering style system where the data is analysed after several visits with decisions made on continuing the observations based on the results seen. Science goals for such an observing strategy could include the determination of whether an atmosphere is primary, secondary or not present.

From this preliminary study, we appreciate that providing significant time to observe smaller planets would be valuable for their more in-depth chemical/cloud characterisation after an initial survey. Here we have presented a possible option including the in-depth analysis of ∼110 small planets, but of course different com-

binations of strategies could and will be considered in this and future mission Phases to optimise the breadth and depth of the Ariel sample during its mission lifetime and prioritise its science objectives. If much of the primary mission is dedicated to an in-depth survey of smaller planets, the total number of planets observed by Ariel would be reduced. Hence, some of the more speculative questions could be left for a potential extended mission. This study shows that Ariel has the potential to characterise the atmospheres of planets of all sizes. Data from such a multifarious population would be invaluable for our knowledge of planetary formation and evolution.

8.3 Discussion

8.3.1 Dependence of Predicted Yields on the Accuracy of Planetary Occurrence Statistics

Here, expected TESS detections have been used to estimate the number, and type, of exoplanets that could be potential targets for ARIEL. Predicted yields for future missions are, of course, speculative in nature and highly dependent on the assumptions of the study. In [4] the planetary occurrence statistics for AFGK stars were taken from [77] and from [9] for M dwarfs. More recent studies may suggest higher occurrence rates for some classes of small planets (e.g. [299, 82]) and the differences between these could affect the yield of TESS. Recently, TESS finished observing the southern hemisphere. During the analysis process, stars which show events which could be due to a transiting planet are labelled at TESS Objects of Interest (TOI). These TOIs are then followed-up, with ground-based instruments obtaining more photometry light curves or spectroscopic information, to confirm the presence of a planet. So far there have been over 1000 TOIs identified, with 29 confirmed TESS detections in the NASA Exoplanet Catalogue and papers for many more submitted to journals. Although the analysis of data from the southern hemisphere is still ongoing [e.g. 300], one can start to compare the current yield of TESS with that from [4]. 1113 TOIs have been registered in the southern sectors, compared to 2197 predicted planets, and Figure 8.9 shows a histogram of the plan-

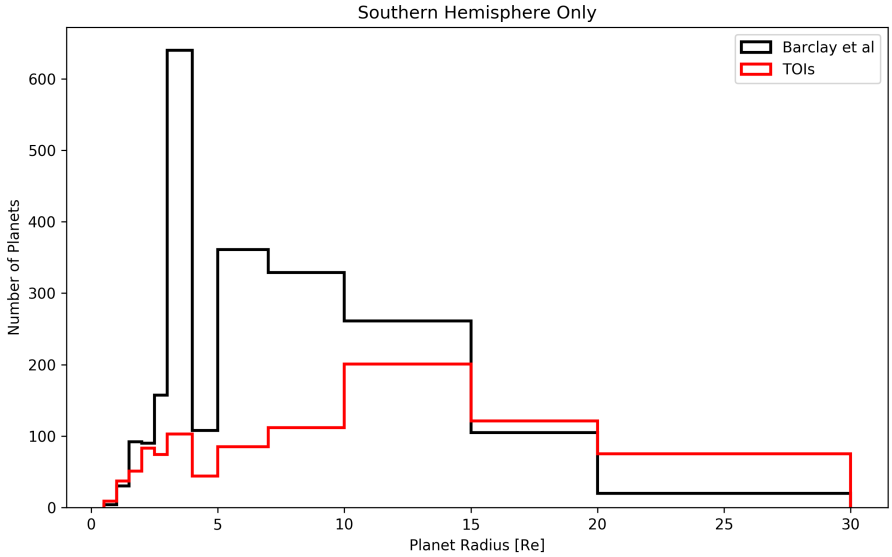

Figure 8.9: Histogram of current TESS Objects of Interest in the southern hemisphere and the Barclay predictions for the same sectors [4].

etary radii of these yields. It appears that far fewer sub-Neptunes are being detected than expected, with an additional dearth in Neptune/Saturn regime but an excess in the large, gaseous planets (>15 $R_{\oplus}$).

It is perhaps still too early to comment on the accuracy of the predicted TESS yield. All these current TESS planets are found to be excellent targets for study with Ariel. Further constraints on the occurrence of planets on short periods is likely to be a key outcome of the TESS mission, particularly for M dwarfs. In any case, the primary mission of TESS is due to finish in 2020 [84] and, while the data analysis will continue for many years to come, the yield from this mission will be known long before Ariel launches. Additionally, TESS has been granted a mission extension, allowing the satellite to survey the sky for an additional two years. This is expected to dramatically increase the number of detections, particularly fro longer period planets.

8.3.2 Scheduling of Observations

Here, the scheduling of observations has not been considered although studies in the Ariel consortium are being undertaken which will utilise the Mission Refer-

ence Sample [301, 302]. Such studies will provide a greater understanding of the impact of scheduling constraints (telescope housekeeping, slewing between targets etc.) and a key issue may be observation overlaps (i.e. two planets transiting at the same time). Having additional, back-up targets is likely to be useful for scheduling purposes and this study shows that there should be an over-saturation of suitable planets for characterisation. The list of potential targets constructed here will be used as an input for such efforts.

8.3.3 Tiering System for Smaller Planets

The ambiguity in the atmospheric composition of smaller planets causes complexities when planning via the originally proposed three tier observing structure. Additionally, the major constituents of an atmosphere could be recovered at resolutions below that of Tier 2. Therefore, a separate tiering system for smaller planets which is based around confirming the presence (or absence) of a clear atmosphere of a given mean molecular weight may be required. Once the catalogue of potential planets is completely formed of known planets, additional considerations in the selection of smaller planets such as photo-evaporation and isolation flux (e.g. [83, 303]) will need to be taken into account to ensure a diverse population of planets are studied.

8.3.4 Next Steps and Final Selection of the Mission Reference Sample

The Mission Reference Sample presented here is merely one example of a population of planets that Ariel could observe. The selection of the final list of targets will require far more discussion and input from scientists from across the exoplanet community, particularly as the predicted planets from this list are replaced with actual detections. In the coming years, observations with current ground and space-based facilities (e.g. VLT, Hubble, Spitzer) and future observatories (e.g. E-ELT [304], JWST [106], Twinkle [305]) will further characterise the atmospheres of the known exoplanet population. These studies will increase our knowledge of these distant worlds and may begin to highlight trends in atmospheric chemistry. Such insights

will inevitably be used to optimise the Ariel Mission Reference Sample, maximising the synergies between different facilities, and to this end a website has been created to host the list of potentially observable planets [1]. This open-access site will contain all available datasets on these planets, highlighting planetary systems for which further characterisation would be beneficial (e.g. refinement of ephemerides or stellar parameters) and providing the chance for the entire community to contribute to the Ariel target selection. Therefore, Ariel will embrace the exoplanet community by offering open involvement in the observation planning process as well as providing regular timely public releases of high quality data products at various processing levels throughout the mission. Additionally, targets within the list are being used as the basis for simulated data in several data challenges organised to engage the exoplanet community in Ariel[2]. These efforts, particularly the continuous dialogue with the wider community, will ensure that the Ariel observation strategy facilitates the maximum possible science yield for the entire exoplanet field.

8.4 Conclusions

An updated analysis of the currently-known planets and predicted TESS discoveries, as well as Ariel predicted performances, supports and improves the conclusions of the previous Mission Reference Sample (MRS) study from Phase A: Ariel will be capable of characterising 1000 exoplanet atmospheres during the primary mission life. The total number of potential planets to choose this MRS from is found to be over 2000 meaning there is a surplus of targets. Within this list of planets there is a large range of planetary and stellar parameters, ensuring that the MRS is diverse; a key requirement for meeting Ariel's mission objectives. The example MRS selected here allows for 1000 planets to be studied, with high-quality spectroscopic data being obtained for 600 of these during the 4 year primary mission life. The selection also reserves mission time for other observation strategies (Tier 4). These could include phase-curves, non-transiting planets or targets of interest which are not captured by the current tier system.

[1] `https://arielmission.space/target-list/`
[2] `https://ariel-datachallenge.azurewebsites.net`

Additionally we have explored the mission capability to perform an in depth analysis of small planets' atmospheres, which are expected to be more diverse compared to the gaseous ones. Given the increased observational difficulty to probe atmospheres heavier than H/He, significant mission time may have to be allocated to this task. Trade-offs between studying more planets, observing fewer targets but in greater detail, and/or choosing interesting planets which require more observational time, will form a key part in the selection of the final Mission Reference Sample. Generating an optimal catalogue of potential candidates is key in these efforts and this list of targets will be constantly updated with new planet discoveries.

Chapter 9

Characterising Exoplanets with Twinkle

> ”Giants are not what we think they are. The same qualities that appear to give them strength are often the sources of great weakness.”
>
> Malcolm Gladwell

Perhaps Twinkle's most promising science case is the characterisation of exoplanets and their atmospheres. Here I will discuss the studies undertaken thus far to understand Twinkle's capabilities, proving that smaller space-based telescopes can provide cutting-edge data. Firstly, an adapted version of the radiometric model from Puig et al. [256] has been used to study Twinkle's capacity for observing the catalogue of known and predicted planets from Chapter 7. Additionally, Twinkle data has been simulated and the ability to recover the input atmosphere explored. Finally, the time-domain simulator Terminus [262] has been used to provide more realistic simulations of Twinkle observations, including adding gaps due to Earth obscuration.

Contributions: This chapter is based upon published work led by myself (Edwards et al., 2018, Exoplanet spectroscopy and photometry with the Twinkle space telescope, Experimental Astronomy, doi: 10.1007/s10686-018-9611-4). Giovanna Tinetti, Marcell Tessenyi, Malena Rice, Tiziano Zingales and Giorgio Savini also contributed significantly to this publication.

9.1 Targets within Twinkle's Field of Regard

As previously discussed, Twinkles field of regard, the region of sky in which it can be pointed, is a cone, centred on the anti-sun vector and extending to $\pm 40^{\circ}$ from the ecliptic plane. Twinkle's sky visibility is therefore similar to that of CHEOPS but is in contrast to TESS, JWST and Ariel, all of which have continuous coverage around the ecliptic poles and a partial visibility of the whole sky at lower latitudes. Here, we compare Twinkle's 40° field of regard to the celestial coordinates of planet-hosting stars to determine the number of known and predicted targets within Twinkle's view.

Figure 9.1 displays the locations of the planets within the catalogue discussed in Chapter 7 and highlights those within the sweep of Twinkle's field of regard. We note that the original Kepler field (which accounts for over 2000 transiting planets) lies far from the ecliptic and thus cannot be observed with a 40° field of regard centred on the anti-sun vector. An extension of the field of regard to 60° from the ecliptic may allow some of these targets to be observed. However, Twinkle is best-suited for observing planets around bright stars and thus is not impeded by being unable to observe planets in the Kepler field which are generally hosted by fainter stars. At the time of this study (July 2018), 548 of the 685 transiting planets not discovered by the original Kepler mission lie within Twinkle's field of regard.

The predicted TESS planets are also shown in Figure 9.1 and we find that of the 4376 targets plotted, 1815 lie within the 40° field of regard of Twinkle. TESS is also predicted to discover more than 10,000 planets around fainter stars and whilst some of these will be within Twinkle's field of regard, most are unlikely to be suitable targets for observation with Twinkle. However, some larger, hotter planets may be observable.

9.2 Assessing Target Suitability

Twinkle will enable the study of exoplanets simultaneously at multiple wavelengths through transit, eclipse and phase-curve observations. Here, we consider transit and eclipse observations which, via spectroscopy, can allow for the atmospheric composition of the planet to be obtained. Additionally, photometric or low reso-

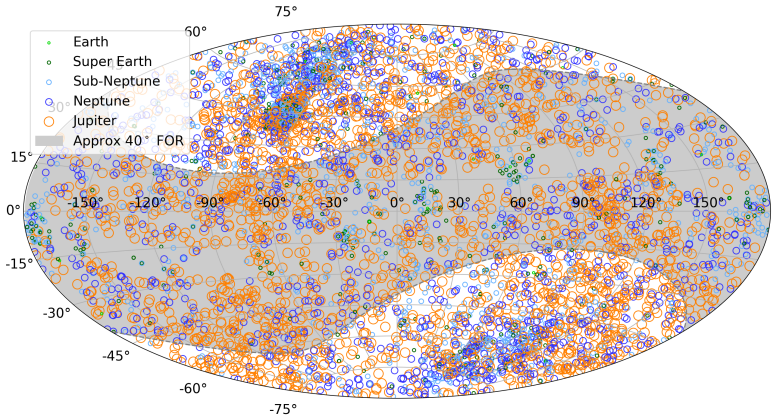

Figure 9.1: Sky location of currently-known transiting exoplanets and those predicted to be discovered by TESS, their planetary classification and the sweep of Twinkle's field of regard. The initial Kepler field is the densely populated region at RA -70°, Dec 45° and the locations of some well-known exoplanets are noted.

lution observations in the optical and infrared can be utilised to refine planetary and orbital parameters, monitor stellar activity over time (e.g. [306]) or search for transit time variations (TTVs, [307]) and transit duration variations (TDVs, [308]). TTVs have been extensively used as a valuable technique for finding additional planets within systems and constraining planetary masses and orbits (e.g. [309, 310, 67, 311, 312]). Combined TTV and TDV signals are paramount to search for exomoons [313]. The temporal binning required for Twinkle's observations will depend upon the brightness of the host star but for brighter targets will be very short ($<$30 seconds) and therefore may be utilised to provide precise measurements of TTV and TDV due to low mass objects present in some planetary systems. For fainter stars, a temporal binning of a few minutes may be required, depending on the wavelength range considered. While other future space facilities may also be able to detect TTV and TDV signals, Twinkle can obtain NIR light curves which exhibit highly reduced distortion from limb darkening and stellar activity. Additionally, multi-colour light curves significantly attenuate degeneracy of fitted limb darkening parameters across all wavelengths. Therefore Twinkle's capabilities for both high and low resolution transit (and eclipse) observations are considered here.

9.2.1 A Radiometric Model for Twinkle

Terminus, the radiometric model for Twinkle, has been created using the methods described for calculating the signal and noise contributions for other exoplanet infrared spectroscopic missions in [256, 294] and in Chapter 7. The radiometric model simulates observational and instrumentation effects, utilising target characteristics to assess whether emission or transmission spectroscopy is preferable and to estimate the required number of observations to achieve a desired resolving power and signal to noise ratio (SNR).

Information from the planet catalogue was inserted into the model and the average SNR across each spectrometer for one transit or eclipse was obtained for the maximum resolving power. In post-processing, the resolving power can be decreased from its native value in order to increase the SNR per wavelength bin. Stacking multiple observations increases the SNR of the final dataset and for this exercise the increase in SNR has been calculated from:

$$SNR_N = \sqrt{N} \times SNR_1 \tag{9.1}$$

where N is the number of observations. Defining a requirement for SNR ≥ 7 on the atmosphere, Figures 9.2, 9.3 and 9.4 display the number of planets that could be observed in channels 0, 1 and 2, at a given resolution, for a given number of transit or eclipse observations. Assuming the same SNR requirement, the resolution achieved over a given number of transits or eclipses is displayed in Figures 9.5, 9.6 and 9.7 showing the distribution of the radius of observable planets along with the planet's temperature class. The SNR requirement will depend upon the user's preferences and the observations undertaken and therefore should be taken only as an indicative value.

We find that in one observation Twinkle could study 89 known planets and 469 predicted TESS planets in channel 1 with R $<$ 20 and 12 known planets and 29 predicted TESS planets at higher resolutions. With ten transits or eclipses, spectroscopy is possible for 81 known and 307 TESS planets at R$>$20, and for 144 known and 1041 TESS planets at lower resolution. In each case the majority of

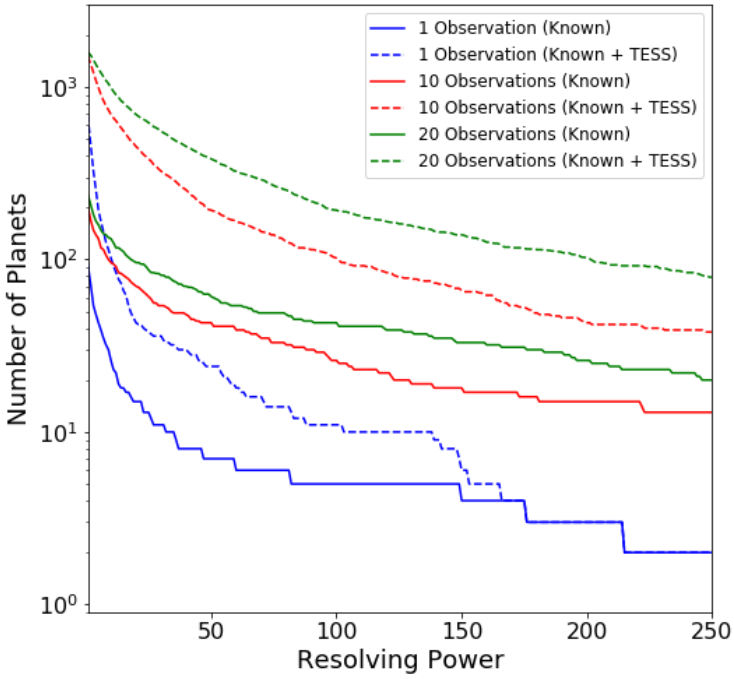

Figure 9.2: Number of known and predicted TESS planets with Twinkle's field of regard for which SNR ≥ 7 is achievable at a given resolving power in channel 0 (0.4 - 1.0 μm)

targets are large gaseous planets (e.g. 84.5% Jupiters and 15% Neptunes/Sub-Neptunes for R >20 in 10 observations). With a larger number of observations, the atmospheres of 46 smaller, potentially rocky planets (R<1.7 $R_\oplus$) are characterisable using low resolution spectroscopy (R<20) in channel 1 with 20 observations. The relations between stellar magnitude, planetary radius and the achievable resolving power are shown in Figures 9.8-9.10.

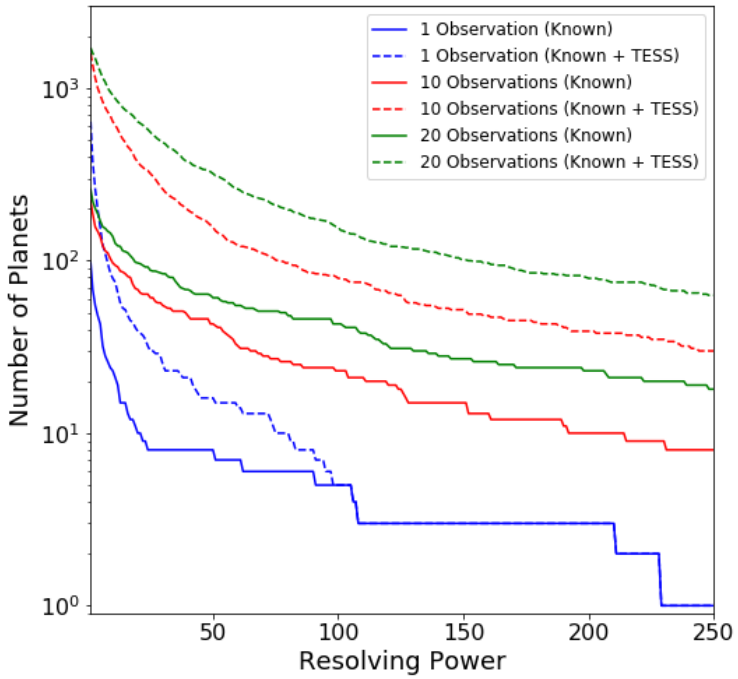

Figure 9.3: Number of known and predicted TESS planets with Twinkle's field of regard for which SNR ≥ 7 is achievable at a given resolving power in channel 1 (1.3 - 2.42 μm)

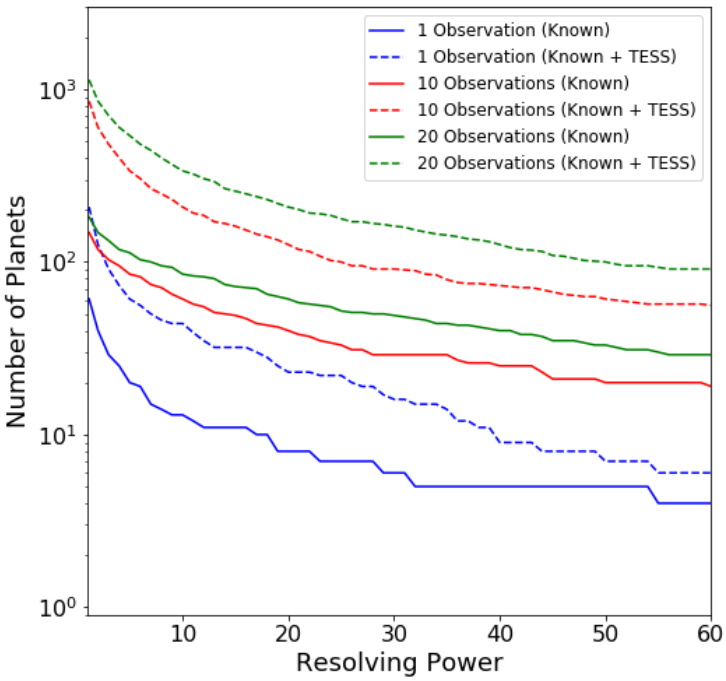

Figure 9.4: Number of known and predicted TESS planets with Twinkle's field of regard for which SNR ≥ 7 is achievable at a given resolving power in channel 2 (2.42 - 4.5 μm)

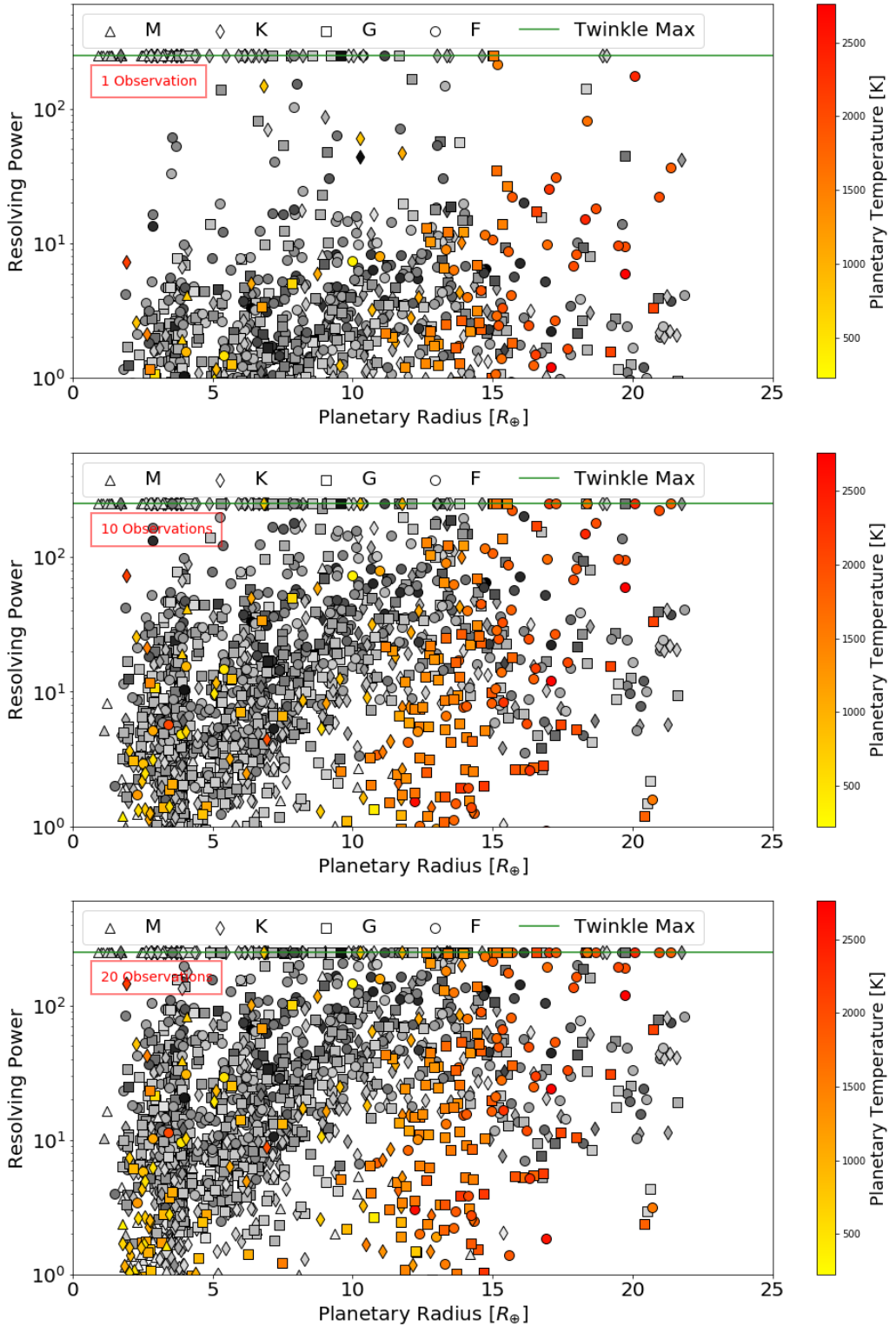

Figure 9.5: Achievable resolving power in infrared channel 0 (0.4 - 1.0 μm) for currently known (coloured) and expected TESS planets (grey) assuming a requirement of SNR ≥ 7 for a given number of transit or eclipse observations. The shape of the points indicates the stellar type of the host star and the green line represents Twinkle's maximum resolving power in the channel

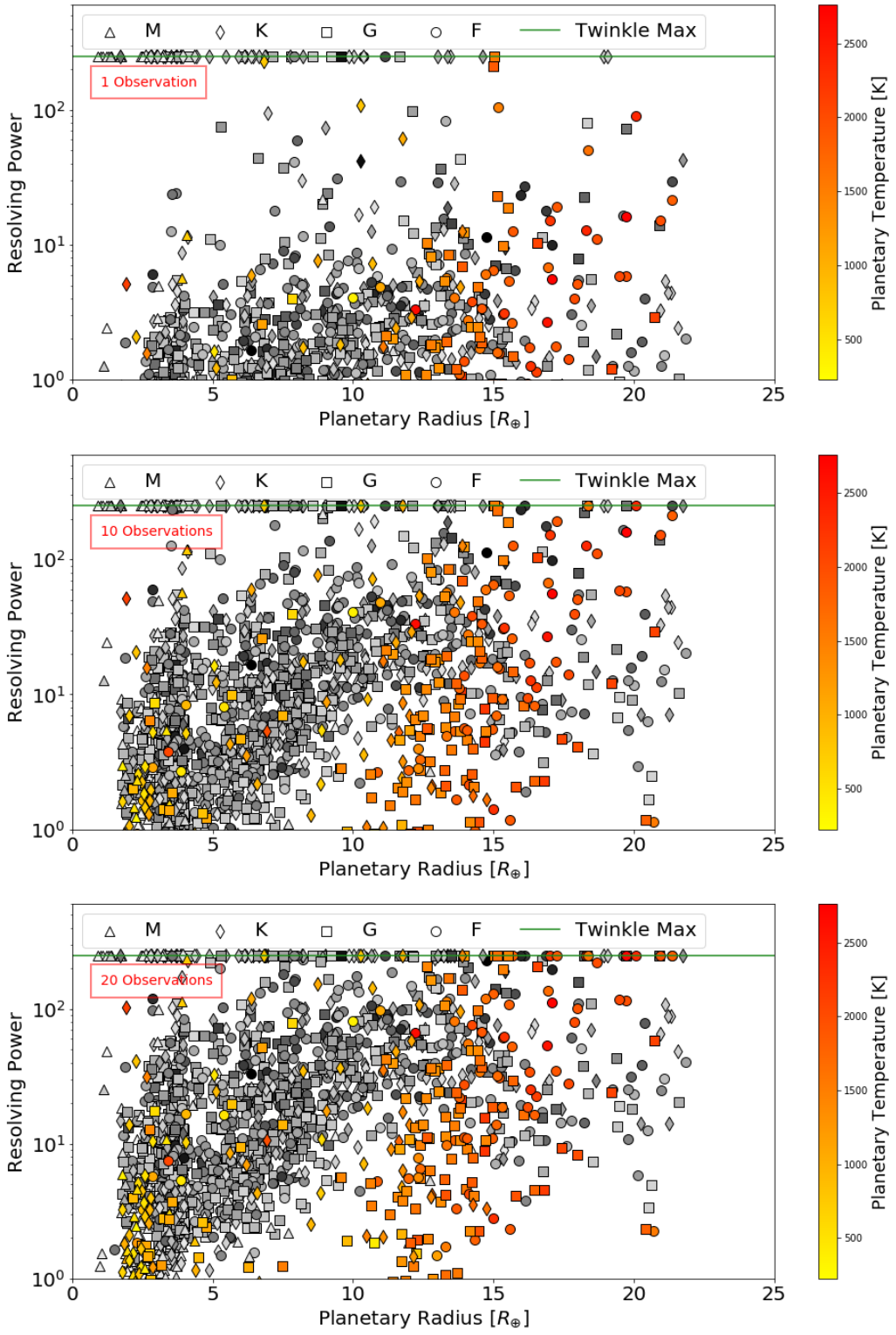

Figure 9.6: Achievable resolving power in infrared channel 1 (1.3 - 2.42 μm) for currently known (coloured) and expected TESS planets (grey) assuming a requirement of SNR ≥ 7 for a given number of transit or eclipse observations. The shape of the points indicates the stellar type of the host star and the green line represents Twinkle's maximum resolving power in the channel

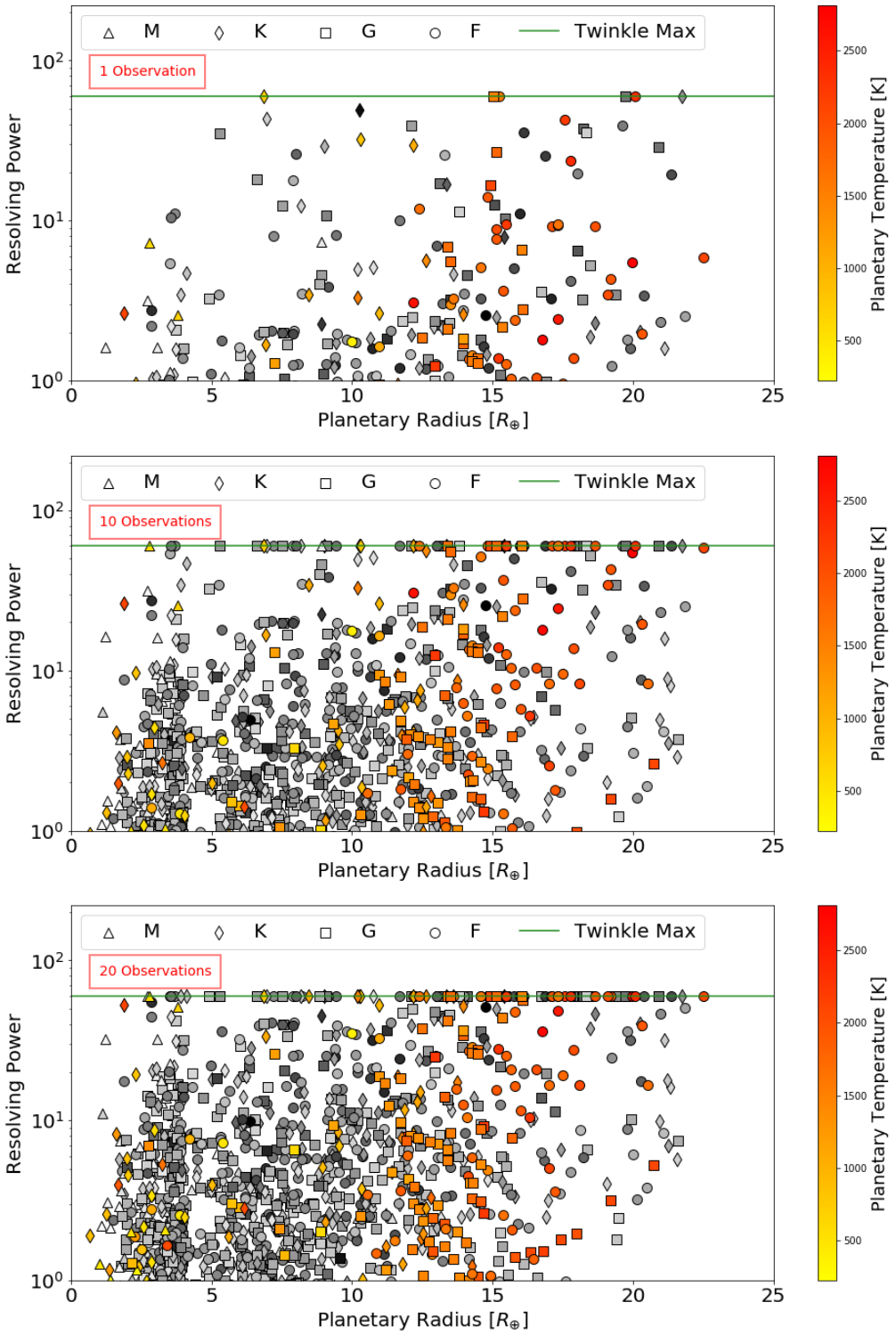

Figure 9.7: Achievable resolving power in infrared channel 2 (2.42 - 4.5 μm) for currently known (coloured) and expected TESS planets (grey) assuming a requirement of SNR ≥ 7 for a given number of transit or eclipse observations. The shape of the points indicates the stellar type of the host star and the green line represents Twinkle's maximum resolving power in the channel

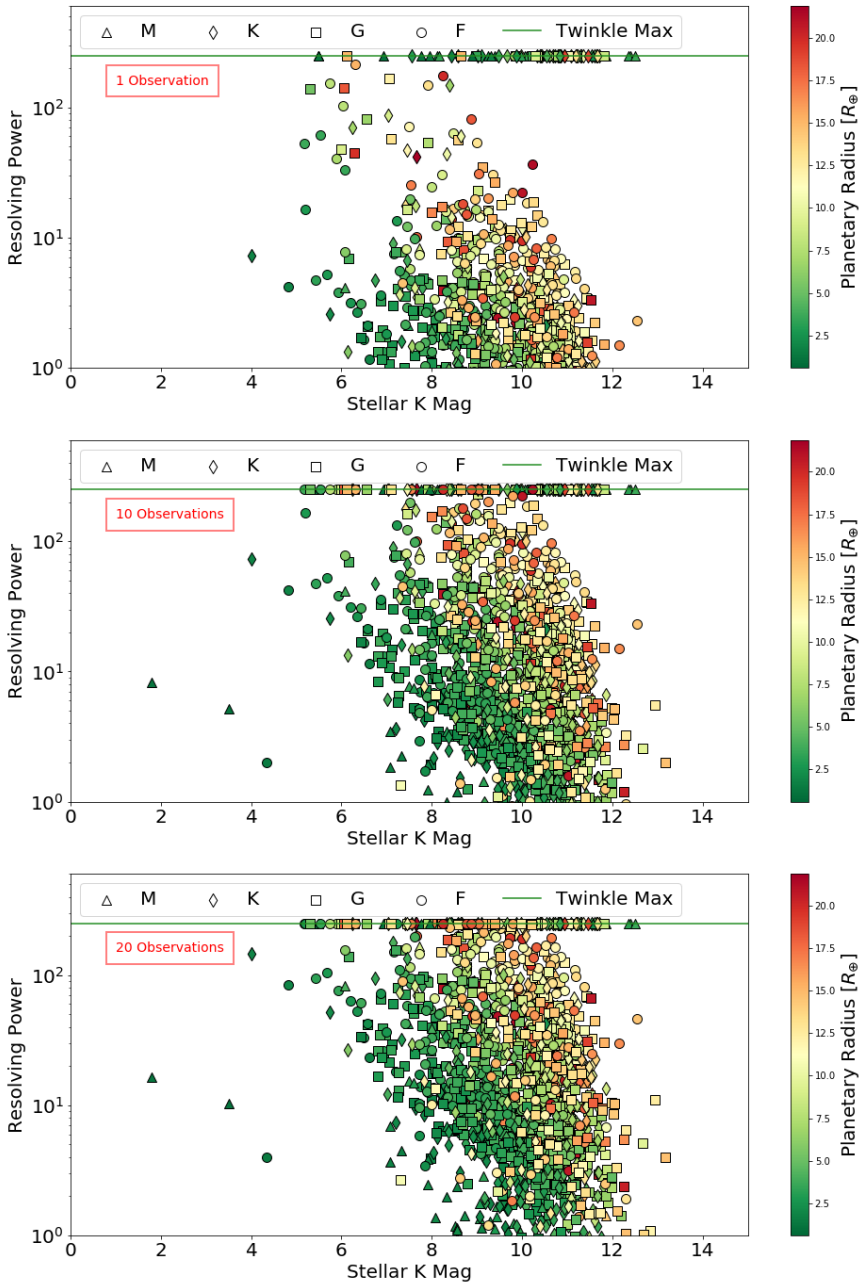

Figure 9.8: Achievable resolving power in the visible channel (0.4 - 1.0 μm) for currently-known exoplanets and predicted TESS planets within Twinkle's field of regard assuming a requirement of SNR $\geq$ 7 for a given number of transit or eclipse observations. The colour of the point indicates the planetary radius, the shape indicates the stellar type of the host star and the green line represents Twinkle's maximum resolving power in the channel

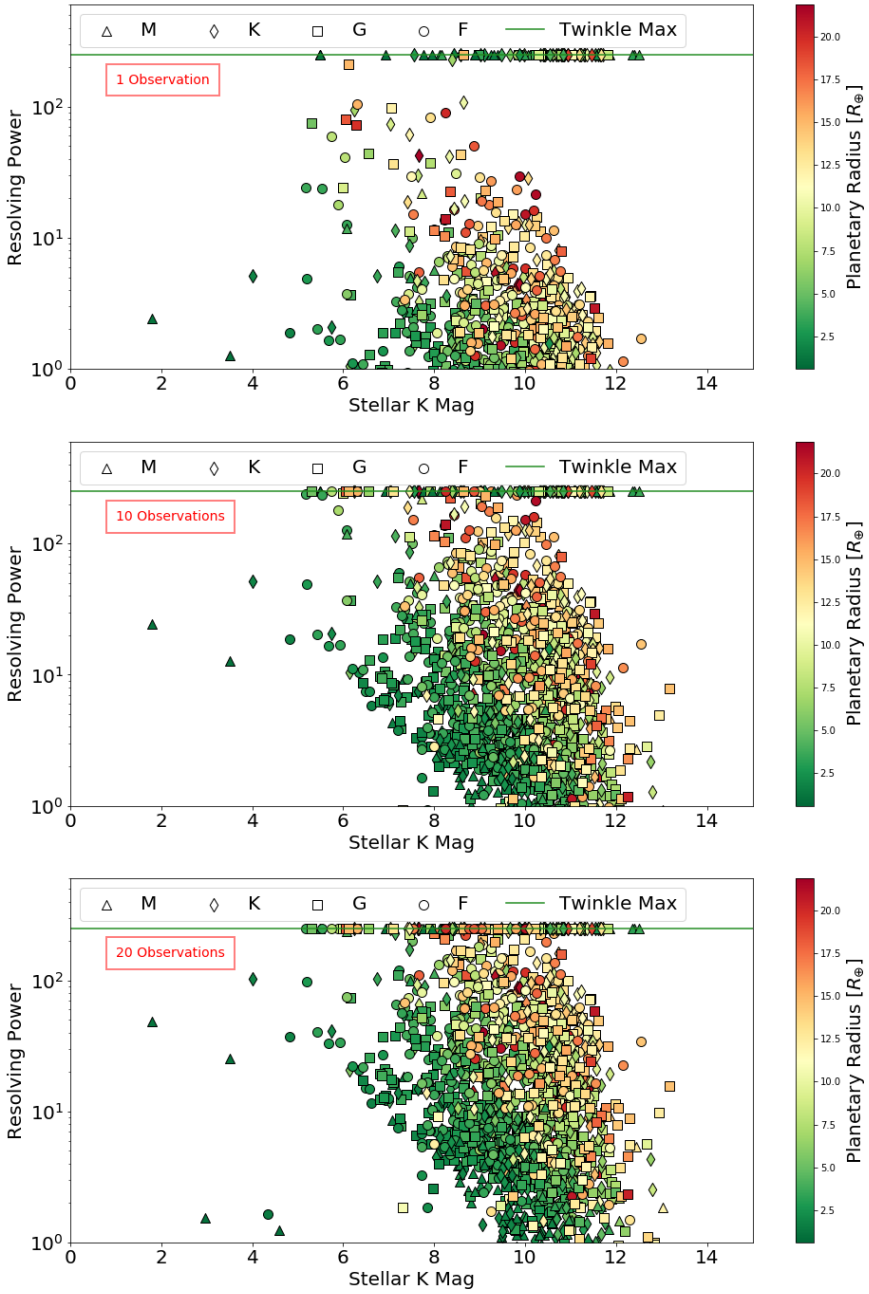

Figure 9.9: Achievable resolving power in the first infrared channel (1.3 - 2.42 μm) for currently-known exoplanets and predicted TESS planets within Twinkle's field of regard assuming a requirement of SNR $\geq$ 7 for a given number of transit or eclipse observations. The colour of the point indicates the planetary radius, the shape indicates the stellar type of the host star and the green line represents Twinkle's maximum resolving power in the channel

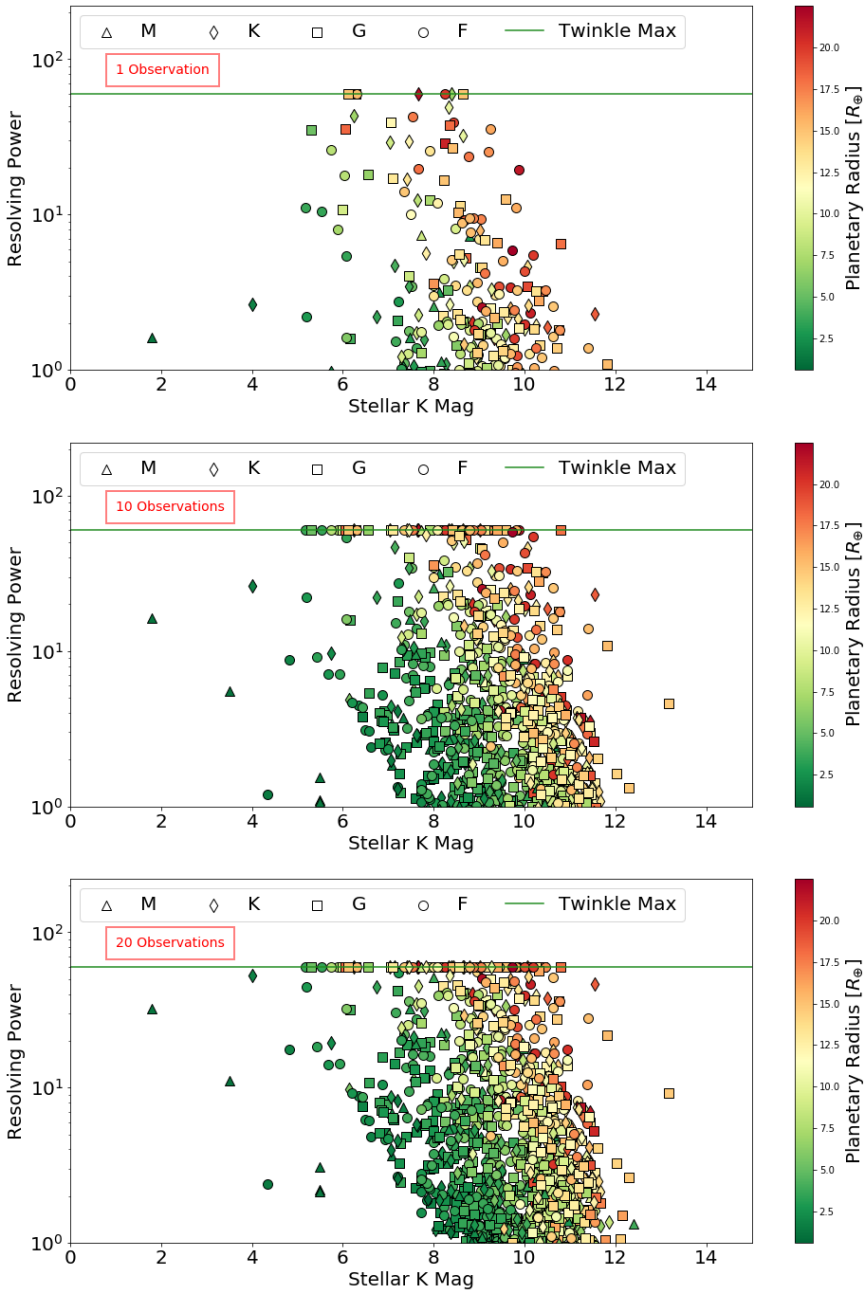

Figure 9.10: Achievable resolving power in the second infrared channel (2.42 - 4.5 μm) for currently-known exoplanets and predicted TESS planets within Twinkle's field of regard assuming a requirement of SNR $\geq$ 7 for a given number of transit or eclipse observations. The colour of the point indicates the planetary radius, the shape indicates the stellar type of the host star and the green line represents Twinkle's maximum resolving power in the channel

9.2.2 Spectral Retrievals

Determining the composition of exoplanetary atmospheres, and thus gaining an understanding of the atmospheric properties, provides insight about the processes occurring on these planets, as well as the presence or absence of clouds an important constraint to understand atmospheric dynamics. Many molecules have absorption lines within Twinkle's spectral bands including H_2O, carbon-bearing molecules (CO_2, CO, CH_4, C_2H_2, C_2H_4, C_2H_6), exotic metallic compounds (TiO, VO, SiO, TiH) and nitrogen/sulphur-bearing species (H_2S, SO_2, NH_3 and HCN).

We have performed several spectral retrieval simulations to assess the information content of the spectra obtainable through Twinkle observations. The known population of exoplanets is diverse and thus to better assess Twinkle's capabilities we focus here on three well known, but very different, planets: HD 209458 b, GJ 3470 b and 55 Cnc e. These planets all orbit very bright stars with K magnitudes of 6.31, 7.99 and 4.02 respectively.

To simulate emission and transmission forward models and atmospheric retrievals we use the open-source exoplanet atmospheric retrieval framework TauREx [272, 241] described in Chapter 7. We have adopted TauREx to simulate retrievals at various resolutions. The assumed planetary characteristics are contained in Table 9.1. For HD 209458 b we take the atmospheric composition retrieved from observations with Hubble WFC3 [240, 314]. We note that, while the spectral range for WFC3 is ideal for detecting water, constraining other molecules is more difficult with many models fitting the data. These degeneracies cause the retrieved abundances to differ from those expected from chemistry models [315].

For the three chosen planets, we calculate the resolution achievable to reach an SNR > 7 for each channel with a given number of transits/eclipses and run Tau-REx spectral retrievals with the observation parameters contained in Table 9.2.

HD 209458 b could be observed, in a single transit, at the highest resolution possible with Twinkle's instrumentation and the subsequent retrieval correctly identifies the abundances and cloud pressure as shown in Figures 9.11 and 9.12 and Table 9.3. Figure 9.13 displays the retrieval for GJ 3470 b and it can be seen that

Table 9.1: Planetary characteristics utilised for simulating atmospheric retrievals

Planet	Equilibrium Temperature [K]	Clouds?	Mean Molecular Weight	Molecular Abundances (Source)		
55 Cnc e	2000	No	2.33	CO C_2H_2 HCN	$1x10^{-3}$ $1x10^{-5}$ $1x10^{-5}$	[316]
GJ 3470 b	700	Yes	2.54	H_20 CH_4 CO NH_3 CO_2	$1x10^{-2}$ $4x10^{-3}$ $1x10^{-3}$ $1x10^{-4}$ $1x10^{-5}$	[317]
HD 209458 b	1000	Yes	2.34	H_2O HCN NH_3 CH_4	$1x10^{-5}$ $1x10^{-6}$ $1x10^{-6}$ $1x10^{-8}$	[240] [314]

Table 9.2: Parameters of the simulated atmospheric retrievals with Tau-REx

Planet	Number of Observations	R (λ <2.42 μm)	R (λ >2.42 μm)	Observation Type
HD 209458 b	1	250	60	Transit
GJ 3470 b	10	65	20	Transit
55 Cnc e	10	10	20	Eclipse

after 10 transits, at a resolution in channel 1 similar to the max resolution of Hubble WFC3, the molecular abundance of H_2O, CH_4, NH_3 and CO_2 have been correctly recovered, even with a cloudy atmosphere (assuming a grey cloud with a cloud top pressure of 10 mbar). However, as shown in Table 9.3 and Figure 9.14, the CO abundance is not recovered as the strongest CO band accessible to Twinkle is at 4.7 μm which is at the edge of its observable wavelength range and often masked by other molecular constituents.

Due to its small size, 55 Cnc e is challenging to observe and thus 10 eclipse observations are required to obtain low resolution spectra. Despite this difficulty, TauREx retrievals of 55 Cnc e resulted in the main constituents of the simulated atmosphere (CO and HCN) being identified well (Figures 9.15 and 9.16, Table 9.3). Increasing the number of visits to 20 results in the accurate recovery of the simulated abundances of CO and HCN as well as more accurately retrieving C_2H_2. The retrievability of C_2H_2 highlights the benefit of higher resolution spectra when measuring abundances of complex carbon molecules.

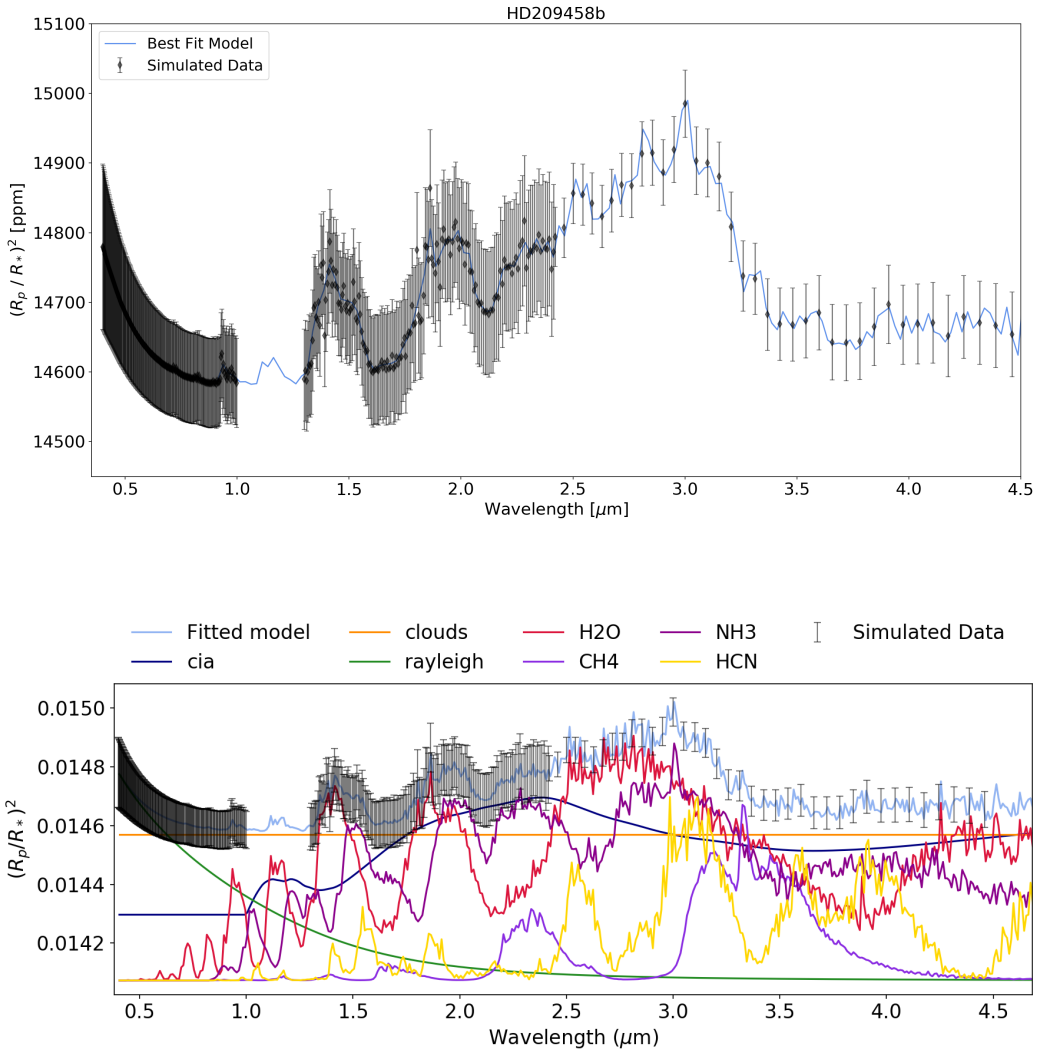

Figure 9.11: Spectral retrieval of HD 209458 b (input values: P_{Clouds} = 1x10^4 Pa, H_20 = 1x10^{-5}, HCN = 1x10^{-6}, NH_3 = 1x10^{-6}, CH_4 = 1x10^{-8}) at R = 250 ($\lambda <$ 2.42 μm) and R = 60 ($\lambda >$ 2.42 μm) with 1 complete transit observation which recovers the main molecular composition but does not constrain CH_4 due to the very low abundance of the molecule. The bottom panel shows the individual contributions of each molecule and of Rayleigh scattering, collision induced absorption (cia) and clouds.

Table 9.3: The original and retrieved abundances for each planet from the simulated retrievals with Tau-REx. We note that we correctly retrieve the abundances for HD 209458 b as well as most of the abundances for GJ 3470 b and 55 Cnc e. However, the CO abundance is not recovered for GJ 3470 b and for 55 Cnc e C_2H_2 is also not constrained. This is due to other molecules obscuring the absorption features as can be seen in the contributions plots in Figures 9.13 and 9.15

Planet	Molecule	Input Abundance (log10)	Retrieved Abundance (log10)	Retrieval Abundance Uncertainty (log10)
HD 209458 b	H_2O	-5.00	-5.02	+0.17 -0.17
	HCN	-6.00	-6.09	+0.33 -0.44
	NH_3	-6.00	-5.98	+0.14 -0.14
	CH_4	-8.00	-9.61	+1.54 -1.63
GJ 3460 b	H_2O	-2.00	-2.03	+0.36 -0.51
	CH_4	-2.40	-2.45	+0.37 -0.46
	CO	-3.00	-7.49	+3.39 -3.01
	NH_3	-4.00	-4.15	+0.38 -0.44
	CO_2	-5.00	-5.13	+0.44 -0.52
55 Cnc e	CO	-3.00	-3.10	+0.42 -0.41
	HCN	-5.00	-5.02	+0.17 -0.17
	C_2H_2	-5.00	-7.47	+2.60 -2.98

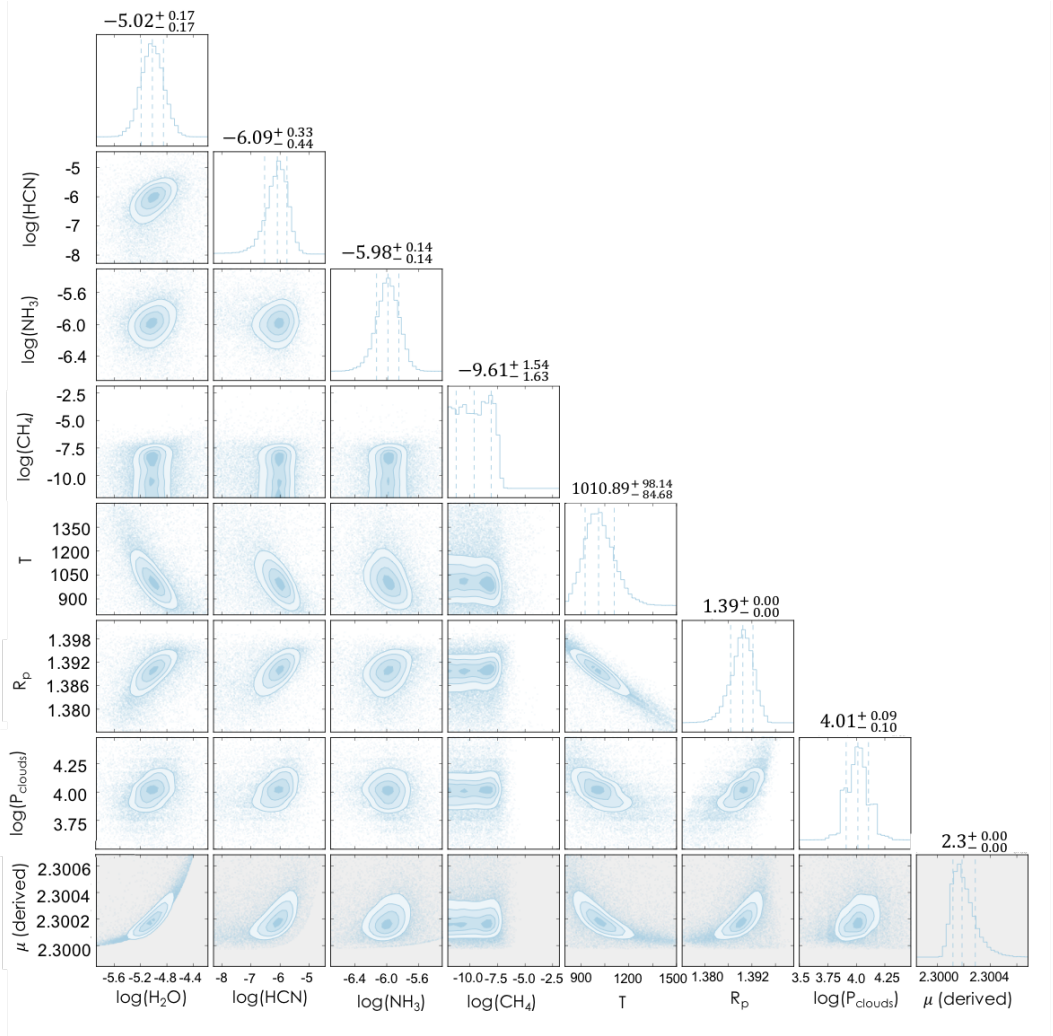

Figure 9.12: Posteriors for spectral retrieval of HD 209458 b (P_{Clouds} = 1x10^4, H_20 = 1x10^{-5}, HCN = 1x10^{-6}, NH_3 = 1x10^{-6}, CH_4 = 1x10^{-8}) at R = 250 ($\lambda <$ 2.42 μm) and R = 60 ($\lambda >$ 2.42 μm) with 1 transit observation which correctly recovers the major molecular abundances and cloud pressure but does not constrain CH_4

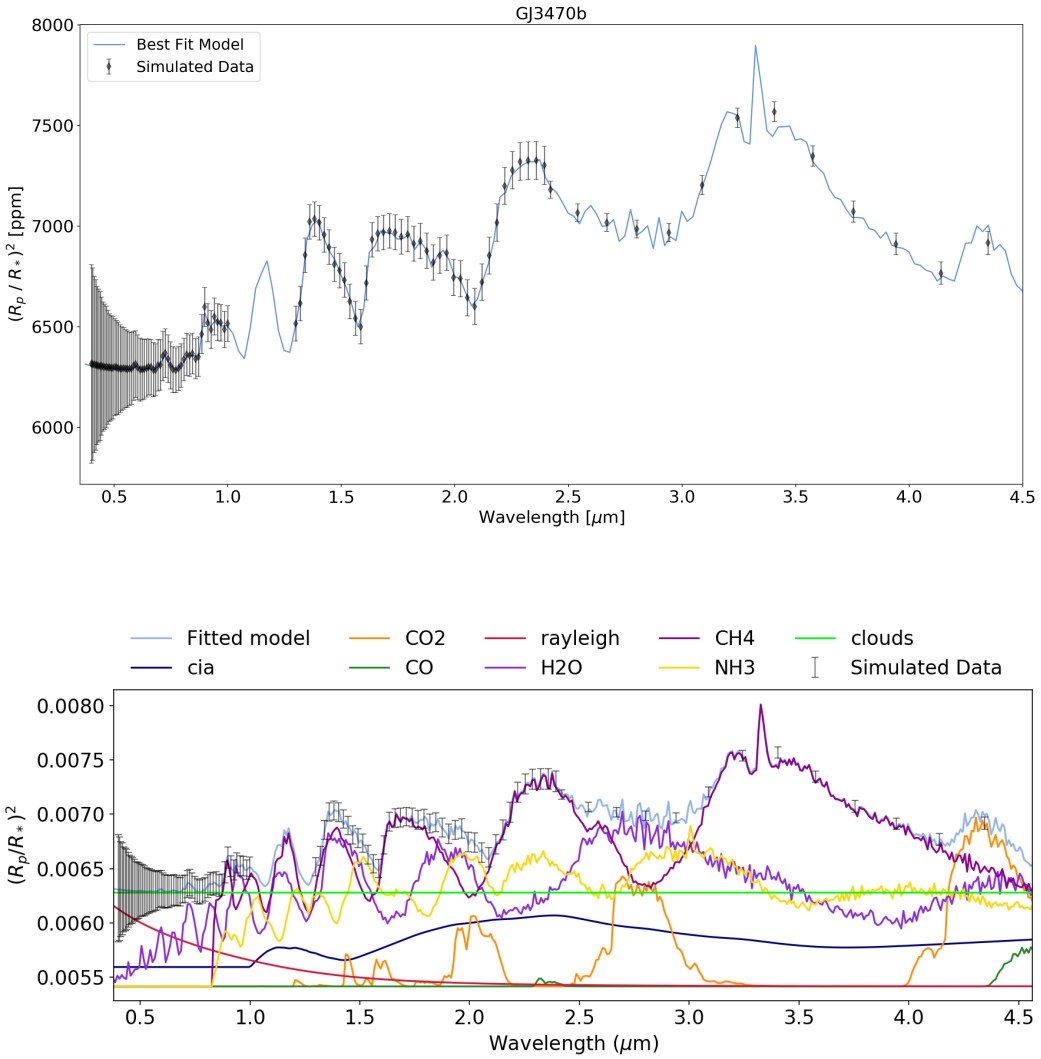

Figure 9.13: Spectral retrieval for GJ 3470 b (input values: P_{Clouds} = 1x10^3 Pa, H_20 = 1x10^{-2}, CH_4 = 4x10^{-3}, CO = 1x10^{-3}, NH_3 = 1x10^{-4}, CO_2 = 1x10^{-5}) at R = 65 ($\lambda < 2.42$ μm) and R = 20 ($\lambda > 2.42$ μm) with 10 complete transit observations which correctly recovers the major molecular abundances and cloud pressure but does not detect CO. The bottom panel shows the individual contributions of each molecule and of Rayleigh scattering, collision induced absorption (cia) and clouds.

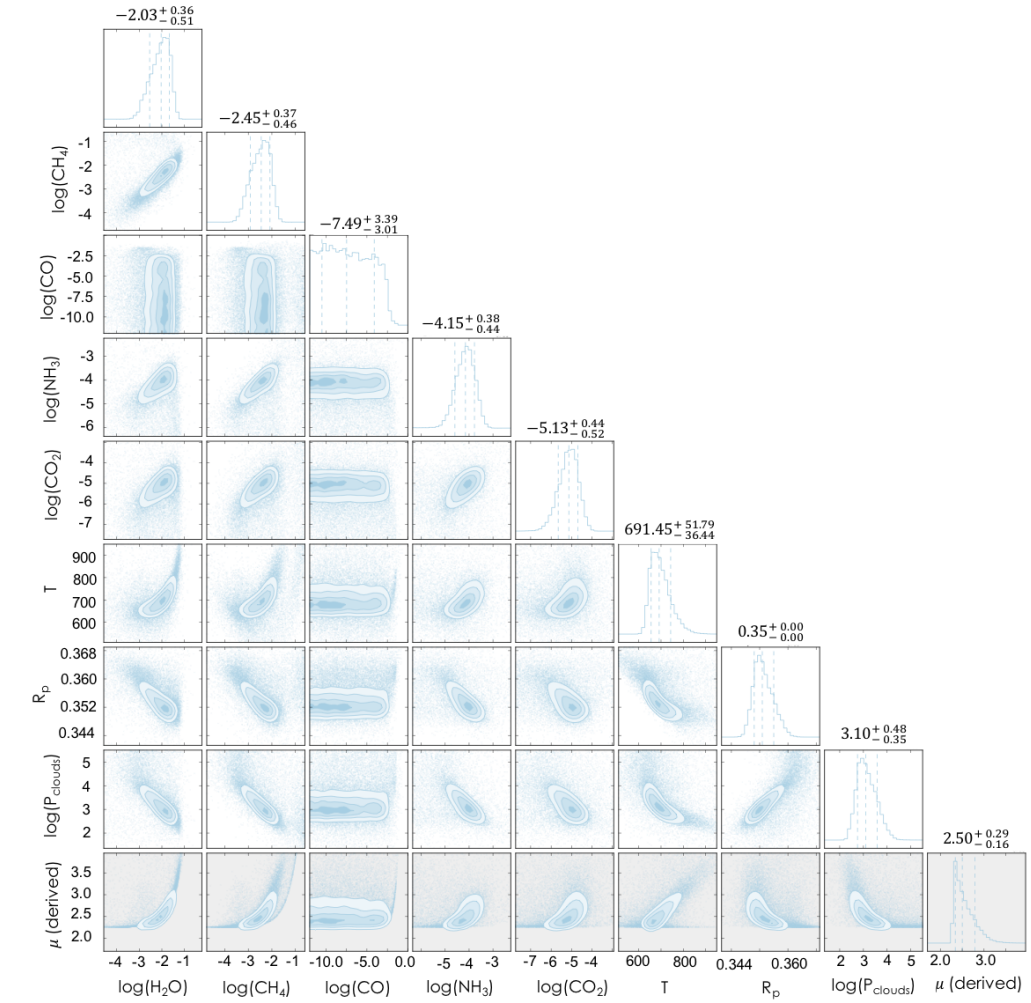

Figure 9.14: Posteriors for spectral retrieval for GJ 3470 b (P_{Clouds} = 1x10^{3}, H_20 = 1x10^{-2}, CH_4 = 4x10^{-3}, CO = 1x10^{-3}, NH_3 = 1x10^{-4}, CO_2 = 1x10^{-5}) at R = 65 ($\lambda < 2.42\ \mu$m) and R = 20 ($\lambda > 2.42\ \mu$m) with 10 transit observations which correctly recovers the major molecular abundances and cloud pressure but does not constrain CO

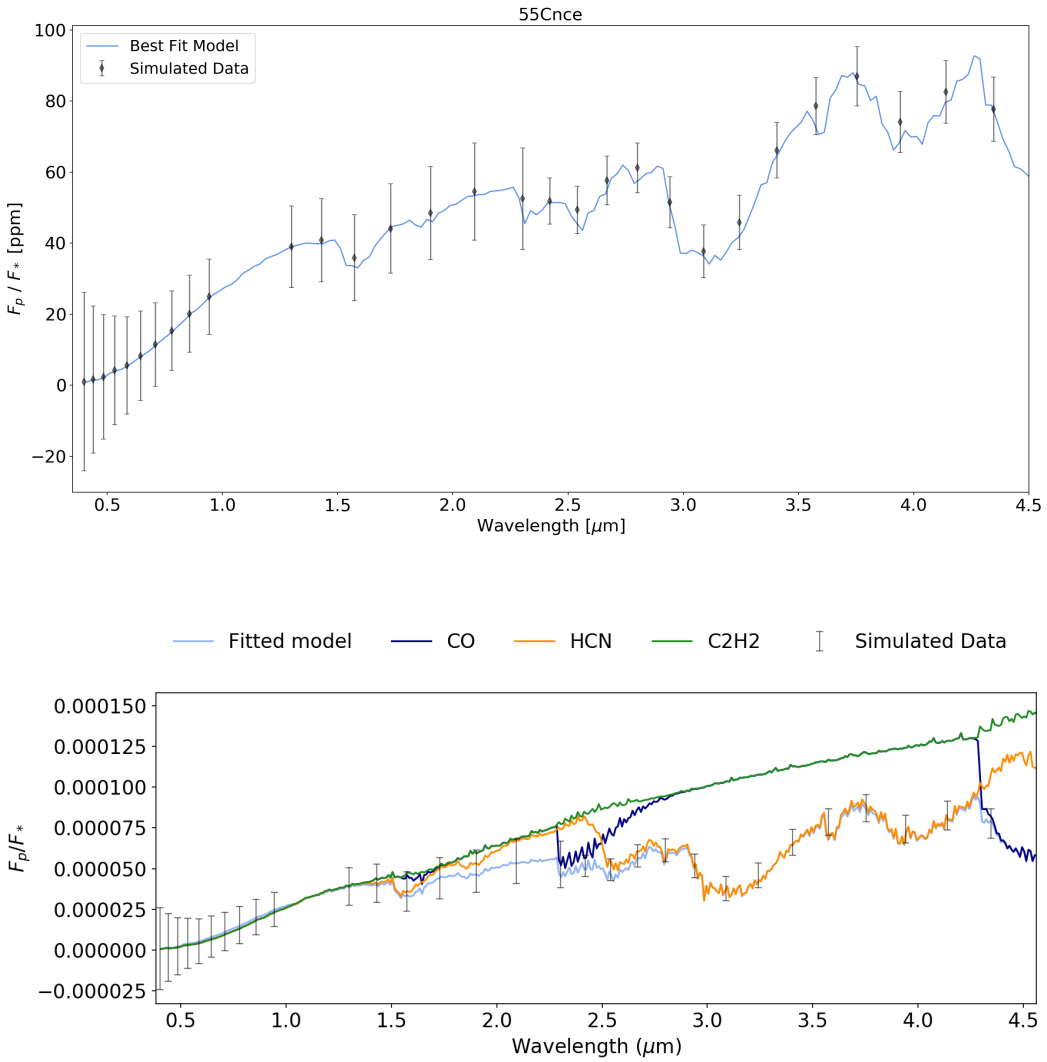

Figure 9.15: Spectral retrieval for 55 Cnc e (input values: cloud free, CO = 1x10^{-3} Pa, C_2H_2 = 1x10^{-5}, HCN = 1x10^{-5}) at R = 10 ($\lambda < 2.42$ μm) and R = 20 ($\lambda > 2.42$ μm) with 10 complete eclipse observations which correctly recovers the HCN and CO abundances but does not constrain the C_2H_2 abundance. The bottom panel shows the individual contributions of each molecule and of Rayleigh scattering, collision induced absorption (cia) and clouds.

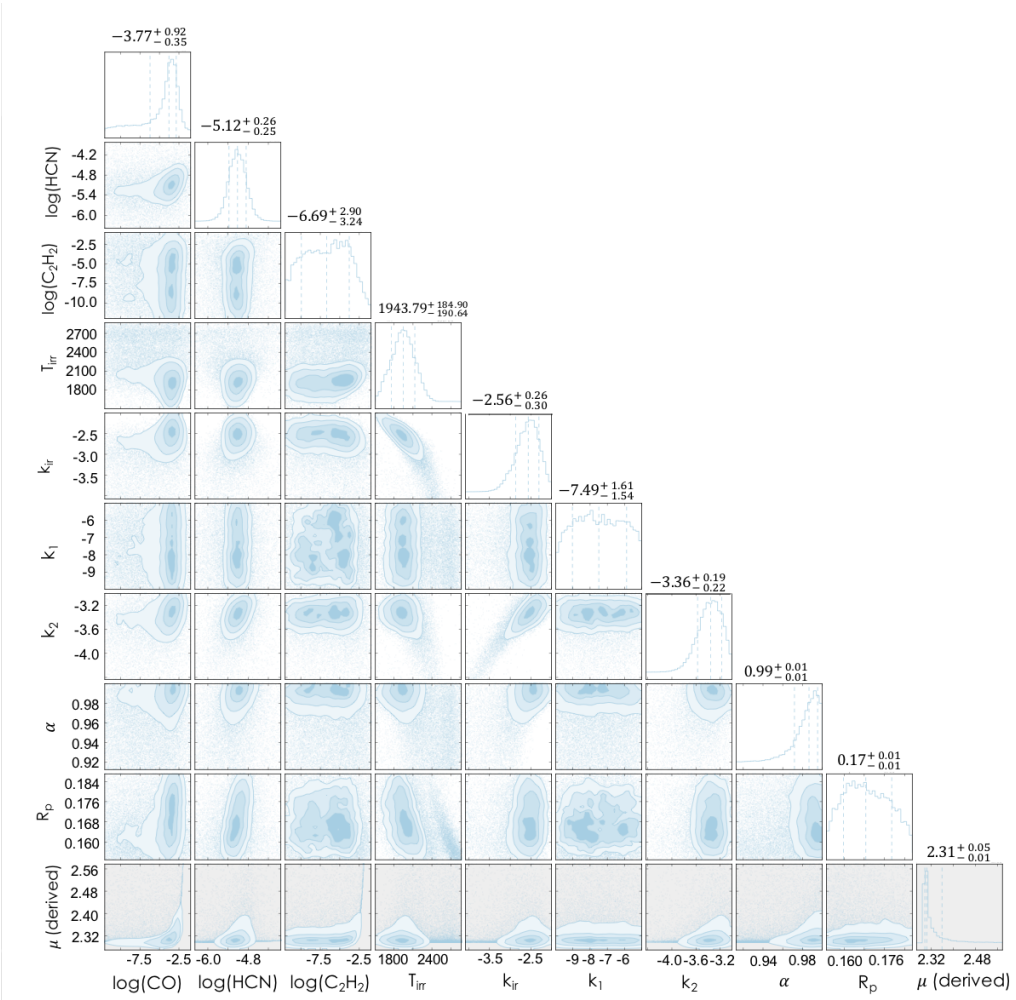

Figure 9.16: Posteriors for spectral retrieval for 55 Cnc e (cloud free, CO = 1x10^{-3}, C_2H_2 = 1x10^{-5}, HCN = 1x10^{-5}) at R = 10 ($\lambda < 2.42$ μm) and R = 20 ($\lambda > 2.42$ μm) with 10 eclipse observations which correctly recovers the HCN and CO abundances but does not obtain the correct C_2H_2 abundance

9.3 Earth Obscuration

Thus far it has been assumed that a full light curve is observed. However, in reality, for space-telescopes in a low-Earth orbit (Hubble, CHEOPS, Twinkle etc.), sometimes only partial light curves will be obtained due to Earth obscuration. The radiometric model used here calculates the SNR achieved based upon observing a full transit or occultation.These gaps cannot be completely accounted for in radiometric models and thus a time-domain code is required.

For this purpose, Terminus was developed. The mission design, analysis and operation software Freeflyer[1] has been used to model the obscurations of the target by the Earth throughout 2023. FreeFlyer has previously been used to support planning for several missions including NASAs Solar Dynamics Observatory (SDO). As Freeflyer only models the physical obscuration of the target star by Earth, the length of the gaps was increased by: 1). 5 minutes to account for stray light limit (i.e. how close Twinkle can observe to the Earth-limb); 2). 5 minutes to account for target re-acquisition after Earth obscuration. Freeflyer also allows one to simulate the view from the spacecraft and Figure 9.17 highlights this issue of Earth obscuration.

Twinkle's field of regard means targets are not constantly observable. In 2023, 17 transits of HD 209458 b would be observable by Twinkle and each of these, including simulated instrument noise for the spectral bin 0.4-0.402 μm, is plotted in Figure 9.18.

The standard methodology of analysing transiting exoplanet data is to fit to the light curves for Rp/Rs to achieve a spectrum with error bars. This distils time-domain observations down to a single point and thus much information about the orbital parameters of the system is lost. Fitting of full light curves (no gaps) usually retrieves the orbital parameters accurately but gaps can lead to less certainty. This potential degeneracy is lost in the standard method and so, to bring the data analysis one step closer to the raw data, retrievals with Terminus generated data are now conducted using the light curves and the methodology described in [243]. This so

[1] https://ai-solutions.com/freeflyer/

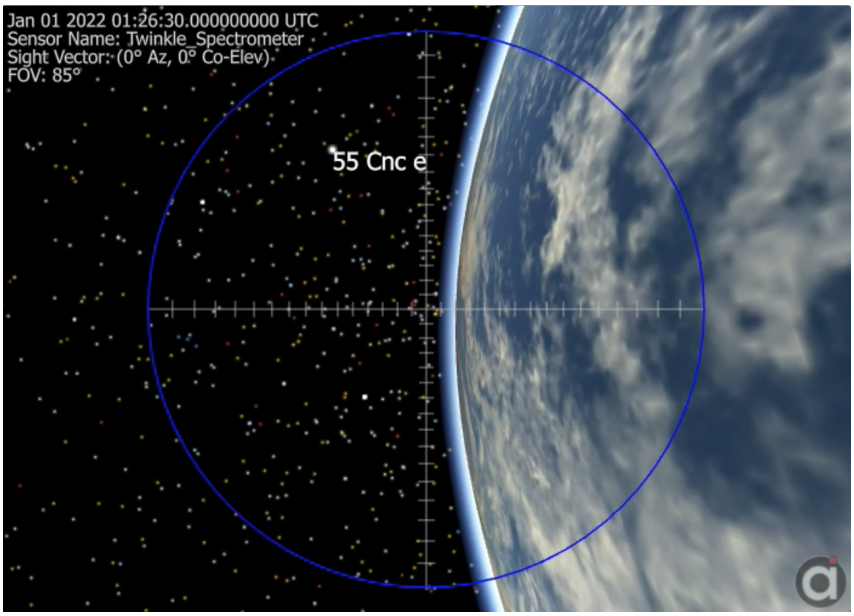

Figure 9.17: Screenshot from Freeflyer highlighting Twinkle's field of regard (blue circle), some of which is obscured by the Earth at this time.

called "L-retrieval" allows for the orbital parameters (e.g. inclination, semi-major axis) to be free parameters in the retrieval to ensure that orbital degeneracies are accounted for.

For each of the available transits, a retrieval is run and the recovered atmospheric parameters are summarised in Figure 9.19. Additionally, a retrieval is run with a set of complete light curves (i.e. no gaps), also fitted through the L-retrieval. In the case of HD 209458 b the gaps are relatively small and these appear to have little effect on the retrieved atmospheric properties. However, it should be noted that in all cases the cloud pressure and NH_3 abundance are overestimated, with the temperature of the planet being slightly cooler than originally modelled. As with the standard retrieval method, the HCN and CH_4 abundances are not well constrained due to the low input values. Adding a second transit would improve the accuracy of the retrieval.

Some planets may have larger gaps and thus may be affected more significantly. For these planets, the scheduling of observations is likely to be highly important. Terminus is able to provide input into studies exploring the affects of partial light curves. Obtaining a full transit, or eclipse, light curve is obviously the ideal

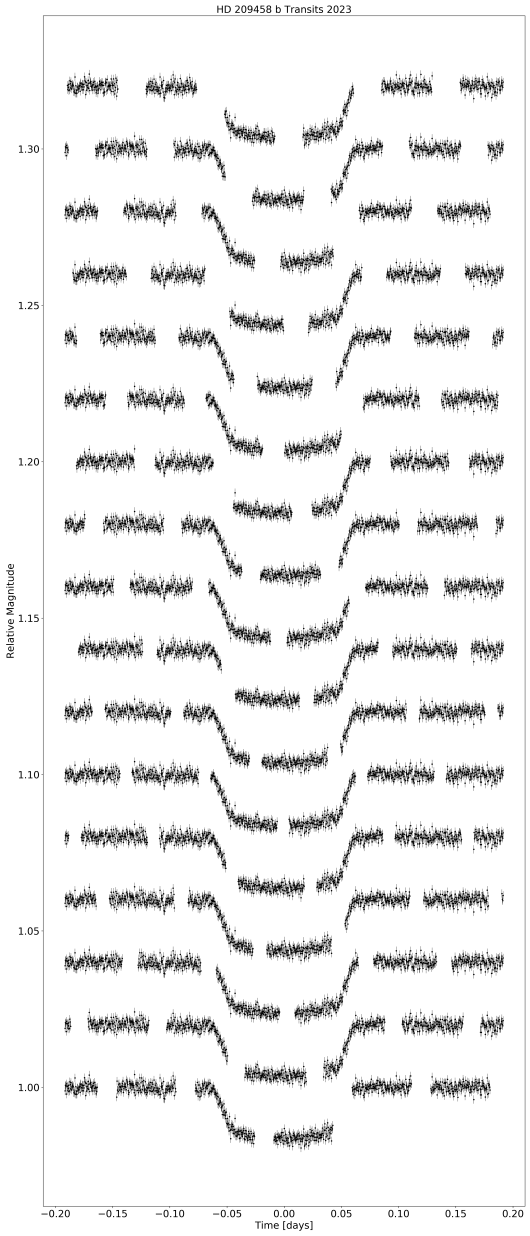

Figure 9.18: Observable transits of HD 209458 b with Twinkle in 2023. The gaps are due to Earth obscuration and have been modelled with Freeflyer. Additionally, the gaps have been lengthened to account for stray light limits and target re-acquisition.

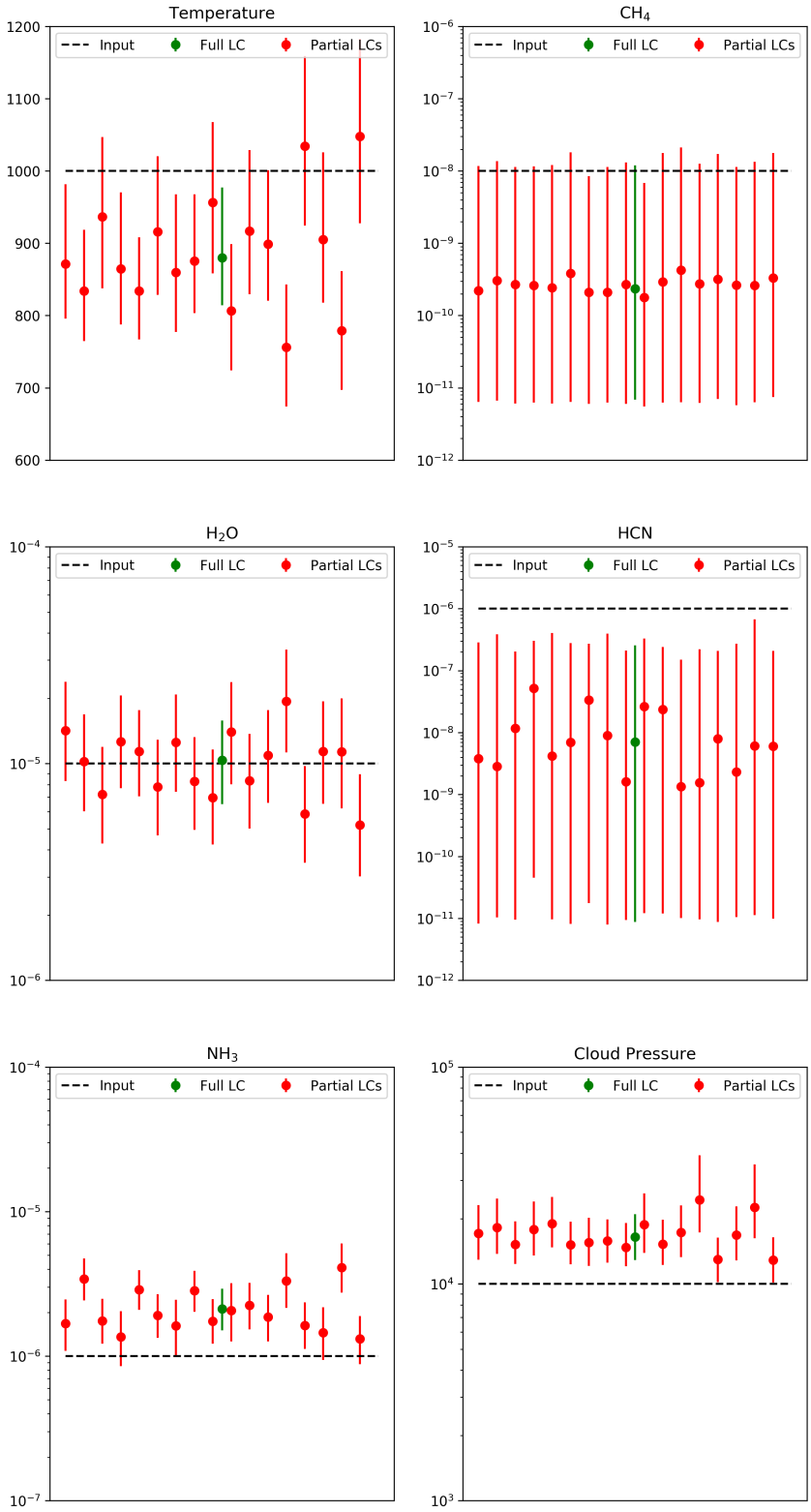

Figure 9.19: Retrieval results for simulated observations of all available light curves of HD 209458 b during 2023 (red). In each case, the light curves are used in the retrieval and the results from an uninterrupted observation (green) and the inputs values (black) are also shown.

case but when it is not possible, such as for HD 209458 b, an optimisation of the location, and length, of the gaps is required. However, as of yet, a full study of the nature and effect of these gaps is yet to be completed.

9.4 Discussion

This first iteration of assessing Twinkle's performance for exoplanetary science has shown that many planets are potentially observable with Twinkle. Twinkle is currently entering a Phase B design review and thus the technical specifications may change. An updated analysis will be published when the design is finalised using the tools discussed here.

We find that a large number of targets could be studied with multi-band photometry (i.e. photons binned into a limited number of broad photometric bands) or low resolution spectroscopy in a single observation. Simultaneous photometric measurements in the optical and infrared would allow for rigorous constraints on the planetary, stellar and orbital parameters of a system. Eclipse photometry in the visible and infrared provide the bulk temperature and albedo of the planet, thereby allowing an estimate of the planetary energy balance and insight into whether the planet has an additional energy input, such as an internal heat source. For the planets discovered by TESS and other transit surveys, constraining planetary ephemerides will be a key requirement to allow for spectroscopic observations further into the future. The planets which have deeper transits could be observed from the ground but fainter and shallower transits will require space-based facilities. Twinkle may also be able to detect TTVs and TDVs but this capability will depend upon the cadence of the observations as well as the impact of Earth obscuration and therefore requires further analysis on specific targets. The temporal binning for brighter targets will be very short ($<$30 seconds) while for fainter stars, a temporal binning of a few minutes may be required, depending on the wavelength range considered. Such a cadence is suitable for TTV and TDV analysis and Twinkle's ability to obtain IR light curves will be useful for studying limb darkening and stellar activity which are expected to exhibit highly reduced distortion over this spectral range compared to

visible wavelengths. Additionally, multi-colour light curves significantly attenuate degeneracy of fitted limb darkening parameters across all wavelengths.

Simulations shown here indicate that, for very bright targets, Twinkle will be capable of spectroscopy with resolutions R $>$20 and sufficient precision to probe the major species present in their atmospheres and constrain lower abundance molecules. For some planets, such as HD 209458 b, this will be achievable in one transit or eclipse while others may require between 10 to 20 observations. When the achievable resolution is plotted as a function of stellar k magnitude (Figures 9.8 - 9.10, a cut-off limit of K mag $\sim$12 for spectroscopy (R$>$20) is uncovered. Hence many Kepler planets orbit stars too faint for spectroscopic follow-up with Twinkle but TESS is expected to provide a multitude of suitable targets. The majority of planets that can be observed spectroscopically with Twinkle are hot, giant planets or Neptunes although some smaller or cooler planets around very bright stars might be feasible.

By simultaneously providing spectroscopic data over a large wavelength range, Twinkle will be able to reduce the degeneracies that affect current observations with Hubble and Spitzer. While the spectral range of WFC3 is ideal for detecting water vapour and characterising clouds, Twinkle's wavelength range contains absorption features from a wide variety of molecules (e.g. H_2O, CH_4, CO_2, CO, NH_3, HCN, TiO, VO). The instrument spectral resolving power allows in principle the detection of many trace gases, the only limiting factor being the precision achieved which depends upon the integration time (i.e. the number of transit or eclipse events). Twinkle's observations will be demand-based and thus the requirements in terms of spectral resolution and SNR will depend on the user's preferences. The values here utilised for retrievals have been selected to provide an overview of the capabilities of the satellite and to allow a potential user to assess Twinkle's suitability for the observations they desire. From the spectral retrievals conducted here it is found that the major constituents of an atmosphere could potentially be recovered with low resolution spectroscopy (R$\sim$20). However, for weaker molecular transitions or to retrieve trace gas abundances more accurately, longer integration time may

be required (e.g. Figure 9.15). In the case of Figure 9.15, the underlying issue may be the cross-section utilised for C_2H_2 which has been determined at Earth-like temperatures, not the $\sim$2000 K assumed here for 55 Cnc e. This highlights the need for accurate line lists over a wide temperature range and the importance of the work of groups such as ExoMol [318].

The visible part of the spectrum can be utilised to measure the planetary albedo, Rayleigh scattering and detect/characterise clouds. Star spots and faculae may affect the observed transit depth at wavelengths shorter than 2 μm and Twinkle's spectral coverage should allow stellar activity to be monitored and to remove, or mitigate, its impact on the observations. For hotter planets, metallic resonance line (e.g. Na and K) dominate the opacities over visible wavelengths [319]. The spectral resolving power considered for Twinkle in the optical (R$\sim$250) will allow for such detections on planets orbiting very bright stars. A wide spectral range will also be advantageous in the search for condensates or hazes with many species expected to condense in exoplanetary atmospheres, as suggested by current observations [15, 3].

In the thermal regime, usually probed in the infrared through eclipse observations, redundancy in molecular detection is also necessary to allow for the retrieval of the vertical thermal structure and molecular abundances (e.g. [320, 321]). The capability to observe multiple absorption bands of the same molecule provides some redundancy and significantly improves the reliability of a detection. Additionally, insights into the vertical distribution of species can be gained by observing bands of different intensity which probe different atmospheric levels.

For a more refined list of targets and performances, several factors not studied in this paper must also be accounted for. These are detailed in Sections 9.4.2 - 9.4.4 below.

9.4.1 Complimentary with Other Facilities

Twinkle could be utilised to provide preliminary observations of targets for other observatories such as JWST and Ariel, refining transit times and reducing the risk of missing transits due to poor ephemeris data. Given its capabilities, JWST time will be extremely precious [111], with over-subscription likely to be an issue, and

thus any insight about the atmospheres of recently discovered planets will be highly advantageous to guide the selection of the very best targets. Ariel will be launched in 2028 and aims at observing a very large population of exoplanet atmospheres [125]. A key decision for Ariel is the selection of optimal and diverse targets before its launch and Twinkle could be utilised to inform these decisions as well as provide initial insights into the mission's science objectives. Ariel will require a robust and efficient schedule to observe a large population of exoplanets. Hence providing constraints on the planetary, stellar and orbital parameters with Twinkle would enhance the mission's scientific yield.

Additionally, Twinkle could enhance ground-based observations. Ground-based surveys are capable of extremely high resolution spectroscopy over narrow wavebands, but the spectral continuum is unknown. By observing the same target over a broader wavelength range from space, at a lower resolution, Twinkle will be able to provide the missing, highly complementary information.

9.4.2 Earth Obscuration

The radiometric model used for the population study calculates the SNR achieved based upon observing a full transit or occultation. However, due to Twinkle's low Earth orbit, it will not always be possible to view the transits (or eclipses) in their entirety. Observing partial transits/eclipses will reduce the SNR achieved for a given number of observations and thus the number of transits (or eclipses) predicted by the radiometric model is, in these cases, an underestimate of the number that will need to be observed. Work is continuing to assess the impact of Earth obscuration and the effect on the number of potentially observable targets.

9.4.3 Scheduling

The observability of a target has been determined by assuming that a given number of complete transits or eclipses could be viewed during the mission lifetime. In addition to Earth obscuration, scheduling constraints, such as telescope housekeeping, slewing between targets and observations of other targets, will impact the number of transits or eclipses that are observable in a given time period. Such constraints have

not been included in this exercise and the development of an optimised schedule is dependent upon an improved understanding of the additional observations required due to Earth obscuration.

The expectation is that the main issue may be observation overlaps (i.e. two planets transiting at the same time) rather than an insufficient number of potential observations. Our analysis finds that, for currently-known planets within Twinkle's field of regard, around 85% of targets have at least 5 transits/eclipses which could be viewed in a year while over 60% of targets have 10 potential observations or more per year. Therefore, during the mission lifetime, most planets will have many transits and eclipses which could be observed. Further target selection studies will occur in due course and will incorporate these constraints.

9.4.4 Future Planet Discoveries

The main focus of this work is on Twinkle's capability to observe currently-known planets whilst also considering the predicted TESS yield. Additionally to TESS, by the launch date, other space-based missions such as Gaia, CHEOPS and K2, as well as ground-based surveys including NGTS, SPECULOOS, and WASP, are expected to have discovered hundreds of new planets around bright stars within Twinkle's field of regard. This will provide an expanded list of planets including many that are anticipated to be observable by Twinkle.

Predicted TESS detections were included in this study to provide an indication of the number, and type, of planets projected to be discovered which will be suitable for observations with Twinkle. We find that discoveries from the TESS survey could more than double the number of exoplanet atmospheres that Twinkle is capable of observing. As further planets are discovered they will be added to this analysis to produce a comprehensive Twinkle target list.

9.5 Conclusion

This chapter has presented an initial survey of Twinkle's capability for optical and infrared observations of exoplanets. For the several hundred currently-known planets which lie within Twinkle's field of regard and whose parameters are known, the

spectral resolution which could be obtained for a given number of transit or eclipse events has been estimated.

Within a single transit or eclipse observation, it is predicted that 82 existing targets could be observed in at R <20 in channel 1 (1.3 - 2.42 μm) whilst 68 planets could be observed spectroscopically (R >20) with 10 transits or eclipses. The planets observable spectroscopically are found to be generally hot, with planetary radii greater than 10 $R_{\oplus}$, and orbiting bright stars (K magnitude<11).

Spectral retrieval simulations of HD 209458 b, GJ 3470 b and 55 Cnc e highlight the expected capability of Twinkle for atmospheric characterisation in case of planets around very bright stars. We find that most abundant molecular species, cloud and atmospheric key parameters can be retrieved reasonably well at the spectral resolution obtainable with Twinkle.

Future surveys will reveal thousands of new exoplanets, some of which will be located within Twinkle's field of regard. Analysis of the predicted detections suggests the number of exoplanets, and exoplanet atmospheres, Twinkle is capable of characterising will dramatically increase from planets found with TESS.

Chapter 10

Further Applications of Radiometric Models

> ”Any darn fool can make something complex; it takes a genius to make something simple.”
>
> Pete Seeger

Space-based telescopes take a long time to develop, build and launch. During this time, is it useful to begin to explore the capabilities of the instrumentation, hence the need for the development of the tools discussed thus far. These models provide a useful means of showing the wider scientific community the expected performance of the mission and for preparing the necessary pipelines and techniques needed to analyse the data. The focus of this chapter is on how these instrument models can be used for specific science cases. Firstly an overview of literature uses is given before discussing the need for more complex chemistry profiles in atmospheric retrievals. Finally the three tools developed and discussed here are used to compare the capabilities of future missions by performing retrievals on simulated

Contributions: The sections on two layer chemistry and K2-18b are based upon a papers led by Quentin Changeat to which I have contributed significantly (Changeat, Edwards, et al. 2019, Towards a more complex description of chemical profiles in exoplanet retrievals: A 2-layer parameterisation, ApJ. & Changeat, Edwards, et al., in prep, Disentangling Atmospheric Compositions of K2-18 b with Next Generation Facilities). The rest of the results presented here are original work which has not been published.

data for a hot-Jupiter and a Super-Earth.

10.1 Uses In The Literature

A key area of investigation surrounding the performance of upcoming instruments is into the current assumptions and simplifications used in atmospheric retrievals. Present data, with its low SNR and narrow wavelength coverage is not of sufficient quality for complex atmospheric profiles to be disentangled. However, future observatories can be expected to provide spectra which require more complex analysis than the current 1-D, isothermal, isochemical atmospheres. For instance, [322] have demonstrated that the assumption of constant atmospheric thermal profiles will be inadequate to correctly interpret future transit spectra recorded from space. By simulating JWST observations of HD 209458 b with a temperature that varies with altitude and attempting to retrieve an isothermal profile, [322] showed that biases would be introduced in the retrieved chemical abundances.

In standard retrievals, atmospheres are considered be 1-D, that is a homogeneous collection of thin columns where changes occur only with altitude. This is, of course, a huge simplification and one can imagine that large gaseous exoplanets have circulation patterns similar to Jupiter. Several studies have looked into the differences in atmospheric spectra when accounting for further dimensionality.

On tidally-locked planets we expect there to be strong thermal, and compostional, gradients between the day and night side. These would cause heterogeneties across the limb which would consequently affect the observed spectrum. [323] developed a 3D radiative transfer model to generate transmission spectra through such atmospheres and, for GJ 1214 b, found that the differences between the 1-D and 3-D models were greater than the noise expected on JWST observations. Retrievals for this planet, and for HD 209458 b, revealed systematic biases on the retrieved temperature and chemical abundances. Disturbingly, the 1-D retrievals provided an excellent fit to the data and the biases would not be easily detectable.

Similarly, [324] explored the effects of an inhomogeneous horizontal temperature structure on emission retrievals. They derive an analytical criterion which

can be used to find the SNR required to disentangle inhomogeneous temperature structure, finding that the SNR needed increases at longer wavelengths. Again, by retrieving a 2-D input with a 1-D model, the chemistry retrieved is biased. However, [324] show that applying a dilution factor to the 1-D model results in a capability similar to that of a 2-D retrieval and, for quenched atmospheres where the chemistry across the disc is close to uniform, biases in the chemistry would not be introduced with this methodology. This dilution factor is used to scale the model to preferentially sample the hotter regions of the atmosphere, which have a greater contribution to the observed spectrum, instead of performing a disc-averaged retrieval. The study also shows that the effects of the 2-D model are more evident at shorter wavelengths but can still bias the longer wavelengths, even when there is no apparent evidence for using a 2-D retrieval over a 1-D.

Another major focus of studies has been the ability of JWST to study the atmospheres of rocky planets, particularly those within the habitable zone of their star. Since its discovery, the TRAPPIST-1 system of seven Earth-sized planets has been the epicentre of this movement. Orbiting an M-dwarf (T_{Eff} = 2500 K, R_* = 0.12 $R_\odot$ [67]), these planets have large transit depths and thus any atmosphere present will provide a higher SNR than for a similar planet around a F/G/K star. Additionally, due to the coolness of TRAPPIST-1, the habitable zone lies close to the star and so the planets within it, TRAPPIST-1 d, e, f and g, have periods between 4 and 12 days [67]. A short period is crucial because, even with the large transit signal, many transits will need to be stacked to observe any atmospheric features with high confidence. Given the potential habitability of these worlds, much effort has been expended on studies attempting to quantify the amount of JWST time required to detect features, especially those due to water or carbon dioxide. For example, work by [325] concludes that transmission spectroscopy with NIRSpec Prism is optimal for detecting terrestrial, CO_2 containing atmospheres. They conclude that is can potentially be achieved in fewer than 10 transits for all seven TRAPPIST-1 planets, if they lack high altitude aerosols. However, the additional of H_2SO_4, an aerosol present on Venus, would increase the number of observations required to detect an

atmosphere by up to an order of magnitude. It should be noted that this study calculated the number of observations required to rule out a featureless spectrum (i.e. no atmosphere) for different compositions at an SNR of 5. To distinguish between different types of atmospheres, and comprehensively detect molecules, would likely require far more observations and would certainly also be hindered by the presence of clouds. Another study explored whether GJ 1132 b or LHS 1140 b would potential provide better opportunities for characterising the atmospheres of small, rocky planets. While LHS 1140 b was found to be unsuitable, the atmsophere of GJ 1132 b could be observed in a few eclipses using the MIRI instrument [326].

However, work by [242] shows that stellar contamination can have hugely detrimental effects on the near-infrared spectra of the TRAPPIST-1 system. By modelling spots and faculae they showed that stellar contamination can affect the transmission depth of these planets with strengths of 1-15x the strength of the atmospheric features. Additionally, as TRAPPIST-1 is a fast rotating star, across a single transit around a third of the visible stellar hemisphere will be different between the beginning and the end of the transit. Such a rapid change means that stellar contamination will not only be different between different transits, but will change even during a single transit, making potential star spot modelling and correction even more difficult [16]. Hence, JWST spectroscopy of the system may be extremely difficult, particularly if multiple instruments are combined.

10.2 Exploring Two Layer Chemistry

State of the art spectral retrieval models of exoplanet atmospheres assume constant chemical profiles with altitude. The isochemical assumption is justified by the information content of current datasets which do not allow, in most cases, for the molecular abundances as a function of pressure to be constrained.

In the context of the next generation of telescopes, a more accurate description of chemical profiles may become crucial to interpret observations and gain new insights into atmospheric physics. We have explored the possibility of retrieving pressure-dependent chemical profiles from transit spectra, without injecting any

priors from theoretical chemical models in our retrievals. The "2-layer" parameterisation presented here allows for the independent extraction of molecular abundances above and below a certain atmospheric pressure.

By simulating various cases, we demonstrate that this evolution from constant chemical abundances is justified by the information content of spectra provided by future space instruments. Comparisons with traditional retrieval models show that assumptions made on chemical profiles may significantly impact retrieved parameters, such as the atmospheric temperature, and justify the attention we give here to this issue.

We find that the 2-layer retrieval accurately captures discontinuities in the vertical chemical profiles, which could be caused by disequilibrium processes – such as photochemistry – or the presence of clouds/hazes. The 2-layer retrieval could also help to constrain the composition of clouds and hazes by exploring the correlation between the chemical changes in the gaseous phase and the pressure at which the condensed phase occurs.

The 2-layer retrieval presented here therefore represents an important step forward in our ability to constrain theoretical chemical models and cloud/haze composition from the analysis of future observations. The approach taken here is to increase the number of free variables for each molecular species considered. Applying this approach to currently available data is not justifiable as it would simply increase the degeneracy of the retrieved solutions. By contrast, attempts to use models of inadequate complexity to analyse spectra observed by next generation facilities are likely to provide incomplete pictures and misleading results. The importance of moving towards a more complete description of chemical profiles through the analysis of simulated transit data from Ariel is explored. In this context, we consider the example of a 2-layer parametrisation with 3 degrees of freedom.

10.2.1 Methodology

This work focuses on retrievals of transit spectra, so that, for simplicity, the thermal profile can be assumed isothermal in some benchmark cases. In eclipse spectroscopy, the thermal gradients and the chemical profiles are always entangled, mak-

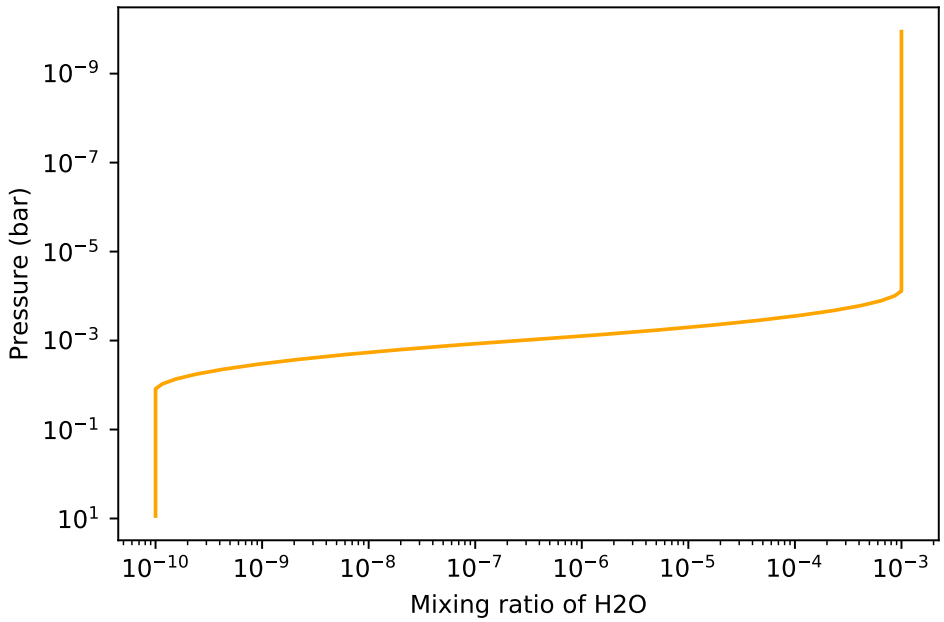

Figure 10.1: Example of a 2-layer chemical profile with H_2O which can be used as input for forward simulations of exoplanet spectra, as well as for fitting data in retrievals. Here, the surface layer is depleted with a mixing ratio $X_S(H_2O)$ of 10^{-10} and the top layer has a large quantity of H_2O, with $X_T(H_2O) = 10^{-3}$. The separation pressure of the two layers is set to $P_I(H_2O) = 10^{-3}$ bar and the transition is smoothed over 10% of the atmosphere (10 layers).

ing it a more complex case which will be considered in future work. The 2-layer parametrisation has been adopted for its simplicity and because it does not rely on external physical assumptions which could bias the results of the retrieval. While our model is clearly not representative of all real atmospheres, it allows us to consider a departure from the constant mixing ratios case.

A new 2-layer module has been added to the Tau-REx code. The chemical parametrisation we used can be described by three variables: the surface/bottom abundance X_S, the top abundance X_T and the pressure defining the separation of the two layers (Input Pressure Point, P_I, for the forward model and Retrieved Pressure Point, P_R). The chemical profile is linearly interpolated in log space – smoothing over 10% of the atmosphere – to avoid a sharp transition in the profile. An example of a 2-layer chemical profile for water vapour is given in Figure 10.1.

For all the tests reported, we follow a 3-step procedure. Firstly, high reso-

lution input spectra are generated with Tau-REx. These are then combined with an instrument model to simulate realistic observations. Although the observations modelled here are only for Ariel, with errors from ArielRad, the same technique can be applied with Terminus and ExoWebb for Twinkle and JWST.

We then run TauREx in retrieval mode and use the simulated observed spectra as input to the retrieval. The retrieved parameters include our chemical setup (3 variables per chemical species), the isothermal temperature value and the planet radius. We therefore have a minimum of 5 free parameters that we attempt to retrieve. In the case where the mixing ratios were assumed constant with altitude (1-layer forward model), the Retrieved Pressure Point has been fixed, so that we have only 2 free variables per chemical species or a minimum of 4 free parameters. In our retrieval scheme, we use uniform priors for all the free parameters. In all our retrievals, chemical abundances are allowed to explore the bounds 10^{-12} to 10^{-1}. In Section 10.2.4 we allow the pressure point to explore 10^{-1} bar to 10^{-7} bar. For the isothermal temperature retrievals, the priors span $\pm$ 30 percent of the ground truth value. In Section 10.2.4, since we investigate more realistic examples, we retrieve a 3-point temperature profile [241].

By applying the 3-step methodology, a number of cases are simulated. Firstly, we verify that the 2-layer retrieval is able to recover the more basic 1-layer input (i.e. a constant chemical profile). We then investigate the "retrievability" of the 2-layer input spectrum by a 2-layer retrieval in the case of Ariel observations. Finally, we explore the advantage of using a 2-layer approach by comparing how a 2-layer input spectrum is recovered by both 1- and 2-layer retrievals.

10.2.2 Retrieving a 1-layer input with a 2-layer parametrisation

As a sanity check, we test that the more complex 2-layer model can indeed recognise the simple case of constant chemistry. A 1-layer simulated spectrum is generated and we attempt to recover the solution using the 2-layer model. Here, the retrieval of the pressure point (P_R) is disabled as this parameter introduces intrinsic degeneracy in the specific case of constant chemistry. As any value for this point would work, we arbitrarily choose to set it at $P_I = 10^{-1.3}$ bar. The retrieved posterior distributions

for an input spectrum generated with 1-layer parametrisation with a single species, H_2O, is presented in Figure 10.2. In orange, we show the retrieved posterior distribution of the parameters, while the true value is marked in blue. The mixing ratio of H_2O used for this example was 10^{-5}. The 2-layer model successfully retrieved the same abundance for both layers and, as the result matches the input abundance, confirms that the 2-layer parametrisation can recover the 1-layer input. The example showcases a situation where the complexity of the retrieval model is higher than the input.

10.2.3 Comparison of the 1-layer and 2-layer retrievals

By comparing the results obtained with the 1-layer and 2-layer retrievals, we aim to illustrate issues that may occur when performing a retrieval with a model of inappropriate complexity. Therefore, we simulate planetary atmospheres with 2-layer chemical profiles and analyse the results if the retrieval is performed with a 1-layer chemical approach. For this test, we use Ariel simulations to illustrate our results. In particular, two main issues could occur and need to be tested:

1. The observed spectrum cannot be explained using the 1-layer retrieval, as the best solution retrieved does not fit the data.

2. The 1-layer retrieval manages to achieve a "good" fit but the retrieved parameters are wrong compared to the ground-truth. This issue is more subtle as there is little evidence and no direct way to spot the error.

These two points can be tested by considering the following examples. For the former, we assume an atmosphere with a single CH_4 profile with a surface layer of $X_S(CH_4) = 10^{-5}$ up to $P_I(CH_4) = 10^{-2}$ bar and $X_T(CH_4) = 10^{-10}$ above that pressure, corresponding to a depleted layer. For the latter, we simulate a single H_2O profile where the planet contains $X_S(H_2O) = 10^{-10}$ up to 10^{-2} bar and the mixing ratio is $X_T(H_2O) = 10^{-3}$ for lower pressures.

We show here the results of the test where the input spectrum was generated assuming CH_4 only with $X_S(CH_4) = 10^{-5}$ up to $P_I(CH_4) = 10^{-2}$ bar and $X_T(CH_4) = 10^{-10}$. $X_T(CH_4) = 10^{-10}$ does not produce any observable feature,

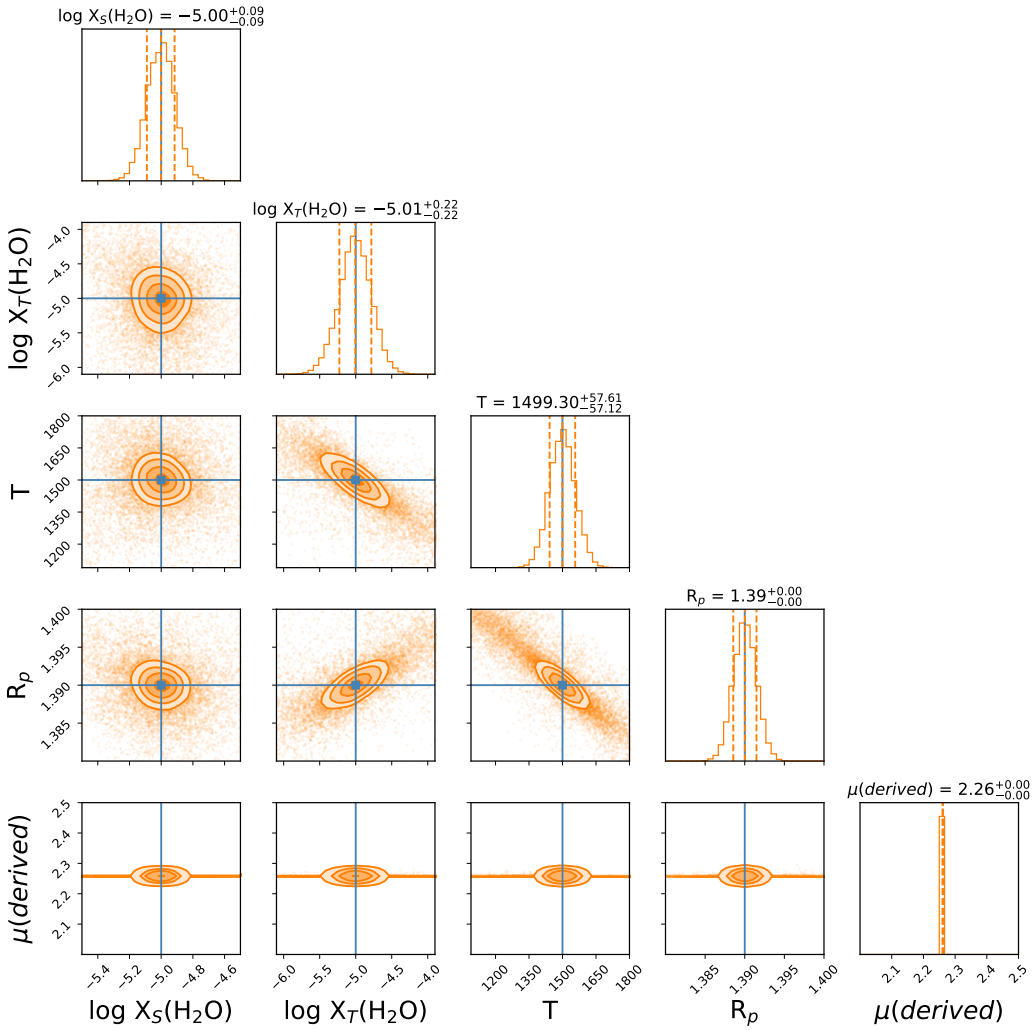

Figure 10.2: Posterior distributions of a 1-layer input atmosphere retrieved using the 2-layer model. The input spectrum was generated by assuming a constant profile for H_2O with a mixing ratio of 10^{-5}. In this example, the Retrieved Pressure Point is disabled and arbitrarily set at $P_I = 10^{-1.3}$ bar. For each free parameter, we report the mean and 1-sigma iso-likelihood levels with the dashed lines. The retrieved values match the input values within the retrieved uncertainties.

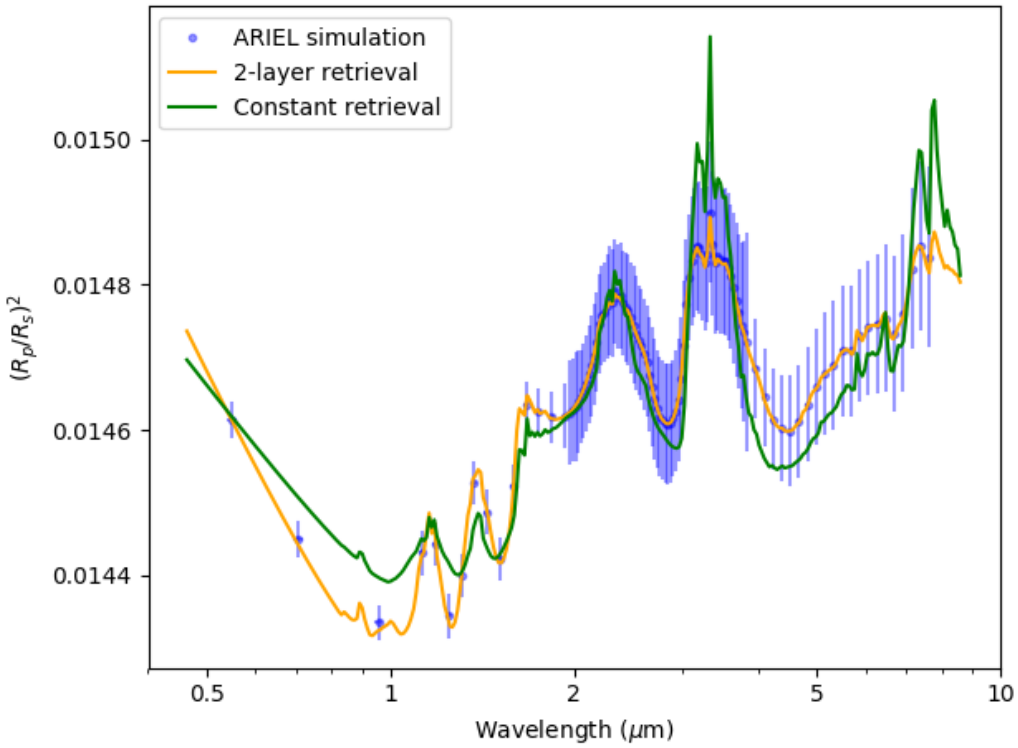

Figure 10.3: Observed input spectrum obtained with a 2-layer CH_4 profile and retrieved spectrum obtained with a 1-layer retrieval. The example showcases that the 1-layer retrieval is inadequate to interpret the data. The correct 2-layer retrieval is also shown. The Nested Sampling Global Evidence is $log(E) = 737$ for the 1-layer and $log(E) = 885$ for the 2-layer retrieval. This implies $log(B) = 148$, which is decisively in favour of the 2-layer scenario.

so for this layer we expect to retrieve only an upper limit in the posteriors. In this example, the 1-layer retrieval has difficulties in fitting the observed spectrum, as shown in Figure 10.3. In this case, the 1-layer retrieval lacks flexibility which visibly leads to a poor fit of the spectrum. The need for a 2-layer retrieval is confirmed by the lower Nested Sampling Global Evidence for the 1-layer scenario: 737 for the 1-layer and 885 for the 2-layer ($\Delta log(E) = 148$).

Concerning the test where the input spectrum was generated with H_2O only and assuming $X_S(H_2O) = 10^{-10}$ and $X_T(H_2O) = 10^{-3}$ above 10^{-2} bar, both the 1-layer and 2-layer retrievals converged to a solution and, as shown in Figure 10.4, gave satisfactory fits of the input spectrum. The posterior distributions are presented in Figure 10.6. Unsurprisingly, the 2-layer retrieval managed to recover the correct

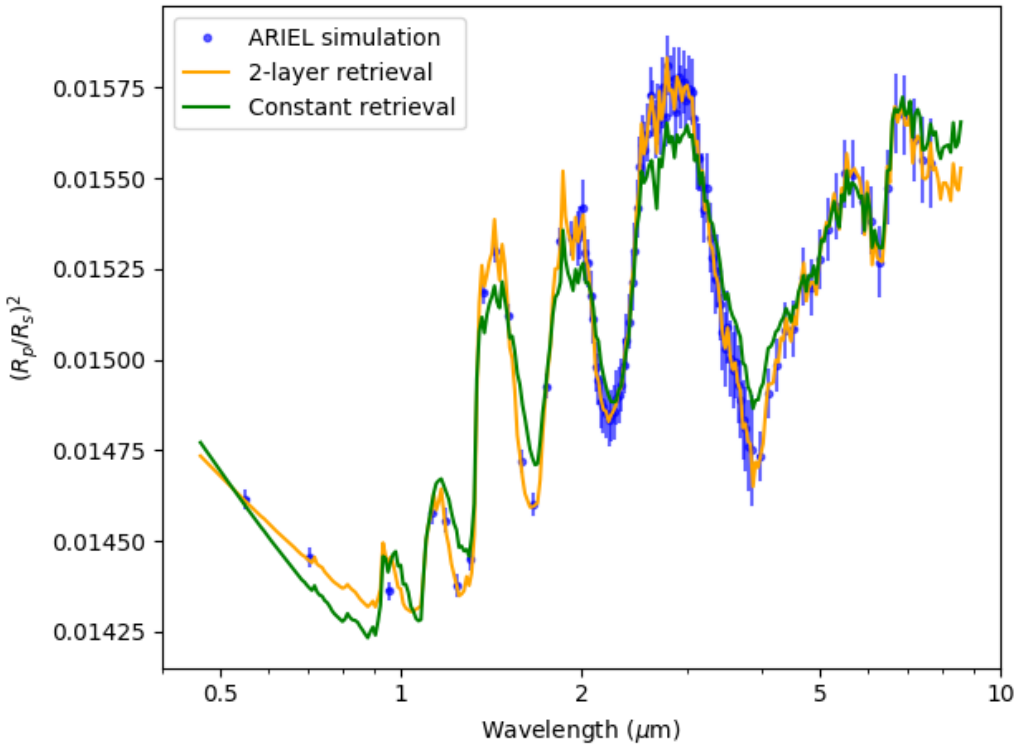

Figure 10.4: Observed spectrum generated with a 2-layer H_2O profile as input and best retrieved solutions obtained with a 1-layer and 2-layer retrievals. While the 2-layer retrieval captures better the observations, the differences with the 1-layer fit are relatively small. The Nested Sampling Global Evidence is $log(E) = 733$ for the 1-layer and $log(E) = 883$ for the 2-layer retrieval.

input parameters. However, while fitting the spectrum, significant differences appear for the 1-layer model in the retrieved parameters. The 1-layer retrieval tries to compensate the lack of flexibility in the chemical profile by increasing the temperature to 2100 K (instead of the 1500 K ground truth temperature). The input chemical and thermal profiles for both retrievals are shown in Figure 10.5 where retrieved temperature by the 1-layer retrieval is significantly off compared to the input, while the retrieved H_2O mixing ratio approximates the atmospheric average.

This example illustrates well the importance of exploring and understanding more complex chemical models in retrievals. Here the retrieved spectrum using the 1-layer approximation (Figure 10.4) gives an acceptable fit while leading to a wrong solution, which is a serious issue. Small differences compared to the observations are noticeable which, in this case, would still permit the selection of the

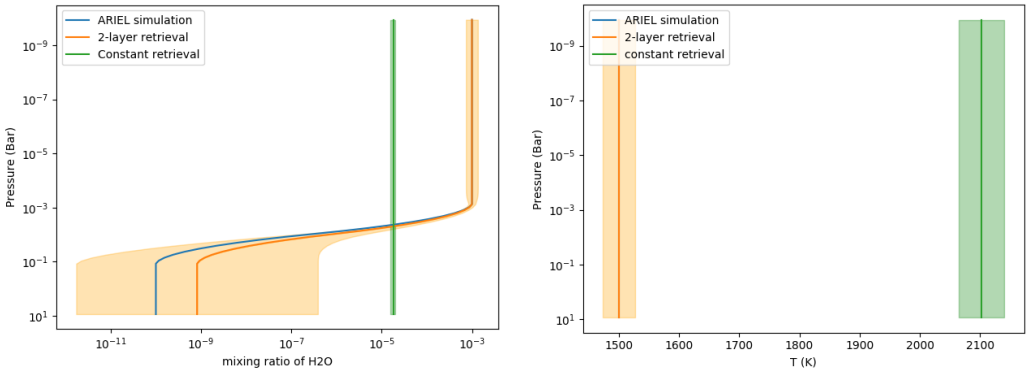

Figure 10.5: Chemical (left) and temperature (right) profiles for the input atmospheric model, the 2-layer and 1-layer retrievals. For the temperature, the 1-layer model is strongly biased. The input model temperature is not clearly visible as it overlaps with the retrieved value of the 2-layer retrieval at 1500K.

2-layer solution, provided that both retrievals are performed. More importantly, the correct solution can be determined by comparing the Nested Sampling Global Log-Evidence of the retrieval. The 2-layer retrieval obtained a value of $log(E) = 883$ while the 1-layer only had $log(E) = 733$, indicating a clear preference for the 2-layer scenario (difference of $\Delta log(E) = 150$).

10.2.4 A more realistic example: WASP-33 b

The previous sections demonstrated the theoretical possibility and, in some cases, the necessity of retrieving 2-layer chemical profiles in a number of select, simplified examples. Here we test the 2-layer approach by applying it a case inspired by WASP-33 b.

Current analyses of ground and space-based observations of WASP-33 b suggest extreme temperatures reaching 3800 K and a possible thermal inversion in the atmosphere [327, 328]. TiO or VO, which are strong absorbers at short wavelengths, could very efficiently capture high-energy stellar photons at the top of the atmosphere and cause the inversion [329, 330]. In parallel, other observations have suggested the presence of TiO in WASP-121 b [331] and WASP-76 b [15].

Here we investigate this process by attempting to detect a TiO layer in the upper atmosphere of a simulated planet resembling WASP-33 b. Our input model includes only two molecules: H_2O and TiO. The simulation consists of a constant

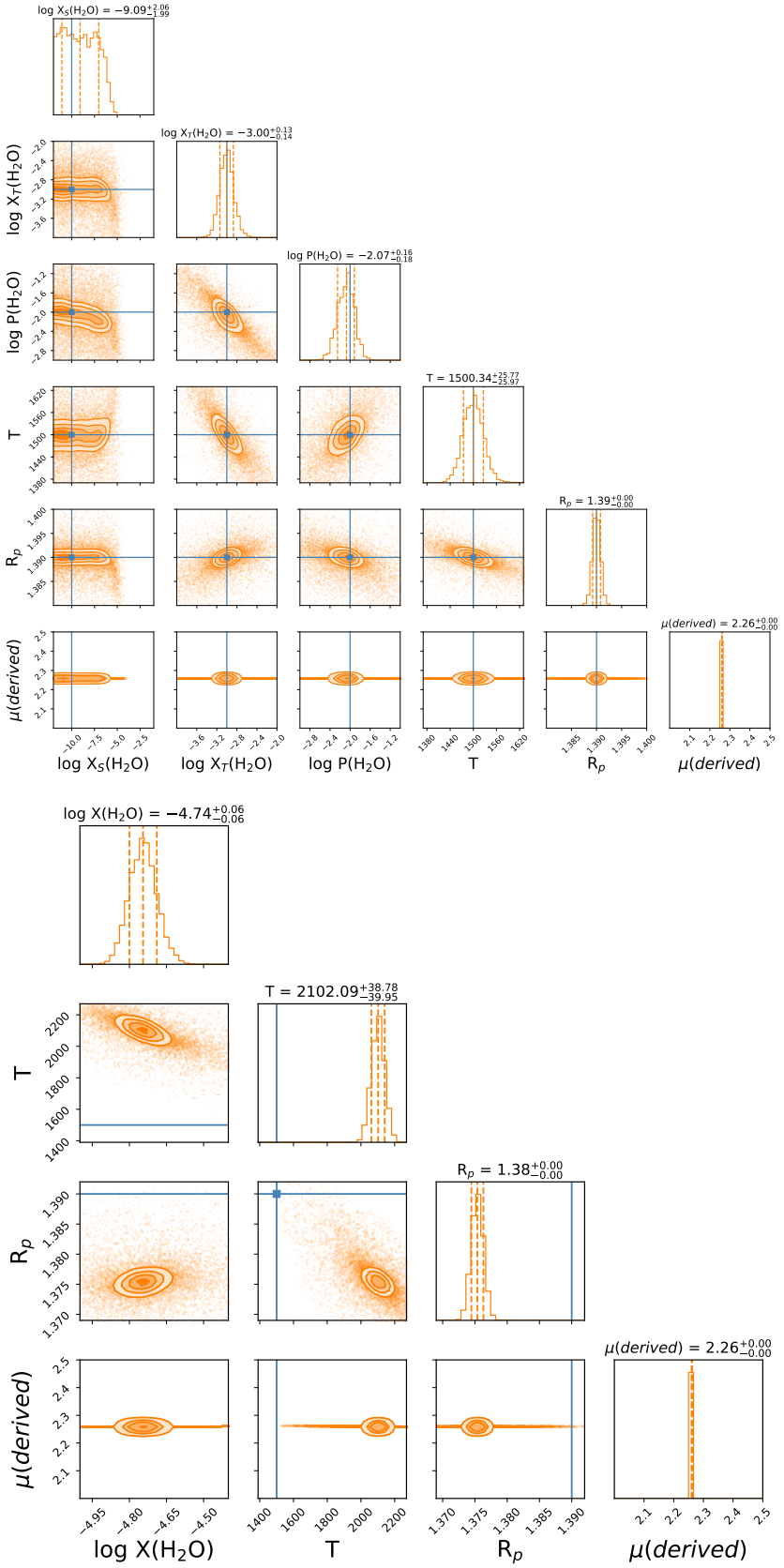

Figure 10.6: Posteriors of the 2-layer retrieval (top) and the constant retrieval (bottom) for a simulated Ariel observation of a planet with an inverted H_2O profile. The top layer contains $X_T(H_2O) = 10^{-3}$ for pressures lower than $P_l(H_2O) = 10^{-2}$ bar and the surface layer is depleted with a mixing ratio of only $X_S(H_2O) = 10^{-10}$.

mixing ratio of 10^{-4} for H_2O and an inverted temperature-pressure (TP) profile from 2800 K to 3700 K, which is inspired by [327]. For the temperature-pressure profile we used a 3-point model [272]. The model interpolates a smooth TP profile using 5 free parameters: surface temperature and two temperature-pressure points. The temperature variations allow us to explore the possibility of retrieving both thermal and chemical parametric profiles at the same time. For the retrieval, we explore uniform priors on the pressure bounds 10^{-2} - 10^{1} bar for first point and 10^{-5} - 10^{-1} bar for the second. The temperature bounds are the same for all 3 retrieved points and cover a range 30 percent lower/higher than the input minimum and maximum temperatures (1960 K - 4690 K). For a real observation, these priors could be informed by the knowledge of the equilibrium temperature and the physics of the atmosphere. To simulate a stratospheric TiO layer, we assumed abundances of $X_T(\mathrm{TiO}) = 10^{-4}$ for the top layer (down to $P_I = 10^{-4}$ bar) and $X_S(\mathrm{TiO}) = 10^{-7}$ at the surface. The spectrum, as well as the temperature and chemical profiles, are presented in Figure 10.7 while the full posterior is shown in Figure 10.8.

These results demonstrate the possibility of accurately retrieving the vertical distribution of the TiO layer. In particular, the TiO profile is well constrained between 10^{-6} bar and 10^{-3} bar as a result of the strong features between 0.4 μm and 1 μm. The shape of the thermal profile is also correctly retrieved, although with larger uncertainties at higher pressures as shown by the posterior distribution. The retrievability of the thermal and chemical profiles at the same time indicates that retrievals of future transit spectra should take these two effects into account. The flexibility of the 2-layer approach allows for the confirmation (or rejection) of potential correlations between molecules/condensates and thermal inversions which is an important application of the 2-layer approach.

10.2.5 The need for non-isochemical profiles

We have shown in the previous sections that simulated atmospheres with a 2-layer chemical profile would induce spectral features that need to be properly accounted for in retrievals to avoid incorrect conclusions. However, one could ask whether such families of chemical profiles can be found in exoplanetary atmospheres.

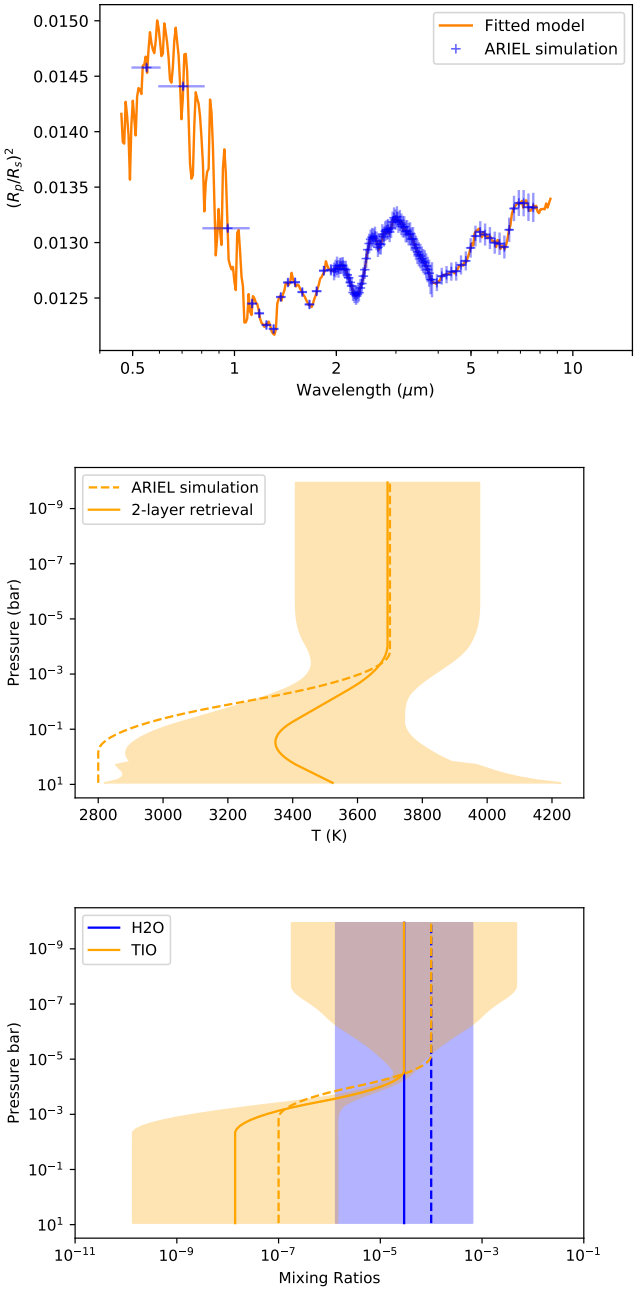

Figure 10.7: Outcome of the WASP-33 b retrieval simulations. Top: fitted spectrum; Middle: retrieved temperature profile; Bottom: retrieved chemical profiles of H_2O and TiO. The dashed lines correspond to the input values assumed in the forward model while the solid lines indicate the retrieved profiles. For this run log(E) = 880.

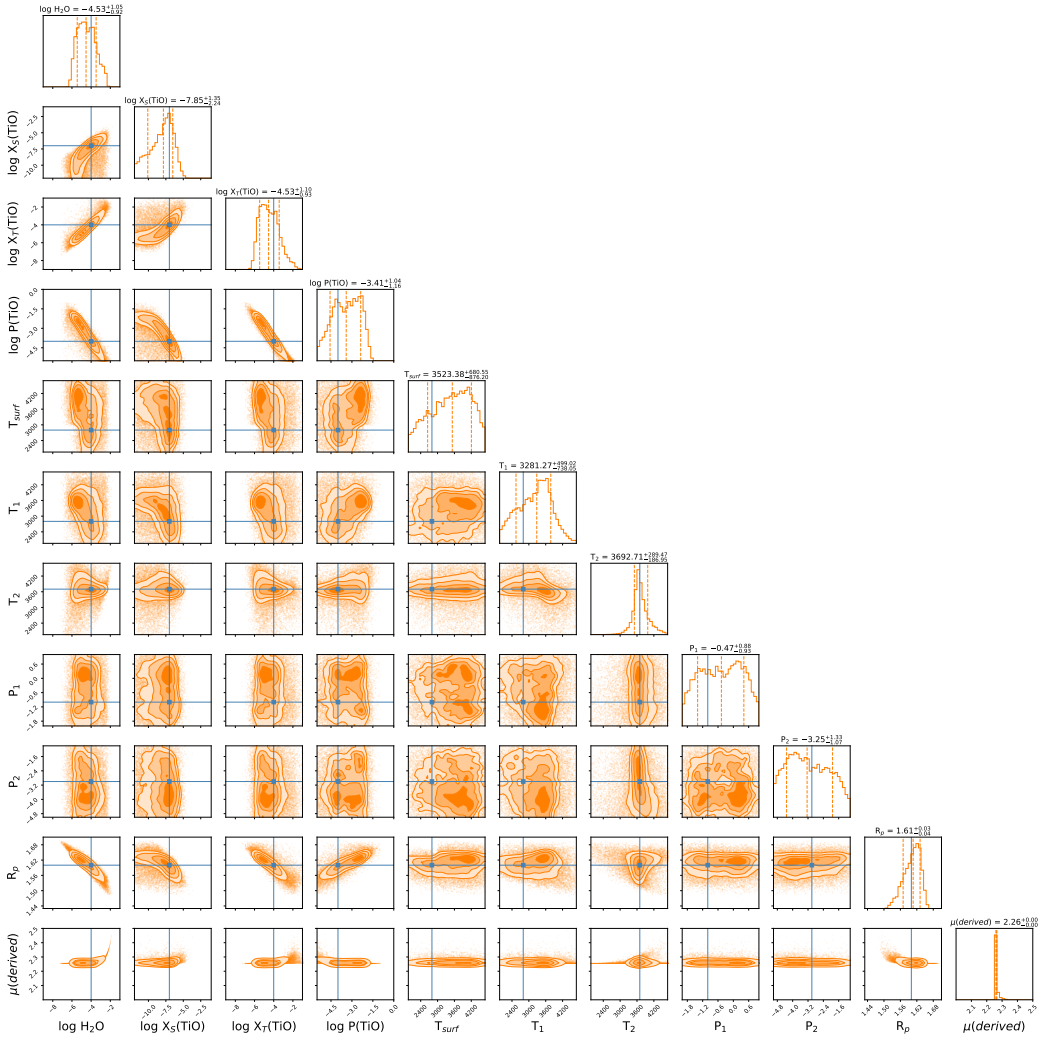

Figure 10.8: Posteriors distribution for the retrieval of WASP-33 b. The planet presents constant H_2O abundance and a TiO 2-layer profile with a large abundance in the upper atmosphere.

Simulations by [332] suggest at least two typical behaviours for chemical profiles in exoplanetary atmospheres of the type HD 209458b. Some molecules of interest, such as H_2O and CO, are predicted to have constant mixing ratios as a function of pressure. Others, like NH_3 or CH_4, are expected to vary with altitude. In the deep atmosphere (generally pressures higher than 1 bar / 10^5 Pa) chemical reactions are close to their thermochemical equilibrium values. In the higher part of the atmosphere ($\sim 10^{-4}$ bar / 10 Pa) photo-chemistry and disequilibrium processes may modify the overall mix by dissociation and creation of atomic species and new molecules. In addition, [333] investigated the composition of Hot Neptunes

like GJ 436 b with a wide range of metallicities and the resulting chemical profiles demonstrated complex behaviours, highlighting the need for adapted retrieval techniques. These disequilibrium processes are expected to be more prominent and important in colder atmospheres [125].

Future space instruments should be able to probe roughly between 1 bar and 10^{-5} bar, depending on the composition and temperature of the atmosphere, allowing us to constrain chemical models with direct observations. Figure 10.9 illustrates the contribution functions and their wavelength dependencies for planets similar to HD 209458 b and WASP-33 b.

10.2.6 Should we always use the 2-layer model?

The increase in complexity in chemical models must be done with care. In some cases, the introduction of additional degrees of freedom comes at the expense of model convergence. The flexibility of the retrieval should depend on the quality of the input data which opens up the question of model selection. Indeed, should we prefer models with increased flexibility at the risk of increasing model degeneracies and over-fitting, or should we prefer simpler models but returning only "acceptable" fits?

In the 2-layer case, this issue can be illustrated by the retrieval of a constant input. Initially, we disabled the Retrieved Pressure Point to ensure the convergence of the 2-layer retrieval. The choice was justified by the fact that the Input Pressure Point does not exist in constant chemical profiles, making any Retrieved Pressure Point suitable and therefore introducing an intrinsic degeneracy. In Figure 10.10 the constant chemical profile used as input is here retrieved with the Retrieved Pressure Point activated (log $P(H_2O)$). The point is however not well constrained and the retrieved abundances become more difficult to interpret. The posteriors are compatible with a bi-modal solution peaked at pressures where observations are no longer sensitive.

This example highlights the circumstances under which the model used in the retrieval is too complex. The issue was solved previously in Figure 10.2 by fixing the Retrieved Pressure to an arbitrary value (reduction of the model complexity),

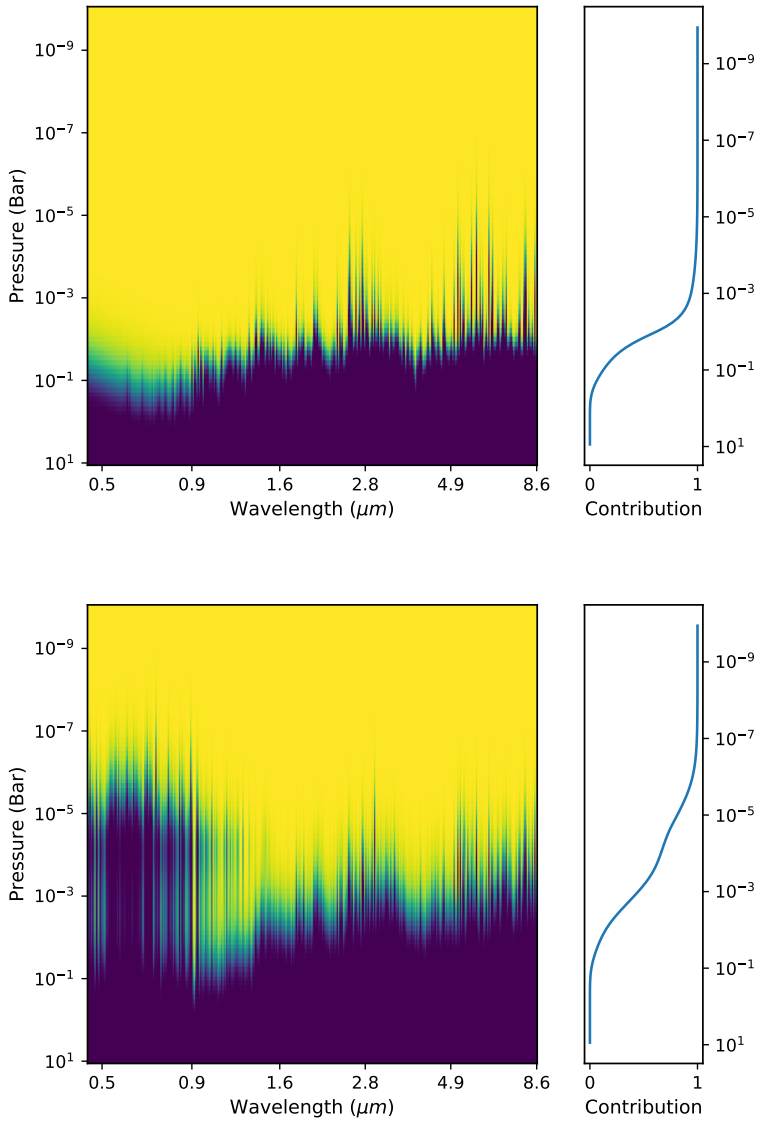

Figure 10.9: Opacity contribution functions for: Top: a hot-jupiter (e.g. HD 209458 b); Bottom: an ultra hot-Jupiter (e.g. WASP-33 b). In each plot, the left panel shows the contribution function as function of wavelength (horizontal axis) and the pressure (vertical axis). The right panel is the same function averaged over all wavelengths. For a Hot Jupiter like HD 209458 b, the pressures probed range from 1 bar to 10^{-4} bar. For an Ultra-Hot Jupiter of the type WASP-33 b, the contribution ranges from 10^{-1} bar to 10^{-7} bar.

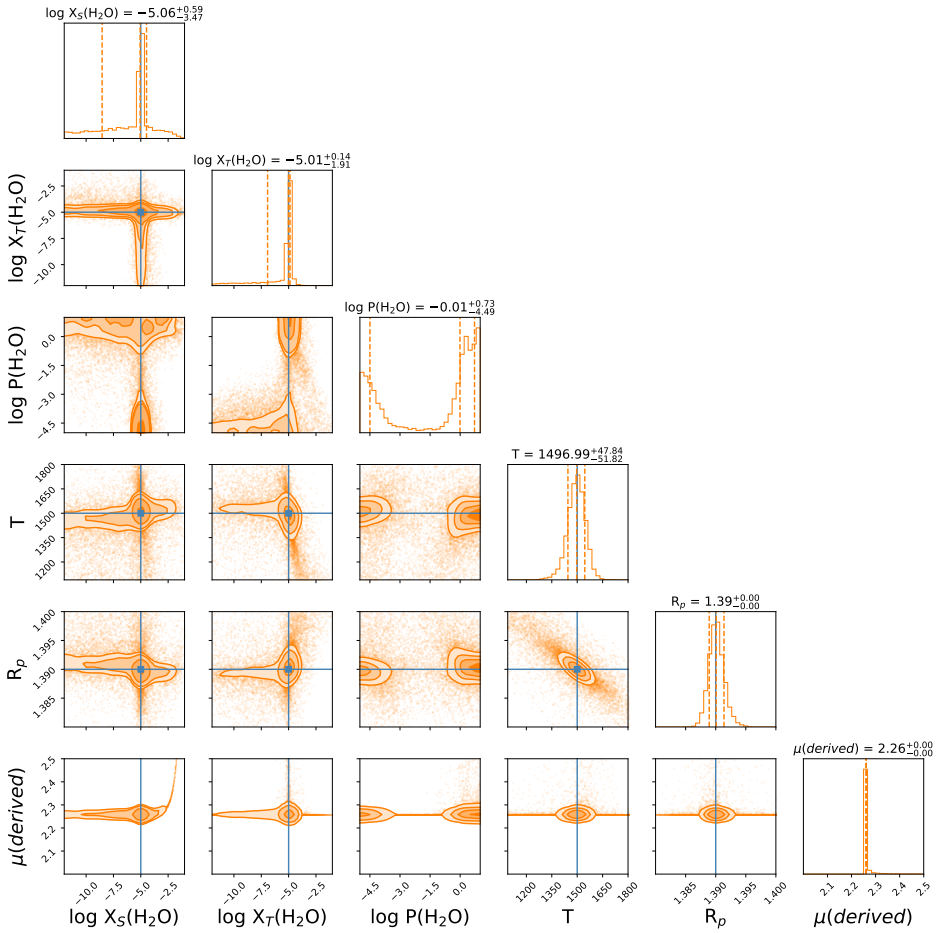

Figure 10.10: Posterior distribution for the retrieval of a constant H_2O input profile using the 2-layer model with the Retrieved Pressure Point activated. The model cannot converge as multiple solutions for this point exist which indicates that the number of free parameters is too high and we need to revert to a simpler retrieval.

illustrating that if/when the 2-layer model is too complex for the data, one needs to decrease the number of free parameters and revert back to a simpler chemical parameterisation. The overcomplexity of the model can clearly be seen from the pressure point divergence in posterior distribution.

10.3 Comparing Facilities

With three upcoming observatories which will be capable of characterising exoplanet atmospheres through transit spectroscopy it is useful not only to understand their individual performances but to measure their relative adeptness. Such studies allow us to understand the strengths of each instrument and are crucial for ensuring that each observatory is used in the most effective way. Here data from Twinkle, Ariel and JWST have been simulated for the same targets, and retrievals performed, to highlight both the similarities and differences in the expected performance.

10.3.1 Hot-Jupiters

For bright hot jupiters, it has already been shown that Ariel and JWST have similar information content, thus indicating that Ariel will be able to characterise atmospheres to a similar degree of accuracy [125]. A similar analysis is replicated here but with an additional comparison to Twinkle. Here Twinkle's capability is again based on the Phase A design, which may be subject to change, and assumes that there are no gaps in the light curve. To analyse the capability of these instruments when studying a stereotypical hot-Jupiter, a planet similar to WASP-69 b has been simulated. WASP-69 b is a potential Tier 3 target for Ariel and one for which an SNR >7 can be reached on the atmosphere in 1 transit. As a comparison, 1 transit of Twinkle has also been modelled while, for JWST, 1 observation with NIRISS G700XD has been simulated alongside 1 transit with NIRSpec G395M. No spectral studies have yet been conducted for WASP-69 b but the atmosphere assumed, which is detailed in Table 10.1, is generic and not unreasonable considering the constituents found in similar planets. The observed spectra for each of the observatories are shown in Figure 10.11 along with the high resolution model from TauREx.

A retrieval was performed on these spectra using the same priors and the resulting posteriors are over-plotted in Figure 10.12. These show that, for a typical hot-Jupiter around a bright star, Twinkle and Ariel will give a similar performance in 1 transit as JWST would with 2 transits. In such a case, JWST is limited by two factors: the need to combine multiple instruments to cover a wide wavelength range and the fast saturation time which causes a poor on-sky efficiency. Therefore, for

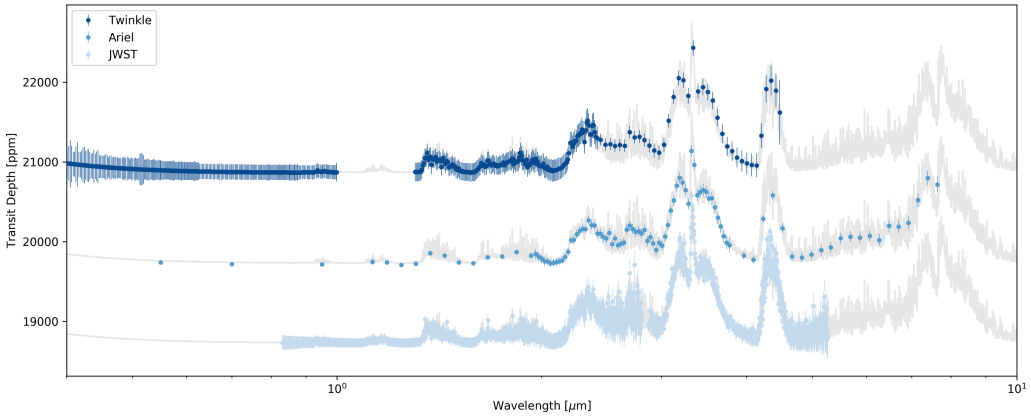

Figure 10.11: WASP-69 spectra with Twinkle, JWST and Ariel.

Parameter	Value	Priors
Radius [R_J]	1.11	0.89 to 1.33
Temperature [K]	982	700 to 1300
log(H_2O)	-5	-3 to -10
log(CH_4)	-5	-3 to -10
log(CO_2)	-6	-3 to -10
log(P_{Clouds})	3	0 to 5

Table 10.1: Input parameters used for WASP-69 b simulations and the priors for the retrievals.

bright hot-Jupiters, JWST is far from the ideal facility. However, the NIRSpec instrument on JWST features a prism which offers spectral coverage from 0.5-5.3 μm in one shot at low resolution (R$\sim$30-300). The NIRSpec prism has the advantage of covering the same wavelength range as NIRISS and NIRSpec G395M combined but the drawback is an extremely fast saturation time which means it cannot be used for bright targets. Nevertheless, one can consider using it for fainter targets, taking advantage of JWST's enormous collecting area.

In reality, WASP-69 is situated 50 parsecs from Earth and has a K band magnitude of 7.5. If we consider a star with the same characteristics as WASP-69 but at a distance of 200 parsecs (K_{Mag} = $\sim$11), the NIRSpec clear prism could be used. Imagining that this star, F-69, had a planet, which was identical to the previously modelled WASP-69 b, we simulate observations with Twinkle, Ariel and JWST. In this case, 20 Twinkle observations are used, along with 10 for Ariel, while only 1 is modelled for JWST. When retrievals are performed upon these simulated observa-

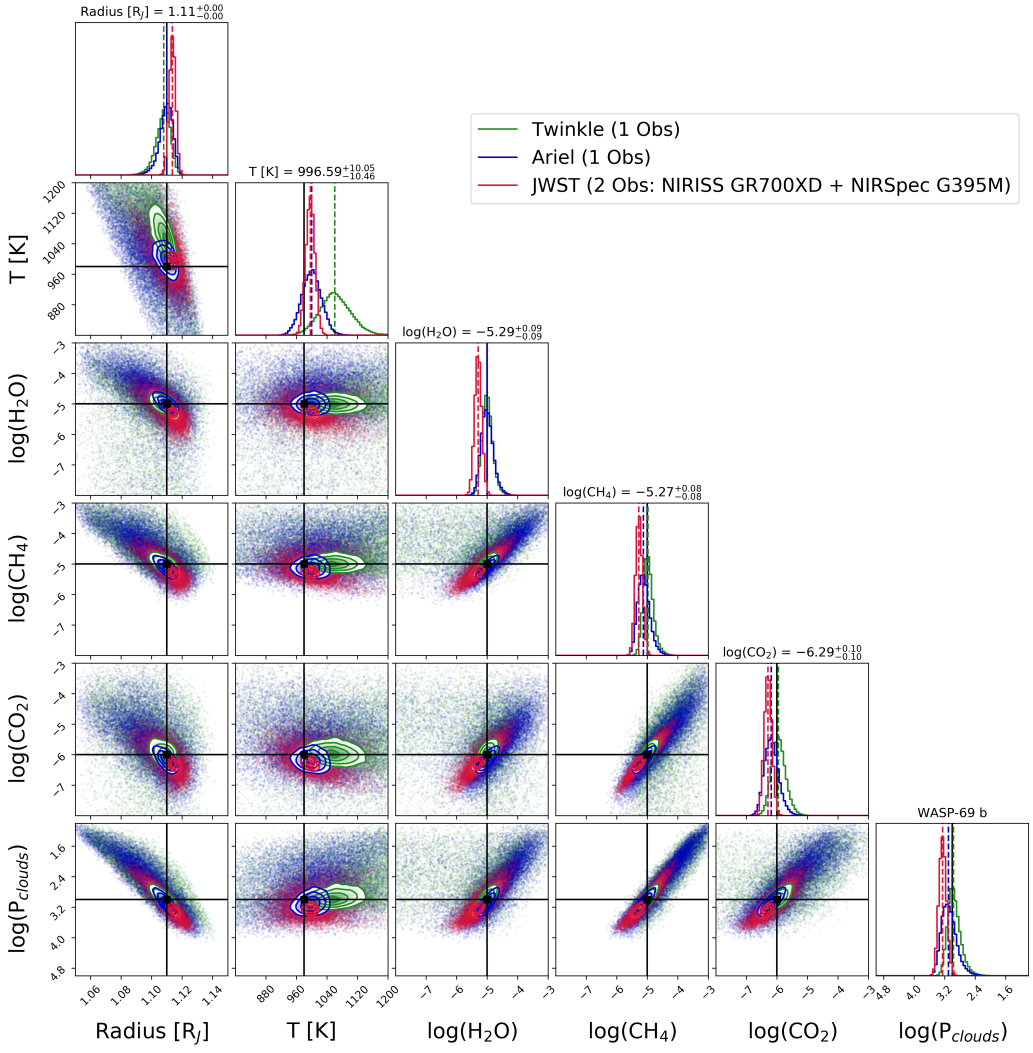

Figure 10.12: Retrieval posteriors for WASP-69 b for Twinkle (green), Ariel (blue) and JWST (red). The results are roughly consistent but the JWST data would require 2 observations to obtain. As there is no overlap between the JWST instruments, there may be issues with stellar variability or instrument systematics which are not modelled here.

tions, all instruments converge to the correct solutions. However, JWST has a better performance as shown in the posteriors in Figure 10.13. Comparing the JWST retrievals of this fictional, fainter planet, to the same planet but around a bright star in Figure 10.14, we can see that the performance is roughly equivalent. While the retrieval of the faint planet has wider 1 sigma errors, the best fit values are closer to the ground truth. The result suggests that, if one wishes to observe hot-Jupiters with JWST, one should pick fainter targets. Such a finding is perhaps initally counter initiative but, while it may not be true in every case, the approach should certainly be considered for several reasons. Firstly, given how precious JWST time will be, reducing the number of observations is always a bonus. Additionally, for bright targets the observations of multiple instruments must be stitched together. Given that these will be taken at different times and will include instrument systematics, the same issues as found for Hubble observations of HAT-P-11 b may be incurred. A single observation with the NIRSpec prism would avoid this. Finally, as the performance for the brighter hot-Jupiter is approximately equivalent for Twinkle, Ariel and JWST, it would be wasteful to use such a powerful observatory for these targets particularly as JWST has been shown to be far more capable of observing larger, gaseous planets around fainter stars than these other missions. Utilising JWST to study these would therefore open up a new set of planets that are too faint for other space-based instruments in the next decade.

10.3.2 K2-18 b

Recent observations of K2-18 b with Hubble have, for the first time, revealed the presence of water in the atmosphere of a Super-Earth orbiting within the habitable zone of its star. The detection, confirmed by two independent studies, [18] and [334], is particularly exciting as it contrasts with the most of the relatively featureless planets so far analysed in the Super-Earth/Sub-Neptune regime. In the two K2-18 b retrieval studies, while the water feature is evident, it was not possible to constrain precisely the abundance of the main gases (e.g whether or not the planet possess a secondary atmosphere).

From the Hubble observations, three main solutions have been identified. The

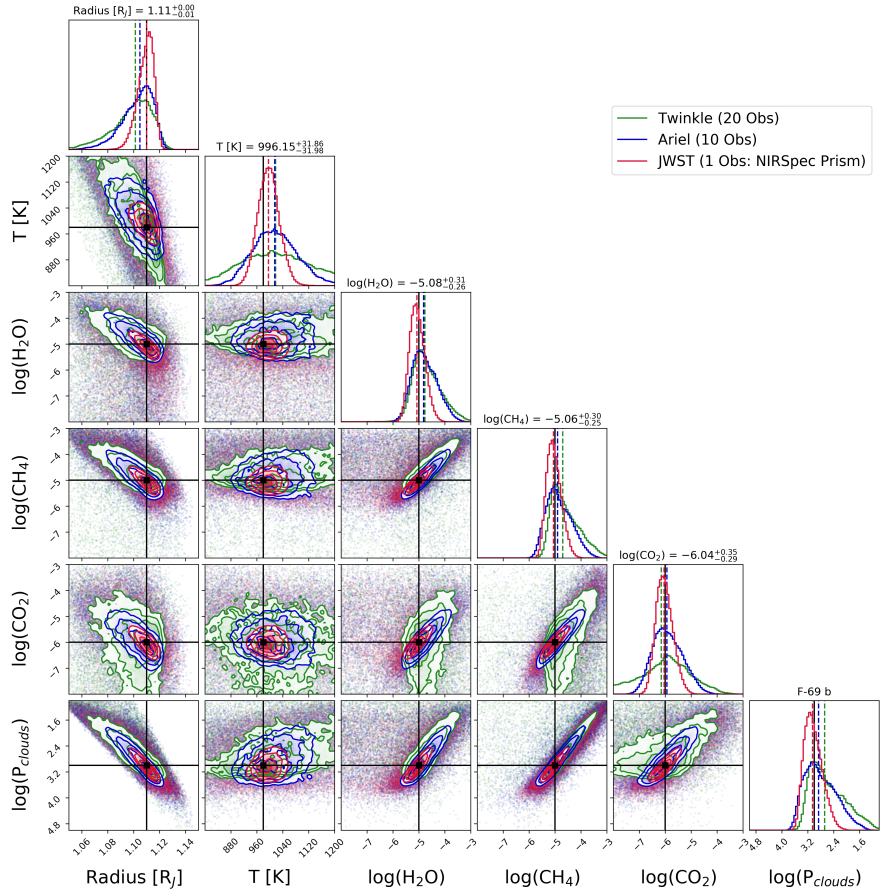

Figure 10.13: Retrieval posteriors for F-69 b for Twinkle (green), Ariel (blue) and JWST (red). JWST provides far tighter posteriors in one observation that Ariel and Twinkle can with 10 and 20 transits respectively.

first one describes a secondary atmosphere with a high mean molecular weight explained by a large abundance in water (up to 50 percent). The second solution is a secondary atmosphere with some trace water and the presence of one or multiple main absorbers. From the HST spectrum, these must be relatively featureless between 1.1 μm and 1.6 μm, so a worst case scenario would be the presence of an inactive gas such as N_2. Finally, the third case is a lighter atmosphere composed mainly of hydrogen, helium and some trace water, but where the features are muted by high altitude clouds. In essence, the nature of K2-18 b atmosphere is still unconstrained and will require further observations from the next generation telescopes. We have simulated observations of the atmosphere with JWST and Ariel for each of these scenarios and the parameters used are summarised in Table 10.2. For this

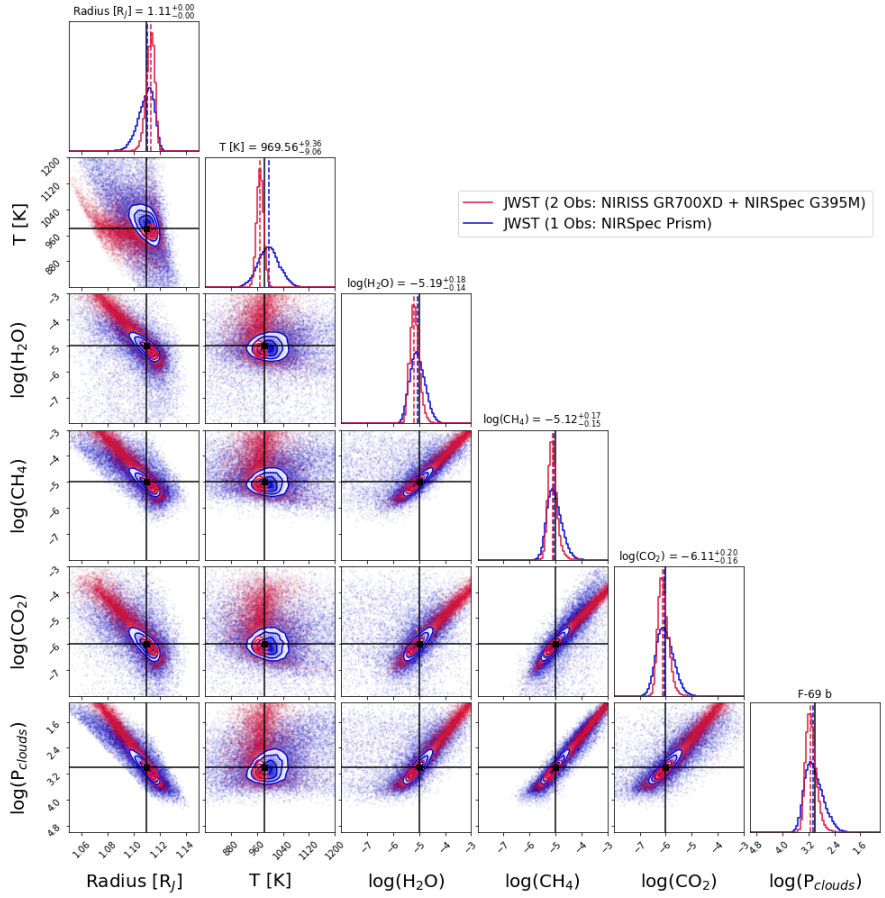

Figure 10.14: Retrieval posteriors for WASP-69 b (red) and its imaginary fainter twin, F-69 b (blue). In the latter case only a single transit is required yet the fit to the data is similar to observing a brighter target which requires two observations.

Parameter	Model 1	Model 2	Model 3
Radius (R_J)	0.219	0.219	0.216
Temperature (K)	286	286	288
H_2O/H_2	0.541	3.71×10^{-4}	1.28×10^{-3}
N_2/H_2	7.82×10^{-7}	0.0592	6.74×10^{-7}
P_{Clouds} (bar)	2.85	2.85	6.92×10^{-2}

Table 10.2: Parameters used for our 3 atmosphere scenarios. Model 1 is a heavy atmosphere with hydrogen and water. Model 2 is a heavy atmosphere with hydrogen, nitrogen and traces of water. Model 3 is a cloudy lighter atmosphere with hydrogen, water. These input parameters are taken from the results in [18].

case, Twinkle observations have not been simulated due to the faintness of the star and the small spectral signature searched for.

In the case of JWST, we assume observations are made with NIRISS and NIRSpec and we always state the total number of observations performed which are

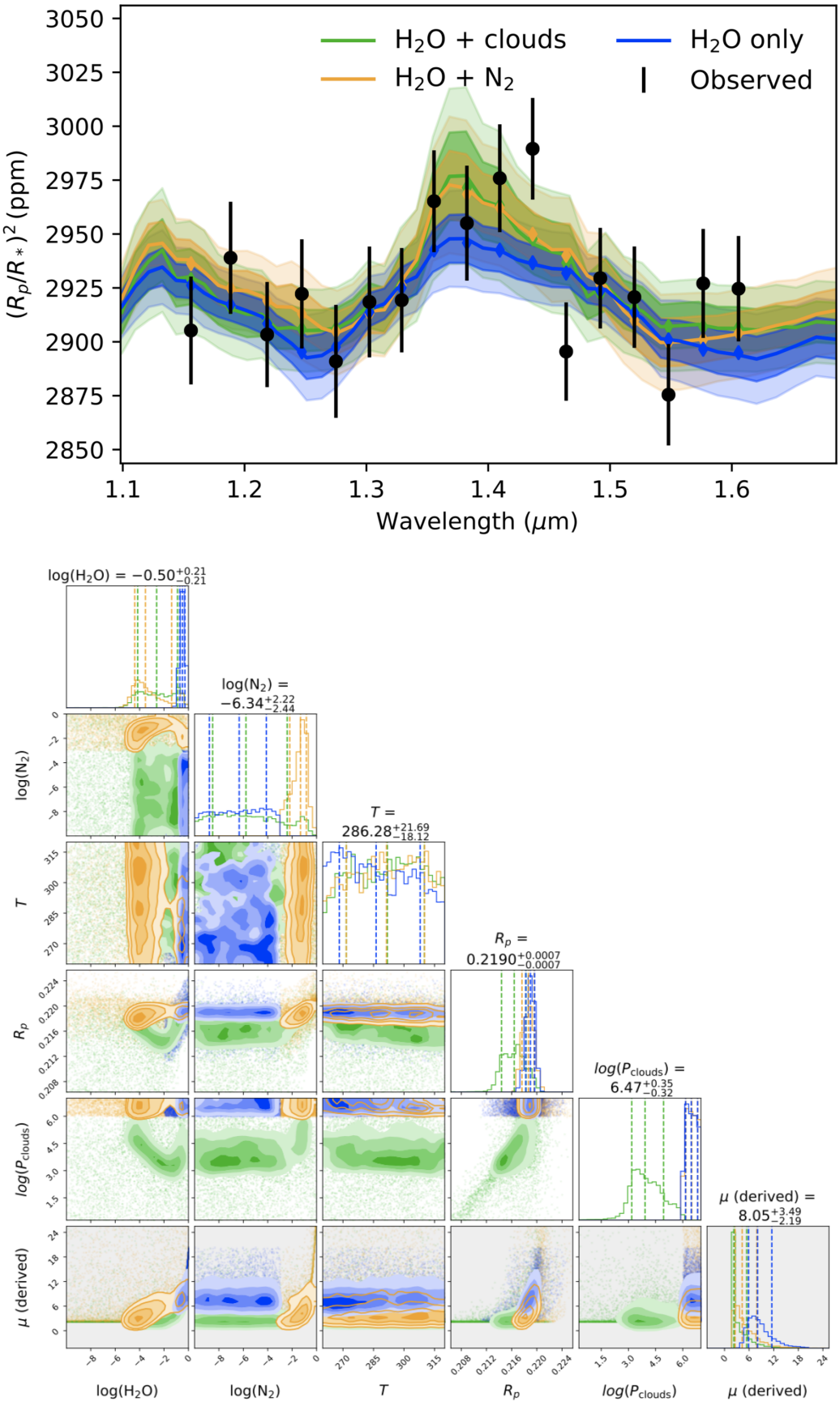

Figure 10.15: Current observational data of K2-18 b. Top: Hubble spectrum with best fit solutions overplotted including 1 and 3 sigma errors. Bottom: retrieval posteriors from Tau-REx. Both plots are reproductions from [18].

Parameter	NIRISS	NIRSpec
Filter/Grism	GR700XD ORD1	F290LP-G395m
Spectral Coverage [μm]	0.83 - 2.81	2.87 - 5.27
Number Groups	31	25
Time [s]	164.7	21.7
Max Saturation Level	78%	78%
In Transit Integrations	58	430
Out Transit Integrations	116	860

Table 10.3: JWST instrument setups used in ExoWebb for this work.

Telescope	Number of Transits	Resolving Power
Ariel	10	10/12/10
Ariel	20	10/12/10
Ariel	50	10/50/15
JWST	2	30
JWST	10	100
JWST	20	100

Table 10.4: Cases investigated with Ariel and JWST. We indicate the number of transits for each case. For Ariel, we state the resolution used for NIRSpec, AIRS 0 and AIRS 1. In the case of JWST simulations, we use the same resolution for NIRISS and NIRSpec.

equally split between the instruments. For example, 2 observations correspond to the addition of 1 transit with NIRISS and 1 with NIRSpec. The combination of these two instruments ensures an optimal wavelength coverage from 0.8 μm to 5 μm and the instrument setup used is summarised in Table 10.3.

For both missions we investigate these 3 cases by varying the number of observations to fully explore the possibilities of these two telescopes to constrain the main chemical composition of K2-18 b. With an orbital period of approximately 33 days, we restrain our maximum number of transits to 50 for Ariel and 20 transits for JWST (10 NIRISS and 10 NIRSpec). Since K2-18 is around the ecliptic, around half of the transits would not observable, which means our Ariel 50 transits case is an optimistic upper limit. The list of investigated cases is presented in Table 10.4.

Figure 10.16 shows 50 observations of K2-18 b with Ariel simulated for the 3 scenarios. We can see that the 3 scenarios are visually distinguishable. In the 20 observations case, the spectra remained very similar which highlighted the interest

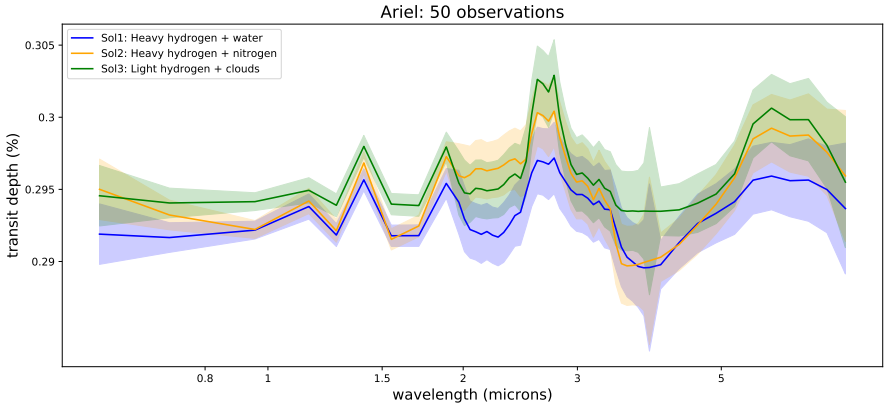

Figure 10.16: Simulated forward models for the 3 scenarios of K2-18b case as seen by Ariel with 50 stacked transits. We can already see the spectra are distinguishable, especially for the section between 2μm and 5μm.

of pushing for more observations. Figure 10.17 illustrates the case of 10 K2-18 b observations with JWST NIRISS/NIRSpec. The 3 scenarios now show large differences.

Our input scenarios include 3 atmosphere models and 6 observation simulations, so we performed a retrieval for each of the 18 cases. In each case, we retrieved the following free parameters: planet radius, temperature (T), water to hydrogen ratio (H_2O/H_2), nitrogen to hydrogen ratio (N_2/H_2) and cloud pressure (P_{clouds}). For each of the fitted parameters, we used the same uniform priors to avoid biases and ensure that our results can be compared.

Overall, we find that Ariel and JWST will be able to distinguish between the 3 scenarios presented in [18], evidence for which can be seen in Figure 10.18 where we show the posterior distributions for two particular cases: 10 observations with NIRISS and NIRSpec for JWST and 50 Ariel observations. In general, this is also true for the other investigated cases and we compiled the results of our retrievals in Figures 10.19 - 10.22. We show the combined posterior distributions in each telescope case for the 3 scenarios of atmospheres (we show the case Ariel 10 transits separately as the distinction between the different solutions is less evident).

The required number of observations for this target varies. With 1 transit with both NIRISS and NIRSpec, JWST should be able to inform us on the nature of

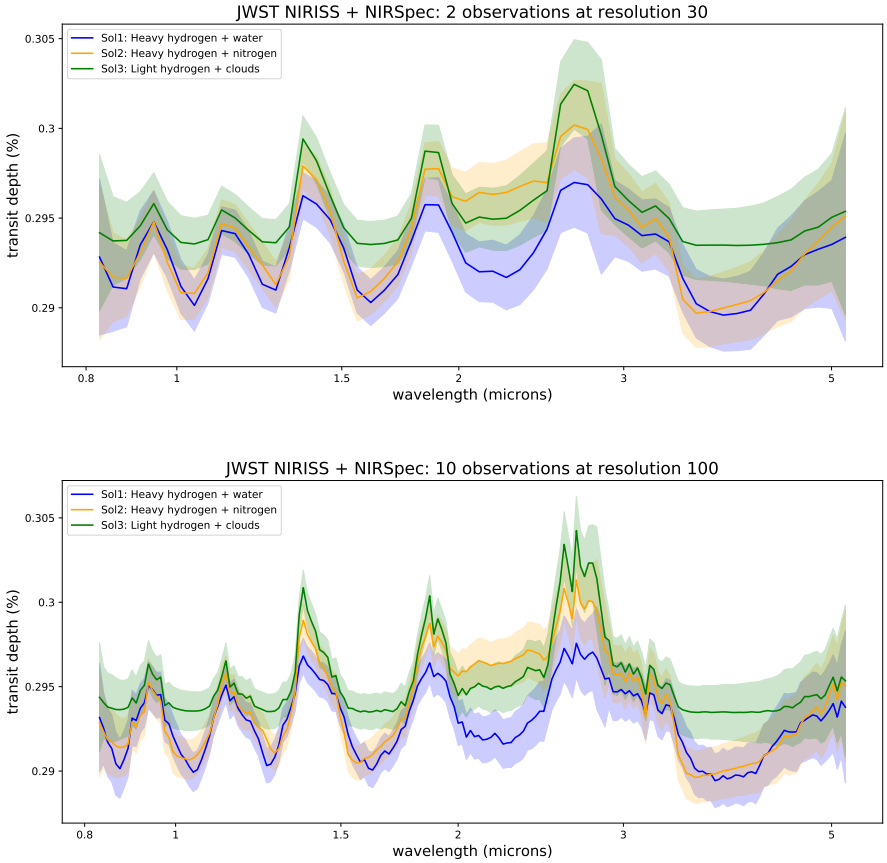

Figure 10.17: Simulated forward models with JWST for the 3 scenarios of K2-18b. Top: 2 stacked transits. Bottom: 10 stacked transits. Differences between the input forward models can be observed.

K2-18 b. Ariel can also reach the same conclusions, but it will require far more observations. While our 10 observations scenario with Ariel starts to bring indications of the atmospheric differences (see Figure 10.22), it is only after 20 observations that we significantly see the divergence between heavy water atmosphere, heavy nitrogen atmosphere or lighter cloudy atmosphere. The 50 observations scenario, which would require to observe all transits in the primary and extended mission of the telescope, provides a real insight on the atmospheric composition. In our comparative study, the Ariel 50 observations scenario provides similar posterior distributions to the combined JWST observation of a single NIRISS and NIRSpec transit. Such a finding demonstrates the advantage of using large telescopes for the study of challenging targets such as Super-Earths with secondary atmospheres, but

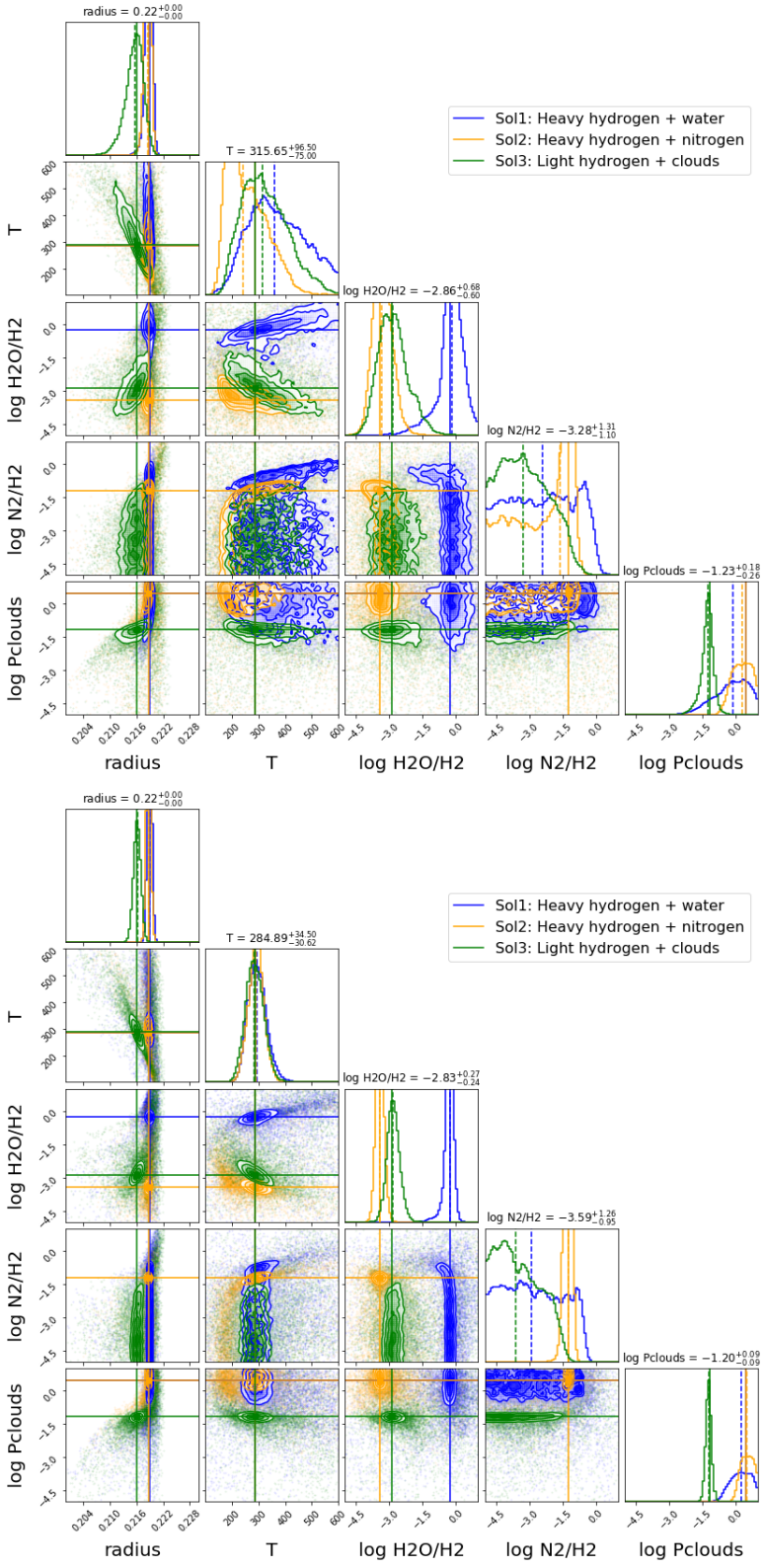

Figure 10.18: Summarising plots of the retrieval posteriors for the 3 atmospheric scenarios in the case of Ariel 50 observations (top) and JWST 10 observations (bottom). For both cases, the 3 solutions can easily be distinguished from the posterior distributions of the parameters.

also shows that dedicated telescopes of smaller diameters like Ariel have the potential to go after similar targets, provided that enough transits are observed. K2-18 b is included within the current version of Ariel's Mission Reference Sample and, as discussed in Chapter 8, some portion of mission may be dedicated to studying smaller planets.

In all our cases, the radius is very well constrained (less than 2 percent for the worst case Ariel 10 transits). The temperature however is only constrained accurately for high SNR observations (e.g. only in the cases with JWST for more than 5 observations). The JWST single combined observations as well all Ariel cases are not able to converge to the appropriate solutions and lead to large uncertainties in the retrieved temperature. The water abundance is always well constrained due to the strong molecular features. Similarly, in the case of secondary atmosphere with trace water, the ratio of N_2/H_2 is well retrieved as the model requires a large mean molecular weight while the trace water is well constrained thanks to the molecular features. On the 2 other scenarios (heavy atmosphere with mainly water and lighter cloudy atmosphere), the retrievals are only able to provide an upper limit on the N_2 abundance. Finally, the clouds are always retrieved correctly, with a very low uncertainty when they were present in the input forward model.

Our best case scenario with 20 JWST observations shows very tight posterior distributions, allowing for a very precise characterisation of the atmospheric main gases in K2-18 b, the isothermal temperature and the clouds. Hence, by performing a retrieval analysis of the potential scenarios for K2-18 b, we show that the next generation of space telescopes will be able to distinguish between the 3 cases. We can therefore highly recommend the consideration of this target for atmospheric follow-up.

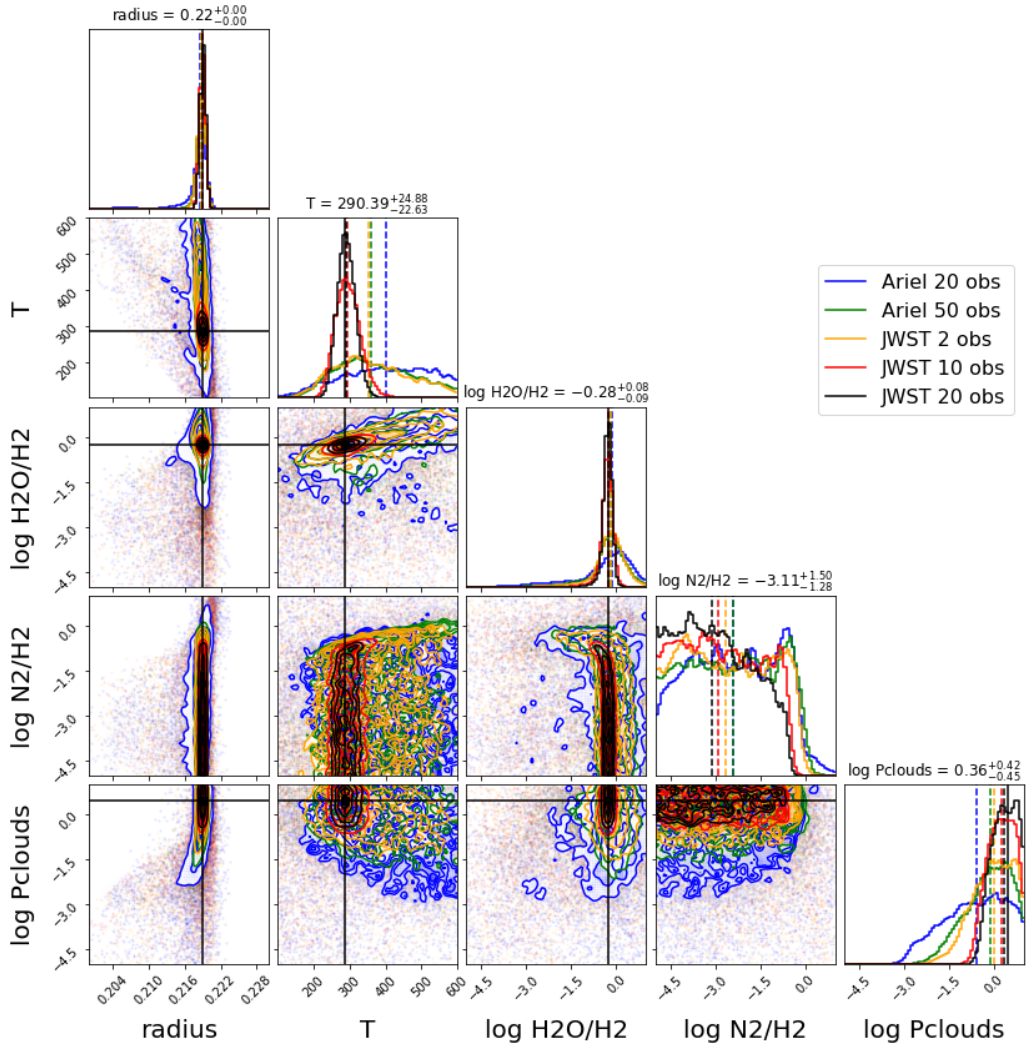

Figure 10.19: Retrieval posteriors for the atmospheric scenario 1: Heavy atmosphere composed of hydrogen and water.

10.4 Conclusions

The next generation of space-based telescopes for exoplanet characterisation will cause a revolution. The increase in the quality of the data, both in terms of SNR and wavelength coverage, will facilitate the detection of numerous molecular species in the atmospheres of extrasolar planets. However, this data will be of such a quality that many current assumptions used in the retrieval of atmospheric properties will be inadequate. Therefore, the complexity of retrieval codes must be increased to match the intricacy of the data. The use of oversimplified models is likely to lead to, at best, poor fits to the data or, at worst, seemingly good fits but with inher-

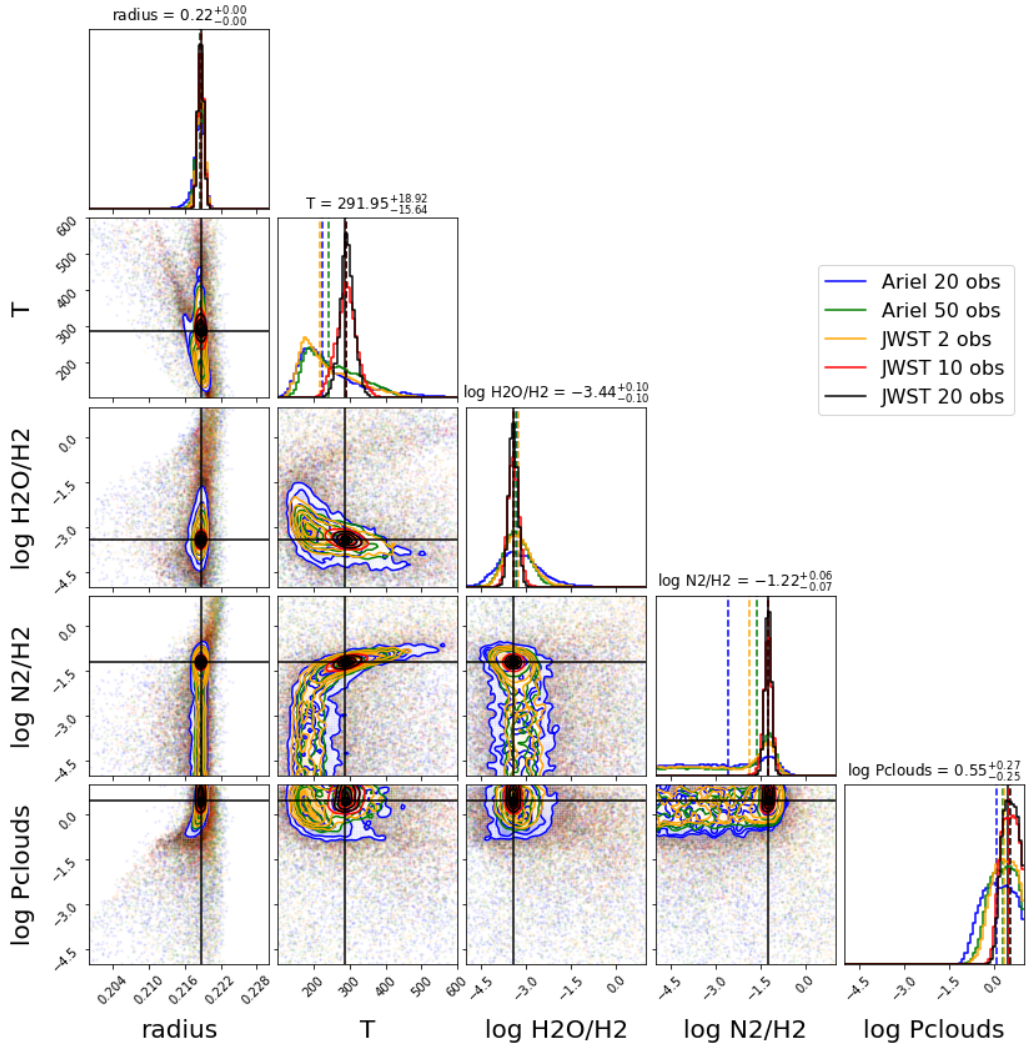

Figure 10.20: Retrieval posteriors for the atmospheric scenario 2: Heavy atmosphere composed of hydrogen and nitrogen. Traces of water are also present.

ent bias in the chemistry or atmospheric properties. Upcoming instruments have a variety of wavelength coverages and resolutions. Comparing their capabilities suggests that Twinkle, Ariel and JWST all give similar levels of characterisation for large gaseous planets around bright stars. However, Twinkle and Ariel are more suited for these targets as they achieve this spectra in a single visit. If one wishes to study gas giants with JWST, one would be better off observing planets around fainter stars so that the NIRSpec prism, which provides the same wavelength coverage as combining NIRISS GR700XD and NIRSpec G395m but in a single visit, can be utilised. For smaller, potentially rocky planets, JWST is the most suitable

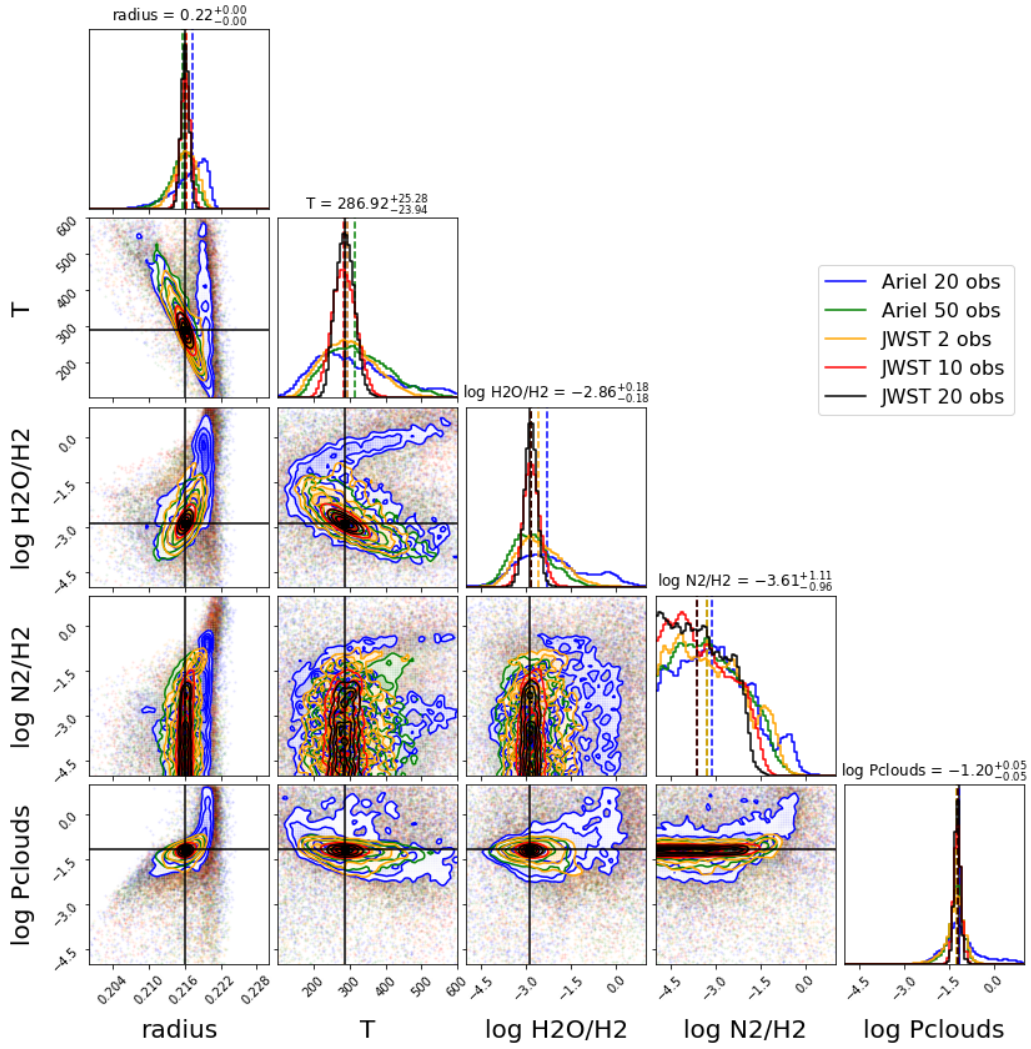

Figure 10.21: Retrieval posteriors for the atmospheric scenario 3: Light atmosphere composed of hydrogen and clouds. Traces of water are also present.

observatory, particularly for temperate worlds, due to its unparalleled sensitivity.

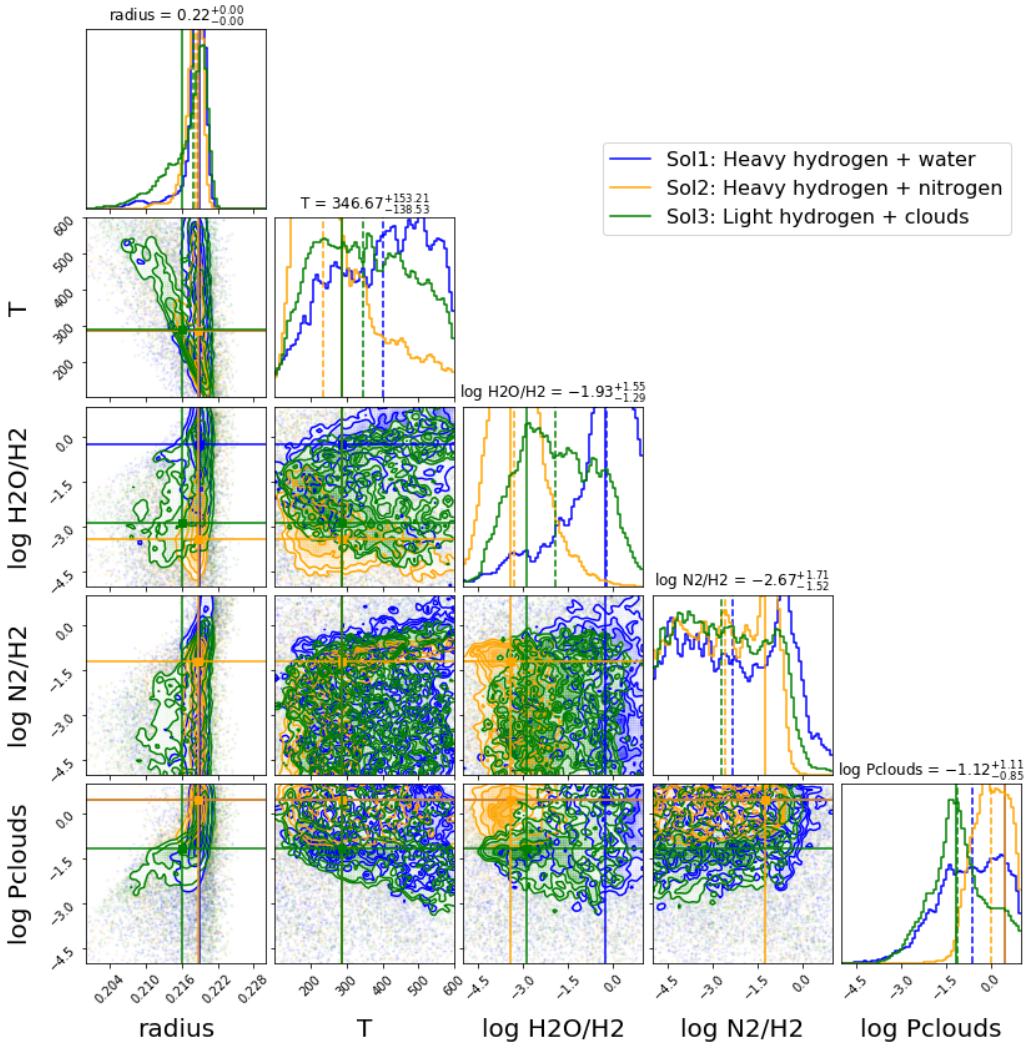

Figure 10.22: Retrieval posteriors for the 3 scenarios in the case of 10 Ariel transits. The solutions are close, but we start seeing the convergence to the 3 scenarios.

Chapter 11

Maintaining Exoplanet Ephemerides

> ”Better three hours too soon, than one minute too late.”
>
> William Shakespeare

Shakespeare’s wise words apply to many situations in life and certainly ring true for exoplanet observers for whom missing a transit (or eclipse) is costly. However, observing a target star for many hours before an event for fear of missing it is an inefficient use of what is usually a highly expensive facility. Thus accurate ephemeris data, that is knowledge of a planet’s orbit and hence when a transit or eclipse event will occur, is of the utmost importance to ensure effective use of telescope time while minimising risk. When considering the next generation of facilities for exoplanet atmospheric characterisation (JWST, E-ELT, Ariel etc.), this is particularly true as observing time on these exceptional facilities will be precious. Therefore, observations of transiting exoplanets will need to have a limited time window while ensuring that enough margin is included to avoid a transit event being partially, or completely, missed. Large errors in the ephemeris of a planet increase the observation time required to ensure the full transit is captured and thus reduce the efficiency, and science yield, of these missions.

Contributions: The majority of this chapter is novel work which has not been published. I led the ORBYTS ephemeris refinement project, with support from Quentin Changeat, Gordon Yip and Angelos Tsiaras, and a paper has recently been submitted (Edwards et al., submitted, Original Research By Young Twinkle Students (ORBYTS): Ephemeris Refinement of Transiting Exoplanets, MNRAS).

Just after discovery, the time of the next transit for a planet is well known. Unfortunately the accuracy of predicted future transits degrades over time due to the increased number of epochs since the last observation and the stacking of the period error. In extreme cases this can mean the transit time is practically lost, with errors of several hours (e.g. Corot-24 b & c, [335]). In addition to this, extrapolating transit times from only a few data points over a limited baseline can easily introduce bias (e.g. [70]). Finally, we could expect transit times to shift due to dynamical phenomena such as tidal orbital decay, apsidal precession or from gravitational interactions with other bodies in the system (see e.g. [307, 336, 337]). These can only be understood, and mitigated for, by regularly observing targets over a long baseline. In the era of TESS, this will become increasingly difficult and require a coordinated effort by many groups and telescope networks to prepare for characterisation by the next generation facilities. The campaign will need data from both ground-based facilities and space-based telescopes such as TESS, Spitzer, CHEOPS and Twinkle.

This chapter focuses on the potential avenues for following-up of exoplanets with large uncertainties in their transit times. Different opportunities are explored from both the ground and space. Additionally, an example project for ephemeris refinement as part of the outreach program ORBYTS (Original Research By Young Twinkle Students) is presented. The project used a fully robotic ground-based telescope network, citizen astronomers and data from TESS.

11.1 Ground-based Follow-up

Since the first planetary transit was discovered [338, 339], ground-based telescopes have regularly discovered and characterised exoplanets via transit photometry. Across the globe, thousands of small telescopes are capable of transit photometry and many of these belong to citizen astronomers. TESS will extend the number of targets that can be observed, as well as relaxing constraints on the telescope size and instrumentation quality. Ground-based follow-up will require not only a large number of telescopes but a good deal of man hours to plan observations and

Minimum Transit Depth	Number of Planets	Percentage of Target List
1 millimag	1433	71%
2 millimag	1096	55%
3 millimag	874	44%

Table 11.1: Number of planets that could be follow-up from the ground assuming a max transit duration of 6 hours and various minimum transit depths.

process the data. Hence, citizen astronomers, citizen science and educational outreach offer an excellent opportunity to support future space missions. The ability of small ground-based telescopes to contribute to exoplanet science is well known (e.g. [340]) and, given the brightness of the host stars of planets found by TESS, even modestly sized telescopes can be used to re-observe planetary systems, reducing the errors on their ephemeris.

The limits of which planetary transits can be observed depend upon the size of the telescope and the instrumentation. Here a depth of 2 millimag has been taken as the shallowest transit which can be detected by ground-based facilites. The Next Generation Transit Survey (NGTS, [97]) has shown that sub-millimag precision is achievable by simultaneously observing the same transit with many identical small telescopes and combining data. Using such methods could expand the number of exoplanets that are observable from the ground but are not in the realm of most observers. The length of a transit can also be prohibitive. Given that, for good ephemeris, the entire transit should be captured along with a significant baseline, a max duration of 6 hours has been assumed. Applying these constraints to the list of potential targets for Ariel yields over 1000 planets and Table 11.1 shows that even with more conservative limits on the transit depth, nearly 900 planets could be follow-up up from the ground.

We can therefore expect that ground-based follow-up will be possible for hundreds, if not thousands, of planets over the coming decade to ensure exoplanet ephemeris are kept up to date. To achieve regular observations of all known exoplanets, telescope time must be efficiently utilised. However, it is not always clear when the most recent observations of a target occurred which can result in the unnecessary use of telescope (and observer) time. To combat this, particularly in the

TESS era, follow-up observations need to be coordinated to maximise the effectiveness of the data. Several ongoing projects aim to contribute to this and these are described below.

11.1.1 Exoplanet Transit Database

The Exoplanet Transit Database (ETD, [341]) was established in 2008 and is a web-based application which is open to any exoplanet observer. The ETD is a project of the Variable Star and Exoplanet Section of the Czech Astronomical Society and the site consists of three parts, the first of which provides predictions of the upcoming transits. The second section allows for users to upload new data and the final function is the display of the observed - calculated diagrams (O-C). The ETD has hundreds of contributors and the database contains thousands of observations. While all observations are analysed by the ETD system to produce these graphs, the data can also be downloaded. The ETD does not facilitate a ranking of planets based on their current uncertainties.

11.1.2 ExoWorlds Spies

ExoWorlds Spies[1] is a project that started in early 2018, aiming to monitor transiting exoplanets through long-term regular observations using small and medium scale telescopes. The effort is supported by citizen astronomers, the Holomon Astronomical Station and the Telescope Live network[2]. The project promotes the idea that research is an effort that everyone can contribute to and thus it is open to collaborations with the public, including school and university students. User-friendly data analysis tools and a dedicated website have been developed as part of the project, in order to disseminate the material to as many people as possible. The website includes audiovisual material, information on the project, data analysis tools, instructions, observational data and graphics. All sources are online, free, and available for everyone both in English and Greek. So far, the ExoWorlds Spies database includes approximately 60 transit observations of more than 25 different exoplanets, from both the North and the South hemisphere, including recently dis-

[1] https://exoworldsspies.com
[2] https://telescope.live

covered planets with limited data available. A number of these transits are already available on the website for members of the general public, students, and citizens to analyse.

11.1.3 ExoClock

ExoClock has been established as part of the ground-based characterisation campaign for the Ariel space mission. Ariel aims to observe 1000 exoplanets during its primary mission, characterising their atmospheres and seeking to understand the chemical diversity of planets in our galaxy [125]. The Ariel Mission Reference Sample (MRS), the planets observed by the mission, will be selected from a large list of potential targets. The selection criteria will aim to produce a multifarious population of planets for study. However, the lack of basic knowledge such as stellar variability and the expected transit time of the system, may mean a planet is not selected for observation, potentially reducing the impact of the mission. ExoClock aims to facilitate a coordinated program of ground-based observations to maximise the efficiency of the Ariel mission. The program also aims to stimulate engagement with citizen astronomers, allowing them to contribute to an upcoming ESA mission. The site ranks the potential Ariel targets from [124], prioritising those that have a large uncertainty in their next transit time. These can then be filtered by the location of the observer and the telescope size, providing a list of exoplanet transits which would be observable in the near future. The ExoClock initiative has the explicit rule that all those who upload data for a planetary system will be included on any subsequent publications.

11.2 Space-based Follow-up

Up to 70% of TESS detections, and 50% of the Ariel target list, may not be observable from the ground due to long or shallow transits [342] and a number of space-based telescopes offer the opportunity to observe exoplanet transits. The potential of these missions to contribute towards improved ephemeris data is considered here.

11.2.1 TESS

During its primary mission, TESS is surveying almost the entire sky. While the prime objective of the mission is to discover new planets, TESS will also observe stars which are known to host planets and the data has a number of uses. Firstly, one can search for additional planets in these systems or for transits of planets discovered by radial velocity surveys. For large, close-in planets around bright stars, TESS provides optical phase curves of a quality which allows for the scattering properties of the atmosphere to be studied, gleaning hints of the cloud coverage and particle size. By re-observing known plants, TESS is also allowing observers to refine the orbital parameters of these worlds.

However, while TESS will provide an excellent source of ephemeris data during the primary mission life, the satellite's impact in the longer term is less certain and is dependent upon the extension of the mission and the strategy proposed. These scenarios could include searching for planets close to the ecliptic plane, a Kepler-style long stare and a repeat of the full-sky survey with longer staring periods or different 'postage-stamp' stars. If TESS continues to observe the whole sky, it will be possible to gain transit observations of many of the currently-known planets as well as those discovered by the mission in its nominal lifetime. However, certain planets (e.g. those on longer periods, close to the ecliptic or around fainter stars) may not be observed by TESS and other extended operations could be chosen. Additionally there will be a huge number of planets discovered by TESS that need follow-up.

In any case, to assess the possibility of ephemeris refinement of planets within the Ariel target list with TESS, a pipeline has been built to find, acquire, reduce, and analyse the data. For a given target, the code searches the Mikulski Archive for Space Telescopes (MAST[3]) and returns all the data collected on the host star from various observatories. The list is filtered to see if TESS has observed the star and, if so, the Presearch Data Conditioning (PDC) light curve, which has had non-astrophysical variability removed and 'bad data' eliminated through the methods

[3] `http://archive.stsci.edu`

outlined in the TESS guide[4], is downloaded. The data product is a time-series for each sector ($\sim$27 days) with a cadence of two minutes. Next, pylightcurve is used provide an initial quick fit of the data to locate the first transit event. Once the time of this initial transit has been established, the data is split using the literature period to create individual time-series of each transit event. The pipeline then fits each of these and uses the fitting of these transits, along with literature values, to update the orbital period and transit time of the planet.

As of November 2019, TESS has observed the host stars of 150 planets within the Ariel target list. However, data of sufficient quality has not necessarily been obtained for each of these. Figure 11.1 shows examples of the two minute cadence data for two bright targets, WASP-4 b and KELT-15 b, and a fainter target, Kepler-18 b. The transits of the bright targets are easily visible by eye, even without phase folding. However, for Kepler-18 b, even when the data is binned to a two hour cadence and phase folded, the errors on each data point are far greater than the transit depth of the planet. Thus, while TESS will undoubtedly be a great resource for the refinement of transit times, the extent of this contribution needs further exploration.

11.2.2 Hubble and Spitzer

Spitzer has been used to follow-up several exoplanets with ephemeris uncertainties (e.g. [70, 71, 72]) but, while there are ongoing programs, the spacecraft will cease operations in early 2020. The Hubble Space Telescope (HST) has been delivering spectroscopic observations of exoplanets since 2001. Although most observations are interrupted due to Earth obscuration, the precision can still be sufficient for measuring accurate transit times. HST may well be used to observe new TESS detections and could therefore provide ephemeris refinement but, should the uncertainty on the transit time become too great, could also be restricted in terms of choice of target. Therefore, neither of these missions can be expected to have a major impact on any ephemeris refinement project.

[4] `https://spacetelescope.github.io/notebooks/notebooks/MAST/TESS/beginner_tour_lc_tp/beginner_tour_lc_tp.html`

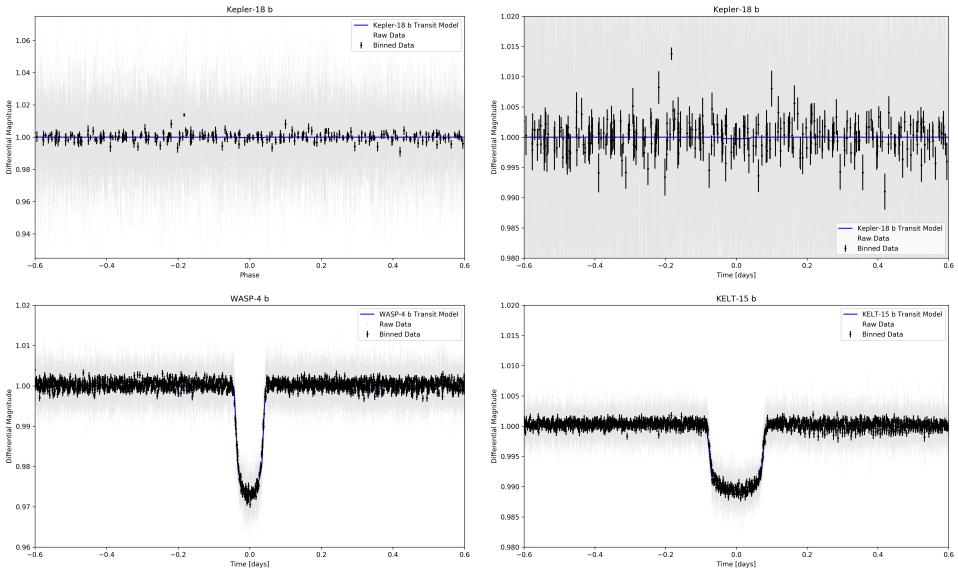

Figure 11.1: TESS observations of Kepler-18 b, WASP-4 b and KELT-15 b. The latter two cases provide excellent quality data for ephemeris refinement while for Kepler-18 b, the transit signal is far smaller than the noise even when the data is binned to a cadence of 2 hours and phase-folded.

11.2.3 CHEOPS

CHEOPS will be launched in December 2019 and is anticipated to follow-up a large number of TESS discoveries, refining both planetary and orbital parameters via high precision photometry. The mission has reserved around 20% of the telescope time for guest observers which equates to 946 orbits, or 1578 hours, in the first year. To allow potential users to explore the capabilities of CHEOPS, a simulator has been developed which has a web interface[5]. By inputting the star type and magnitude, along with the observation duration, a noise prediction is returned. The web-based simulator has been utilised to understand the performance for ephemeris refinement of planets within the Ariel target list. CHEOPS cannot observe the ecliptic poles, which are the continuous viewing zones for JWST and Ariel, and planets outside the field of regard have been removed. Having done so, Figure 11.2 shows the predicted error on the transit depth from one CHEOPS observation, assuming one transit duration is observed as a baseline both before and after the event. Over-plotted are lines which indicate the SNR on the transit depth and Table 11.2 contains the number of

[5] `https://cheops.unige.ch/pht2/exposure-time-calculator`

planets for which these SNRs could be achieved in 1 transit. The target list has been split into those that could be observed from the ground (transit depth >2 mmag and transit duration <6 hours) and those for which space-based follow-up will be required (transit depth <2 mmag and/or transit duration >6 hours), to estimate the number of planets which CHEOPS could contribute.

To put these SNRs into context, Figure 11.3 shows some simulated data for various SNRs. It should be noted that while the calculation of the predicted error in Figure 11.2 does account for gaps in the light curve due to Earth obscuration, the simulated data does not. The position of these gaps will no doubt affect the accuracy of the fitted ephemeris and so a code like Terminus would be needed to ensure the data quality was sufficient. Time-domain information is not available in the CHEOPS online simulator although an average efficiency is given. Further investigation is needed to ascertain the exact number of targets for which CHEOPS could reduce the transit uncertainties but it would seem likely that the final figure will be of the order of several hundred. Future work will attempt to refine the basic calculations made here by simulating gaps due to Earth obscuration, fitting the mock data and calculating the number of observations needed to reduce the transit uncertainties to acceptable levels. Here it is assumed that CHEOPS would be able to provide ephemeris refinement for all planets for which an SNR >5 is achieved on a single transit, though, in some cases, multiple transits may be required.

From CHEOPS and ground-based surveys alone, a first analysis suggests that nearly 80% of the Ariel target list could be followed-up. The calculation assumes that the time on CHEOPS is allocated to an ephemeris project with the scope of preparing targets for Ariel. Figure 11.4 displays the location in the sky of the Ariel targets and the method with which they can be followed-up. Those that cannot be followed-up with ground-based photometry or CHEOPS would require observations with other space-based telescopes or ephemeris refinement via radial velocity measurements (e.g. [343]).

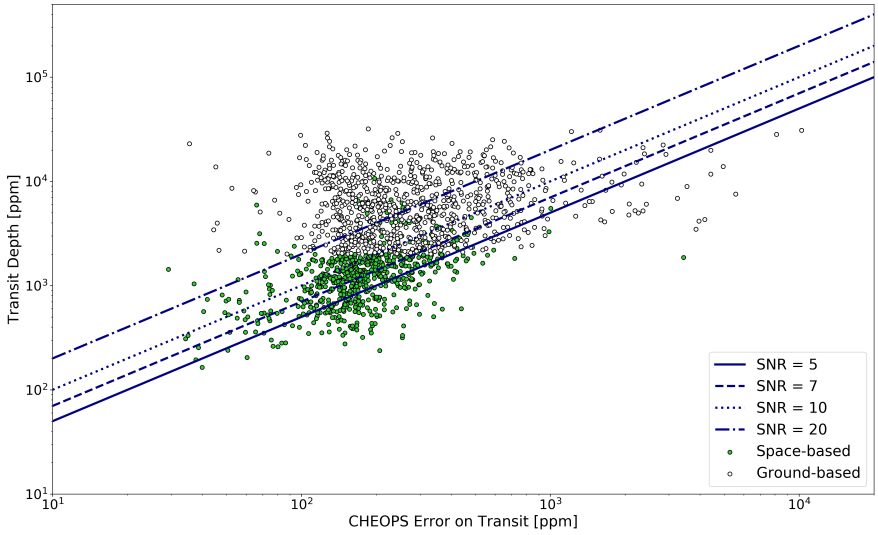

Figure 11.2: Predicted error on the transit depth with one CHEOPS observation compared to the transit depth. Planets requiring space-based follow-up are defined as those which have a transit depth shallower than 3mmag and/or a transit duration that is longer than 6 hours.

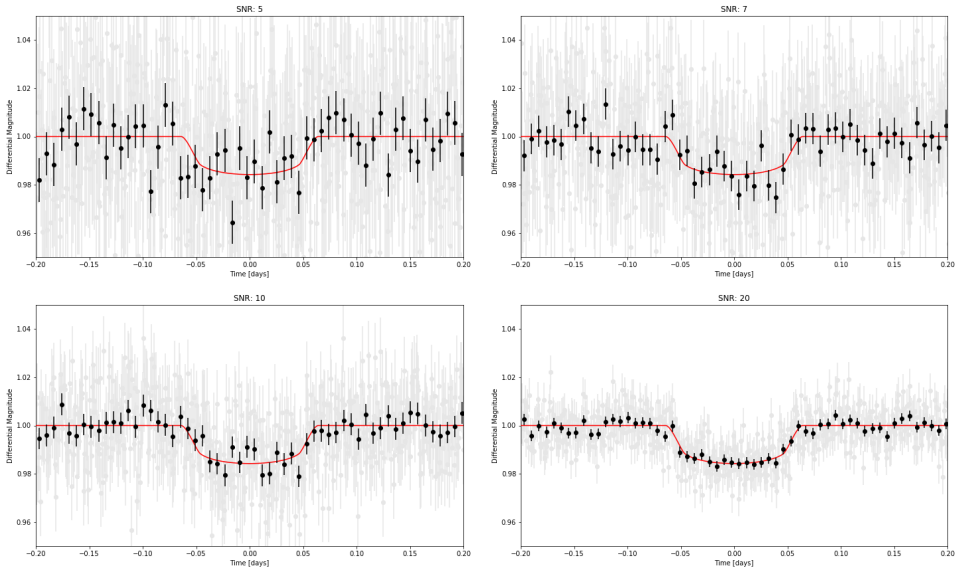

Figure 11.3: Simulated observations of a Jupiter-sized planet orbiting a G-type star at different SNRs. In each case the cadences are 1 minute and 10 minutes for original and binned data respectively.

SNR	All Planets	Space-based Required
5	1286	454
7	1093	304
10	820	132
20	453	22

Table 11.2: Number of planets within the Ariel target list for which a given SNR can be reached in 1 transit with CHEOPS. Planets requiring space-based follow-up are defined as those which have a transit depth shallower than 3mmag and/or a transit duration that is longer than 6 hours.

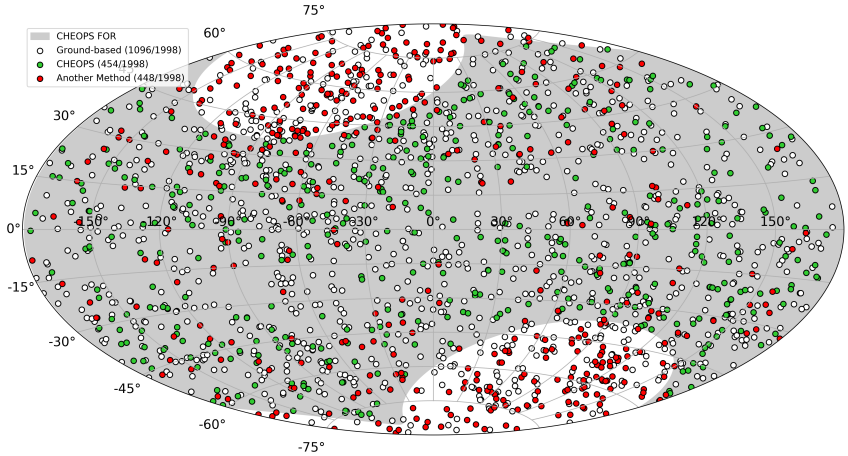

Figure 11.4: Sky location of potential planets for study with Ariel. The colour of the marker indicates the method with which they could be followed-up based on the analysis here. Note that many of the planets currently defined as "another method' could be followed-up with TESS during the extended mission.

11.2.4 Twinkle

Twinkle's instrumentation is capable of transit and eclipse spectroscopy of exoplanets around bright stars in the visible and near-infrared and this data could also be utilised to refine the ephemeris times. Binning Twinkle data into broadband photometric points may also allow fainter targets to be observed. Twinkle, as with CHEOPS, cannot observe the ecliptic poles and some portion of observations will be affected by Earth obscuration. Additionally, Twinkle, like HST, Spitzer and CHEOPS, is only capable of observing a single target at any one time. Therefore, the total observing time on this facility may not be sufficient to follow-up all targets.

11.2.5 Cubesats

Cubesats such as the Microvariability and Oscillation of Stars (MOST, [344]) and Arcsecond Space Telescope Enabling Research in Astrophysics (ASTERIA, [345]) have been used to observe transiting planets (e.g. [346]) while PicSat aimed to observe a possible transit of the giant planet β Pictoris b's Hill sphere [347] and the Colorado Ultraviolet Transit Experiment (CUTE, [348]) will attempt to observe atmospheric mass loss from Hot-Jupiters. Space-based follow-up using cubesats will continue to be explored and future missions with capabilities similar to these missions could also play a large part in ephemeris follow-up. Nevertheless, the concept of CURE (CUbesat for Refining Ephemerides) has been proposed and studied. CURE would aim to observe the ecliptic poles, the constant viewing zone of JWST and Ariel but an area of sky that cannot be covered by CHEOPS. Hence CURE would provide a space-based alternative to TESS in case the mission does not sufficiently re-observe the poles or is not funded until the launch of Ariel. CURE's baseline design is on PicSat with an 8 cm diameter primary mirror and a fibre-fed instrument. However, while CURE would likely have considerable capabilities for transit photometry, cubesats are relatively expensive (>£1 million), often unreliable due to issues with their attitude and orbital control systems (AOCS), and usually have a limited lifespan (<2 years).

11.3 An Example Ephemeris Refinement Project

To prove the feasibility of engaging with citizen science and educational outreach for ephemeris refinement, a project has run through the Original Research By Young Twinkle Students (ORBYTS) scheme. ORBYTS is an educational programme in which secondary school pupils work on original research linked to the Twinkle Space Mission under the tuition of PhD students and other young scientists [349, 350]. The ORBYTS program has been run since 2012 and is jointly managed by Blue Skies Space Ltd. (BSSL) and University College London (UCL). A key science case for Twinkle is the observation of extrasolar planets via transit and eclipse spectroscopy. ORBYTS offers school pupils the chance to enrich our understanding

Planet	Planet Radius [R_J]	Star V Mag	Uncertainty [minutes]	Last Observed	Reference
CoRoT-6 b	1.17	13.9	2.7	2010	[354]
KELT-15 b	1.44	11.2	15.7	2015	[355]
KPS-1 b	1.03	13.0	57.6	2018	[356]
K2-237 b	1.65	11.6	13.0*	2018	[357]
WASP-45 b	1.16	12.0	5.3	2012	[358]
WASP-83 b	1.04	12.9	11.9	2015	[359]
WASP-119 b	1.40	12.2	15.7	2016	[360]
WASP-122 b	1.74	11.0	4.9†	2016	[361]

*The independent discovery paper [362] suggests an uncertainty 3.8 minutes
†The independent discovery paper [355] suggests an uncertainty 3.4 minutes

Table 11.3: Exoplanets for which observations were acquired and the calculated uncertainty in their transit mid time on 1st July 2019 based on data from the NASA Exoplanet Archive.

of these new worlds by improving our knowledge of the molecules they're made of, their orbits and their physical properties. The program provides a unique opportunity for pupils to undertake cutting-edge science that has a meaningful impact on a future space mission.

ORBYTS partners dynamic, passionate science researchers with secondary schools, where, through fortnightly school visits over an academic year, the researcher teaches the students undergraduate-level physics. The goal of every partnership is that school students will have the opportunity to use this new knowledge to contribute towards publishable research. Pupils get hands on experience of scientific research and work closely with young scientists. By partnering schools with relatable researchers, the programme aims to not only improve student aspirations and scientific literacy, but also help to address diversity challenges by dispelling harmful stereotypes, challenging any preconceptions about who can become a scientist. The organisers and tutors strongly believe that all school students should have the opportunity to become involved in active scientific research and to be culturally connected to space missions. Previous projects have included calculating molecular transitions with the ExoMol group [351, 352, 353] as these line lists are key for atmospheric retrievals. During this project the students selected suitable follow-up targets, scheduled observations and analysed the subsequent data.

11.3.1 Target Selection

There are several major exoplanet catalogues from which one can compile a list of potential planets. The most widely used and comprehensive is the NASA Exoplanet

Archive[6] [363]. The NASA catalogue was accessed in February 2019 and the transit error by mid 2019 (the end time of this project) was calculated for each planet. Unlike some previously studies (e.g. [364]), we included all transiting planets, regardless of their discovery facility. The next transit of a planet, T_c, can be calculated from

$$T_c = T_0 + n \cdot P \tag{11.1}$$

where P is the period of the planet, T_0 is the last measured transit time and n is the number of epochs since this last observation. Both T_0 and P have errors associated with their measurement and thus the error on the predicted transit time, ΔT_c is given by

$$\Delta T_c = \sqrt{\Delta T_0^2 + (n \cdot \Delta P)^2} \tag{11.2}$$

assuming no co-variance between the two parameters. There is, of course, a correlation between the fitted period and mid time but this co-variance is generally negligible. Suitable targets were found by filtering this list to include only those with a large transit uncertainty (>10 minutes) or those that had not been observed for 3 or more years. We note that the ephemeris of many of the large, gaseous planets with significant transit uncertainties were refined in [364] and these were excluded from the study. The choice of targets was restricted by the size of the telescopes (0.35 - 0.6 m, see Section 11.3.2) due to the star magnitude and transit depth but still many planets with substantial ephemeris errors were found to be observable.

11.3.2 Data Acquisition

Observations were attempted for a large number of targets, though some were frustrated due to sky coverage and unforeseen issues such as poor weather. Table 11.3 contains the planets for which good quality data was obtained and the expected transit error on 1^{st} July 2019. Although some of the planets observed here are around fainter stars, they are all potentially suitable for spectroscopic follow-up and could be observed by Ariel [124]. They may also be potential targets for characterisation by Twinkle, JWST or ground-based facilities. Observations of these targets were

[6] `https://exoplanetarchive.ipac.caltech.edu`

scheduled between February and April 2019.

11.3.2.1 Robotic Ground-based Telescope Network

For the new observations presented here we use the Telescope Live network of robotic telescopes[7]. Telescope Live is a web application offering end-users the possibility to purchase images obtained on-demand from a network of robotic telescopes. It has been developed by Konica Minolta Laboratory Europe[8], the European research and development group of Konica Minolta Inc. and it is operated by Spaceflux Ltd., a space sector start-up based in the United Kingdom. Telescope Live kindly provided access to their telescopes for a total of 100 hours. At the time of writing the network consists of three telescopes: a Planewave CDK24 (with a main mirror diameter of 0.6 m) located at at El Sauce Observatory in Chile, a Meade LX200 (0.35 m) at Warrumbungle Observatory in Australia, and a Officina Stellare RILA 400 (0.4 m) at Nunki Observatory in Greece. We obtained a single transit observation of K2-237 b and WASP-119 b along with 2 of KELT-15 b and WASP-83 b. Additionally we obtained a light curve of WASP-122 b with a 0.4 m telescope from the Las Cumbres Observatory (LCO) network[9] thanks to the Educational Proposal FTPEPO2014A-004 led by Paul Roche.

11.3.2.2 ETD and ExoWorldSpies

For the selected planets, the Exoplanet Transit Database (ETD, [341]) was searched for additional observations. Having removed unsuitable light curves via visual inspection, we found a total of 29 light curves from citizen astronomers: 5 of CoRoT-6 b, 18 of KPS-1 b, 3 of WASP-45 b, 1 of WASP-83 b and 2 of WASP-122 b. All these observations were undertaken as part of the TRansiting ExoplanetS and CAndidates (TRESCA) project[10] and are summarised in Table 11.4. From ExoWorldSpies, we included an observation of WASP-83 b in our analysis. Additionally, the new observations taken as part of this work have been added to the ExoWorldsSpies and ExoClock databases.

[7] https://telescope.live
[8] https:///research.konicaminolta.eu
[9] https://lco.global
[10] http://var2.astro.cz/EN/tresca

11.3.2.3 TESS

TESS recently finished surveying the south hemisphere and thus has observed several of the planets studied here. We searched the Mikulski Archive for Space Telescopes (MAST[11]) and found that TESS has observed K2-237 b, KELT-15 b, WASP-45 b, WASP-83 b, WASP-119 b and WASP-122 b. The pipeline described in Section 11.2.1 was used to download and clean the data. After excluding the poor data, we recovered 7 K2-237 b transits, 12 for KELT-15 b, 8 for WASP-45 b, 4 of WASP-83 b along with 37 for WASP-119 b and 14 of WASP-122 b. We note that Sector 8 TESS data for KELT-15 b was not available. All TESS data used here has a cadence of 2 minutes.

11.3.3 Data Reduction and Analysis

The LCO and Telescope Live networks automatically gathers calibration frames and provide the data in a reduced format (though the raw and calibration frames can also be downloaded). These frames were analysed using the HOlomon Photometric Software (HOPS, (Tsiaras, in prep)) which aligns the frames and normalises the flux of the target star by using selected comparison stars. The software was developed as part of the ExoWorldSpies project, is open-source and is available on Github[12]. The final output of HOPS is a time-series photometric light curve. The data from ExoWorldSpies was also analysed with HOPS while the observations from ETD were obtained as space, tab or comma-separated files containing the light curve.

The photometric light curves from all sources were fitted using PyLightcurve (Tsiaras, in prep), another open-source code which is also publicly available[13]. Initially fit parameters were the orbital semi-major axis scaled by the stellar radius (a/R_*), the orbital inclination (i), the planet-star radius ratio (R_p/R_*), the midpoint of the transit (T) and the orbital period (P). In each case the MCMC was run with 250,000 iterations, a burn of 100,000 and 200 walkers. The limb darkening coefficients were fixed to theoretical values from [365, 366] according to the stellar parameters obtained from the planet discovery papers. Previous analyses show

[11] `http://archive.stsci.edu`
[12] `https://github.com/HolomonAstronomicalStation/hops`
[13] `https://github.com/ucl-exoplanets/pylightcurve`

Table 11.4: General information about the observations conducted and analysed in this work

Planet	Date	Telescope	Filter
CoRoT-6 b	09 July 2010	ETD, Sauer	Clear
	17 July 2010	ETD, Sauer	Clear
	17 June 2015	ETD, Molina	Clear
	19 July 2018	ETD, Kang	R
	22 June 2019	ETD, Evans	Clear
K2-237 b	16 April	El Sauce	V
	26 May 2019 till 18 June 2019	TESS	I
KELT-15 b	08 January 2019 till 27 March 2019	TESS	I
	19 February 2019	Warrumbungle	V
	21 March 2019	Warrumbungle	V
KPS-1 b	12 March 2019	ETD, Jongen	Clear
	22 March 2019	ETD, Wunsche	V
	22 March 2019	ETD, Wunsche	Clear
	22 March 2019	ETD, Raetz	Clear
	22 March 2019	ETD, Jongen	Clear
	22 March 2019	ETD, Guerra	Clear
	29 March 2019	ETD, Wunsche	Clear
	29 March 2019	ETD, Jongen	Clear
	29 March 2019	ETD, Friedli/Kropf	V
	29 March 2019	ETD, Watkin	R
	29 March 2019	ETD, Guerra	I
	20 April 2019	ETD, Wunsche	Clear
	20 April 2019	ETD, Jongen	Clear
	02 May 2019	ETD, Raetz	Clear
	14 May 2019	ETD, Bretton	I
	14 May 2019	ETD, Guerra	V
	14 May 2019	ETD, Raetz	Clear
	14 May 2019	ETD, Bosch	V
WASP-45 b	15 August 2011	ETD, Evans	Clear
	16 July 2012	ETD, Sauer	R
	27 December 2016	ETD, Lajus	R
	23 August 2018 till 20 September 2019	TESS	I
WASP-83 b	28 March 2018	El Sauce	R
	02 April 2019	El Sauce	R
	11 March 2019	El Sauce	V
	29 March 2019	ETD, Chatela	R
	28 March 2019 till 22 April 2019	TESS	I
WASP-119 b	27 July 2018 till 13 November 2018	TESS	I
	07 March 2019	Warrumbungle	V
WASP-122 b	18 January 2017	ETD, Evans	R
	30 January 2017	ETD, Evans	R
	02 March 2019	LCO	V
	08 January 2019 till 01 February 2019	TESS	I

that the trends in the light curves can be approximated with simple functions of only very few free parameters, for example low order polynomials over time (e.g. [266, 336, 367, 364]). Hence we detrended all light curves using a simple second-order polynomial. We then removed all data points with residuals greater than 3 sigma from the best-fit model. For planets with TESS data, we refined all transit parameters. However, for the other targets we do not attempt this refinement because a significant fraction of the light curves used here either miss parts of the transit event or do not reach millimag-precision.

Next we fitted each light curve individually with a/R_*, i and R_p/R_* allowed to vary within 1 sigma of the values from the literature (or the new values computed here) while T was fit with far wider bounds. The uncertainties on each fitted mid-time are obtained from the posterior distributions of the MCMC chains. We convert all our mid-times into BJD_{TDB} using the tool from [368]. Having fit the mid transit time for all the data, we use a weighted least squares fit to obtain a linear period for the data analysed in this work and any previous mid-times from the literature (also converted to BJD_{TDB}). We varied the timing zero point, T_0, and report the value which minimised the co-variance between T_0 and P. We used the ephemeris that are available in the literature to compute 'observed minus calculated' residuals for all transit times.

11.3.4 Results

Our analysis uncovered significant drifts in the transit times of all planets studied here, with only one planet (KPS-1 b) having observed transits within the 1 sigma errors on the expected time. Even in this case, the observed transit was considerably offset from the predicted. K2-237 b, KELT-15 b, WASP-45 b, WASP-83 b, WASP-119 b and WASP-122 b were observed by TESS in the first year of operations and we demonstrate the great potential the mission has for refining orbital parameters. The capability of TESS to provide accurate updated ephemerides for bright, short period planets has previously been shown in [337].

As the primary two year mission covers almost the entire sky, the ephemerides of many of the known planets could be updated once the data is released. For short

period planets, TESS data gives multiple, high-precision, complete transits allowing the uncertainty on both the period and T_0 of these planets to be reduced. A summary of the findings for each planet is given below.

CoRoT-6 b: [369] found that CoRoT planets seemed to have slightly underestimated uncertainties in their ephemerides and our analysis of CoRoT-6 b agrees with their findings. The final transit of CoRoT-6 b was found to be 23 minutes from the calculated time despite the predicted uncertainity being less than 3 minutes. The new observations help reduce the uncertainity on the transit time but we note that the fit of linear period for CoRoT-6 b is poor so more data is required to accurately assess the period.

K2-237 b: There are two independent discovery papers for K2-237 b. Using the ephemeris data from [357] one could expect an uncertainty of 13 minutes in the transit mid time while [362] claims a greater precision on the period and thus predicts an uncertainty of 3 minutes. In reality we discover a shift of nearly 15 minutes and find our data to have a closer fit to the ephemeris of [357]. However, given the short period of the planet ($\sim$2.18 days), over 400 orbits have occurred since the discovery. The difference is therefore equivalent to an error in the period of $\sim$1.5 seconds, compared to a claimed uncertainty in the period of 0.5 seconds), and shows how an overconfidence in the accuracy of exoplanet ephemerides can lead to significant deviations from the expected transit time, highlighting the benefit of following-up targets on a regular basis.

KELT-15 b: This hot-jupiter had not been re-observed with transit photometry since its discovery meaning the uncertainity in its transit time had risen to nearly 16 minutes. In the 4 years since, several hundred orbits had occurred and a 20 minute deviation from the expected transit time was found.

KPS-1 b: The newly observed transits for this planet were the only ones to fall within the 1 sigma errors in our sample. However, a deviation from the expected was found of over 30 minutes which is still a substantial residual. The uncertainty on the transit time of KPS-1 b is predicted to be less than 10 minutes until after the launch of Ariel.

WASP-45 b: The predicted uncertainty on WASP-45 b was around 5 minutes but it had not been re-observed for several years. The O-C plot from ETD showed a slight divergence from the expected but it was not until the TESS data was analysed the the full extent became clear with the transit arriving 15 minutes early.

WASP-83 b: For WASP-83 b, the newly observed transits occurred $\sim$30 minutes after the expected time, well outside the 1 sigma error of $\sim$12 minutes. Having not been observed since 2015, 300 orbits had passed. Thus the literature orbit differs by around 6 seconds from the updated value reported here, again highlighting the need for consistent follow-up.

WASP-119 b: With a reported discovery ephemeris in 2013 and an uncertainty of over 10 minutes, WASP-119 b was an obvious choice for follow-up. The combination of TESS data and a ground-based observations uncovered a drift of nearly 20 minutes over the 700 orbits since discovery.

WASP-122 b: Also known as KELT-14 b, this planet has two independent discovery papers [361, 355]. These predicted uncerainities of 3.4 and 4.9 minutes but again the planet had not been re-observed since. Our observations found the transits of WASP-122 b to be occuring around 5 minutes early, just outside the 1 sigma errors. We find our data has a better fit to the period from [361].

Hence we detect significant variations in the observed transit time from the expected for most of the planets studied here. An overconfidence in the predicted transit time is a known issue and analysis of measured-to-predicted timing deviations of 21 exoplanets in [364] indicated a trend of slightly underestimated uncertainties of the ephemerides while [369] made a similar finding for CoRoT planets.

Here our analysis claims an uncertainty on the period of K2-237 b of 0.2s which should keep the uncertainty in the transit time of this planet to below 15 minutes until well after the launch of Ariel in 2028 (see Figure 11.6). Nevertheless, we would advocate further follow up of this planet, the others studied here and further planets with seemingly accurate ephemeris data to ensure errors are not underestimated. Sources of larger than expected uncertainties can be due to underestimated systematics in the data, stellar activity, tidal effects or transit timing

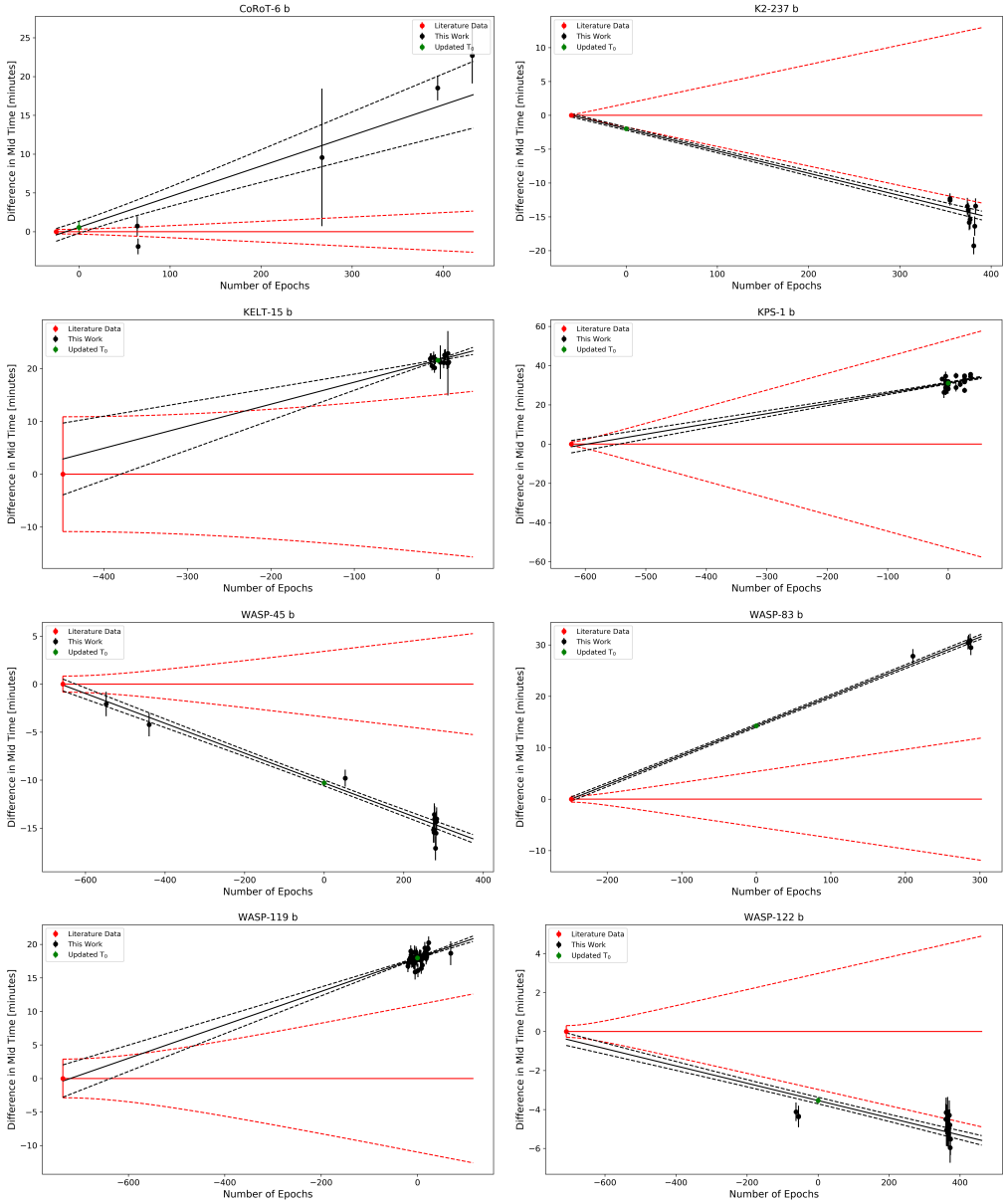

Figure 11.5: Observed minus calculated mid-transit times for all planet studied here. Measurements resulting from this work are shown in black, while literature values included in our calculation are in red. The green data point shows the updated T_0 reported. The black line denotes the new ephemeris of this work with the dashed lines showing the associated uncertainties. For comparison, the previous ephemeris of the discovery paper are in red.

variations (TTVs) due to other bodies in the system. These effects can only be mitigated for by regularly observing transits over a long time period and to achieve this a well-organised ground and space-based campaign is required.

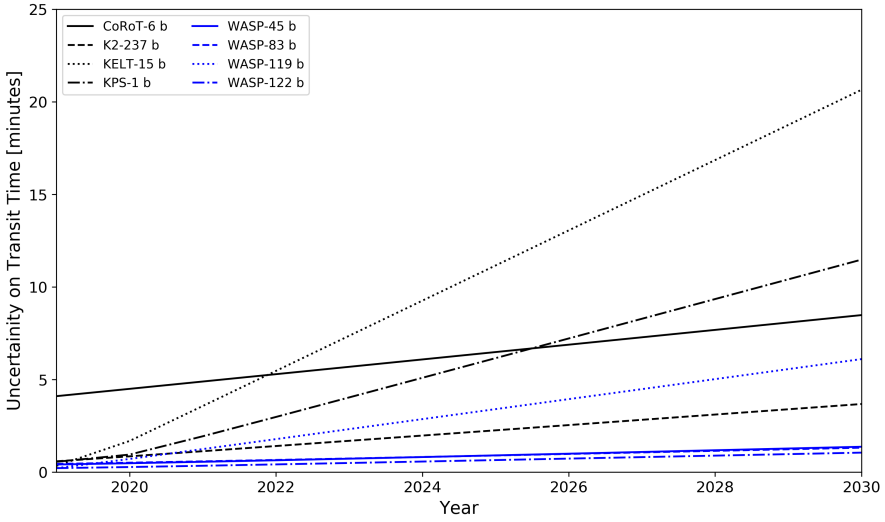

Figure 11.6: Projected uncertainties in the transit times of the planets studied here. While the uncertainties for all planets are predicted to be small for at least a decade, overconfidence in exoplanet ephemeris is a known issue and thus we advocate further follow-up of these planets in the coming years.

11.3.5 Next Steps

Here we homogeneously analyse the data but the reduction has differed between observers which can lead to inconsistencies due to varying reduction methods between observers. The ETD provides a rating of the quality of the uploaded data, from 1-5, but its vetting is perhaps not as extensive as other databases such as the Minor Planet Center. A systematic approach is required, with guidelines that ensure all data is processed in the correct manner. For exoplanet observations, the choice of comparison stars, the provision of correct timing and overall consistency are paramount. Performing such quality checks on the data can be complex, requiring significant data storage and processing capabilities, but are critical if high precision ephemerides are to be obtained. Thus future projects should allow the submission of raw images, along with the necessary calibration files, to allow for the data to homogeneously reduced and analysed and, if an observer wishes to download data, the output format needs to be consistent to ensure efficacy. Being able to accept, and return, various data products from the raw frames to the light curve will increase the functionality of such a project. Alternatively, easy-to-use codes which automatically process the data without the need for human input (e.g. in the choice

of comparison stars) could be used. ExoClock aims to implement such a process for planets that could potentially be studied by Ariel via an open access website which will host all available data on these planetary systems.

11.4 Conclusions

This chapter has focused on the need for follow-up observations for ephemeris refinement to ensure the next generation of facilities can be used efficiently. Community-wide citizen science efforts, such as the ExoClock, need to be established to create a network of individuals and groups to monitor new discoveries. The program need not be limited to citizen astronomers but should include all research groups with access to telescopes of all sizes and build upon the work of existing schemes. Researcher engagement with citizen astronomers, citizen science and in educational outreach offers an excellent opportunity to support future space missions. Stimulating this engagement and devising a coordinated approach to maintaining exoplanet ephemeris will be imperative in the coming years. An initial project to refine ephemerides through one of these schemes found that transit times of seven of the eight planets observed differed greatly from their expected timing. Such a result highlights the need for an ephemeris refinement project in preparation for Ariel. Initial results suggests the combination of ground-based and space-based photometry should be capable of keeping transit timing uncertainties within suitable limits for the majority of the target list.

Chapter 12

Conclusion

> ”An idea, which is man-conceived, unlike most of the myriad effects which comprise our universe, is seldom perfectly balanced. Inevitably, it bears the imprint of man’s own frailty; it may fluctuate from the meagre to the grandiose.”
>
> Bryan Aldiss, Non-Stop

The idea of sending satellites into space to observe distant worlds is certainly grandiose. By studying other planets we learn more about the small, fragile rock, travelling endlessly through the vastness of space, that we call home. It is human nature to be curious and to ponder what conditions are like on these bodies around other stars, wondering if someone, or something, else out there is thinking the same. Space-based telescopes offer an increasingly tantalising opportunity to lift the veil on the conditions on, and diversity of, other planets, allowing us to further develop our understanding of planetary formation and evolution.

However, each mission is, in its very essence, flawed, with no one spacecraft capable of achieving everything. Specialised spacecraft, such as those in-situ around other Solar System bodies, provide astonishing detail about an object or system, but miss the bigger picture, while general observatories cater to many science cases but lack the granularity or time to solve all questions in a field. Mis-

sions which seek to push the boundaries, both from a scientific and engineering perspective, are inevitably expensive and over-subscribed due to their vast capabilities. Smaller, cheaper projects can still offer cutting edge science and therefore to achieve the maximum scientific progress, space agencies should undertake a myriad of projects, each with differing strengths and weakness that accumulate into a well-rounded program of investigation. Already bigger, more complex and more expensive successors to JWST have been proposed to NASA to be the large space-based telescope of the 2030s. The objectives of these facilities, with respect to exoplanet science, revolve around discovering and studying potentially habitable worlds in the search of biosignatures and life. However, it would seem unlikely that such a project would be delivered within budget or on schedule and many studies into their capabilities contain considerable simplifications or assumptions. It would therefore be naive of the exoplanet field to put all its emphasis on such a project in the pursuit of biosignatures and habitability when we understand so little about exoplanetary atmospheres in general. While striving for such goals we must also answer simpler questions such as: how chemically diverse are exoplanets?; how does atmospheric chemistry correlate to other, more basic parameters such as stellar metallicity?; do smaller, rocky planets have an atmosphere and if so, what is main constituent?

Missions that can begin to answer these are on the horizon and here the capabilities of spacecraft ranging in sizes from grams to tonnes have been compared and while undoubtedly a larger telescope aperture results in a greater scientific capability, much can still be accomplished with smaller missions. Although Hubble, Spitzer and ground-based telescopes are providing data which has lead to the characterisation of a number of exoplanet atmospheres (and small bodies), progress is currently limited by the quantity of data, the narrow wavelength regions covered, and the lack of dedicated facilities. The fields of small bodies research and exoplanet science are desperately in need of spectroscopic survey missions that can provide high-quality data, with a broad wavelength coverage, for a large, diverse population of targets. Facilities that are due to launch in the next decade have this capability and promise to revolutionise our understanding of planetary systems.

Many of the results from these observatories can be expected to be serendipitous and thus caution must be applied in the analysis of the data. Incorrect assumptions, particularly simplified physics, can lead to drastic misinterpretations.

The exoplanet field in particular must therefore not stand idle and simply wait for these facilities as, to maximise the efficiency of use and the scientific yield of these missions, there is a great deal of preparatory work required. This work includes exploring the addition of further complexity into retrievals to ensure the complexity of the analysis is well matched to the quality of the data. Additionally more basic preparation, such as refining exoplanet ephemerides, will be critical in ensuring time on the next generation of telescopes is utilised effectively and that the most interesting targets can be observed. Projects to achieve this can be hugely enhanced through engagement with citizen science, amateur astronomers and educational outreach. Not only do such activities benefit the researchers running them, they also allow potential future scientists to have the opportunity to become involved in active scientific research and to be culturally connected to upcoming space missions.

Bibliography

[1] James Norwood, Heidi Hammel, Stefanie Milam, John Stansberry, Jonathan Lunine, Nancy Chanover, Dean Hines, George Sonneborn, Matthew Tiscareno, Michael Brown, and Pierre Ferruit. Solar System Observations with the James Webb Space Telescope. *Publications of the Astronomical Society of the Pacific*, 128(960):025004, Feb 2016.

[2] Fumihiko Usui, Daisuke Kuroda, Thomas G. Müller, Sunao Hasegawa, Masateru Ishiguro, Takafumi Ootsubo, Daisuke Ishihara, Hirokazu Kataza, Satoshi Takita, Shinki Oyabu, Munetaka Ueno, Hideo Matsuhara, and Takashi Onaka. Asteroid Catalog Using Akari: AKARI/IRC Mid-Infrared Asteroid Survey. *Publications of the Astronomical Society of Japan*, 63:1117–1138, Oct 2011.

[3] D. K. Sing, J. J. Fortney, N. Nikolov, H. R. Wakeford, T. Kataria, T. M. Evans, S. Aigrain, G. E. Ballester, A. S. Burrows, D. Deming, J.-M. Désert, N. P. Gibson, G. W. Henry, C. M. Huitson, H. A. Knutson, A. Lecavelier Des Etangs, F. Pont, A. P. Showman, A. Vidal-Madjar, M. H. Williamson, and P. A. Wilson. A continuum from clear to cloudy hot-Jupiter exoplanets without primordial water depletion. *Nature*, 529:59–62, January 2016.

[4] T. Barclay, J. Pepper, and E. V. Quintana. A Revised Exoplanet Yield from the Transiting Exoplanet Survey Satellite (TESS). *ArXiv e-prints 1804.05050*, April 2018.

[5] C. M. Pieters and T. Hiroi. RELAB (Reflectance Experiment Laboratory): A NASA Multiuser Spectroscopy Facility. In S. Mackwell and E. Stansbery,

editors, *Lunar and Planetary Science Conference*, volume 35 of *Lunar and Planetary Inst. Technical Report*, March 2004.

[6] A. W. Howard. Observed Properties of Extrasolar Planets. *Science*, 340:572–576, May 2013.

[7] N. M. Batalha, J. F. Rowe, S. T. Bryson, T. Barclay, C. J. Burke, D. A. Caldwell, J. L. Christiansen, F. Mullally, S. E. Thompson, T. M. Brown, A. K. Dupree, D. C. Fabrycky, E. B. Ford, J. J. Fortney, R. L. Gilliland, H. Isaacson, D. W. Latham, G. W. Marcy, S. N. Quinn, D. Ragozzine, A. Shporer, W. J. Borucki, D. R. Ciardi, T. N. Gautier, III, M. R. Haas, J. M. Jenkins, D. G. Koch, J. J. Lissauer, W. Rapin, G. S. Basri, A. P. Boss, L. A. Buchhave, J. A. Carter, D. Charbonneau, J. Christensen-Dalsgaard, B. D. Clarke, W. D. Cochran, B.-O. Demory, J.-M. Desert, E. Devore, L. R. Doyle, G. A. Esquerdo, M. Everett, F. Fressin, J. C. Geary, F. R. Girouard, A. Gould, J. R. Hall, M. J. Holman, A. W. Howard, S. B. Howell, K. A. Ibrahim, K. Kinemuchi, H. Kjeldsen, T. C. Klaus, J. Li, P. W. Lucas, S. Meibom, R. L. Morris, A. Prša, E. Quintana, D. T. Sanderfer, D. Sasselov, S. E. Seader, J. C. Smith, J. H. Steffen, M. Still, M. C. Stumpe, J. C. Tarter, P. Tenenbaum, G. Torres, J. D. Twicken, K. Uddin, J. Van Cleve, L. Walkowicz, and W. F. Welsh. Planetary Candidates Observed by Kepler. III. Analysis of the First 16 Months of Data. *The Astrophysical Journal Supplement*, 204:24, February 2013.

[8] A. Cassan, D. Kubas, J.-P. Beaulieu, M. Dominik, K. Horne, J. Greenhill, J. Wambsganss, J. Menzies, A. Williams, U. G. Jørgensen, A. Udalski, D. P. Bennett, M. D. Albrow, V. Batista, S. Brillant, J. A. R. Caldwell, A. Cole, C. Coutures, K. H. Cook, S. Dieters, D. Dominis Prester, J. Donatowicz, P. Fouqué, K. Hill, N. Kains, S. Kane, J.-B. Marquette, R. Martin, K. R. Pollard, K. C. Sahu, C. Vinter, D. Warren, B. Watson, M. Zub, T. Sumi, M. K. Szymański, M. Kubiak, R. Poleski, I. Soszynski, K. Ulaczyk, G. Pietrzyński, and Ł. Wyrzykowski. One or more bound planets per Milky Way star from microlensing observations. *Nature*, 481:167–169, January 2012.

[9] C. D. Dressing and D. Charbonneau. The Occurrence Rate of Small Planets around Small Stars. *The Astrophysical Journal*, 767:95, April 2013.

[10] J. T. Wright, G. W. Marcy, A. W. Howard, J. A. Johnson, T. D. Morton, and D. A. Fischer. The Frequency of Hot Jupiters Orbiting nearby Solar-type Stars. *ApJ*, 753:160, July 2012.

[11] M. Brogi, I. A. G. Snellen, R. J. de Kok, S. Albrecht, J. Birkby, and E. J. W. de Mooij. The signature of orbital motion from the dayside of the planet τ Boötis b. *Nature*, 486:502–504, June 2012.

[12] C. Majeau, E. Agol, and N. B. Cowan. A Two-dimensional Infrared Map of the Extrasolar Planet HD 189733b. *The Astrophysical Journal Letters*, 747:L20, March 2012.

[13] K. B. Stevenson, J.-M. Désert, M. R. Line, J. L. Bean, J. J. Fortney, A. P. Showman, T. Kataria, L. Kreidberg, P. R. McCullough, G. W. Henry, D. Charbonneau, A. Burrows, S. Seager, N. Madhusudhan, M. H. Williamson, and D. Homeier. Thermal structure of an exoplanet atmosphere from phase-resolved emission spectroscopy. *Science*, 346:838–841, November 2014.

[14] Guangwei Fu, Drake Deming, Heather Knutson, Nikku Madhusudhan, Avi Mandell, and Jonathan Fraine. Statistical Analysis of Hubble /WFC3 Transit Spectroscopy of Extrasolar Planets. *The Astrophysical Journal Letters*, 847(2):L22, 2017.

[15] A. Tsiaras, I. P. Waldmann, T. Zingales, M. Rocchetto, G. Morello, M. Damiano, K. Karpouzas, G. Tinetti, L. K. McKemmish, J. Tennyson, and S. N. Yurchenko. A Population Study of Gaseous Exoplanets. *AJ*, 155:156, April 2018.

[16] Zhanbo Zhang, Yifan Zhou, Benjamin V. Rackham, and Dániel Apai. The Near-infrared Transmission Spectra of TRAPPIST-1 Planets b, c, d, e, f, and

g and Stellar Contamination in Multi-epoch Transit Spectra. *AJ*, 156(4):178, Oct 2018.

[17] Jonathan Fraine, Drake Deming, Bjorn Benneke, Heather Knutson, Andrés Jordán, Néstor Espinoza, Nikku Madhusudhan, Ashlee Wilkins, and Kamen Todorov. Water vapour absorption in the clear atmosphere of a Neptune-sized exoplanet. *Nature*, 513(7519):526–529, Sep 2014.

[18] Angelos Tsiaras, Ingo P. Waldmann, Giovanna Tinetti, Jonathan Tennyson, and Sergey N. Yurchenko. Water vapour in the atmosphere of the habitable-zone eight-Earth-mass planet K2-18 b. *Nature Astronomy*, Sept 2019.

[19] M. Mayor, F. Pepe, D. Queloz, F. Bouchy, G. Rupprecht, G. Lo Curto, G. Avila, W. Benz, J. L. Bertaux, X. Bonfils, Th. Dall, H. Dekker, B. Delabre, W. Eckert, M. Fleury, A. Gilliotte, D. Gojak, J. C. Guzman, D. Kohler, J. L. Lizon, A. Longinotti, C. Lovis, D. Megevand, L. Pasquini, J. Reyes, J. P. Sivan, D. Sosnowska, R. Soto, S. Udry, A. van Kesteren, L. Weber, and U. Weilenmann. Setting New Standards with HARPS. *The Messenger*, 114:20–24, Dec 2003.

[20] R. Follert, R. J. Dorn, E. Oliva, J. L. Lizon, A. Hatzes, N. Piskunov, A. Reiners, U. Seemann, E. Stempels, U. Heiter, T. Marquart, M. Lockhart, G. Anglada-Escude, T. Löwinger, D. Baade, J. Grunhut, P. Bristow, B. Klein, Y. Jung, D. J. Ives, F. Kerber, E. Pozna, J. Paufique, H. U. Kaeufl, L. Origlia, E. Valenti, D. Gojak, M. Hilker, L. Pasquini, A. Smette, and J. Smoker. *CRIRES+: a cross-dispersed high-resolution infrared spectrograph for the ESO VLT*, volume 9147 of *Society of Photo-Optical Instrumentation Engineers (SPIE) Conference Series*, page 914719. SPIE, 2014.

[21] H. Jens Hoeijmakers, David Ehrenreich, Kevin Heng, Daniel Kitzmann, Simon L. Grimm, Romain Allart, Russell Deitrick, Aurélien Wyttenbach, Maria Oreshenko, Lorenzo Pino, Paul B. Rimmer, Emilio Molinari, and Luca

Di Fabrizio. Atomic iron and titanium in the atmosphere of the exoplanet KELT-9b. *Nature*, 560(7719):453–455, Aug 2018.

[22] Ignas A. G. Snellen, Remco J. de Kok, Ernst J. W. de Mooij, and Simon Albrecht. The orbital motion, absolute mass and high-altitude winds of exoplanet HD209458b. *Nature*, 465(7301):1049–1051, Jun 2010.

[23] Brendan P. Bowler. Imaging Extrasolar Giant Planets. *Publications of the Astronomical Society of the Pacific*, 128(968):102001, Oct 2016.

[24] A. M. Lagrange, M. Bonnefoy, G. Chauvin, D. Apai, D. Ehrenreich, A. Boccaletti, D. Gratadour, D. Rouan, D. Mouillet, S. Lacour, and M. Kasper. A Giant Planet Imaged in the Disk of the Young Star β Pictoris. *Science*, 329(5987):57, Jul 2010.

[25] Paul Kalas, James R. Graham, Eugene Chiang, Michael P. Fitzgerald, Mark Clampin, Edwin S. Kite, Karl Stapelfeldt, Christian Marois, and John Krist. Optical Images of an Exosolar Planet 25 Light-Years from Earth. *Science*, 322(5906):1345, Nov 2008.

[26] M. Perryman, J. Hartman, G. Á. Bakos, and L. Lindegren. Astrometric Exoplanet Detection with Gaia. *ApJ*, 797:14, December 2014.

[27] C. P. Sonett. A Summary Review of the Scientific Findings of the Mariner Venus Mission. *Space Science Reviews*, 2:751–777, December 1963.

[28] M. G. G. T. Taylor, N. Altobelli, B. J. Buratti, and M. Choukroun. The Rosetta mission orbiter science overview: the comet phase. *Philosophical Transactions of the Royal Society of London Series A*, 375:20160262, May 2017.

[29] F. Capaccioni, A. Coradini, G. Filacchione, S. Erard, G. Arnold, P. Drossart, M. C. De Sanctis, D. Bockelee-Morvan, M. T. Capria, F. Tosi, C. Leyrat, B. Schmitt, E. Quirico, P. Cerroni, V. Mennella, A. Raponi, M. Ciarniello, T. McCord, L. Moroz, E. Palomba, E. Ammannito, M. A. Barucci,

G. Bellucci, J. Benkhoff, J. P. Bibring, A. Blanco, M. Blecka, R. Carlson, U. Carsenty, L. Colangeli, M. Combes, M. Combi, J. Crovisier, T. Encrenaz, C. Federico, U. Fink, S. Fonti, W. H. Ip, P. Irwin, R. Jaumann, E. Kuehrt, Y. Langevin, G. Magni, S. Mottola, V. Orofino, P. Palumbo, G. Piccioni, U. Schade, F. Taylor, D. Tiphene, G. P. Tozzi, P. Beck, N. Biver, L. Bonal, J. Ph. Combe, D. Despan, E. Flamini, S. Fornasier, A. Frigeri, D. Grassi, M. Gudipati, A. Longobardo, K. Markus, F. Merlin, R. Orosei, G. Rinaldi, K. Stephan, M. Cartacci, A. Cicchetti, S. Giuppi, Y. Hello, F. Henry, S. Jacquinod, R. Noschese, G. Peter, R. Politi, J. M. Reess, and A. Semery. The organic-rich surface of comet 67P/Churyumov-Gerasimenko as seen by VIRTIS/Rosetta. *Science*, 347(6220):aaa0628, Jan 2015.

[30] Kathrin Altwegg, Hans Balsiger, and Stephen A. Fuselier. Cometary Chemistry and the Origin of Icy Solar System Bodies, the view after Rosetta. *arXiv e-prints*, page arXiv:1908.04046, Aug 2019.

[31] D. S. Lauretta, S. S. Balram-Knutson, E. Beshore, W. V. Boynton, C. Drouet d'Aubigny, D. N. DellaGiustina, H. L. Enos, D. R. Golish, C. W. Hergenrother, E. S. Howell, C. A. Bennett, E. T. Morton, M. C. Nolan, B. Rizk, H. L. Roper, A. E. Bartels, B. J. Bos, J. P. Dworkin, D. E. Highsmith, D. A. Lorenz, L. F. Lim, R. Mink, M. C. Moreau, J. A. Nuth, D. C. Reuter, A. A. Simon, E. B. Bierhaus, B. H. Bryan, R. Ballouz, O. S. Barnouin, R. P. Binzel, W. F. Bottke, V. E. Hamilton, K. J. Walsh, S. R. Chesley, P. R. Christensen, B. E. Clark, H. C. Connolly, M. K. Crombie, M. G. Daly, J. P. Emery, T. J. McCoy, J. W. McMahon, D. J. Scheeres, S. Messenger, K. Nakamura-Messenger, K. Righter, and S. A. Sand ford. OSIRIS-REx: Sample Return from Asteroid (101955) Bennu. *Space Science Reviews*, 212(1-2):925–984, Oct 2017.

[32] Jr. Spitzer, L. The First Known Report Concerning the Astronomical Importance of an Extraterrestrial Telescope. *Astronomy Quarterly*, 7:129–142, Jan 1990.

[33] Hiroshi Murakami, Hajime Baba, Peter Barthel, David L. Clements, Mar-

tin Cohen, Yasuo Doi, Keigo Enya, Elysandra Figueredo, Naofumi Fujishiro, Hideaki Fujiwara, Mikio Fujiwara, Pedro Garcia-Lario, Tomotsugu Goto, Sunao Hasegawa, Yasunori Hibi, Takanori Hirao, Norihisa Hiromoto, Seung Soo Hong, Koji Imai, Miho Ishigaki, Masateru Ishiguro, Daisuke Ishihara, Yoshifusa Ita, Woong-Seob Jeong, Kyung Sook Jeong, Hidehiro Kaneda, Hirokazu Kataza, Mitsunobu Kawada, Toshihide Kawai, Akiko Kawamura, Martin F. Kessler, Do Kester, Tsuneo Kii, Dong Chan Kim, Woojung Kim, Hisato Kobayashi, Bon Chul Koo, Suk Minn Kwon, Hyung Mok Lee, Rosario Lorente, Sin'itirou Makiuti, Hideo Matsuhara, Toshio Matsumoto, Hiroshi Matsuo, Shuji Matsuura, Thomas G. MÜller, Noriko Murakami, Hirohisa Nagata, Takao Nakagawa, Takahiro Naoi, Masanao Narita, Manabu Noda, Sang Hoon Oh, Akira Ohnishi, Youichi Ohyama, Yoko Okada, Haruyuki Okuda, Sebastian Oliver, Takashi Onaka, Takafumi Ootsubo, Shinki Oyabu, Soojong Pak, Yong-Sun Park, Chris P. Pearson, Michael Rowan-Robinson, Toshinobu Saito, Itsuki Sakon, Alberto Salama, Shinji Sato, Richard S. Savage, Stephen Serjeant, Hiroshi Shibai, Mai Shirahata, Jungjoo Sohn, Toyoaki Suzuki, Toshinobu Takagi, Hidenori Takahashi, Toshihiko TanabÉ, Tsutomu T. Takeuchi, Satoshi Takita, Matthew Thomson, Kazunori Uemizu, Munetaka Ueno, Fumihiko Usui, Eva Verdugo, Takehiko Wada, Lingyu Wang, Toyoki Watabe, Hidenori Watarai, Glenn J. White, Issei Yamamura, Chisato Yamauchi, and Akiko Yasuda. The Infrared Astronomical Mission AKARI*. *Publications of the Astronomical Society of Japan*, 59:S369–S376, Oct 2007.

[34] T. Onaka, H. Matsuhara, T. Wada, N. Fujishiro, H. Fujiwara, M. Ishigaki, D. Ishihara, Y. Ita, H. Kataza, W. Kim, T. Matsumoto, H. Murakami, Y. Ohyama, S. Oyabu, I. Sakon, T. Tanabé, T. Takagi, K. Uemizu, M. Ueno, F. Usui, H. Watarai, M. Cohen, K. Enya, T. Ootsubo, C. P. Pearson, N. Takeyama, T. Yamamuro, and Y. Ikeda. The Infrared Camera (IRC) for AKARI – Design and Imaging Performance. *Publications of the Astronomical Society of Japan*, 59:S401, Oct 2007.

[35] Fumihiko Usui, Sunao Hasegawa, Takafumi Ootsubo, and Takashi Onaka. AKARI/IRC near-infrared asteroid spectroscopic survey: AcuA-spec. *Publications of the Astronomical Society of Japan*, 71(1):1, Jan 2019.

[36] E. L. Wright, P. R. M. Eisenhardt, A. K. Mainzer, M. E. Ressler, R. M. Cutri, T. Jarrett, J. D. Kirkpatrick, D. Padgett, R. S. McMillan, M. Skrutskie, S. A. Stanford, M. Cohen, R. G. Walker, J. C. Mather, D. Leisawitz, T. N. Gautier, III, I. McLean, D. Benford, C. J. Lonsdale, A. Blain, B. Mendez, W. R. Irace, V. Duval, F. Liu, D. Royer, I. Heinrichsen, J. Howard, M. Shannon, M. Kendall, A. L. Walsh, M. Larsen, J. G. Cardon, S. Schick, M. Schwalm, M. Abid, B. Fabinsky, L. Naes, and C.-W. Tsai. The Wide-field Infrared Survey Explorer (WISE): Mission Description and Initial On-orbit Performance. *AJ*, 140:1868–1881, December 2010.

[37] A. Mainzer, J. Bauer, T. Grav, J. Masiero, R. M. Cutri, J. Dailey, P. Eisenhardt, R. S. McMillan, E. Wright, R. Walker, R. Jedicke, T. Spahr, D. Tholen, R. Alles, R. Beck, H. Brandenburg, T. Conrow, T. Evans, J. Fowler, T. Jarrett, K. Marsh, F. Masci, H. McCallon, S. Wheelock, M. Wittman, P. Wyatt, E. DeBaun, G. Elliott, D. Elsbury, T. Gautier, IV, S. Gomillion, D. Leisawitz, C. Maleszewski, M. Micheli, and A. Wilkins. Preliminary Results from NEOWISE: An Enhancement to the Wide-field Infrared Survey Explorer for Solar System Science. *ApJ*, 731:53, April 2011.

[38] A. Mainzer, J. Bauer, R. M. Cutri, T. Grav, J. Masiero, R. Beck, P. Clarkson, T. Conrow, J. Dailey, P. Eisenhardt, B. Fabinsky, S. Fajardo-Acosta, J. Fowler, C. Gelino, C. Grillmair, I. Heinrichsen, M. Kendall, J. D. Kirkpatrick, F. Liu, F. Masci, H. McCallon, C. R. Nugent, M. Papin, E. Rice, D. Royer, T. Ryan, P. Sevilla, S. Sonnett, R. Stevenson, D. B. Thompson, S. Wheelock, D. Wiemer, M. Wittman, E. Wright, and L. Yan. Initial Performance of the NEOWISE Reactivation Mission. *ApJ*, 792:30, September 2014.

[39] C. R. Nugent, A. Mainzer, J. Masiero, J. Bauer, R. M. Cutri, T. Grav,

E. Kramer, S. Sonnett, R. Stevenson, and E. L. Wright. NEOWISE Reactivation Mission Year One: Preliminary Asteroid Diameters and Albedos. *ApJ*, 814:117, Dec 2015.

[40] C. R. Nugent, A. Mainzer, J. Bauer, R. M. Cutri, E. A. Kramer, T. Grav, J. Masiero, S. Sonnett, and E. L. Wright. NEOWISE Reactivation Mission Year Two: Asteroid Diameters and Albedos. *AJ*, 152:63, Sep 2016.

[41] Joseph R. Masiero, C. Nugent, A. K. Mainzer, E. L. Wright, J. M. Bauer, R. M. Cutri, T. Grav, E. Kramer, and S. Sonnett. NEOWISE Reactivation Mission Year Three: Asteroid Diameters and Albedos. *AJ*, 154:168, Oct 2017.

[42] W. B. Sparks, K. P. Hand, M. A. McGrath, E. Bergeron, M. Cracraft, and S. E. Deustua. Probing for Evidence of Plumes on Europa with HST/STIS. *ApJ*, 829(2):121, Oct 2016.

[43] A. Vidal-Madjar, A. Lecavelier des Etangs, J.-M. Désert, G. E. Ballester, R. Ferlet, G. Hébrard, and M. Mayor. An extended upper atmosphere around the extrasolar planet HD209458b. *Nature*, 422:143–146, March 2003.

[44] D. Ehrenreich, V. Bourrier, X. Bonfils, A. Lecavelier des Etangs, G. Hébrard, D. K. Sing, P. J. Wheatley, A. Vidal-Madjar, X. Delfosse, S. Udry, T. Forveille, and C. Moutou. Hint of a transiting extended atmosphere on 55 Cancri b. *A&A*, 547:A18, Nov 2012.

[45] D. K. Sing, F. Pont, S. Aigrain, D. Charbonneau, J. M. Désert, N. Gibson, R. Gilliland, W. Hayek, G. Henry, H. Knutson, A. Lecavelier Des Etangs, T. Mazeh, and A. Shporer. Hubble Space Telescope transmission spectroscopy of the exoplanet HD 189733b: high-altitude atmospheric haze in the optical and near-ultraviolet with STIS. *MNRAS*, 416(2):1443–1455, Sep 2011.

[46] V. Bourrier, A. Lecavelier des Etangs, H. Dupuy, D. Ehrenreich, A. Vidal-Madjar, G. Hébrard, G. E. Ballester, J. M. Désert, R. Ferlet, D. K. Sing,

and P. J. Wheatley. Atmospheric escape from HD 189733b observed in H I Lyman-α: detailed analysis of HST/STIS September 2011 observations. *A&A*, 551:A63, Mar 2013.

[47] D. Jewitt, J. Agarwal, H. Weaver, M. Mutchler, and S. Larson. The Extraordinary Multi-tailed Main-belt Comet P/2013 P5. *The Astrophysical Journal Letters*, 778:L21, November 2013.

[48] Paul D. Feldman, Harold A. Weaver, Michael F. A'Hearn, Michael R. Combi, and Neil Dello Russo. Far-ultraviolet Spectroscopy of Recent Comets with the Cosmic Origins Spectrograph on the Hubble Space Telescope. *AJ*, 155(5):193, May 2018.

[49] Jessica Agarwal, David Jewitt, Max Mutchler, Harold Weaver, and Stephen Larson. A binary main-belt comet. *Nature*, 549(7672):357–359, Sep 2017.

[50] David Jewitt, Harold Weaver, Max Mutchler, Stephen Larson, and Jessica Agarwal. Hubble Space Telescope Observations of Main-Belt Comet 596 Scheila. *The Astrophysical Journal*, 733(1):L4, apr 2011.

[51] Zachory K. Berta, David Charbonneau, Jean-Michel Désert, Eliza Miller-Ricci Kempton, Peter R. McCullough, Christopher J. Burke, Jonathan J. Fortney, Jonathan Irwin, Philip Nutzman, and Derek Homeier. The Flat Transmission Spectrum of the Super-Earth GJ1214b from Wide Field Camera 3 on the Hubble Space Telescope. *ApJ*, 747(1):35, Mar 2012.

[52] C. M. Huitson, D. K. Sing, F. Pont, J. J. Fortney, A. S. Burrows, P. A. Wilson, G. E. Ballester, N. Nikolov, N. P. Gibson, D. Deming, S. Aigrain, T. M. Evans, G. W. Henry, A. Lecavelier des Etangs, A. P. Showman, A. Vidal-Madjar, and K. Zahnle. An HST optical-to-near-IR transmission spectrum of the hot Jupiter WASP-19b: detection of atmospheric water and likely absence of TiO. *MNRAS*, 434(4):3252–3274, Oct 2013.

[53] Thomas G. Beatty, Nikku Madhusudhan, Angelos Tsiaras, Ming Zhao, Ronald L. Gilliland, Heather A. Knutson, Avi Shporer, and Jason T. Wright.

Evidence for Atmospheric Cold-trap Processes in the Noninverted Emission Spectrum of Kepler-13Ab Using HST/WFC3. *AJ*, 154(4):158, Oct 2017.

[54] Nicolas Crouzet, Peter R. McCullough, Drake Deming, and Nikku Madhusudhan. Water Vapor in the Spectrum of the Extrasolar Planet HD 189733b. II. The Eclipse. *ApJ*, 795(2):166, Nov 2014.

[55] J. R. Houck, T. L. Roellig, J. van Cleve, W. J. Forrest, T. Herter, C. R. Lawrence, K. Matthews, H. J. Reitsema, B. T. Soifer, D. M. Watson, D. Weedman, M. Huisjen, J. Troeltzsch, D. J. Barry, J. Bernard-Salas, C. E. Blacken, B. R. Brandl, V. Charmandaris, D. Devost, G. E. Gull, P. Hall, C. P. Henderson, S. J. U. Higdon, B. E. Pirger, J. Schoenwald, G. C. Sloan, K. I. Uchida, P. N. Appleton, L. Armus, M. J. Burgdorf, S. B. Fajardo-Acosta, C. J. Grillmair, J. G. Ingalls, P. W. Morris, and H. I. Teplitz. The Infrared Spectrograph (IRS) on the Spitzer Space Telescope. *The Astrophysical Journal Supplement*, 154:18–24, September 2004.

[56] M. A. Barucci, S. Fornasier, E. Dotto, P. L. Lamy, L. Jorda, O. Groussin, J. R. Brucato, J. Carvano, A. Alvarez-Candal, D. Cruikshank, and M. Fulchignoni. Asteroids 2867 Steins and 21 Lutetia: surface composition from far infrared observations with the Spitzer space telescope. *A&A*, 477:665–670, January 2008.

[57] J. P. Emery, D. P. Cruikshank, J. van Cleve, and J. A. Stansberry. Mineralogy of Asteroids from Observations with the Spitzer Space Telescope. In S. Mackwell and E. Stansbery, editors, *36th Annual Lunar and Planetary Science Conference*, volume 36 of *Lunar and Planetary Inst. Technical Report*, March 2005.

[58] D. E. Trilling, B. Bhattacharya, M. Blaylock, J. A. Stansberry, M. V. Sykes, and L. H. Wasserman. The Spitzer Asteroid Catalog: Albedos And Diameters of 35,000 Asteroids. In *AAS/Division for Planetary Sciences Meeting*

Abstracts #39, volume 39 of *Bulletin of the American Astronomical Society*, page 484, October 2007.

[59] C. A. Thomas, J. P. Emery, D. E. Trilling, M. Delbó, J. L. Hora, and M. Mueller. Physical characterization of Warm Spitzer-observed near-Earth objects. *Icarus*, 228:217–246, January 2014.

[60] D. E. Trilling, M. Mueller, J. L. Hora, A. W. Harris, B. Bhattacharya, W. F. Bottke, S. Chesley, M. Delbo, J. P. Emery, G. Fazio, A. Mainzer, B. Penprase, H. A. Smith, T. B. Spahr, J. A. Stansberry, and C. A. Thomas. ExploreNEOs I: Description and first results from the Warm Spitzer NEO Survey. *ArXiv e-prints*, July 2010.

[61] William T. Reach, Michael S. Kelley, and Jeremie Vaubaillon. Survey of cometary CO_2, CO, and particulate emissions using the Spitzer Space Telescope. *Icarus*, 226(1):777–797, Sep 2013.

[62] Giovanna Tinetti, Alfred Vidal-Madjar, Mao-Chang Liang, Jean-Philippe Beaulieu, Yuk Yung, Sean Carey, Robert J. Barber, Jonathan Tennyson, Ignasi Ribas, Nicole Allard, Gilda E. Ballester, David K. Sing, and Franck Selsis. Water vapour in the atmosphere of a transiting extrasolar planet. *Nature*, 448(7150):169–171, Jul 2007.

[63] David Charbonneau, Lori E. Allen, S. Thomas Megeath, Guillermo Torres, Roi Alonso, Timothy M. Brown, Ronald L. Gilliland, David W. Latham, Georgi Mandushev, Francis T. O'Donovan, and Alessandro Sozzetti. Detection of Thermal Emission from an Extrasolar Planet. *ApJ*, 626(1):523–529, Jun 2005.

[64] B.-O. Demory, M. Gillon, J. de Wit, N. Madhusudhan, E. Bolmont, K. Heng, T. Kataria, N. Lewis, R. Hu, J. Krick, V. Stamenković, B. Benneke, S. Kane, and D. Queloz. A map of the large day-night temperature gradient of a super-Earth exoplanet. *Nature*, 532:207–209, April 2016.

[65] Laura Kreidberg, Daniel D. B. Koll, Caroline Morley, Renyu Hu, Laura Schaefer, Drake Deming, Kevin B. Stevenson, Jason Dittmann, Andrew Vanderburg, David Berardo, Xueying Guo, Keivan Stassun, Ian Crossfield, David Charbonneau, David W. Latham, Abraham Loeb, George Ricker, Sara Seager, and Roland Vand erspek. Absence of a thick atmosphere on the terrestrial exoplanet LHS 3844b. *Nature*, 573(7772):87–90, Aug 2019.

[66] Arazi Pinhas, Nikku Madhusudhan, Siddharth Gandhi, and Ryan MacDonald. H_2O abundances and cloud properties in ten hot giant exoplanets. *MNRAS*, 482(2):1485–1498, Jan 2019.

[67] M. Gillon, A. H. M. J. Triaud, B.-O. Demory, E. Jehin, E. Agol, K. M. Deck, S. M. Lederer, J. de Wit, A. Burdanov, J. G. Ingalls, E. Bolmont, J. Leconte, S. N. Raymond, F. Selsis, M. Turbet, K. Barkaoui, A. Burgasser, M. R. Burleigh, S. J. Carey, A. Chaushev, C. M. Copperwheat, L. Delrez, C. S. Fernandes, D. L. Holdsworth, E. J. Kotze, V. Van Grootel, Y. Almleaky, Z. Benkhaldoun, P. Magain, and D. Queloz. Seven temperate terrestrial planets around the nearby ultracool dwarf star TRAPPIST-1. *Nature*, 542:456–460, February 2017.

[68] L. Delrez, M. Gillon, A. H. M. J. Triaud, B.-O. Demory, J. de Wit, J. G. Ingalls, E. Agol, E. Bolmont, A. Burdanov, A. J. Burgasser, S. J. Carey, E. Jehin, J. Leconte, S. Lederer, D. Queloz, F. Selsis, and V. Van Grootel. Early 2017 observations of TRAPPIST-1 with Spitzer. *MNRAS*, 475:3577–3597, April 2018.

[69] Simon L. Grimm, Brice-Olivier Demory, Michaël Gillon, Caroline Dorn, Eric Agol, Artem Burdanov, Laetitia Delrez, Marko Sestovic, Amaury H. M. J. Triaud, Martin Turbet, Émeline Bolmont, Anthony Caldas, Julien de Wit, Emmanuël Jehin, Jérémy Leconte, Sean N. Raymond, Valérie Van Grootel, Adam J. Burgasser, Sean Carey, Daniel Fabrycky, Kevin Heng, David M. Hernandez, James G. Ingalls, Susan Lederer, Franck Selsis, and

Didier Queloz. The nature of the TRAPPIST-1 exoplanets. *A&A*, 613:A68, May 2018.

[70] Björn Benneke, Michael Werner, Erik Petigura, Heather Knutson, Courtney Dressing, Ian J. M. Crossfield, Joshua E. Schlieder, John Livingston, Charles Beichman, Jessie Christiansen, Jessica Krick, Varoujan Gorjian, Andrew W. Howard, Evan Sinukoff, David R. Ciardi, and Rachel L. Akeson. Spitzer Observations Confirm and Rescue the Habitable-zone Super-Earth K2-18b for Future Characterization. *ApJ*, 834(2):187, Jan 2017.

[71] John H. Livingston, Ian J. M. Crossfield, Michael W. Werner, Varoujan Gorjian, Erik A. Petigura, David R. Ciardi, Courtney D. Dressing, Benjamin J. Fulton, Teruyuki Hirano, and Joshua E. Schlieder. Spitzer Transit Follow-up of Planet Candidates from the K2 Mission. *AJ*, 157(3):102, Mar 2019.

[72] Molly R. Kosiarek, Ian J. M. Crossfield, Kevin K. Hardegree-Ullman, John H. Livingston, Björn Benneke, Gregory W. Henry, Ward S. Howard, David Berardo, Sarah Blunt, and Benjamin J. Fulton. Bright Opportunities for Atmospheric Characterization of Small Planets: Masses and Radii of K2-3 b, c, and d and GJ3470 b from Radial Velocity Measurements and Spitzer Transits. *AJ*, 157(3):97, Mar 2019.

[73] P. Bordé, D. Rouan, and A. Léger. Exoplanet detection capability of the COROT space mission. *A&A*, 405:1137–1144, July 2003.

[74] R. Alonso, A. Alapini, S. Aigrain, M. Auvergne, A. Baglin, M. Barbieri, P. Barge, A. S. Bonomo, P. Bordé, F. Bouchy, S. Chaintreuil, R. de La Reza, H. J. Deeg, M. Deleuil, R. Dvorak, A. Erikson, M. Fridlund, F. de Oliveira Fialho, P. Gondoin, T. Guillot, A. Hatzes, L. Jorda, H. Lammer, A. Léger, A. Llebaria, P. Magain, T. Mazeh, C. Moutou, M. Ollivier, M. Pätzold, F. Pont, D. Queloz, H. Rauer, D. Rouan, J. Schneider, and G. Wuchterl. The secondary eclipse of CoRoT-1b. *Astronomy and Astrophysics*, 506(1):353–358, Oct 2009.

[75] A. Léger, D. Rouan, J. Schneider, P. Barge, M. Fridlund, B. Samuel, M. Ollivier, E. Guenther, M. Deleuil, H. J. Deeg, M. Auvergne, R. Alonso, S. Aigrain, A. Alapini, J. M. Almenara, A. Baglin, M. Barbieri, H. Bruntt, P. Bordé, F. Bouchy, J. Cabrera, C. Catala, L. Carone, S. Carpano, Sz. Csizmadia, R. Dvorak, A. Erikson, S. Ferraz-Mello, B. Foing, F. Fressin, D. Gand olfi, M. Gillon, Ph. Gondoin, O. Grasset, T. Guillot, A. Hatzes, G. Hébrard, L. Jorda, H. Lammer, A. Llebaria, B. Loeillet, M. Mayor, T. Mazeh, C. Moutou, M. Pätzold, F. Pont, D. Queloz, H. Rauer, S. Renner, R. Samadi, A. Shporer, Ch. Sotin, B. Tingley, G. Wuchterl, M. Adda, P. Agogu, T. Appourchaux, H. Ballans, P. Baron, T. Beaufort, R. Bellenger, R. Berlin, P. Bernardi, D. Blouin, F. Baudin, P. Bodin, L. Boisnard, L. Boit, F. Bonneau, S. Borzeix, R. Briet, J. T. Buey, B. Butler, D. Cailleau, R. Cautain, P. Y. Chabaud, S. Chaintreuil, F. Chiavassa, V. Costes, V. Cuna Parrho, F. de Oliveira Fialho, M. Decaudin, J. M. Defise, S. Djalal, G. Epstein, G. E. Exil, C. Fauré, T. Fenouillet, A. Gaboriaud, A. Gallic, P. Gamet, P. Gavalda, E. Grolleau, R. Gruneisen, L. Gueguen, V. Guis, V. Guivarc'h, P. Guterman, D. Hallouard, J. Hasiba, F. Heuripeau, G. Huntzinger, H. Hustaix, C. Imad, C. Imbert, B. Johlander, M. Jouret, P. Journoud, F. Karioty, L. Kerjean, V. Lafaille, L. Lafond, T. Lam-Trong, P. Landiech, V. Lapeyrere, T. Larqué, P. Laudet, N. Lautier, H. Lecann, L. Lefevre, B. Leruyet, P. Levacher, A. Magnan, E. Mazy, F. Mertens, J. M. Mesnager, J. C. Meunier, J. P. Michel, W. Monjoin, D. Naudet, K. Nguyen-Kim, J. L. Orcesi, H. Ottacher, R. Perez, G. Peter, P. Plasson, J. Y. Plesseria, B. Pontet, A. Pradines, C. Quentin, J. L. Reynaud, G. Rolland , F. Rollenhagen, R. Romagnan, N. Russ, R. Schmidt, N. Schwartz, I. Sebbag, G. Sedes, H. Smit, M. B. Steller, W. Sunter, C. Surace, M. Tello, D. Tiphène, P. Toulouse, B. Ulmer, O. Vandermarcq, E. Vergnault, A. Vuillemin, and P. Zanatta. Transiting exoplanets from the CoRoT space mission. VIII. CoRoT-7b: the first super-Earth with measured radius. *Astronomy and Astrophysics*, 506(1):287–302, Oct 2009.

[76] William J. Borucki, David Koch, Gibor Basri, Natalie Batalha, Timothy Brown, Douglas Caldwell, John Caldwell, Jørgen Christensen-Dalsgaard, William D. Cochran, Edna DeVore, Edward W. Dunham, Andrea K. Dupree, Thomas N. Gautier, John C. Geary, Ronald Gilliland, Alan Gould, Steve B. Howell, Jon M. Jenkins, Yoji Kondo, David W. Latham, Geoffrey W. Marcy, Søren Meibom, Hans Kjeldsen, Jack J. Lissauer, David G. Monet, David Morrison, Dimitar Sasselov, Jill Tarter, Alan Boss, Don Brownlee, Toby Owen, Derek Buzasi, David Charbonneau, Laurance Doyle, Jonathan Fortney, Eric B. Ford, Matthew J. Holman, Sara Seager, Jason H. Steffen, William F. Welsh, Jason Rowe, Howard Anderson, Lars Buchhave, David Ciardi, Lucianne Walkowicz, William Sherry, Elliott Horch, Howard Isaacson, Mark E. Everett, Debra Fischer, Guillermo Torres, John Asher Johnson, Michael Endl, Phillip MacQueen, Stephen T. Bryson, Jessie Dotson, Michael Haas, Jeffrey Kolodziejczak, Jeffrey Van Cleve, Hema Chandrasekaran, Joseph D. Twicken, Elisa V. Quintana, Bruce D. Clarke, Christopher Allen, Jie Li, Haley Wu, Peter Tenenbaum, Ekaterina Verner, Frederick Bruhweiler, Jason Barnes, and Andrej Prsa. Kepler Planet-Detection Mission: Introduction and First Results. *Science*, 327(5968):977, Feb 2010.

[77] F. Fressin, G. Torres, D. Charbonneau, S. T. Bryson, J. Christiansen, C. D. Dressing, J. M. Jenkins, L. M. Walkowicz, and N. M. Batalha. The False Positive Rate of Kepler and the Occurrence of Planets. *ApJ*, 766:81, April 2013.

[78] J. L. Christiansen, B. D. Clarke, C. J. Burke, S. Seader, J. M. Jenkins, J. D. Twicken, J. D. Catanzarite, J. C. Smith, N. M. Batalha, M. R. Haas, S. E. Thompson, J. R. Campbell, A. Sabale, and A. Kamal Uddin. Measuring Transit Signal Recovery in the Kepler Pipeline II: Detection Efficiency as Calculated in One Year of Data. *ApJ*, 810:95, September 2015.

[79] III Gautier, Thomas N., David Charbonneau, Jason F. Rowe, Geoffrey W. Marcy, Howard Isaacson, Guillermo Torres, Francois Fressin,

Leslie A. Rogers, Jean-Michel Désert, Lars A. Buchhave, David W. Latham, Samuel N. Quinn, David R. Ciardi, Daniel C. Fabrycky, Eric B. Ford, Ronald L. Gilliland, Lucianne M. Walkowicz, Stephen T. Bryson, William D. Cochran, Michael Endl, Debra A. Fischer, Steve B. Howell, Elliott P. Horch, Thomas Barclay, Natalie Batalha, William J. Borucki, Jessie L. Christiansen, John C. Geary, Christopher E. Henze, Matthew J. Holman, Khadeejah Ibrahim, Jon M. Jenkins, Karen Kinemuchi, David G. Koch, Jack J. Lissauer, Dwight T. Sanderfer, Dimitar D. Sasselov, Sara Seager, Kathryn Silverio, Jeffrey C. Smith, Martin Still, Martin C. Stumpe, Peter Tenenbaum, and Jeffrey Van Cleve. Kepler-20: A Sun-like Star with Three Sub-Neptune Exoplanets and Two Earth-size Candidates. *ApJ*, 749(1):15, Apr 2012.

[80] S. B. Howell, C. Sobeck, M. Haas, M. Still, T. Barclay, F. Mullally, J. Troeltzsch, S. Aigrain, S. T. Bryson, D. Caldwell, W. J. Chaplin, W. D. Cochran, D. Huber, G. W. Marcy, A. Miglio, J. R. Najita, M. Smith, J. D. Twicken, and J. J. Fortney. The K2 Mission: Characterization and Early Results. *Publications of the Astronomical Society of the Pacific*, 126:398, April 2014.

[81] Jon K. Zink, Kevin K. Hardegree-Ullman, Jessie L. Christiansen, Ian J. M. Crossfield, Erik A. Petigura, Chris J. Lintott, John H. Livingston, David R. Ciardi, Geert Barentsen, Courtney D. Dressing, Alexander Ye, Joshua E. Schlieder, Kevin Acres, Peter Ansorge, Dario Arienti, Elisabeth Baeten, Victoriano Canales Cerdá, Itayi Chitsiga, Maxwell Daly, James Damboiu, Martin Ende, Adnan Erdag, Stiliyan Evstatiev, Joseph Henderson, David Hine, Tony Hoffman, Emmanuel Lambrou, Gabriel Murawski, Mark Nicholson, Mason Russell, Hans Martin Schwengeler, Alton Spencer, Aaron Tagliabue, Christopher Tanner, Melina Thévenot, Christine Unsworth, and Jouni Uusi-Simola. Catalog of New K2 Exoplanet Candidates from Citizen Scientists. *Research Notes of the American Astronomical Society*, 3(2):43, Feb 2019.

[82] B. J. Fulton and E. A. Petigura. The California Kepler Survey VII. Precise

Planet Radii Leveraging Gaia DR2 Reveal the Stellar Mass Dependence of the Planet Radius Gap. *ArXiv e-prints*, May 2018.

[83] J. E. Owen and Y. Wu. The Evaporation Valley in the Kepler Planets. *ApJ*, 847:29, September 2017.

[84] G. R. Ricker, J. N. Winn, R. Vanderspek, D. W. Latham, G. Á. Bakos, J. L. Bean, Z. K. Berta-Thompson, T. M. Brown, L. Buchhave, N. R. Butler, R. P. Butler, W. J. Chaplin, D. Charbonneau, J. Christensen-Dalsgaard, M. Clampin, D. Deming, J. Doty, N. De Lee, C. Dressing, E. W. Dunham, M. Endl, F. Fressin, J. Ge, T. Henning, M. J. Holman, A. W. Howard, S. Ida, J. Jenkins, G. Jernigan, J. A. Johnson, L. Kaltenegger, N. Kawai, H. Kjeldsen, G. Laughlin, A. M. Levine, D. Lin, J. J. Lissauer, P. MacQueen, G. Marcy, P. R. McCullough, T. D. Morton, N. Narita, M. Paegert, E. Palle, F. Pepe, J. Pepper, A. Quirrenbach, S. A. Rinehart, D. Sasselov, B. Sato, S. Seager, A. Sozzetti, K. G. Stassun, P. Sullivan, A. Szentgyorgyi, G. Torres, S. Udry, and J. Villasenor. Transiting Exoplanet Survey Satellite (TESS). In *Space Telescopes and Instrumentation 2014: Optical, Infrared, and Millimeter Wave*, volume 9143 of *Proceedings of the SPIE*, page 914320, August 2014.

[85] C. X. Huang, J. Burt, A. Vanderburg, M. N. Günther, A. Shporer, J. A. Dittmann, J. N. Winn, R. Wittenmyer, L. Sha, S. R. Kane, G. R. Ricker, R. K. Vanderspek, D. W. Latham, S. Seager, J. M. Jenkins, D. A. Caldwell, K. A. Collins, N. Guerrero, J. C. Smith, S. N. Quinn, S. Udry, F. Pepe, F. Bouchy, D. Ségransan, C. Lovis, D. Ehrenreich, M. Marmier, M. Mayor, B. Wohler, K. Haworth, E. H. Morgan, M. Fausnaugh, D. R. Ciardi, J. Christiansen, D. Charbonneau, D. Dragomir, D. Deming, A. Glidden, A. M. Levine, P. R. McCullough, L. Yu, N. Narita, T. Nguyen, T. Morton, J. Pepper, A. Pál, J. E. Rodriguez, K. G. Stassun, G. Torres, A. Sozzetti, J. P. Doty, J. Christensen-Dalsgaard, G. Laughlin, M. Clampin, J. L. Bean, L. A. Buchhave, G. Á. Bakos, B. Sato, S. Ida, L. Kaltenegger, E. Palle, D. Sasselov, R. P. Butler,

J. Lissauer, J. Ge, and S. A. Rinehart. TESS Discovery of a Transiting Super-Earth in the pi Mensae System. *The Astrophysical Journal Letters*, 868:L39, December 2018.

[86] Roland Vanderspek, Chelsea X. Huang, Andrew Vanderburg, George R. Ricker, David W. Latham, Sara Seager, Joshua N. Winn, Jon M. Jenkins, Jennifer Burt, Jason Dittmann, Elisabeth Newton, Samuel N. Quinn, Avi Shporer, David Charbonneau, Jonathan Irwin, Kristo Ment, Jennifer G. Winters, Karen A. Collins, Phil Evans, Tianjun Gan, Rhodes Hart, Eric L. N. Jensen, John Kielkopf, Shude Mao, William Waalkes, François Bouchy, Maxime Marmier, Louise D. Nielsen, Gaël Ottoni, Francesco Pepe, Damien Ségransan, Stéphane Udry, Todd Henry, Leonardo A. Paredes, Hodari-Sadiki James, Rodrigo H. Hinojosa, Michele L. Silverstein, Enric Palle, Zachory Berta-Thompson, Ian Crossfield, Misty D. Davies, Diana Dragomir, Michael Fausnaugh, Ana Glidden, Joshua Pepper, Edward H. Morgan, Mark Rose, Joseph D. Twicken, Jesus Noel S. Villaseñor, Liang Yu, Gaspar Bakos, Jacob Bean, Lars A. Buchhave, Jørgen Christensen-Dalsgaard, Jessie L. Christiansen, David R. Ciardi, Mark Clampin, Nathan De Lee, Drake Deming, John Doty, J. Garrett Jernigan, Lisa Kaltenegger, Jack J. Lissauer, P. R. McCullough, Norio Narita, Martin Paegert, Andras Pal, Stephen Rinehart, Dimitar Sasselov, Bun'ei Sato, Alessandro Sozzetti, Keivan G. Stassun, and Guillermo Torres. TESS Discovery of an Ultra-short-period Planet around the Nearby M Dwarf LHS 3844. *The Astrophysical Journal Letters*, 871(2):L24, Feb 2019.

[87] N. E. Bowles, C. Snodgrass, A Gibbings, J. P. Sanchez, J. A. Arnold, P. Eccleston, T. Andert, A. Probst, G. Naletto, A. C. Vandaele, J. de Leon, A. Nathues, I. R. Thomas, N. Thomas, L. Jorda, V. Da Deppo, H. Haack, S. F. Green, B. Carry, K. L. Donaldson Hanna, J. Leif Jorgensen, A. Kereszturi, F. E. DeMeo, M. R. Patel, J. K. Davies, F. Clarke, K. Kinch, A. Guilbert-Lepoutre, J. Agarwal, A. S. Rivkin, P. Pravec, S. Fornasier, M. Granvik, R. H. Jones, N. Murdoch, K. H. Joy, E. Pascale, M. Tecza, J. M. Barnes, J. Lican-

dro, B. T. Greenhagen, S. B. Calcutt, C. M. Marriner, T. Warren, and I. Tosh. CASTAway: An Asteroid Main Belt Tour and Survey. *ArXiv e-prints*, October 2017.

[88] H. H. Hsieh and D. Jewitt. A Population of Comets in the Main Asteroid Belt. *Science*, 312:561–563, April 2006.

[89] C. Snodgrass, J. Agarwal, M. Combi, A. Fitzsimmons, A. Guilbert-Lepoutre, H. H. Hsieh, M.-T. Hui, E. Jehin, M. S. P. Kelley, M. M. Knight, C. Opitom, R. Orosei, M. de Val-Borro, and B. Yang. The Main Belt Comets and ice in the Solar System. *The Astronomy and Astrophysics Review*, 25:5, November 2017.

[90] C. Snodgrass, G. H. Jones, H. Boehnhardt, A. Gibbings, M. Homeister, N. Andre, P. Beck, M. S. Bentley, I. Bertini, N. Bowles, M. T. Capria, C. Carr, M. Ceriotti, A. J. Coates, V. Della Corte, K. L. Donaldson Hanna, A. Fitzsimmons, P. J. Gutiérrez, O. R. Hainaut, A. Herique, M. Hilchenbach, H. H. Hsieh, E. Jehin, O. Karatekin, W. Kofman, L. M. Lara, K. Laudan, J. Licandro, S. C. Lowry, F. Marzari, A. Masters, K. J. Meech, F. Moreno, A. Morse, R. Orosei, A. Pack, D. Plettemeier, D. Prialnik, A. Rotundi, M. Rubin, J. P. Sánchez, S. Sheridan, M. Trieloff, and A. Winterboer. The Castalia mission to Main Belt Comet 133P/Elst-Pizarro. *Advances in Space Research*, 62:1947–1976, October 2018.

[91] G. H. Jones, C. Snodgrass, and R. T. Wicks. A Proposed ESA Mission to a Dynamically New Comet. *AGU Fall Meeting Abstracts*, December 2018.

[92] A. K. Mainzer and NEOCam Science Team. The Near-Earth Object Camera. In *AAS/Division for Planetary Sciences Meeting Abstracts #49*, volume 49 of *AAS/Division for Planetary Sciences Meeting Abstracts*, page 219.01, October 2017.

[93] B. Carry. Solar system science with ESA Euclid. *A&A*, 609:A113, January 2018.

[94] Olivier Doré, Michael W. Werner, Matthew L. N. Ashby, Lindsey E. Bleem, Jamie Bock, Jennifer Burt, Peter Capak, Tzu-Ching Chang, Jonás Chaves-Montero, Christine H. Chen, Francesca Civano, I. Ilsedore Cleeves, Asantha Cooray, Brendan Crill, Ian J. M. Crossfield, Michael Cushing, Sylvain de la Torre, Tiziana DiMatteo, Niv Dvory, Cora Dvorkin, Catherine Espaillat, Simone Ferraro, Douglas Finkbeiner, Jenny Greene, Jackie Hewitt, David W. Hogg, Kevin Huffenberger, Hyun-Sung Jun, Olivier Ilbert, Woong-Seob Jeong, Jennifer Johnson, Minjin Kim, J. Davy Kirkpatrick, Theresa Kowalski, Phil Korngut, Jianshu Li, Carey M. Lisse, Meredith MacGregor, Eric E. Mamajek, Phil Mauskopf, Gary Melnick, Brice Ménard, Mark Neyrinck, Karin Öberg, Alice Pisani, Jennifer Rocca, Mara Salvato, Emmanuel Schaan, Nick Z. Scoville, Yong-Seon Song, Daniel J. Stevens, Ananth Tenneti, Harry Teplitz, Volker Tolls, Stephen Unwin, Meg Urry, Benjamin Wandelt, Benjamin F. Williams, David Wilner, Rogier A. Windhorst, Scott Wolk, Harold W. Yorke, and Michael Zemcov. Science Impacts of the SPHEREx All-Sky Optical to Near-Infrared Spectral Survey II: Report of a Community Workshop on the Scientific Synergies Between the SPHEREx Survey and Other Astronomy Observatories. *arXiv e-prints*, page arXiv:1805.05489, May 2018.

[95] C. Broeg, A. Fortier, D. Ehrenreich, Y. Alibert, W. Baumjohann, W. Benz, M. Deleuil, M. Gillon, A. Ivanov, R. Liseau, M. Meyer, G. Oloffson, I. Pagano, G. Piotto, D. Pollacco, D. Queloz, R. Ragazzoni, E. Renotte, M. Steller, and N. Thomas. CHEOPS: A transit photometry mission for ESA's small mission programme. In *European Physical Journal Web of Conferences*, volume 47 of *European Physical Journal Web of Conferences*, page 03005, April 2013.

[96] G. Scandariato, D. Ehrenreich, I. Pagano, D. Queloz, Y. Alibert, R. Alonso, T. Bárczy, W. Baumjohann, W. Benz, X. Bonfils, A. Brandeker, L. Borsato, C. Broeg, J. Cabrera, S. Charnoz, A. C. Cameron, M. Davies, O. Demangeon, M. Deleuil, A. Erikson, A. Fortier, L. Fossati, M. Fridlund, D. Gandolfi,

M. Gillon, M. Güdel, K. Isaak, L. Kiss, J. Laskar, C. Lovis, M. R. Meyer, V. Nascimbeni, G. Oloffson, E. Pallé, G. Piotto, D. Pollacco, R. Ragazzoni, N. Rando, É. Renottes, I. Ribas, N. C. Santos, S. Sousa, T. Spohnl, M. Steller, G. Szabó, N. Thomas, S. Udry, N. Walton, D. Barrado y Novascués, A. Gutierrez Peña, A. Lecavelier des Etangs, and V. Van Grootel. CHEOPS (Characterising Exoplanets Satellite) Mission. In *Frontier Research in Astrophysics II*, page 89, May 2016.

[97] Peter J. Wheatley, Richard G. West, Michael R. Goad, James S. Jenkins, Don L. Pollacco, Didier Queloz, Heike Rauer, Stéphane Udry, Christopher A. Watson, and Bruno Chazelas. The Next Generation Transit Survey (NGTS). *MNRAS*, 475(4):4476–4493, Apr 2018.

[98] H. Rauer, C. Catala, C. Aerts, T. Appourchaux, W. Benz, A. Brandeker, J. Christensen-Dalsgaard, M. Deleuil, L. Gizon, M. J. Goupil, M. Güdel, E. Janot-Pacheco, M. Mas-Hesse, I. Pagano, G. Piotto, D. Pollacco, Ċ. Santos, A. Smith, J. C. Suárez, R. Szabó, S. Udry, V. Adibekyan, Y. Alibert, J. M. Almenara, P. Amaro-Seoane, M. Ammler-von Eiff, M. Asplund, E. Antonello, S. Barnes, F. Baudin, K. Belkacem, M. Bergemann, G. Bihain, A. C. Birch, X. Bonfils, I. Boisse, A. S. Bonomo, F. Borsa, I. M. Brand ão, E. Brocato, S. Brun, M. Burleigh, R. Burston, J. Cabrera, S. Cassisi, W. Chaplin, S. Charpinet, C. Chiappini, R. P. Church, Sz. Csizmadia, M. Cunha, M. Damasso, M. B. Davies, H. J. Deeg, R. F. Díaz, S. Dreizler, C. Dreyer, P. Eggenberger, D. Ehrenreich, P. Eigmüller, A. Erikson, R. Farmer, S. Feltzing, F. de Oliveira Fialho, P. Figueira, T. Forveille, M. Fridlund, R. A. García, P. Giommi, G. Giuffrida, M. Godolt, J. Gomes da Silva, T. Granzer, J. L. Grenfell, A. Grotsch-Noels, E. Günther, C. A. Haswell, A. P. Hatzes, G. Hébrard, S. Hekker, R. Helled, K. Heng, J. M. Jenkins, A. Johansen, M. L. Khodachenko, K. G. Kislyakova, W. Kley, U. Kolb, N. Krivova, F. Kupka, H. Lammer, A. F. Lanza, Y. Lebreton, D. Magrin, P. Marcos-Arenal, P. M. Marrese, J. P. Marques, J. Martins, S. Mathis, S. Mathur, S. Messina, A. Miglio, J. Montalban, M. Montalto, M. J. P. F. G. Monteiro,

H. Moradi, E. Moravveji, C. Mordasini, T. Morel, A. Mortier, V. Nascimbeni, R. P. Nelson, M. B. Nielsen, L. Noack, A. J. Norton, A. Ofir, M. Oshagh, R. M. Ouazzani, P. Pápics, V. C. Parro, P. Petit, B. Plez, E. Poretti, A. Quirrenbach, R. Ragazzoni, G. Raimondo, M. Rainer, D. R. Reese, R. Redmer, S. Reffert, B. Rojas-Ayala, I. W. Roxburgh, S. Salmon, A. Santerne, J. Schneider, J. Schou, S. Schuh, H. Schunker, A. Silva-Valio, R. Silvotti, I. Skillen, I. Snellen, F. Sohl, S. G. Sousa, A. Sozzetti, D. Stello, K. G. Strassmeier, M. Švanda, Gy. M. Szabó, A. Tkachenko, D. Valencia, V. Van Grootel, S. D. Vauclair, P. Ventura, F. W. Wagner, N. A. Walton, J. Weingrill, S. C. Werner, P. J. Wheatley, and K. Zwintz. The PLATO 2.0 mission. *Experimental Astronomy*, 38(1-2):249–330, Nov 2014.

[99] Demetrio Magrin, Roberto Ragazzoni, Heike Rauer, Isabella Pagano, Valerio Nascimbeni, Giampaolo Piotto, Valentina Viotto, Daniele Piazza, Timothy Bandy, Stefano Basso, Willy Benz, Maria Bergomi, Federico Biondi, Francesco Borsa, Anko Börner, Alexis Brandeker, Mathias Brändli, Giordano Bruno, Juan Cabrera, Flavia Calderone, Virginie Cessa, Simonetta Chinellato, Thierry De Roche, Marco Dima, Anders Erikson, Jacopo Farinato, Mauro Ghigo, Davide Greggio, Maximilian Klebor, Luca Marafatto, Matteo Munari, Valery Mogulsky, Martin Pertenais, Gisbert Peter, Elisa Portaluri, Martin Rieder, Steve Rockstein, Mario Schweitzer, Daniela Sicilia, Gabriele Umbriaco, Matthias Wieser, Ana M. Heras, Filippo Marliani, Simone Pirrotta, Mario Salatti, Elisabetta Tommasi, Riccardo Bardazzi, Enrico Battistelli, Mauro Brotini, Matteo Burresi, Emanuele Capuano, Massimo Marinai, Andrea Novi, and Claude Català. PLATO: the ESA mission for exo-planets discovery. In *Proceedings of SPIE*, volume 10698 of *Society of Photo-Optical Instrumentation Engineers (SPIE) Conference Series*, page 106984X, Jul 2018.

[100] D. Spergel, N. Gehrels, C. Baltay, D. Bennett, J. Breckinridge, M. Donahue, A. Dressler, B. S. Gaudi, T. Greene, O. Guyon, C. Hirata, J. Kalirai, N. J. Kasdin, B. Macintosh, W. Moos, S. Perlmutter, M. Postman, B. Rauscher,

J. Rhodes, Y. Wang, D. Weinberg, D. Benford, M. Hudson, W. S. Jeong, Y. Mellier, W. Traub, T. Yamada, P. Capak, J. Colbert, D. Masters, M. Penny, D. Savransky, D. Stern, N. Zimmerman, R. Barry, L. Bartusek, K. Carpenter, E. Cheng, D. Content, F. Dekens, R. Demers, K. Grady, C. Jackson, G. Kuan, J. Kruk, M. Melton, B. Nemati, B. Parvin, I. Poberezhskiy, C. Peddie, J. Ruffa, J. K. Wallace, A. Whipple, E. Wollack, and F. Zhao. Wide-Field InfrarRed Survey Telescope-Astrophysics Focused Telescope Assets WFIRST-AFTA 2015 Report. *arXiv e-prints*, page arXiv:1503.03757, Mar 2015.

[101] B. Lacy, D. Shlivko, and A. Burrows. Characterization of Exoplanet Atmospheres with the Optical Coronagraph on WFIRST. *AJ*, 157(3):132, Mar 2019.

[102] Matthew T. Penny, B. Scott Gaudi, Eamonn Kerins, Nicholas J. Rattenbury, Shude Mao, Annie C. Robin, and Sebastiano Calchi Novati. Predictions of the WFIRST Microlensing Survey. I. Bound Planet Detection Rates. *The Astrophysical Journal Supplement*, 241(1):3, Mar 2019.

[103] David P. Bennett, Rachel Akeson, Jay Anderson, Lee Armus, Etienne Bachelet, Vanessa Bailey, Thomas Barclay, Richard Barry, Jean-Phillipe Beaulieu, Andrea Belini, Dominic J. Benford, Aparna Bhattacharya, Padi Boyd, Valerio Bozza, Sebastiano Calchi Novati, Kenneth Carpenter, Arnaud Cassan, David Ciardi, Andrew Cole, Knicole Colon, Christian Coutures, Martin Dominik, Pascal Fouque, Kevin Grady, Tyler Groff, Calen B. Henderson, Keith Horne, Christopher Gelino, Dawn Gelino, Jason Kalirai, Stephen Kane, N. Jeremy Kasdin, Jeffrey Kruk, Seppo Laine, Michiel Lambrechts, Luigi Mancini, Avi Mand ell, Sangeeta Malhotra, Shude Mao, Michael McElwain, Bertrand Mennesson, Tiffany Meshkat, Leonidas Moustakas, Jose A. Munoz, David Nataf, Roberta Paladini, Ilaria Pascucci, Matthew Penny, Radek Poleski, Elisa Quintana, Clement Ranc, Nicholas Rattenbury, James Rhodes, Jason D. Rhodes, Maxime Rizzo, Aki Roberge, Leslie

Rogers, Kailash C. Sahu, Joshua Schlieder, Sara Seager, Yossi Shvartzvald, Remi Soummer, David Spergel, Keivan G. Stassun, Rachel Street, Takahiro Sumi, Daisuke Suzuki, John Trauger, Roeland van der Marel, Benjamin F. Williams, Edward J. Wollack, Jennifer Yee, Atsunori Yonehara, and Neil Zimmerman. The WFIRST Exoplanet Microlensing Survey. *arXiv e-prints*, page arXiv:1803.08564, Mar 2018.

[104] Peter C. Nagler, Billy Edwards, Brian Kilpatrick, Nikole K. Lewis, Pierre Maxted, C. Barth Netterfield, Vivien Parmentier, Enzo Pascale, Subhajit Sarkar, Gregory S. Tucker, and Ingo Waldmann. Observing Exoplanets in the Near-Infrared from a High Altitude Balloon Platform. *Journal of Astronomical Instrumentation*, 8(3):1950011, Jan 2019.

[105] C. Beichman, B. Benneke, H. Knutson, R. Smith, P.-O. Lagage, C. Dressing, D. Latham, J. Lunine, S. Birkmann, P. Ferruit, G. Giardino, E. Kempton, S. Carey, J. Krick, P. D. Deroo, A. Mandell, M. E. Ressler, A. Shporer, M. Swain, G. Vasisht, G. Ricker, J. Bouwman, I. Crossfield, T. Greene, S. Howell, J. Christiansen, D. Ciardi, M. Clampin, M. Greenhouse, A. Sozzetti, P. Goudfrooij, D. Hines, T. Keyes, J. Lee, P. McCullough, M. Robberto, J. Stansberry, J. Valenti, M. Rieke, G. Rieke, J. Fortney, J. Bean, L. Kreidberg, D. Ehrenreich, D. Deming, L. Albert, R. Doyon, and D. Sing. Observations of Transiting Exoplanets with the James Webb Space Telescope (JWST). *Publications of the Astronomical Society of the Pacific*, 126:1134, December 2014.

[106] T. P. Greene, M. R. Line, C. Montero, J. J. Fortney, J. Lustig-Yaeger, and K. Luther. Characterizing Transiting Exoplanet Atmospheres with JWST. *ApJ*, 817:17, January 2016.

[107] D. R. Louie, D. Deming, L. Albert, L. G. Bouma, J. Bean, and M. Lopez-Morales. Simulated JWST/NIRISS Transit Spectroscopy of Anticipated Tess Planets Compared to Select Discoveries from Space-based and Ground-

based Surveys. *Publications of the Astronomical Society of the Pacific*, 130(4):044401, April 2018.

[108] S. N. Milam, J. A. Stansberry, G. Sonneborn, and C. Thomas. The James Webb Space Telescope's Plan for Operations and Instrument Capabilities for Observations in the Solar System. *Publications of the Astronomical Society of the Pacific*, 128(1):018001, January 2016.

[109] C. A. Nixon, R. K. Achterberg, M. Ádámkovics, B. Bézard, G. L. Bjoraker, T. Cornet, A. G. Hayes, E. Lellouch, M. T. Lemmon, M. López-Puertas, S. Rodriguez, C. Sotin, N. A. Teanby, E. P. Turtle, and R. A. West. Titan Science with the James Webb Space Telescope. *Publications of the Astronomical Society of the Pacific*, 128(1):018007, January 2016.

[110] C. A. Thomas, P. Abell, J. Castillo-Rogez, N. Moskovitz, M. Mueller, V. Reddy, A. Rivkin, E. Ryan, and J. Stansberry. Observing Near-Earth Objects with the James Webb Space Telescope. *Publications of the Astronomical Society of the Pacific*, 128(1):018002, January 2016.

[111] N. B. Cowan, T. Greene, D. Angerhausen, N. E. Batalha, M. Clampin, K. Colón, I. J. M. Crossfield, J. J. Fortney, B. S. Gaudi, J. Harrington, N. Iro, C. F. Lillie, J. L. Linsky, M. Lopez-Morales, A. M. Mandell, and K. B. Stevenson. Characterizing Transiting Planet Atmospheres through 2025. *Publications of the Astronomical Society of the Pacific*, 127:311, March 2015.

[112] J. L. Bean, K. B. Stevenson, N. M. Batalha, Z. Berta-Thompson, L. Kreidberg, N. Crouzet, B. Benneke, M. R. Line, D. K. Sing, H. R. Wakeford, H. A. Knutson, E. M.-R. Kempton, J.-M. Désert, I. Crossfield, N. E. Batalha, J. de Wit, V. Parmentier, J. Harrington, J. I. Moses, M. Lopez-Morales, M. K. Alam, J. Blecic, G. Bruno, A. L. Carter, J. W. Chapman, L. Decin, D. Dragomir, T. M. Evans, J. J. Fortney, J. D. Fraine, P. Gao, A. García Muñoz, N. P. Gibson, J. M. Goyal, K. Heng, R. Hu, S. Kendrew,

B. M. Kilpatrick, J. Krick, P.-O. Lagage, M. Lendl, T. Louden, N. Madhusudhan, A. M. Mandell, M. Mansfield, E. M. May, G. Morello, C. V. Morley, N. Nikolov, S. Redfield, J. E. Roberts, E. Schlawin, J. J. Spake, K. O. Todorov, A. Tsiaras, O. Venot, W. C. Waalkes, P. J. Wheatley, R. T. Zellem, D. Angerhausen, D. Barrado, L. Carone, S. L. Casewell, P. E. Cubillos, M. Damiano, M. de Val-Borro, B. Drummond, B. Edwards, M. Endl, N. Espinoza, K. France, J. E. Gizis, T. P. Greene, T. K. Henning, Y. Hong, J. G. Ingalls, N. Iro, P. G. J. Irwin, T. Kataria, F. Lahuis, J. Leconte, J. Lillo-Box, S. Lines, L. Mancini, F. Marchis, N. Mayne, E. Palle, G. Roudier, E. L. Shkolnik, J. Southworth, J. Teske, G. Tinetti, P. Tremblin, G. S. Tucker, R. vanBoekel, I. P. Waldmann, I. C. Weaver, and T. Zingales. The Transiting Exoplanet Community Early Release Science Program for JWST. *ArXiv e-prints*, March 2018.

[113] M. Maszkiewicz, N. Rowlands, D. Aldridge, A. Beaton, S. Delamer, Sheng-Hai Zheng, R. Ohl IV, and P. Coulter. Fine guidance sensor/near-infrared imager and slitless spectrograph on James Webb Space Telescope: pupil alignment methodology and metrology. In Bruno Cugny, Nikos Karafolas, and Zoran Sodnik, editors, *International Conference on Space Optics, ICSO 2016*, volume 10562, pages 596 – 604. International Society for Optics and Photonics, SPIE, 2017.

[114] Stephan M. Birkmann, Pierre Ferruit, Tim Rawle, Marco Sirianni, Catarina Alves de Oliveira, Torsten Böker, Giovanna Giardino, Nora Lützgendorf, Anthony Marston, Martin Stuhlinger, Maurice B. J. te Plate, Peter Jensen, Peter Rumler, Bernhard Dorner, Hermann Karl, Peter Mosner, Raymond H. Wright, and Robert Rapp. The JWST/NIRSpec instrument: update on status and performances. In *Proceedings of SPIE*, volume 9904 of *Society of Photo-Optical Instrumentation Engineers (SPIE) Conference Series*, page 99040B, Jul 2016.

[115] P. Ferruit, S. Birkmann, T. Böker, M. Sirianni, G. Giardino, G. de Marchi,

C. Alves de Oliveira, and B. Dorner. Observing transiting exoplanets with JWST/NIRSpec. In *Proceedings of SPIE*, volume 9143 of *Society of Photo-Optical Instrumentation Engineers (SPIE) Conference Series*, page 91430A, Aug 2014.

[116] Thomas P. Greene, Laurie Chu, Eiichi Egami, Klaus W. Hodapp, Douglas M. Kelly, Jarron Leisenring, Marcia Rieke, Massimo Robberto, Everett Schlawin, and John Stansberry. Slitless spectroscopy with the James Webb Space Telescope Near-Infrared Camera (JWST NIRCam). In *Proceedings of SPIE*, volume 9904 of *Society of Photo-Optical Instrumentation Engineers (SPIE) Conference Series*, page 99040E, Jul 2016.

[117] Thomas Greene, Charles Beichman, Daniel Eisenstein, Scott Horner, Douglas Kelly, Yalan Mao, Michael Meyer, Marcia Rieke, and Fang Shi. Observing exoplanets with the JWST NIRCam grisms. In *Proceedings of SPIE*, volume 6693 of *Society of Photo-Optical Instrumentation Engineers (SPIE) Conference Series*, page 66930G, Sep 2007.

[118] Camilla Danielski, Jean-Loup Baudino, Pierre-Olivier Lagage, Anthony Boccaletti, René Gastaud, Alain Coulais, and Bruno Bézard. Atmospheric Characterization of Directly Imaged Exoplanets with JWST/MIRI. *AJ*, 156(6):276, Dec 2018.

[119] Sarah Kendrew, Silvia Scheithauer, Patrice Bouchet, Jerome Amiaux, Ruymán Azzollini, Jeroen Bouwman, C. H. Chen, D. Dubreuil, Sebastian Fischer, Alistair Glasse, T. P. Greene, P. O. Lagage, Fred Lahuis, Samuel Ronayette, David Wright, and G. S. Wright. The Mid-Infrared Instrument for the James Webb Space Telescope, IV: The Low-Resolution Spectrometer. *Publications of the Astronomical Society of the Pacific*, 127(953):623, Jul 2015.

[120] P. Mollière, R. van Boekel, J. Bouwman, Th. Henning, P. O. Lagage, and

M. Min. Observing transiting planets with JWST. Prime targets and their synthetic spectral observations. *A&A*, 600:A10, Apr 2017.

[121] G. Savini, M. Tessenyi, G. Tinetti, C. Arena, J. Tennyson, T. Zingales, E. Pascale, R. Sudiwala, A. Papageorgiou, S. Sarkar, P.A.R. Ade, M. J. Griffin, K. Barnes, L. Hipwood, P. Knowles, M. Patel, M. Leese, J.P. Mason, M. Crook, Technology Department, I. Tosh, A. Saad, P. Eccleston, B. Shaughnessy, T. Brooke, M. Wells, I. Bryson, A. MacLeod, W. Taylor, N. Bezawada, G. S. Wright, S. Jason, J. Friend, J. Williams, G. Johnston, S. Prasad, A. Vora, C. Saunders, B. Winter, P. Curry, and A. Smith. Twinkle A Low Earth Orbit Visible and Infrared Exoplanet Spectroscopy Observatory. In *Preprint (SPIE astronomical telescopes + instrumentation 2016 paper 9904175)*, 2016.

[122] S. Jason, A. da Silva Curiel, M. Tessenyi, G. Tinetti, G. Savini, J. Tennyson, E. Pascale, J. Williams, Johnson, S. Prasad, A. Vora, C. Saunders, J. Friend, and M. Sweeting. Twinkle: A new idea for commercial astrophysics missions. In *4S Symposium 2016*, 4S Symposium, Valletta, Malta, 30 May 2016, 2016.

[123] M. Wells. The infrared spectrometer for Twinkle. *Proc.SPIE*, 9904:9904 – 176, 2016.

[124] Billy Edwards, Lorenzo Mugnai, Giovanna Tinetti, Enzo Pascale, and Subhajit Sarkar. An Updated Study of Potential Targets for Ariel. *The Astronomical Journal*, 157(6):242, may 2019.

[125] Giovanna Tinetti, Pierre Drossart, Paul Eccleston, Paul Hartogh, Astrid Heske, Jrmy Leconte, Giusi Micela, Marc Ollivier, Gran Pilbratt, Ludovic Puig, Diego Turrini, Bart Vandenbussche, and Paulina Wolkenberg. A chemical survey of exoplanets with ARIEL. *Experimental Astronomy*, 2018.

[126] T. Zingales, G. Tinetti, I. Pillitteri, J. Leconte, G. Micela, and S. Sarkar. The ARIEL mission reference sample. *Experimental Astronomy*, February 2018.

[127] E. Pascale, N. Bezawada, J. Barstow, J.-P. Beaulieu, N. Bowles, V. Coudé Du Foresto, A. Coustenis, L. Decin, P. Drossart, P. Eccleston, T. Encrenaz, F. Forget, M. Griffin, M. Güdel, P. Hartogh, A. Heske, P.-O. Lagage, J. Leconte, P. Malaguti, G. Micela, K. Middleton, M. Min, A. Moneti, J.C. Morales, L. Mugnai, M. Ollivier, E. Pace, A. Papageorgiou, G. Pilbratt, L. Puig, M. Rataj, T. Ray, I. Ribas, M. Rocchetto, S. Sarkar, F. Selsis, W. Taylor, J. Tennyson, G. Tinetti, D. Turrini, B. Vandenbussche, O. Venot, I.P. Waldmann, P. Wolkenberg, G. Wright, M.-R. Zapatero Osorio, and T. Zingales. The ariel space mission. *Proceedings of SPIE - The International Society for Optical Engineering*, 10698, 2018.

[128] T. G. Müller, C. Kiss, P. Scheirich, P. Pravec, L. O'Rourke, E. Vilenius, and B. Altieri. Thermal infrared observations of asteroid (99942) Apophis with Herschel. *A&A*, 566:A22, Jun 2014.

[129] W. Tobiska and A. Nusinov. Status of the ISO Draft Standard for Determining Solar Irradiances (CD 21348). In J.-P. Paillé, editor, *35th COSPAR Scientific Assembly*, volume 35 of *COSPAR Meeting*, page 900, 2004.

[130] C. T. Whitmell. Brightness of a planet. *The Observatory*, 30:96–100, February 1907.

[131] Anthony Mallama. The magnitude and albedo of mars. *Icarus*, 192:404–416, 12 2007.

[132] B. H. Zellner and R. C. Capen. Photometric properties of the Martian satellites. *Icarus*, 23:437–444, November 1974.

[133] P. C. Thomas, D. Adinolfi, P. Helfenstein, D. Simonelli, and J. Veverka. The Surface of Deimos: Contribution of Materials and Processes to Its Unique Appearance. *Icarus*, 123:536–556, October 1996.

[134] D. Morrison, N. D. Morrison, and A. R. Lazarewicz. Four-color photometry of the Galilean satellites. *Icarus*, 23:399–416, November 1974.

[135] D. P. Simonelli and J. Veverka. Voyager disk-integrated photometry of Io. *Icarus*, 59:406–425, September 1984.

[136] B. Buratti and J. Veverka. Voyager photometry of Europa. *Icarus*, 55:93–110, July 1983.

[137] D. P. Simonelli, L. Rossier, P. C. Thomas, J. Veverka, J. A. Burns, and M. J. S. Belton. Leading/Trailing Albedo Asymmetries of Thebe, Amalthea, and Metis. *Icarus*, 147:353–365, October 2000.

[138] D. Morrison, T. V. Johnson, E. M. Shoemaker, L. A. Soderblom, P. Thomas, J. Veverka, and B. A. Smith. *Satellites of Saturn - Geological perspective*, pages 609–639. University of Arizona Press, 1984.

[139] A. Verbiscer, R. French, M. Showalter, and P. Helfenstein. Enceladus: Cosmic Graffiti Artist Caught in the Act. *Science*, 315:815, February 2007.

[140] J. Veverka, R. H. Brown, and J. F. Bell. *Uranus satellites - Surface properties*, pages 528–560. University of Arizona Press, 1991.

[141] M. D. Hicks and B. J. Buratti. The spectral variability of Triton from 1997-2000. *Icarus*, 171:210–218, September 2004.

[142] E. Karkoschka. Sizes, shapes, and albedos of the inner satellites of Neptune. *Icarus*, 162:400–407, April 2003.

[143] P. Thomas, J. Veverka, and P. Helfenstein. Voyager observations of Nereid. *Journal of Geophysical Research*, 96:19, October 1991.

[144] J.-Y. Li, L. A. McFadden, J. W. Parker, E. F. Young, S. A. Stern, P. C. Thomas, C. T. Russell, and M. V. Sykes. Photometric analysis of 1 Ceres and surface mapping from HST observations. *Icarus*, 182:143–160, May 2006.

[145] J. Stansberry, W. Grundy, M. Brown, D. Cruikshank, J. Spencer, D. Trilling, and J.-L. Margot. *Physical Properties of Kuiper Belt and Centaur Objects:*

Constraints from the Spitzer Space Telescope, pages 161–179. University of Arizona Press, 2008.

[146] M. E. Brown. On the Size, Shape, and Density of Dwarf Planet Makemake. *The Astrophysical Journal Letters*, 767:L7, April 2013.

[147] B. Sicardy, J. L. Ortiz, M. Assafin, E. Jehin, A. Maury, E. Lellouch, R. G. Hutton, F. Braga-Ribas, F. Colas, D. Hestroffer, J. Lecacheux, F. Roques, P. Santos-Sanz, T. Widemann, N. Morales, R. Duffard, A. Thirouin, A. J. Castro-Tirado, M. Jelínek, P. Kubánek, A. Sota, R. Sánchez-Ramírez, A. H. Andrei, J. I. B. Camargo, D. N. da Silva Neto, A. R. Gomes, R. V. Martins, M. Gillon, J. Manfroid, G. P. Tozzi, C. Harlingten, S. Saravia, R. Behrend, S. Mottola, E. G. Melendo, V. Peris, J. Fabregat, J. M. Madiedo, L. Cuesta, M. T. Eibe, A. Ullán, F. Organero, S. Pastor, J. A. de Los Reyes, S. Pedraz, A. Castro, I. de La Cueva, G. Muler, I. A. Steele, M. Cebrián, P. Montañés-Rodríguez, A. Oscoz, D. Weaver, C. Jacques, W. J. B. Corradi, F. P. Santos, W. Reis, A. Milone, M. Emilio, L. Gutiérrez, R. Vázquez, and H. Hernández-Toledo. A Pluto-like radius and a high albedo for the dwarf planet Eris from an occultation. *Nature*, 478:493–496, October 2011.

[148] Andrew S. Rivkin, David E. Trilling, Cristina A. Thomas, Francesca DeMeo, Timothy B. Spahr, and Richard P. Binzel. Composition of the l5 mars trojans: Neighbors, not siblings. *Icarus*, 192(2):434 – 441, 2007.

[149] J. Veverka, P. C. Thomas, J. F. Bell, III, M. Bell, B. Carcich, B. Clark, A. Harch, J. Joseph, P. Martin, M. Robinson, S. Murchie, N. Izenberg, E. Hawkins, J. Warren, R. Farquhar, A. Cheng, D. Dunham, C. Chapman, W. J. Merline, L. McFadden, D. Wellnitz, M. Malin, W. M. Owen, Jr., J. K. Miller, B. G. Williams, and D. K. Yeomans. Imaging of asteroid 433 Eros during NEAR's flyby reconnaissance. *Science*, 285:562–564, July 1999.

[150] Jian-Yang Li, Lucille Le Corre, Stefan E. Schröder, Vishnu Reddy, Brett W. Denevi, Bonnie J. Buratti, Stefano Mottola, Martin Hoffmann, Pablo

Gutierrez- Marques, Andreas Nathues, Christopher T. Russell, and Carol A. Raymond. Global photometric properties of Asteroid (4) Vesta observed with Dawn Framing Camera. *Icarus*, 226:1252–1274, November 2013.

[151] Lucy F. Lim, Timothy H. McConnochie, James F. Bell, and Thomas L. Hayward. Thermal infrared (8 13 μm) spectra of 29 asteroids: the Cornell Mid-Infrared Asteroid Spectroscopy (MIDAS) Survey. *Icarus*, 173:385–408, February 2005.

[152] E. F. Tedesco, G. J. Veeder, J. W. Fowler, and J. R. Chillemi. The IRAS Minor Planet Survey. Technical report, Phillips Laboratory, December 1992.

[153] C. A. Hibbitts, R. T. Pappalardo, G. B. Hansen, and T. B. McCord. Carbon dioxide on Ganymede. *Journal of Geophysical Research (Planets)*, 108:5036, May 2003.

[154] B. D. Teolis, G. H. Jones, P. F. Miles, R. L. Tokar, B. A. Magee, J. H. Waite, E. Roussos, D. T. Young, F. J. Crary, A. J. Coates, R. E. Johnson, W.-L. Tseng, and R. A. Baragiola. Cassini finds an oxygen–carbon dioxide atmosphere at saturn's icy moon rhea. *Science*, 330(6012):1813–1815, 2010.

[155] R. J. Cartwright, J. P. Emery, A. S. Rivkin, D. E. Trilling, and N. Pinilla-Alonso. Distribution of CO_2 ice on the large moons of Uranus and evidence for compositional stratification of their near-surfaces. *Icarus*, 257:428–456, September 2015.

[156] J. R. Spencer and W. M. Calvin. Condensed O_2 on Europa and Callisto. *AJ*, 124:3400–3403, December 2002.

[157] Samantha K. Trumbo, Michael E. Brown, Patrick D. Fischer, and Kevin P. Hand. A New Spectral Feature on the Trailing Hemisphere of Europa at 3.78 μm. *AJ*, 153:250, June 2017.

[158] A. S. Rivkin, F. Marchis, J. A. Stansberry, D. Takir, C. Thomas, and JWST Asteroids Focus Group. Asteroids and the James Webb Space Telescope.

Publications of the Astronomical Society of the Pacific, 128(1):018003, January 2016.

[159] B. E. Schmidt, P. C. Thomas, J. M. Bauer, J. Y. Li, L. A. McFadden, M. J. Mutchler, S. C. Radcliffe, A. S. Rivkin, C. T. Russell, J. Wm. Parker, and S. A. Stern. The Shape and Surface Variation of 2 Pallas from the Hubble Space Telescope. *Science*, 326(5950):275, Oct 2009.

[160] Michael S. P. Kelley, Charles E. Woodward, Dennis Bodewits, Tony L. Farnham, Murthy S. Gudipati, David E. Harker, Dean C. Hines, Matthew M. Knight, Ludmilla Kolokolova, Aigen Li, Imke de Pater, Silvia Protopapa, Ray W. Russell, Michael L. Sitko, and Diane H. Wooden. Cometary Science with the James Webb Space Telescope. *Publications of the Astronomical Society of the Pacific*, 128(959):018009, Jan 2016.

[161] N. Schorghofer, S. Byrne, M. E. Landis, E. Mazarico, T. H. Prettyman, B. E. Schmidt, M. N. Villarreal, J. Castillo-Rogez, C. A. Raymond, and C. T. Russell. The Putative Cerean Exosphere. *ApJ*, 850:85, November 2017.

[162] H. Karttunen, P. Kröger, H. Oja, M. Poutanen, and K.J. Donner. *Fundamental Astronomy*. Springer, Springer-Verlag, Berlin, 2017.

[163] C.-I. Lagerkvist and I. P. Williams. Physical studies of asteroids. XV - Determination of slope parameters and absolute magnitudes for 51 asteroids. *Astronomy and Astrophysics Supplement*, 68:295–315, March 1987.

[164] R. Dymock. The H and G magnitude system for asteroids. *Journal of the British Astronomical Association*, 117:342–343, December 2007.

[165] Edward Bowell, Bruce Hapke, Deborah Domingue, Kari Lumme, Jouni Peltoniemi, and Alan W. Harris. Application of photometric models to asteroids. In Richard P. Binzel, Tom Gehrels, and Mildred Shapley Matthews, editors, *Asteroids II*, pages 524–556, Jan 1989.

[166] F. E. DeMeo and B. Carry. The taxonomic distribution of asteroids from multi-filter all-sky photometric surveys. *Icarus*, 226:723–741, September 2013.

[167] F. Vilas and M. J. Gaffey. Phyllosilicate absorption features in main-belt and outer-belt asteroid reflectance spectra. *Science*, 246:790–792, November 1989.

[168] F. Vilas. A cheaper, faster, better way to detect water of hydration on Solar System bodies. *Icarus*, 111:456–467, October 1994.

[169] A. S. Rivkin and E. L. Volquardsen. Rotationally-resolved spectra of Ceres in the 3-μm region. *Icarus*, 206:327–333, March 2010.

[170] A. S. Rivkin and J. P. Emery. Detection of ice and organics on an asteroidal surface. *Nature*, 464:1322–1323, April 2010.

[171] E. A. Cloutis, T. Hiroi, M. J. Gaffey, C. M. O. '. Alexander, and P. Mann. Spectral reflectance properties of carbonaceous chondrites: 1. CI chondrites. *Icarus*, 212:180–209, March 2011.

[172] R. N. Clark, T. V. V. King, M. Klejwa, G. A. Swayze, and N. Vergo. High spectral resolution reflectance spectroscopy of minerals. *Journal of Geophysical Research*, 95:12653–12680, August 1990.

[173] T. Hiroi, M. E. Zolensky, C. M. Pieters, and M. E. Lipschutz. Thermal metamorphism of the C, G, B, and F asteroids seen from the 0.7 micron, 3 micron and UV absorption strengths in comparison with carbonaceous chondrites. *Meteoritics and Planetary Science*, 31:321–327, May 1996.

[174] K. Sato, M. Miyamoto, and M. E. Zolensky. Absorption bands near 3 (m in diffuse reflectance spectra of carbonaceous chondrites: Comparison with asteroids. *Meteoritics and Planetary Science*, 32, July 1997.

[175] T. Osawa, H. Kagi, T. Nakamura, and T. Noguchi. Infrared spectroscopic taxonomy for carbonaceous chondrites from speciation of hydrous components. *Meteoritics and Planetary Science*, 40:71, January 2005.

[176] R. M. Mastrapa, S. A. Sandford, T. L. Roush, D. P. Cruikshank, and C. M. Dalle Ore. Optical Constants of Amorphous and Crystalline H_2O-ice: 2.5-22 μm (4000-455 cm^{-1}) Optical Constants of H_2O-ice. *ApJ*, 701:1347–1356, August 2009.

[177] P. Beck, E. Quirico, G. Montes-Hernandez, L. Bonal, J. Bollard, F.-R. Orthous-Daunay, K. T. Howard, B. Schmitt, O. Brissaud, F. Deschamps, B. Wunder, and S. Guillot. Hydrous mineralogy of CM and CI chondrites from infrared spectroscopy and their relationship with low albedo asteroids. *Geochimica et Cosmochimica Acta*, 74:4881–4892, August 2010.

[178] H. Campins, K. Hargrove, N. Pinilla-Alonso, E. S. Howell, M. S. Kelley, J. Licandro, T. Mothé-Diniz, Y. Fernández, and J. Ziffer. Water ice and organics on the surface of the asteroid 24 Themis. *Nature*, 464:1320–1321, April 2010.

[179] D. Takir, J. P. Emery, H. Y. McSween, C. A. Hibbitts, R. N. Clark, N. Pearson, and A. Wang. Nature and degree of aqueous alteration in CM and CI carbonaceous chondrites. *Meteoritics and Planetary Science*, 48:1618–1637, September 2013.

[180] D. Takir and J. P. Emery. Outer Main Belt asteroids: Identification and distribution of four 3-μm spectral groups. *Icarus*, 219:641–654, June 2012.

[181] J. Licandro, H. Campins, M. Kelley, K. Hargrove, N. Pinilla-Alonso, D. Cruikshank, A. S. Rivkin, and J. Emery. (65) Cybele: detection of small silicate grains, water-ice, and organics. *A&A*, 525:A34, January 2011.

[182] V. Zappalà, P. Bendjoya, A. Cellino, P. Farinella, and C. Froeschlé. Asteroid families: Search of a 12,487-asteroid sample using two different clustering techniques. *Icarus*, 116:291–314, August 1995.

[183] M. Florczak, D. Lazzaro, T. Mothé-Diniz, C. A. Angeli, and A. S. Betzler. A spectroscopic study of the THEMIS family. *Astronomy and Astrophysics Supplement*, 134:463–471, February 1999.

[184] J. de León, N. Pinilla-Alonso, H. Campins, J. Licandro, and G. A. Marzo. Near-infrared spectroscopic survey of B-type asteroids: Compositional analysis. *Icarus*, 218:196–206, March 2012.

[185] H. Campins. Volatiles in asteroids. In K. Muinonen, A. Penttilä, M. Granvik, A. Virkki, G. Fedorets, O. Wilkman, and T. Kohout, editors, *Asteroids, Comets, Meteors 2014*, July 2014.

[186] V. V. Busarev, A. B. Makalkin, F. Vilas, S. I. Barabanov, and M. P. Scherbina. New candidates for active asteroids: Main-belt (145) Adeona, (704) Interamnia, (779) Nina, (1474) Beira, and near-Earth (162,173) Ryugu. *Icarus*, 304:83–94, April 2018.

[187] B. Novaković. P/2017 S5: Another Active Asteroid Associated with the Theobalda Family. *Research Notes of the American Astronomical Society*, 2(3):129, July 2018.

[188] G. R. Hunt. Spectral signatures of particulate minerals in the visible and near infrared. *Geophysics*, 42:501–513, April 1977.

[189] F. Poulet, J.-P. Bibring, J. F. Mustard, A. Gendrin, N. Mangold, Y. Langevin, R. E. Arvidson, B. Gondet, and C. Gomez. Phyllosilicates on Mars and implications for early martian climate. *Nature*, 438:623–627, December 2005.

[190] E. A. Cloutis, P. Hudon, T. Hiroi, M. J. Gaffey, and P. Mann. Spectral reflectance properties of carbonaceous chondrites: 2. CM chondrites. *Icarus*, 216:309–346, November 2011.

[191] A. S. Rivkin, C. A. Thomas, E. S. Howell, and J. P. Emery. The Ch-class Asteroids: Connecting a Visible Taxonomic Class to a 3 μm Band Shape. *AJ*, 150:198, December 2015.

[192] J. M. Sunshine, O. Groussin, P. H. Schultz, M. F. A'Hearn, L. M. Feaga, T. L. Farnham, and K. P. Klaasen. The distribution of water ice in the interior of Comet Tempel 1. *Icarus*, 190:284–294, October 2007.

[193] M. F. A'Hearn, M. J. S. Belton, W. A. Delamere, L. M. Feaga, D. Hampton, J. Kissel, K. P. Klaasen, L. A. McFadden, K. J. Meech, H. J. Melosh, P. H. Schultz, J. M. Sunshine, P. C. Thomas, J. Veverka, D. D. Wellnitz, D. K. Yeomans, S. Besse, D. Bodewits, T. J. Bowling, B. T. Carcich, S. M. Collins, T. L. Farnham, O. Groussin, B. Hermalyn, M. S. Kelley, M. S. Kelley, J.-Y. Li, D. J. Lindler, C. M. Lisse, S. A. McLaughlin, F. Merlin, S. Protopapa, J. E. Richardson, and J. L. Williams. EPOXI at Comet Hartley 2. *Science*, 332:1396, June 2011.

[194] L. M. Feaga, M. F. A'Hearn, T. L. Farnham, D. Bodewits, J. M. Sunshine, A. M. Gersch, S. Protopapa, B. Yang, M. Drahus, and D. G. Schleicher. Uncorrelated Volatile Behavior during the 2011 Apparition of Comet C/2009 P1 Garradd. *AJ*, 147:24, January 2014.

[195] J. K. Davies, T. L. Roush, D. P. Cruikshank, M. J. Bartholomew, T. R. Geballe, T. Owen, and C. de Bergh. The Detection of Water Ice in Comet Hale-Bopp. *Icarus*, 127:238–245, May 1997.

[196] H. Kawakita, J. I. Watanabe, T. Ootsubo, R. Nakamura, T. Fuse, N. Takato, S. Sasaki, and T. Sasaki. Evidence of Icy Grains in Comet C/2002 T7 (LINEAR) at 3.52 AU. *The Astrophysical Journal Letters*, 601:L191–L194, February 2004.

[197] B. Yang, D. Jewitt, and S. J. Bus. Comet 17P/Holmes in Outburst: The Near Infrared Spectrum. *AJ*, 137:4538–4546, May 2009.

[198] J. M. Sunshine, L. M. Feaga, O. Groussin, S. Besse, S. Protopapa, F. Merlin, T. L. Farnham, M. F. A'Hearn, and Dixi Science Team. Icy Grains in Comet 103P/Hartley 2. In *Lunar and Planetary Science Conference*, volume 42 of *Lunar and Planetary Science Conference*, page 2292, March 2011.

[199] S. Protopapa, J. M. Sunshine, L. M. Feaga, M. S. P. Kelley, M. F. A'Hearn, T. L. Farnham, O. Groussin, S. Besse, F. Merlin, and J.-Y. Li. Water ice and dust in the innermost coma of comet 103P/Hartley 2. *Icarus*, 238:191–204, August 2014.

[200] T. Yamamoto. On the molecular composition of a cometary nucleus. In T. I. Gombosi, editor, *Cometary Exploration*, volume 1, pages 85–91, 1983.

[201] J. Crovisier and T. Encrenaz. Infrared fluorescence of molecules in comets - The general synthetic spectrum. *A&A*, 126:170–182, September 1983.

[202] H. A. Weaver and M. J. Mumma. Infrared molecular emissions from comets. *ApJ*, 276:782–797, January 1984.

[203] J. B. Adams. Visible and near-infrared diffuse reflectance spectra of pyroxenes as applied to remote sensing of solid objects in the solar system. *Journal of Geophysical Research*, 79:4829–4836, November 1974.

[204] Roger G. Burns. Crystal field spectra and evidence of cation ordering in olivine minerals. *American Mineralogist*, 55(9-10):1608, 1970.

[205] E. A. Cloutis, M. J. Gaffey, T. L. Jackowski, and K. L. Reed. Calibrations of phase abundance, composition, and particle size distribution for olivine-orthopyroxene mixtures from reflectance spectra. *Journal of Geophysical Research*, 91:11, October 1986.

[206] T. L. Dunn, T. J. McCoy, J. M. Sunshine, and H. Y. McSween. A coordinated spectral, mineralogical, and compositional study of ordinary chondrites. *Icarus*, 208:789–797, August 2010.

[207] M. J. Gaffey, J. F. Bell, R. H. Brown, T. H. Burbine, J. L. Piatek, K. L. Reed, and D. A. Chaky. Mineralogical variations within the S-type asteroid class. *Icarus*, 106:573, December 1993.

[208] J. A. Sanchez, V. Reddy, A. Nathues, E. A. Cloutis, P. Mann, and H. Hiesinger. Phase reddening on near-Earth asteroids: Implications for mineralogical analysis, space weathering and taxonomic classification. *Icarus*, 220:36–50, July 2012.

[209] J. de León, J. Licandro, M. Serra-Ricart, N. Pinilla-Alonso, and H. Campins. Observations, compositional, and physical characterization of near-Earth and Mars-crosser asteroids from a spectroscopic survey. *A&A*, 517:A23, July 2010.

[210] S. S. Lindsay, F. Marchis, J. P. Emery, J. E. Enriquez, and M. Assafin. Composition, mineralogy, and porosity of multiple asteroid systems from visible and near-infrared spectral data. *Icarus*, 247:53–70, February 2015.

[211] V. Reddy, J. M. Carvano, D. Lazzaro, T. A. Michtchenko, M. J. Gaffey, M. S. Kelley, T. Mothé-Diniz, A. Alvarez-Candal, N. A. Moskovitz, E. A. Cloutis, and E. L. Ryan. Mineralogical characterization of Baptistina Asteroid Family: Implications for K/T impactor source. *Icarus*, 216:184–197, November 2011.

[212] T. H. Burbine, P. C. Buchanan, T. Dolkar, and R. P. Binzel. Pyroxene mineralogies of near-Earth vestoids. *Meteoritics and Planetary Science*, 44:1331–1341, October 2009.

[213] P. S. Hardersen, V. Reddy, R. Roberts, and A. Mainzer. More chips off of Asteroid (4) Vesta: Characterization of eight Vestoids and their HED meteorite analogs. *Icarus*, 242:269–282, November 2014.

[214] N. A. Moskovitz, M. Willman, T. H. Burbine, R. P. Binzel, and S. J. Bus. A spectroscopic comparison of HED meteorites and V-type asteroids in the inner Main Belt. *Icarus*, 208:773–788, August 2010.

[215] B. E. Clark, B. Hapke, C. Pieters, and D. Britt. *Asteroid Space Weathering and Regolith Evolution*, pages 585–599. University of Arizona Press, 1510 E. University Blvd., P.O. Box 210055, Tucson, AZ 85721-0055, 2002.

[216] Clark R. Chapman. Space weathering of asteroid surfaces. *Annual Review of Earth and Planetary Sciences*, 32(1):539–567, 2004.

[217] J. Veverka, M. Belton, K. Klaasen, and C. Chapman. Galileo's Encounter with 951 Gaspra: Overview. *Icarus*, 107:2–17, January 1994.

[218] J. Veverka, P. Helfenstein, P. Lee, P. Thomas, A. McEwen, M. Belton, K. Klaasen, T. V. Johnson, J. Granahan, F. Fanale, P. Geissler, and J. W. Head, III. Ida and Dactyl: Spectral Reflectance and Color Variations. *Icarus*, 120:66–76, March 1996.

[219] V. Reddy, A. Nathues, L. Le Corre, H. Sierks, J.-Y. Li, R. Gaskell, T. McCoy, A. W. Beck, S. E. Schröder, C. M. Pieters, K. J. Becker, B. J. Buratti, B. Denevi, D. T. Blewett, U. Christensen, M. J. Gaffey, P. Gutierrez-Marques, M. Hicks, H. U. Keller, T. Maue, S. Mottola, L. A. McFadden, H. Y. McSween, D. Mittlefehldt, D. P. O'Brien, C. Raymond, and C. Russell. Color and Albedo Heterogeneity of Vesta from Dawn. *Science*, 336:700, May 2012.

[220] M. J. Gaffey. Surface Lithologic Heterogeneity of Asteroid 4 Vesta. *Icarus*, 127:130–157, May 1997.

[221] L. Jeremy Richardson, Drake Deming, Karen Horning, Sara Seager, and Joseph Harrington. A spectrum of an extrasolar planet. *Nature*, 445(7130):892–895, Feb 2007.

[222] C. J. Grillmair, D. Charbonneau, A. Burrows, L. Armus, J. Stauffer, V. Meadows, J. Van Cleve, and D. Levine. A Spitzer Spectrum of the Exoplanet HD 189733b. *The Astrophysical Journal Letters*, 658(2):L115–L118, Apr 2007.

[223] J. P. Beaulieu, S. Carey, I. Ribas, and G. Tinetti. Primary Transit of the Planet HD 189733b at 3.6 and 5.8 μm. *ApJ*, 677(2):1343–1347, Apr 2008.

[224] Carl J. Grillmair, Adam Burrows, David Charbonneau, Lee Armus, John Stauffer, Victoria Meadows, Jeffrey van Cleve, Kaspar von Braun, and Deb-

orah Levine. Strong water absorption in the dayside emission spectrum of the planet HD189733b. *Nature*, 456(7223):767–769, Dec 2008.

[225] Jean-Michel Désert, Alain Lecavelier des Etangs, Guillaume Hébrard, David K. Sing, David Ehrenreich, Roger Ferlet, and Alfred Vidal-Madjar. Search for Carbon Monoxide in the Atmosphere of the Transiting Exoplanet HD 189733b. *ApJ*, 699(1):478–485, Jul 2009.

[226] J. M. Désert, D. Sing, A. Vidal-Madjar, G. Hébrard, D. Ehrenreich, A. Lecavelier Des Etangs, V. Parmentier, R. Ferlet, and G. W. Henry. Transit spectrophotometry of the exoplanet HD 189733b. II. New Spitzer observations at 3.6 μm. *A&A*, 526:A12, Feb 2011.

[227] G. Morello, I. P. Waldmann, G. Tinetti, G. Peres, G. Micela, and I. D. Howarth. A New Look at Spitzer Primary Transit Observations of the Exoplanet HD 189733b. *ApJ*, 786(1):22, May 2014.

[228] Mario Morvan, Nikoloas Nikolaou, Angelos Tsiaras, and Ingo Waldmann. Detrending Exoplanetary Transit Light Curves with Long Short-Term Memory Networks. *ApJ*, Nov 2019.

[229] Heather A. Knutson, David Charbonneau, Lori E. Allen, Adam Burrows, and S. Thomas Megeath. The 3.6-8.0 μm Broadband Emission Spectrum of HD 209458b: Evidence for an Atmospheric Temperature Inversion. *ApJ*, 673(1):526–531, Jan 2008.

[230] A. Burrows, I. Hubeny, J. Budaj, H. A. Knutson, and D. Charbonneau. Theoretical Spectral Models of the Planet HD 209458b with a Thermal Inversion and Water Emission Bands. *The Astrophysical Journal Letters*, 668(2):L171–L174, Oct 2007.

[231] Michael R. Line, Kevin B. Stevenson, Jacob Bean, Jean-Michel Desert, Jonathan J. Fortney, Laura Kreidberg, Nikku Madhusudhan, Adam P. Showman, and Hannah Diamond-Lowe. No Thermal Inversion and a Solar Water

Abundance for the Hot Jupiter HD 209458b from HST/WFC3 Spectroscopy. *AJ*, 152(6):203, Dec 2016.

[232] B. Warner, E. L. Robinson, and R. E. Nather. Measurement of limb darkening on the white dwarf BD +16 516B. *MNRAS*, 154:455, Jan 1971.

[233] K. Horne. Images of accretion discs -I. The eclipse mapping method. *MNRAS*, 213:129–141, Mar 1985.

[234] Emily Rauscher, Kristen Menou, Sara Seager, Drake Deming, James Y. K. Cho, and Bradley M. S. Hansen. Toward Eclipse Mapping of Hot Jupiters. *ApJ*, 664(2):1199–1209, Aug 2007.

[235] Peter K. G. Williams, David Charbonneau, Curtis S. Cooper, Adam P. Showman, and Jonathan J. Fortney. Resolving the Surfaces of Extrasolar Planets with Secondary Eclipse Light Curves. *ApJ*, 649(2):1020–1027, Oct 2006.

[236] J. de Wit, M. Gillon, B. O. Demory, and S. Seager. Towards consistent mapping of distant worlds: secondary-eclipse scanning of the exoplanet HD 189733b. *A&A*, 548:A128, Dec 2012.

[237] H. A. Knutson, N. Lewis, J. J. Fortney, A. Burrows, A. P. Showman, N. B. Cowan, E. Agol, S. Aigrain, D. Charbonneau, D. Deming, J.-M. Désert, G. W. Henry, J. Langton, and G. Laughlin. 3.6 and 4.5 μm Phase Curves and Evidence for Non-equilibrium Chemistry in the Atmosphere of Extrasolar Planet HD 189733b. *ApJ*, 754:22, July 2012.

[238] N. P. Gibson, S. Aigrain, F. Pont, D. K. Sing, J. M. Désert, T. M. Evans, G. Henry, N. Husnoo, and H. Knutson. Probing the haze in the atmosphere of HD 189733b with Hubble Space Telescope/WFC3 transmission spectroscopy. *MNRAS*, 422(1):753–760, May 2012.

[239] Mark Swain, Pieter Deroo, Giovanna Tinetti, Morgan Hollis, Marcell Tessenyi, Michael Line, Hajime Kawahara, Yuka Fujii, Adam P. Showman,

and Sergey N. Yurchenko. Probing the extreme planetary atmosphere of WASP-12b. *Icarus*, 225(1):432–445, Jul 2013.

[240] A. Tsiaras, I. P. Waldmann, M. Rocchetto, R. Varley, G. Morello, M. Damiano, and G. Tinetti. A New Approach to Analyzing HST Spatial Scans: The Transmission Spectrum of HD 209458 b. *ApJ*, 832(2):202, Dec 2016.

[241] I. P. Waldmann, G. Tinetti, M. Rocchetto, E. J. Barton, S. N. Yurchenko, and J. Tennyson. Tau-REx I: A Next Generation Retrieval Code for Exoplanetary Atmospheres. *ApJ*, 802:107, April 2015.

[242] Benjamin V. Rackham, Dániel Apai, and Mark S. Giampapa. The Transit Light Source Effect: False Spectral Features and Incorrect Densities for M-dwarf Transiting Planets. *ApJ*, 853(2):122, Feb 2018.

[243] Kai Hou Yip, Ingo P. Waldmann, Angelos Tsiaras, and Giovanna Tinetti. Integrating light-curve and atmospheric modelling of transiting exoplanets. *arXiv e-prints*, page arXiv:1811.04686, March 2019.

[244] Brett M. Morris, Leslie Hebb, James R. A. Davenport, Graeme Rohn, and Suzanne L. Hawley. The Starspots of HAT-P-11: Evidence for a Solar-like Dynamo. *ApJ*, 846(2):99, Sep 2017.

[245] Brett M. Morris, Suzanne L. Hawley, Leslie Hebb, Charli Sakari, James. R. A. Davenport, Howard Isaacson, Andrew W. Howard, Benjamin T. Montet, and Eric Agol. Chromospheric Activity of HAT-P-11: An Unusually Active Planet-hosting K Star. *ApJ*, 848(1):58, Oct 2017.

[246] Brett M. Morris, Suzanne L. Hawley, and Leslie Hebb. Large Starspot Groups on HAT-P-11 in Activity Cycle 1. *Research Notes of the American Astronomical Society*, 2(1):26, Feb 2018.

[247] Joshua N. Winn, John Asher Johnson, Andrew W. Howard, Geoffrey W. Marcy, Howard Isaacson, Avi Shporer, Gáspár Á. Bakos, Joel D. Hartman,

and Simon Albrecht. The Oblique Orbit of the Super-Neptune HAT-P-11b. *The Astrophysical Journal Letters*, 723(2):L223–L227, Nov 2010.

[248] Drake Deming, Pedro V. Sada, Brian Jackson, Steven W. Peterson, Eric Agol, Heather A. Knutson, Donald E. Jennings, Flynn Haase, and Kevin Bays. Kepler and Ground-based Transits of the Exo-Neptune HAT-P-11b. *ApJ*, 740(1):33, Oct 2011.

[249] Roberto Sanchis-Ojeda and Joshua N. Winn. Starspots, Spin-Orbit Misalignment, and Active Latitudes in the HAT-P-11 Exoplanetary System. *ApJ*, 743(1):61, Dec 2011.

[250] Samuel W. Yee, Erik A. Petigura, Benjamin J. Fulton, Heather A. Knutson, Konstantin Batygin, Gáspár Á. Bakos, Joel D. Hartman, Lea A. Hirsch, Andrew W. Howard, Howard Isaacson, Molly R. Kosiarek, Evan Sinukoff, and Lauren M. Weiss. HAT-P-11: Discovery of a Second Planet and a Clue to Understanding Exoplanet Obliquities. *AJ*, 155(6):255, Jun 2018.

[251] Megan Mansfield, Jacob L. Bean, Antonija Oklopčić, Laura Kreidberg, Jean-Michel Désert, Eliza M. R. Kempton, Michael R. Line, Jonathan J. Fortney, Gregory W. Henry, Matthias Mallonn, Kevin B. Stevenson, Diana Dragomir, Romain Allart, and Vincent Bourrier. Detection of Helium in the Atmosphere of the Exo-Neptune HAT-P-11b. *The Astrophysical Journal Letters*, 868(2):L34, Dec 2018.

[252] Yayaati Chachan, Heather A. Knutson, Peter Gao, Tiffany Kataria, Ian Wong, Gregory W. Henry, Björn Benneke, Michael Zhang, Joanna Barstow, Jacob L. Bean, Thomas M. Evans, Nikole K. Lewis, Megan Mansfield, Mercedes López-Morales, Nikolay Nikolov, David K. Sing, and Hannah Wakeford. A Hubble PanCET Study of HAT-P-11b: A Cloudy Neptune with a Low Atmospheric Metallicity. *arXiv e-prints*, page arXiv:1910.07523, Oct 2019.

[253] Gustav Mie. Beitrge zur optik trber medien, speziell kolloidaler metallsungen. *Annalen der Physik*, 330(3):377–445, 1908.

[254] Thomas M. Evans, David K. Sing, Jayesh M. Goyal, Nikolay Nikolov, Mark S. Marley, Kevin Zahnle, Gregory W. Henry, Joanna K. Barstow, Munazza K. Alam, Jorge Sanz-Forcada, Tiffany Kataria, Nikole K. Lewis, Panayotis Lavvas, Gilda E. Ballester, Lotfi Ben-Jaffel, Sarah D. Blumenthal, Vincent Bourrier, Benjamin Drummond, Antonio García Muñoz, Mercedes López-Morales, Pascal Tremblin, David Ehrenreich, Hannah R. Wakeford, Lars A. Buchhave, Alain Lecavelier des Etangs, Éric Hébrard, and Michael H. Williamson. An Optical Transmission Spectrum for the Ultrahot Jupiter WASP-121b Measured with the Hubble Space Telescope. *AJ*, 156(6):283, Dec 2018.

[255] Thomas Mikal-Evans, David K. Sing, Jayesh M. Goyal, Benjamin Drummond, Aarynn L. Carter, Gregory W. Henry, Hannah R. Wakeford, Nikole K. Lewis, Mark S. Marley, Pascal Tremblin, Nikolay Nikolov, Tiffany Kataria, Drake Deming, and Gilda E. Ballester. An emission spectrum for WASP-121b measured across the 0.8-1.1 μm wavelength range using the Hubble Space Telescope. *MNRAS*, 488(2):2222–2234, Sep 2019.

[256] Ludovic Puig, Kate Isaak, Martin Linder, Isabel Escudero, Pierre-Elie Crouzet, Roger Walker, Matthias Ehle, Jutta Huebner, Rainer Timm, Bram de Vogeleer, Pierre Drossart, Paul Hartogh, Christophe Lovis, Giusi Micela, Marc Ollivier, Ignasi Ribas, Ignas Snellen, Bruce Swinyard, G Tinetti, and Paul Eccleston. The phase 0/A study of the ESA M3 mission candidate EChO. *Experimental Astronomy*, 40:393–425, 12 2015.

[257] G. Tinetti, J. P. Beaulieu, T. Henning, M. Meyer, G. Micela, I. Ribas, D. Stam, M. Swain, O. Krause, M. Ollivier, E. Pace, B. Swinyard, A. Aylward, R. van Boekel, A. Coradini, T. Encrenaz, I. Snellen, M. R. Zapatero-Osorio, J. Bouwman, J. Y.-K. Cho, V. Coudé de Foresto, T. Guillot, M. Lopez-Morales, I. Mueller-Wodarg, E. Palle, F. Selsis, A. Sozzetti,

P. A. R. Ade, N. Achilleos, A. Adriani, C. B. Agnor, C. Afonso, C. Allende Prieto, G. Bakos, R. J. Barber, M. Barlow, V. Batista, P. Bernath, B. Bézard, P. Bordé, L. R. Brown, A. Cassan, C. Cavarroc, A. Ciaravella, C. Cockell, A. Coustenis, C. Danielski, L. Decin, R. De Kok, O. Demangeon, P. Deroo, P. Doel, P. Drossart, L. N. Fletcher, M. Focardi, F. Forget, S. Fossey, P. Fouqué, J. Frith, M. Galand, P. Gaulme, J. I. G. Hernández, O. Grasset, D. Grassi, J. L. Grenfell, M. J. Griffin, C. A. Griffith, U. Grözinger, M. Guedel, P. Guio, O. Hainaut, R. Hargreaves, P. H. Hauschildt, K. Heng, D. Heyrovsky, R. Hueso, P. Irwin, L. Kaltenegger, P. Kervella, D. Kipping, T. T. Koskinen, G. Kovács, A. La Barbera, H. Lammer, E. Lellouch, G. Leto, M. Lopez Morales, M. A. Lopez Valverde, M. Lopez-Puertas, C. Lovis, A. Maggio, J. P. Maillard, J. Maldonado Prado, J. B. Marquette, F. J. Martin-Torres, P. Maxted, S. Miller, S. Molinari, D. Montes, A. Moro-Martin, J. I. Moses, O. Mousis, N. Nguyen Tuong, R. Nelson, G. S. Orton, E. Pantin, E. Pascale, S. Pezzuto, D. Pinfield, E. Poretti, R. Prinja, L. Prisinzano, J. M. Rees, A. Reiners, B. Samuel, A. Sánchez-Lavega, J. S. Forcada, D. Sasselov, G. Savini, B. Sicardy, A. Smith, L. Stixrude, G. Strazzulla, J. Tennyson, M. Tessenyi, G. Vasisht, S. Vinatier, S. Viti, I. Waldmann, G. J. White, T. Widemann, R. Wordsworth, R. Yelle, Y. Yung, and S. N. Yurchenko. EChO. Exoplanet characterisation observatory. *Experimental Astronomy*, 34:311–353, October 2012.

[258] Subhajit Sarkar, Andreas Papageorgiou, and Enzo Pascale. Exploring the potential of the ExoSim simulator for transit spectroscopy noise estimation. In *Proceedings of SPIE*, volume 9904 of *Society of Photo-Optical Instrumentation Engineers (SPIE) Conference Series*, page 99043R, Jul 2016.

[259] R. Varley, A. Tsiaras, and K. Karpouzas. Wayne—A Simulator for HST WFC3 IR Grism Spectroscopy. *The Astrophysical Journal Supplement*, 231(1):13, Jul 2017.

[260] L. Mugnai, B. Edwards, and E. Pascale. Ariel Radiometric Model. *Journal*

of Astronomical Instrumentation, 2019.

[261] Billy Edwards, Ahmed Al-Refaie, P.O. Lagage, and Rene Gastaud. ExoWebb: A JWST Radiometric Simulator. *in prep*, 2019.

[262] Billy Edwards. Terminus: A Time-Domian Simulator for Exoplanet Observations with Space-based Telescopes. *in prep*, 2019.

[263] J. L. Christiansen. Exoplanet Catalogues. *ArXiv e-prints 1803.11158*, March 2018.

[264] H. Rein. A proposal for community driven and decentralized astronomical databases and the Open Exoplanet Catalogue. *ArXiv e-prints 1211.7121*, November 2012.

[265] J. Schneider, C. Dedieu, P. Le Sidaner, R. Savalle, and I. Zolotukhin. Defining and cataloging exoplanets: the exoplanet.eu database. *A&A*, 532:A79, August 2011.

[266] J. Southworth. Homogeneous studies of transiting extrasolar planets - IV. Thirty systems with space-based light curves. *MNRAS*, 417:2166–2196, November 2011.

[267] M. Tessenyi, M. Ollivier, G. Tinetti, J. P. Beaulieu, V. Coudé du Foresto, T. Encrenaz, G. Micela, B. Swinyard, I. Ribas, A. Aylward, J. Tennyson, M. R. Swain, A. Sozzetti, G. Vasisht, and P. Deroo. Characterizing the Atmospheres of Transiting Planets with a Dedicated Space Telescope. *ApJ*, 746:45, February 2012.

[268] S. Seager and G. Mallén-Ornelas. A Unique Solution of Planet and Star Parameters from an Extrasolar Planet Transit Light Curve. *ApJ*, 585:1038–1055, March 2003.

[269] J. Chen and D. Kipping. Probabilistic Forecasting of the Masses and Radii of Other Worlds. *The Astrophysical Journal*, 834:17, January 2017.

[270] Isabelle Baraffe, Derek Homeier, France Allard, and Gilles Chabrier. New evolutionary models for pre-main sequence and main sequence low-mass stars down to the hydrogen-burning limit. *Astronomy & Astrophysics*, 577:A42, may 2015.

[271] Bernard J. Rauscher, Ori Fox, Pierre Ferruit, Robert J. Hill, Augustyn Waczynski, Yiting Wen, Wei Xia-Serafino, Brent Mott, David Alexander, Clifford K. Brambora, Rebecca Derro, Chuck Engler, Matthew B. Garrison, Thomas Johnson, Sridhar S. Manthripragada, James M. Marsh, Cheryl Marshall, Robert J. Martineau, Kamdin B. Shakoorzadeh, Donna Wilson, Wayne D. Roher, Miles Smith, Craig Cabelli, James Garnett, Markus Loose, Selmer Wong-Anglin, Majid Zandian, Edward Cheng, Timothy Ellis, Bryan Howe, Miriam Jurado, Ginn Lee, John Nieznanski, Peter Wallis, James York, Michael W. Regan, Donald N. B. Hall, Klaus W. Hodapp, Torsten Böker, Guido De Marchi, Peter Jakobsen, and Paolo Strada. Detectors for the James Webb Space Telescope Near-Infrared Spectrograph. I. Readout Mode, Noise Model, and Calibration Considerations. *Publications of the Astronomical Society of the Pacific*, 119(857):768–786, Jul 2007.

[272] I. P. Waldmann, M. Rocchetto, G. Tinetti, E. J. Barton, S. N. Yurchenko, and J. Tennyson. Tau-REx II: Retrieval of Emission Spectra. *ApJ*, 813:13, November 2015.

[273] S. N. Yurchenko and J. Tennyson. ExoMol: molecular line lists for exoplanet and other atmospheres. In C. Stehlé, C. Joblin, and L. d'Hendecourt, editors, *EAS Publications Series*, volume 58 of *EAS Publications Series*, pages 243–248, February 2012.

[274] L. S. Rothman and I. E. Gordon. Status of the HITRAN and HITEMP databases. In *13th International HITRAN Conference, June 2014, Cambridge, Massachusetts, USA*, June 2014.

[275] I. Gordon, L. S. Rothman, J. S. Wilzewski, R. V. Kochanov, C. Hill, Y. Tan,

and P. Wcislo. HITRAN2016 : new and improved data and tools towards studies of planetary atmospheres. In *AAS/Division for Planetary Sciences Meeting Abstracts #48*, volume 48 of *AAS/Division for Planetary Sciences Meeting Abstracts*, page 421.13, October 2016.

[276] Martin Abel, Lothar Frommhold, Xiaoping Li, and Katharine LC Hunt. Collision-induced absorption by h2 pairs: From hundreds to thousands of kelvin. *The Journal of Physical Chemistry A*, 115(25):6805–6812, 2011.

[277] Leigh N Fletcher, Magnus Gustafsson, and Glenn S Orton. Hydrogen dimers in giant-planet infrared spectra. *The Astrophysical Journal Supplement Series*, 235(1):24, 2018.

[278] Martin Abel, Lothar Frommhold, Xiaoping Li, and Katharine LC Hunt. Infrared absorption by collisional h2–he complexes at temperatures up to 9000 k and frequencies from 0 to 20 000 cm- 1. *The Journal of chemical physics*, 136(4):044319, 2012.

[279] Emma J Barton, C Hill, Sergei N Yurchenko, Jonathan Tennyson, Anna S Dudaryonok, and Nina N Lavrentieva. Pressure-dependent water absorption cross sections for exoplanets and other atmospheres. *Journal of Quantitative Spectroscopy and Radiative Transfer*, 187:453–460, 2017.

[280] Oleg L Polyansky, Aleksandra A Kyuberis, Nikolai F Zobov, Jonathan Tennyson, Sergei N Yurchenko, and Lorenzo Lodi. Exomol molecular line lists xxx: a complete high-accuracy line list for water. *Monthly Notices of the Royal Astronomical Society*, 480(2):2597–2608, 2018.

[281] Christian Hill, Sergei N Yurchenko, and Jonathan Tennyson. Temperature-dependent molecular absorption cross sections for exoplanets and other atmospheres. *Icarus*, 226(2):1673–1677, 2013.

[282] Sergei N. Yurchenko and Jonathan Tennyson. ExoMol line lists - IV. The rotation-vibration spectrum of methane up to 1500 K. *Monthly Notices of the Royal Astronomical Society*, 440(2):1649–1661, May 2014.

[283] K. L. Chubb, J. Tennyson, and S. N. Yurchenko. ExoMol Molecular linelists XX: C_2H_2. *MNRAS*, 2019. (In preparation).

[284] R J Barber, J K Strange, C Hill, O L Polyansky, G Ch Mellau, S N Yurchenko, and Jonathan Tennyson. ExoMol line lists – III. An improved hot rotation-vibration line list for HCN and HNC. *MNRAS*, 437:1828–1835, 2014.

[285] S. N. Yurchenko, R. J. Barber, and J. Tennyson. A variationally computed hot line list for NH_3. *MNRAS*, 413:1828–1834, 2011.

[286] Gang Li, Iouli E Gordon, Laurence S Rothman, Yan Tan, Shui-Ming Hu, Samir Kassi, Alain Campargue, and Emile S Medvedev. Rovibrational line lists for nine isotopologues of the co molecule in the x $1\sigma+$ ground electronic state. *The Astrophysical Journal Supplement Series*, 216(1):15, 2015.

[287] LS Rothman, IE Gordon, RJ Barber, H Dothe, RR Gamache, A Goldman, VI Perevalov, SA Tashkun, and J Tennyson. Hitemp, the high-temperature molecular spectroscopic database. *Journal of Quantitative Spectroscopy and Radiative Transfer*, 111(15):2139–2150, 2010.

[288] David W Schwenke. Opacity of tio from a coupled electronic state calculation parametrized by ab initio and experimental data. *Faraday Discussions*, 109:321–334, 1998.

[289] Laura K. McKemmish, Sergei N. Yurchenko, and Jonathan Tennyson. ExoMol line lists - XVIII. The high-temperature spectrum of VO. *MNRAS*, 463(1):771–793, Nov 2016.

[290] C. Sousa-Silva, A. F. Al-Refaie, J. Tennyson, and S. N. Yurchenko. ExoMol line lists - VII. the rotation-vibration spectrum of phosphine up to 1500 K. *MNRAS*, 446:2337–2347, 2015.

[291] E J Barton, S. N. Yurchenko, and J. Tennyson. ExoMol Molecular linelists – II. The ro-vibrational spectrum of SiO. *MNRAS*, 434:1469–1475, 2013.

[292] D. S. Underwood, J. Tennyson, S. N. Yurchenko, Xinchuan Huang, David W. Schwenke, Timothy J. Lee, S. Clausen, and A. Fateev. ExoMol line lists XIV: A line list for hot SO_2. *MNRAS*, 459:3890–3899, 2016.

[293] A. A. A. Azzam, S. N. Yurchenko, J. Tennyson, and O. V. Naumenko. ExoMol line lists XVI: A Hot Line List for H_2S. *MNRAS*, 460:4063–4074, 2016.

[294] S. Sarkar, A. Papageorgiou, I.A. Argyriou Tsikrikonis, B. Vandenbussche, and E. Pascale. *ARIEL Performance Analysis Report: ARIEL-CRDF-PL-AN-001*, 2017.

[295] A. Léger, F. Selsis, C. Sotin, T. Guillot, D. Despois, D. Mawet, M. Ollivier, A. Labèque, C. Valette, F. Brachet, B. Chazelas, and H. Lammer. A new family of planets? "Ocean-Planets". *Icarus*, 169:499–504, June 2004.

[296] K. Hamano, H. Kawahara, Y. Abe, M. Onishi, and G. L. Hashimoto. Lifetime and Spectral Evolution of a Magma Ocean with a Steam Atmosphere: Its Detectability by Future Direct Imaging. *ApJ*, 806:216, June 2015.

[297] Kristo Ment, Jason A. Dittmann, Nicola Astudillo-Defru, David Charbonneau, Jonathan Irwin, Xavier Bonfils, Felipe Murgas, Jose-Manuel Almenara, Thierry Forveille, Eric Agol, Sarah Ballard, Zachory K. Berta-Thompson, François Bouchy, Ryan Cloutier, Xavier Delfosse, René Doyon, Courtney D. Dressing, Gilbert A. Esquerdo, Raphaëlle D. Haywood, David M. Kipping, David W. Latham, Christophe Lovis, Elisabeth R. Newton, Francesco Pepe, Joseph E. Rodriguez, Nuno C. Santos, Thiam-Guan Tan, Stephane Udry, Jennifer G. Winters, and Anaël Wünsche. A Second Terrestrial Planet Orbiting the Nearby M Dwarf LHS 1140. *AJ*, 157:32, Jan 2019.

[298] B. Charnay, V. Meadows, A. Misra, J. Leconte, and G. Arney. 3D Modeling of GJ1214b's Atmosphere: Formation of Inhomogeneous High Clouds and Observational Implications. *ApJ*, 813:L1, November 2015.

[299] Gijs D. Mulders. *Planet Populations as a Function of Stellar Properties*, page 153. Springer International Publishing, 2018.

[300] Kyle A. Pearson. A search for multi-planet systems with TESS using a Bayesian N-body retrieval and machine learning. *arXiv e-prints*, page arXiv:1907.03377, Jul 2019.

[301] A. Garcia-Piquer, I. Ribas, and J. Colomé. Artificial intelligence for the EChO mission planning tool. *Experimental Astronomy*, 40:671–694, December 2015.

[302] J. C. Morales, J.-P. Beaulieu, V. Coudé du Foresto, M. Ollivier, I. O. Castello, R. Clédassou, J. Jaubert, P. Van-Troostenberghe, R. Varley, I. P. Waldmann, E. Pascale, and M. Tessenyi. Scheduling the EChO survey with known exoplanets. *Experimental Astronomy*, 40:655–670, December 2015.

[303] Mark Swain, Raissa Estrela, Christophe Sotin, Gael Roudier, and Robert Zellem. Two Terrestrial Planet Families With Different Origins. *arXiv e-prints*, page arXiv:1811.07919, November 2018.

[304] B. R. Brandl, O. Absil, T. Agócs, N. Baccichet, T. Bertram, F. Bettonvil, R. van Boekel, L. Burtscher, E. van Dishoeck, M. Feldt, P. J. V. Garcia, A. Glasse, A. Glauser, M. Güdel, C. Haupt, M. A. Kenworthy, L. Labadie, W. Laun, D. Lesman, E. Pantin, S. P. Quanz, I. Snellen, R. Siebenmorgen, and H. van Winckel. Status of the mid-IR ELT imager and spectrograph (METIS). In *Ground-based and Airborne Instrumentation for Astronomy VII*, volume 10702 of *Society of Photo-Optical Instrumentation Engineers (SPIE) Conference Series*, page 107021U, July 2018.

[305] Billy Edwards, Malena Rice, Tiziano Zingales, Marcell Tessenyi, Ingo Waldmann, Giovanna Tinetti, Enzo Pascale, Giorgio Savini, and Subhajit Sarkar. Exoplanet spectroscopy and photometry with the Twinkle space telescope. *Experimental Astronomy*, 47(1-2):29–63, Apr 2019.

[306] G. Bruno, M. Deleuil, J.-M. Almenara, S. C. C. Barros, A. F. Lanza, M. Montalto, I. Boisse, A. Santerne, A.-M. Lagrange, and N. Meunier. Disentangling planetary and stellar activity features in the CoRoT-2 light curve. *A&A*, 595:A89, November 2016.

[307] E. Agol, J. Steffen, R. Sari, and W. Clarkson. On detecting terrestrial planets with timing of giant planet transits. *MNRAS*, 359:567–579, May 2005.

[308] D. M. Kipping. Transit timing effects due to an exomoon. *MNRAS*, 392:181–189, January 2009.

[309] M. J. Holman and N. W. Murray. The Use of Transit Timing to Detect Terrestrial-Mass Extrasolar Planets. *Science*, 307:1288–1291, February 2005.

[310] J. J. Lissauer, D. C. Fabrycky, E. B. Ford, W. J. Borucki, F. Fressin, G. W. Marcy, J. A. Orosz, J. F. Rowe, G. Torres, W. F. Welsh, N. M. Batalha, S. T. Bryson, L. A. Buchhave, D. A. Caldwell, J. A. Carter, D. Charbonneau, J. L. Christiansen, W. D. Cochran, J.-M. Desert, E. W. Dunham, M. N. Fanelli, J. J. Fortney, T. N. Gautier, III, J. C. Geary, R. L. Gilliland, M. R. Haas, J. R. Hall, M. J. Holman, D. G. Koch, D. W. Latham, E. Lopez, S. McCauliff, N. Miller, R. C. Morehead, E. V. Quintana, D. Ragozzine, D. Sasselov, D. R. Short, and J. H. Steffen. A closely packed system of low-mass, low-density planets transiting Kepler-11. *Nature*, 470:53–58, February 2011.

[311] J. C. Yee, G. G. Fazio, R. Benjamin, J. D. Kirkpatrick, M. A. Malkan, D. Trilling, S. Carey, D. R. Ciardi, D. Apai, M. L. N. Ashby, S. Ballard, J. L. Bean, T. Beatty, Z. Berta-Thompson, P. Capak, D. Charbonneau, S. Chesley, N. B. Cowan, I. Crossfield, M. C. Cushing, J. de Wit, D. Deming, M. Dickinson, J. Dittmann, D. Dragomir, C. Dressing, J. Emery, J. K. Faherty, J. Gagne, B. S. Gaudi, M. Gillon, C. J. Grillmair, A. Harris, J. Hora, J. G. Ingalls, T. Kataria, L. Kreidberg, J. E. Krick, P. J. Lowrance, W. A. Mahoney, S. A. Metchev, M. Mommert, M. Migo Mueller, Y. Shvartzvald,

H. Smith, K. B. Stevenson, H. I. Teplitz, and S. P. Willner. The Science Case for an Extended Spitzer Mission. *ArXiv e-prints*, October 2017.

[312] I. Linial, S. Gilbaum, and R. Sari. Modal Decomposition of TTV: Inferring Planet Masses and Eccentricities. *ApJ*, 860:16, June 2018.

[313] A. Teachey, D. M. Kipping, and A. R. Schmitt. HEK. VI. On the Dearth of Galilean Analogs in Kepler, and the Exomoon Candidate Kepler-1625b I. *AJ*, 155:36, January 2018.

[314] R. J. MacDonald and N. Madhusudhan. HD 209458b in new light: evidence of nitrogen chemistry, patchy clouds and sub-solar water. *MNRAS*, 469:1979–1996, August 2017.

[315] O. Venot and M. Agúndez. Chemical modeling of exoplanet atmospheres. *Experimental Astronomy*, 40:469–480, December 2015.

[316] A. Tsiaras, M. Rocchetto, I. P. Waldmann, O. Venot, R. Varley, G. Morello, M. Damiano, G. Tinetti, E. J. Barton, S. N. Yurchenko, and J. Tennyson. Detection of an Atmosphere Around the Super-Earth 55 Cancri e. *ApJ*, 820:99, April 2016.

[317] O. Venot, M. Agúndez, F. Selsis, M. Tessenyi, and N. Iro. The atmospheric chemistry of the warm Neptune GJ 3470b: Influence of metallicity and temperature on the CH_4/CO ratio. *A&A*, 562:A51, February 2014.

[318] Jonathan Tennyson, Sergei N. Yurchenko, Ahmed F. Al-Refaie, Emma J. Barton, Katy L. Chubb, Phillip A. Coles, S. Diamantopoulou, Maire N. Gorman, Christian Hill, Aden Z. Lam, Lorenzo Lodi, Laura K. McKemmish, Yueqi Na, Alec Owens, Oleg L. Polyansky, Tom Rivlin, Clara Sousa-Silva, Daniel S. Underwood, Andrey Yachmenev, and Emil Zak. The exomol database: Molecular line lists for exoplanet and other hot atmospheres. *Journal of Molecular Spectroscopy*, 327:73 – 94, 2016. New Visions of Spectroscopic Databases, Volume II.

[319] T. Encrenaz, G. Tinetti, M. Tessenyi, P. Drossart, P. Hartogh, and A. Coustenis. Transit spectroscopy of exoplanets from space: how to optimize the wavelength coverage and spectral resolving power. *Experimental Astronomy*, 40(2):523–543, Dec 2015.

[320] R. M. Goody and Y. L. Yung. *Atmospheric radiation : theoretical basis*. Oxford University Press, 1989.

[321] G. Tinetti, T. Encrenaz, and A. Coustenis. Spectroscopy of planetary atmospheres in our Galaxy. *The Astronomy and Astrophysics Review*, 21:63, October 2013.

[322] M. Rocchetto, I. P. Waldmann, O. Venot, P. O. Lagage, and G. Tinetti. Exploring Biases of Atmospheric Retrievals in Simulated JWST Transmission Spectra of Hot Jupiters. *ApJ*, 833:120, December 2016.

[323] A. Caldas, J. Leconte, F. Selsis, I. P. Waldmann, P. Bordé, M. Rocchetto, and B. Charnay. Effects of a fully 3D atmospheric structure on exoplanet transmission spectra: retrieval biases due to day-night temperature gradients. *A&A*, 623:A161, Mar 2019.

[324] J. Taylor, V. Parmentier, P. Irwin, S. Aigrain, G. Lee, and J. Krissansen-Totton. Understanding and Mitigating Biases when studying Inhomogeneous Emission Spectra with JWST. *MNRAS*, 2019.

[325] Jacob Lustig-Yaeger, Victoria S. Meadows, and Andrew P. Lincowski. The Detectability and Characterization of the TRAPPIST-1 Exoplanet Atmospheres with JWST. *AJ*, 158(1):27, Jul 2019.

[326] Caroline V. Morley, Laura Kreidberg, Zafar Rustamkulov, Tyler Robinson, and Jonathan J. Fortney. Observing the Atmospheres of Known Temperate Earth-sized Planets with JWST. *ApJ*, 850(2):121, Dec 2017.

[327] Korey Haynes, Avi M. Mandell, Nikku Madhusudhan, Drake Deming, and Heather Knutson. Spectroscopic evidence for a temperature inversion in

the dayside atmosphere of hot jupiter wasp-33b. *The Astrophysical Journal*, 806(2):146, 2015.

[328] Stevanus K. Nugroho, Hajime Kawahara, Kento Masuda, Teruyuki Hirano, Takayuki Kotani, and Akito Tajitsu. High-resolution Spectroscopic Detection of TiO and a Stratosphere in the Day-side of WASP-33b. *AJ*, 154:221, December 2017.

[329] J. J. Fortney, K. Lodders, M. S. Marley, and R. S. Freedman. A Unified Theory for the Atmospheres of the Hot and Very Hot Jupiters: Two Classes of Irradiated Atmospheres. *ApJ*, 678:1419–1435, May 2008.

[330] D. S. Spiegel, K. Silverio, and A. Burrows. Can TiO Explain Thermal Inversions in the Upper Atmospheres of Irradiated Giant Planets? *ApJ*, 699:1487–1500, July 2009.

[331] Thomas M. Evans, David K. Sing, Tiffany Kataria, Jayesh Goyal, Nikolay Nikolov, Hannah R. Wakeford, Drake Deming, Mark S. Marley, David S. Amundsen, Gilda E. Ballester, Joanna K. Barstow, Lotfi Ben- Jaffel, Vincent Bourrier, Lars A. Buchhave, Ofer Cohen, David Ehrenreich, Antonio García Muñoz, Gregory W. Henry, Heather Knutson, Panayotis Lavvas, Alain Lecavelier Des Etangs, Nikole K. Lewis, Mercedes López-Morales, Avi M. Mandell, Jorge Sanz-Forcada, Pascal Tremblin, and Roxana Lupu. An ultrahot gas-giant exoplanet with a stratosphere. *Nature*, 548:58–61, August 2017.

[332] O. Venot, E. Hébrard, M. Agúndez, M. Dobrijevic, F. Selsis, F. Hersant, N. Iro, and R. Bounaceur. A chemical model for the atmosphere of hot Jupiters. *A&A*, 546:A43, October 2012.

[333] J. I. Moses, M. R. Line, C. Visscher, M. R. Richardson, N. Nettelmann, J. J. Fortney, T. S. Barman, K. B. Stevenson, and N. Madhusudhan. Compositional Diversity in the Atmospheres of Hot Neptunes, with Application to GJ 436b. *ApJ*, 777(1):34, Nov 2013.

[334] Björn Benneke, Ian Wong, Caroline Piaulet, Heather A. Knutson, Ian J. M. Crossfield, Joshua Lothringer, Caroline V. Morley, Peter Gao, Thomas P. Greene, Courtney Dressing, Diana Dragomir, Andrew W. Howard, Peter R. McCullough, Eliza M. R. Kempton Jonathan J. Fortney, and Jonathan Fraine. Water Vapor on the Habitable-Zone Exoplanet K2-18b. *arXiv e-prints*, page arXiv:1909.04642, Sep 2019.

[335] R. Alonso, C. Moutou, M. Endl, J. M. Almenara, E. W. Guenther, M. Deleuil, A. Hatzes, S. Aigrain, M. Auvergne, A. Baglin, P. Barge, A. S. Bonomo, P. Bordé, F. Bouchy, C. Cavarroc, J. Cabrera, S. Carpano, Sz. Csizmadia, W. D. Cochran, H. J. Deeg, R. F. Díaz, R. Dvorak, A. Erikson, S. Ferraz-Mello, M. Fridlund, T. Fruth, D. Gandolfi, M. Gillon, S. Grziwa, T. Guillot, G. Hébrard, L. Jorda, A. Léger, H. Lammer, C. Lovis, P. J. MacQueen, T. Mazeh, A. Ofir, M. Ollivier, T. Pasternacki, M. Pätzold, D. Queloz, H. Rauer, D. Rouan, A. Santerne, J. Schneider, M. Tadeu dos Santos, B. Tingley, R. Titz-Weider, J. Weingrill, and G. Wuchterl. Transiting exoplanets from the CoRoT space mission. XXVI. CoRoT-24: a transiting multiplanet system. *A&A*, 567:A112, Jul 2014.

[336] G. Maciejewski, D. Dimitrov, M. Fernández, A. Sota, G. Nowak, J. Ohlert, G. Nikolov, Ł. Bukowiecki, T. C. Hinse, E. Pallé, B. Tingley, D. Kjurkchieva, J. W. Lee, and C. U. Lee. Departure from the constant-period ephemeris for the transiting exoplanet WASP-12. *A&A*, 588:L6, Apr 2016.

[337] L. G. Bouma, J. N. Winn, C. Baxter, W. Bhatti, F. Dai, T. Daylan, J. M. Désert, M. L. Hill, S. R. Kane, K. G. Stassun, J. Villasenor, G. R. Ricker, R. Vanderspek, D. W. Latham, S. Seager, J. M. Jenkins, Z. Berta-Thompson, K. Colón, M. Fausnaugh, Ana Glidden, N. Guerrero, J. E. Rodriguez, J. D. Twicken, and B. Wohler. WASP-4b Arrived Early for the TESS Mission. *AJ*, 157(6):217, Jun 2019.

[338] Gregory W. Henry, Geoffrey W. Marcy, R. Paul Butler, and Steven S.

Vogt. A Transiting “51 Peg-like” Planet. *The Astrophysical Journal Letters*, 529(1):L41–L44, Jan 2000.

[339] David Charbonneau, Timothy M. Brown, David W. Latham, and Michel Mayor. Detection of Planetary Transits Across a Sun-like Star. *The Astrophysical Journal Letters*, 529(1):L45–L48, Jan 2000.

[340] P. Kabath, M. Skarka, S. Sabotta, and E. Guenther. The role of small telescopes as a ground-based support for exoplanetary space missions. *arXiv e-prints*, page arXiv:1905.06126, May 2019.

[341] S. Poddaný, L. Brát, and O. Pejcha. Exoplanet Transit Database. Reduction and processing of the photometric data of exoplanet transits. *New Astronomy*, 15:297–301, March 2010.

[342] Diana Dragomir, Mallory Harris, Joshua Pepper, Thomas Barclay, and Jr Villanueva, Steven. Securing the legacy of TESS through the care and maintenance of TESS planet ephemerides. *arXiv e-prints*, page arXiv:1906.02197, Jun 2019.

[343] A. S. Bonomo, S. Desidera, S. Benatti, F. Borsa, S. Crespi, M. Damasso, A. F. Lanza, A. Sozzetti, G. Lodato, F. Marzari, C. Boccato, R. U. Claudi, R. Cosentino, E. Covino, R. Gratton, A. Maggio, G. Micela, E. Molinari, I. Pagano, G. Piotto, E. Poretti, R. Smareglia, L. Affer, K. Biazzo, A. Bignamini, M. Esposito, P. Giacobbe, G. Hébrard, L. Malavolta, J. Maldonado, L. Mancini, A. Martinez Fiorenzano, S. Masiero, V. Nascimbeni, M. Pedani, M. Rainer, and G. Scandariato. The GAPS Programme with HARPS-N at TNG . XIV. Investigating giant planet migration history via improved eccentricity and mass determination for 231 transiting planets. *A&A*, 602:A107, June 2017.

[344] Slavek Rucinski, Kieran Carroll, Rainer Kuschnig, Jaymie Matthews, and Peter Stibrany. Most (Microvariability & oscillations of stars) Canadian

astronomical micro-satellite. *Advances in Space Research*, 31(2):371–373, Jan 2003.

[345] M. Knapp, S. Seager, M. W. Smith, and C. M. Pong. ASTERIA: Arcsecond Space Telescope Enabling Research in Astrophysics. In *AGU Fall Meeting Abstracts*, volume 2017, pages A33M–07, Dec 2017.

[346] Diana Dragomir, Jaymie M. Matthews, Jason D. Eastman, Chris Cameron, Andrew W. Howard, David B. Guenther, Rainer Kuschnig, Anthony F. J. Moffat, Jason F. Rowe, Slavek M. Rucinski, Dimitar Sasselov, and Werner W. Weiss. MOST Detects Transits of HD 97658b, a Warm, Likely Volatile-rich Super-Earth. *ApJ*, 772(1):L2, Jul 2013.

[347] M. Nowak, S. Lacour, A. Crouzier, L. David, V. Lapeyrère, and G. Schworer. Short life and abrupt death of PicSat, a small 3U CubeSat dreaming of exoplanet detection. In *Space Telescopes and Instrumentation 2018: Optical, Infrared, and Millimeter Wave*, volume 10698 of *Society of Photo-Optical Instrumentation Engineers (SPIE) Conference Series*, page 1069821, Jul 2018.

[348] Brian T. Fleming, Kevin France, Nicholas Nell, Richard Kohnert, Kelsey Pool, Arika Egan, Luca Fossati, Tommi Koskinen, Aline A. Vidotto, and Keri Hoadley. Colorado Ultraviolet Transit Experiment: a dedicated CubeSat mission to study exoplanetary mass loss and magnetic fields. *Journal of Astronomical Telescopes, Instruments, and Systems*, 4:014004, Jan 2018.

[349] L. K. McKemmish, K. L. Chubb, T. Rivlin, J. S. Baker, M. N. Gorman, A. Heward, W. Dunn, and M. Tessenyi. Bringing pupils into the ORBYTS of research. *Astronomy and Geophysics*, 58(5):5.11–5.11, October 2017.

[350] C. Sousa-Silva. Original Research By Young Twinkle Students(ORBYTS): When can students start performing original research? In *American Astronomical Society Meeting Abstracts #231*, volume 231 of *American Astronomical Society Meeting Abstracts*, page 113.09, January 2018.

[351] K. L. Chubb, M. Joseph, J. Franklin, N. Choudhury, T. Furtenbacher, A. G. Császár, G. Gaspard, P. Oguoko, A. Kelly, S. N. Yurchenko, J. Tennyson, and C. Sousa-Silva. MARVEL analysis of the measured high-resolution rovibrational spectra of C_2H_2. *Journal of Quantitative Spectroscopy & Radiative Transfer*, 204:42–55, January 2018.

[352] Katy L. Chubb, Olga Naumenko, Stefan Keely, Sebestiano Bartolotto, Skye Macdonald, Mahmoud Mukhtar, Andrey Grachov, Joe White, Eden Coleman, Anwen Liu, Alexander Z. Fazliev, Elena R. Polovtseva, Veli-Matti Horneman, Alain Campargue, Tibor Furtenbacher, Attila G. Császár, Sergei N. Yurchenko, and Jonathan Tennyson. MARVEL analysis of the measured high-resolution rovibrational spectra of $H_2^{32}S$. *Journal of Quantitative Spectroscopy & Radiative Transfer*, 218:178–186, Oct 2018.

[353] Laura K. McKemmish, Jasmin Borsovszky, Katie L. Goodhew, Samuel Sheppard, Aphra F. V. Bennett, Alfie D. J. Martin, Amrik Singh, Callum A. J. Sturgeon, Tibor Furtenbacher, Attila G. Császár, and Jonathan Tennyson. MARVEL Analysis of the Measured High-resolution Rovibronic Spectra of $^{90}Zr^{16}O$. *ApJ*, 867(1):33, Nov 2018.

[354] M. Fridlund, G. Hébrard, R. Alonso, M. Deleuil, D. Gandolfi, M. Gillon, H. Bruntt, A. Alapini, Sz. Csizmadia, and T. Guillot. Transiting exoplanets from the CoRoT space mission. IX. CoRoT-6b: a transiting "hot Jupiter" planet in an 8.9d orbit around a low-metallicity star. *A&A*, 512:A14, Mar 2010.

[355] J. E. Rodriguez, K. D. Colón, K. G. Stassun, D. Wright, P. A. Cargile, D. Bayliss, J. Pepper, K. A. Collins, R. B. Kuhn, M. B. Lund, R. J. Siverd, G. Zhou, B. S. Gaudi, C. G. Tinney, K. Penev, T. G. Tan, C. Stockdale, I. A. Curtis, D. James, S. Udry, D. Segransan, A. Bieryla, D. W. Latham, T. G. Beatty, J. D. Eastman, G. Myers, J. Bartz, J. Bento, E. L. N. Jensen, T. E. Oberst, and D. J. Stevens. KELT-14b and KELT-15b: An Independent Discovery of WASP-122b and a New Hot Jupiter. *AJ*, 151:138, June 2016.

[356] A. Burdanov, P. Benni, E. Sokov, V. Krushinsky, A. Popov, L. Delrez, M. Gillon, G. Hébrard, M. Deleuil, P. A. Wilson, O. Demangeon, Ö. Baştürk, E. Pakštiene, I. Sokova, S. A. Rusov, V. V. Dyachenko, D. A. Rastegaev, A. Beskakotov, A. Marchini, M. Bretton, S. Shadick, and K. Ivanov. KPS-1b: The First Transiting Exoplanet Discovered Using an Amateur Astronomer's Wide-field CCD Data. *Publications of the Astronomical Society of the Pacific*, 130(7):074401, July 2018.

[357] M. G. Soto, M. R. Díaz, J. S. Jenkins, F. Rojas, N. Espinoza, R. Brahm, H. Drass, M. I. Jones, M. Rabus, J. Hartman, P. Sarkis, A. Jordán, R. Lachaume, B. Pantoja, M. Vučković, D. R. Ciardi, I. Crossfield, C. Dressing, E. Gonzales, and L. Hirsch. K2-237 b and K2-238 b: discovery and characterization of two new transiting hot Jupiters from K2. *MNRAS*, 478:5356–5365, August 2018.

[358] D. R. Anderson, A. Collier Cameron, M. Gillon, C. Hellier, E. Jehin, M. Lendl, P. F. L. Maxted, D. Queloz, B. Smalley, and A. M. S. Smith. WASP-44b, WASP-45b and WASP-46b: three short-period, transiting extrasolar planets. *MNRAS*, 422(3):1988–1998, May 2012.

[359] C. Hellier, D. R. Anderson, A. Collier Cameron, L. Delrez, M. Gillon, E. Jehin, M. Lendl, P. F. L. Maxted, F. Pepe, D. Pollacco, D. Queloz, D. Ségransan, B. Smalley, A. M. S. Smith, J. Southworth, A. H. M. J. Triaud, O. D. Turner, S. Udry, and R. G. West. Three WASP-South Transiting Exoplanets: WASP-74b, WASP-83b, and WASP-89b. *AJ*, 150:18, July 2015.

[360] P. F. L. Maxted, D. R. Anderson, A. Collier Cameron, L. Delrez, M. Gillon, C. Hellier, E. Jehin, M. Lendl, M. Neveu-VanMalle, F. Pepe, D. Pollacco, D. Queloz, D. Ségransan, B. Smalley, A. M. S. Smith, J. Southworth, A. H. M. J. Triaud, S. Udry, T. Wagg, and R. G. West. Five transiting hot Jupiters discovered using WASP-South, Euler, and TRAPPIST: WASP-119 b, WASP-124 b, WASP-126 b, WASP-129 b, and WASP-133 b. *A&A*, 591:A55, Jun 2016.

[361] O. D. Turner, D. R. Anderson, A. Collier Cameron, L. Delrez, D. F. Evans, M. Gillon, C. Hellier, E. Jehin, M. Lendl, P. F. L. Maxted, F. Pepe, D. Pollacco, D. Queloz, D. Ségransan, B. Smalley, A. M. S. Smith, A. H. M. J. Triaud, S. Udry, and R. G. West. WASP-120 b, WASP-122 b, AND WASP-123 b: Three Newly Discovered Planets from the WASP-South Survey. *Publications of the Astronomical Society of the Pacific*, 128(964):064401, Jun 2016.

[362] A. M. S. Smith, S. Csizmadia, D. Gandolfi, S. Albrecht, R. Alonso, O. Barragán, J. Cabrera, W. D. Cochran, F. Dai, H. Deeg, P. Eigmüller, M. Endl, A. Erikson, M. Fridlund, A. Fukui, S. Grziwa, E. W. Guenther, A. P. Hatzes, D. Hidalgo, T. Hirano, J. Korth, M. Kuzuhara, J. Livingston, N. Narita, D. Nespral, P. Niraula, G. Nowak, E. Palle, M. Pätzold, C. M. Persson, J. Prieto-Arranz, H. Rauer, S. Redfield, I. Ribas, and V. Van Eylen. K2-295 b and K2-237 b: two transiting hot Jupiters. *arXiv e-prints*, July 2018.

[363] R. L. Akeson, X. Chen, D. Ciardi, M. Crane, J. Good, M. Harbut, E. Jackson, S. R. Kane, A. C. Laity, S. Leifer, M. Lynn, D. L. McElroy, M. Papin, P. Plavchan, S. V. Ramírez, R. Rey, K. von Braun, M. Wittman, M. Abajian, B. Ali, C. Beichman, A. Beekley, G. B. Berriman, S. Berukoff, G. Bryden, B. Chan, S. Groom, C. Lau, A. N. Payne, M. Regelson, M. Saucedo, M. Schmitz, J. Stauffer, P. Wyatt, and A. Zhang. The NASA Exoplanet Archive: Data and Tools for Exoplanet Research. *Publications of the Astronomical Society of the Pacific*, 125:989, August 2013.

[364] M. Mallonn, C. von Essen, E. Herrero, X. Alexoudi, T. Granzer, M. Sosa, K. G. Strassmeier, G. Bakos, D. Bayliss, R. Brahm, M. Bretton, F. Campos, L. Carone, K. D. Colón, H. A. Dale, D. Dragomir, N. Espinoza, P. Evans, F. Garcia, S. H. Gu, P. Guerra, Y. Jongen, A. Jordán, W. Kang, E. Keles, T. Kim, M. Lendl, D. Molina, M. Salisbury, F. Scaggiante, A. Shporer, R. Siverd, E. Sokov, I. Sokova, and A. Wünsche. Ephemeris refinement of

21 hot Jupiter exoplanets with high timing uncertainties. *A&A*, 622:A81, Feb 2019.

[365] A. Claret, P. H. Hauschildt, and S. Witte. New limb-darkening coefficients for PHOENIX/1D model atmospheres. I. Calculations for 1500 K $\leq$ T_{eff} $\leq$ 4800 K Kepler, CoRot, Spitzer, uvby, UBVRIJHK, Sloan, and 2MASS photometric systems. *A&A*, 546:A14, Oct 2012.

[366] A. Claret, P. H. Hauschildt, and S. Witte. New limb-darkening coefficients for Phoenix/1d model atmospheres. II. Calculations for 5000K $\leq$ T_{eff} $\leq$ 10 000 K Kepler, CoRot, Spitzer, uvby, UBVRIJHK, Sloan, and 2MASS photometric systems. *A&A*, 552:A16, April 2013.

[367] F. Mackebrandt, M. Mallonn, J. M. Ohlert, T. Granzer, S. Lalitha, A. García Muñoz, N. P. Gibson, J. W. Lee, A. Sozzetti, J. D. Turner, M. Vaňko, and K. G. Strassmeier. Transmission spectroscopy of the hot Jupiter TrES-3 b: Disproof of an overly large Rayleigh-like feature. *A&A*, 608:A26, Dec 2017.

[368] J. Eastman, R. Siverd, and B. S. Gaudi. Achieving Better Than 1 Minute Accuracy in the Heliocentric and Barycentric Julian Dates. *Publications of the Astronomical Society of the Pacific*, 122:935, August 2010.

[369] St Raetz, A. M. Heras, M. Fernández, V. Casanova, and C. Marka. Transit analysis of the CoRoT-5, CoRoT-8, CoRoT-12, CoRoT-18, CoRoT-20, and CoRoT-27 systems with combined ground- and space-based photometry. *MNRAS*, 483(1):824–839, Feb 2019.